The University Of Sheffield.

The Relevance of Chromosome 6 to Uveal Melanoma: Relationship to Prognosis and Identification of Possibly Candidate Driver Genes

By

Mohammed Alfawaz

Supervisor: Dr. Karen Sisley

A thesis submitted in partial fulfilment of the requirements for the degree of Doctor of Philosophy

The University of Sheffield

Faculty of Medicine, Dentistry and Health

Department of Oncology and Human Metabolism

March 2020

Acknowledgements

In the name of Allah, the most gracious and merciful.

Firstly, I want to thank Allah for giving me the strength and health to finish my PhD journey and helped me through tough times.

I want to express my sincere thanks my supervisor Dr. Karen Sisley whom her support, inspiration and guidance during my study lead me to believe that I can enjoy this journey to the end. Also, I want to thank Dr. David Hammond who started guiding me through the first two years my PhD study and retired to fight cancer which thankfully he succeeded.

I want to thank our amazing Rare Tumour Research Group (RTRG) for their support and assistance in many techniques in the lab, especially Mr. Allan Birkett and Ms. Claire Greaves. Special thanks also to the lead technician Ms. Maggie Glover for her help and support in the histology lab.

Amazing years I spent in Sheffield and I felt home because of all my friends who encourage and supported me during my downtimes especially my colleague and friend Mr. Ahmad Alshammari which he helped me in and out the lab, and I learned a lot from him through these years.

I can't express my thanks to the two most inspiring people in my life, my mother Nawal and father Saleh, who stand by me all the time and when I decided to continue my education with unconditional love. My deepest thanks also to my wonderful brothers Abdullah, Osama and Abdulmalik and my lovely sisters Arwa, Atheer and Amjad for their continuous encouragement to finish this journey.

A very special thanks to my gorgeous wife Ms. Lamya Algasem for her endless support, compassion and patience since the first day she came to Sheffield because she believed that her husband can do it.

Finally, I dedicated this work to the creator and sustainer Allah.

Abstract

Uveal melanoma (UM) is the most common primary intraocular disease of adults and has a high mortality rate compared to other melanomas. Non-random chromosomal aberrations have been associated with UM, such as monosomy 3, gain of chromosome 8q, loss of chromosome 1p and gain of chromosome 6p and loss of 6q (isochromosome 6p). Monosomy 3 and gain of chromosome 8q have the strongest association with poor prognosis for UM. That said, although structural aberrations of chromosome 6 have been detected in some studies of UM, the alterations in this chromosome have been underestimated, possibly because of the focus on other chromosomes or the use of classical technologies such as karyotyping and comparative genomic hybridisation (CGH).

This thesis, therefore, will look to identify candidate genes on altered chromosome 6 that may contribute to the development, prognosis and metastasis of UM.

This thesis aims to associate different alterations of chromosome 6 with the known genetic mutations in UM. In order to achieve this, the aberrations within chromosome 6 will be analysed in detail using a specifically designed high-resolution array-CGH for UM in order to determine candidate genes that have an association with UM. Ultimately, these candidate genes will be explored using various technologies to corroborate their effect on the UM.

Table of contents

LIST OF PUBLICATIONS

- Doherty, R. E., Alfawaz, M., Francis, J., Lijka-Jones, B. and Sisley, K. (2018) 'Genetics of Uveal Melanoma', in Scott, J.F. & Gerstenblith, M.R. (eds.) *Noncutaneous Melanoma*. Brisbane (AU). – Book chapter.

- “Introduction to CRISPR/Cas9 Genome editing”– certificate of attending the workshop organised by Thermofisher™.

LIST OF FIGURES

LIST OF TABLES

List of Abbreviations

°C	Degrees Celsius
ABC	Avidin-Biotin-peroxidase complex
ABL	Abelson murine leukaemia viral oncogene
ADM-2	Aberration detection method-2
AE	Elution buffer
AL	Lysis buffer
AMD1	Adenosylmethionine decarboxylase 1
Array-CGH	Array comparative genomic hybridisation
ATL	Tissue lysis buffer
AW1	Washing buffer 1
AW2	Washing buffer 2
BAC	Bacterial artificial chromosome
BAP1	BRCA1-associated protein 1
BCR	Breakpoint cluster region
bp	base pair
BRAF	B-Raf proto oncogene
BSA	Bovine serum albumin
C	Cysteine
Cas9	CRIPSR associated endonuclease protein 9
CML	Chronic myeloid leukaemia
CO_2	Carbon dioxide
COMS	Collaborative Ocular Melanoma Study
CRISPR	Clustered regularly interspaced short palindromic repeats
CRUK	Cancer Research United Kingdom
Cy3	Cyanine-3
Cy5	Cyanine-5
CYSLTR2	cysteinyl-leukotriene receptor 2
DAB	3,3'-dianimobenzidine
ddNTPs	Dideoxyribonucleotide triphosphates
dH2O	Deionized water
DLRS	Derivative log ratio spread
DNA	Deoxyribonucleic acid
dNTPs	Deoxyribonucleotide triphosphates
DPBS	Dulbecco's phosphate buffer saline
DPX	Mixture of Distyrene, plasticiser and xylene
E	Glutamate
E2F1	E2F transcription factor 1
EBV	Epstein-Barr virus
EDTA	Ethylenediaminetetraacetic acid
EIF1AX	Eukaryotic translation initiation factor 1A, X-linked

EtOH	Ethanol
ETS	E-twenty-six
ESC	Embryonic stem cell
FACS	Fluorescence activated cell sorting
FARS2	Phenylalanyl-tRNA synthetase 2
FASST2	Fast adaptive states segmentation technique 2
FE	Feature extraction
FFPE	Formalin Fixed Paraffin-Embedded
FISH	Fluorescence in situ hybridisation
FNAB	Fine-needle aspiration biopsy
FOXQ1	Forkhead box Q1
g	Gram
GCD	Genomic cleavage detection
gDNA	Genomic DNA
GISTIC	Genomic identification of significant targets in cancer
GNA11	Guanine nucleotide-binding protein alpha 11
GNAQ	Guanine nucleotide-binding protein Q polypeptide
H	Histidine
H_2O_2	Hydrogen peroxide
HDR	Homology directed repair
HMM	Hidden Markov model
HPV	Human papilloma virus
HRP	Horseradish peroxidase
ICC	Immunocytochemistry
IHC	Immunohistochemistry
K	Lysine
KDa	Kilo Dalton
KIT	Kit proto-oncogene receptor tyrosine kinase
KO	Knockout
L	Leucine
MAPK	Mitogen-activated protein kinase
mg	Milligram
Ml	Millilitre
MLPA	Multiple ligation-dependent probe amplification
mm	Millimetre
MSA	Microsatellite Analysis
mTORC1	Mechanistic target of rapamycin complex-1
MTT	(4, 5-Dimethylthiazol-2-yl)-2, 5-diphenyltetrazolium bromide
NA	Not applicable
ng/µl	Nanogram per microliter
NGS	Next-generation sequencing
NHEJ	Non-homologues end joining

nm	Nanometre
NRAS	Neuroblastoma Ras viral oncogene
O.D.	Optical density
ODC	Ornithine decarboxylase
P	Proline
PAM	protospacer adjacent motif
PBS	Phosphate buffer saline
PBST	Phosphate buffer saline with tween 20
PCR	Polymerase chain reaction
PFS	progression-free survival
PLCB4	phospholipase C Beta 4
Pre-mRNA	Precursor messenger RNA
PVDF	Polyvinylidene fluoride
Q	Glutamine
QC	Quality control
R	Arginine
RNA	Ribonucleic acid
RNP	Ribonucleoprotein
RPM	Revolution per minute
SCNA	Somatic copy number aberrations
SDS-PAGE	Sodium dodecyl sulphate-polyacrylamide gel electrophoresis
SEM	Standard error of mean
SF3B1	Splicing factor 3B subunit 1
SKY	Spectral karyotyping
SNR	Signal to noise ratio
STAC	Significance testing for aberrant copy number
TAE	Tris-Acetate-EDTA
TCGA	The Cancer Genome Atlas
TE	Tris-EDTA
TERTp	Telomerase reverse transcriptase promoter
TGF	Transforming growth factor
TIDE	Tracking of indel by decomposition
UM	Uveal melanoma
UV	Ultraviolet
WB	Western blot
WES	Whole exome sequencing
WHO	World Health Organization
WT	Wild type
YAP	Yes-associated protein
µg	Microgram
µl	microliter

Chapter 1: Introduction

1.1 Introduction

Cancer is a genetic disease arising as a result of a failure to control cell growth. Most cancers are considered sporadic or somatic events, although there are some germline mutations that influence hereditary malignancy. According to the World Health Organization (WHO), malignant neoplasms are now considered to be the leading cause of death in Europe and North America (Bray et al., 2018). According to Cancer Research UK (CRUK), in 2016, there were more than 300,000 new cancer cases registered in the U.K. (Cancer Research UK, 2016). The number of new cases is expected to rise by 2% annually in the next two decades to be more than half million cases by 2035 (Smittenaar et al., 2016). Although some types of cancer can be treated effectively, others still have no effective treatment. This combination of the increasing number of cases of cancer and the lack of effective treatment highlights the need for new and improved ways of understanding and promoting suitable treatments for the disease.

1.1.1 Historical aspect of cancer as a genetic disease

Many theories have tried to explain the role of genetics in cancer and how its development is initiated. According to Balmain (2001), the first theory was established by Boveri (1902), who hypothesised that chromosomal changes occur in cancer cells that do not necessarily transpire in normal cells. According to Wunderlich (2007), meanwhile, Tyzzer (1916) was the first to use the term “somatic mutation” to describe the events of cancer progression. It was not until 1960, however, that Nowell and Hungerford became the first to discover a particular chromosomal translocation, now referred to as the Philadelphia chromosome, that could be linked to the incidence of chronic myeloid leukaemia (CML) (Nowell and Hungerford, 1960). In the Philadelphia chromosome, translocation occurred between chromosomes 9 and 22, resulting in tyrosine kinase gene fusion between the breakpoint cluster region (*BCR*) and Abelson murine leukaemia viral oncogene (*ABL*) (Rowley, 1973a, Rowley, 1973b, Thijsen et al., 1999). The final product of this *BCR-ABL* gene fusion is a new protein that led to a constitutive activation of the tyrosine kinase and increased myeloid cell

proliferation in the bone marrow and blood stream, which is an essential step in the transformation towards malignancy in CML (Daley and Baltimore, 1988).

This led to a hypothesis called the ‘two hits hypothesis’, that was proposed by Knudson (1971), and which stated that tumour suppressor genes should have two mutations, consequently affecting both alleles to cause a carcinogenesis, as reviewed by Knudson (2001). This hypothesis was evaluated on hereditary and non-hereditary retinoblastoma using age and family history, with the findings indicating that the retinoblastoma 1 (*Rb1*) gene was mutated on both alleles and was involved in both cell proliferation and the cell cycle (Murphree and Benedict, 1984, Knudson, 1988, Knudson, 1993). However, this theory did not explain other cancer characteristics, such as haploinsufficiency or epigenetic hypermethylation of the gene, rather than genetic mutation (Merlo et al., 1995, Tsihlias et al., 1999). For instance, *PTEN* is a tumour suppressor gene and it was found that haploinsufficiency of this gene is correlated with prostate cancer (Muller et al., 2000). In addition, the promoter hypermethylation of *PTEN* found in various types of cancers such as gastric, cervical and lung (Kang et al., 2002, Soria et al., 2002, Rizvi et al., 2011).

In 1947, Berenblum and Shubik proposed another theory, arguing that, rather than cancer resulting from a single genetic mutation, a multistage process is involved, where DNA is damaged first, and this unrepaired DNA segment then progresses into further cancer cell growth, which may finally convert into a fully-fledged malignant disease. Subsequently, many studies have provided evidence in support of this contention, as reviewed in Jeggo et al. (2016).

At the beginning of the twenty-first century, a remarkable paper was published by Hanahan and Weinberg (2000) explaining six important capabilities acquired in cell physiology that together dictate cancer development: self-sufficiency in growth signals, insensitivity to antigrowth signals, evasion from apoptosis, limitless replicative potential, sustained angiogenesis and tissue evasion and metastasis. A decade later, Hanahan and Weinberg (2011) expanded these capabilities to include four new ones: genome instability and mutation, tumour-promoting inflammation, avoiding immune surveillance and deregulation of

cellular energetics. These capabilities have helped researchers gain a greater understanding of cancer development and its essential mechanisms.

1.1.2 Aetiology of cancer development

Carcinogenesis may be promoted because of different aetiologies such as environmental agents, bacterial and viral infection as well as the ageing process. As reviewed by Luch (2005), Brookes and Lawley (1964) were the first to document the carcinogenic effect of DNA adducts and chemical agents, such as mustard gas. These researchers showed how alkylating agents can directly react with DNA to form a stable chemical adduct that might disrupt the normal function of the DNA molecule. The chemical adducts that bind with DNA induced the DNA repair machinery, which may result in DNA mutations that is correlated with an increased chance of carcinogenesis. Another example is smoking tobacco, which plays a definitive role in oral, lung and other types of cancers due to the fact that it increases the chemical adducts in the DNA molecule which in turn can damage the DNA to such a point that it can no longer be repaired, and this may initiate cancer (Hecht, 2002, Ma and Li, 2017, O'Keeffe et al., 2018). In addition, many reports have emphasised the role of obesity in oesophageal, colorectal and breast cancer, among others (Calle et al., 2003, Renehan et al., 2008, Basen-Engquist and Chang, 2011). Thus, there are myriad environmental factors that can cause cancer, some of which are not yet fully known; and an individual's risk for cancer will therefore reflect exposure to these numerous environmental factors.

Microorganisms, such as bacteria and viruses, also play an important role in increasing the likelihood of an individual developing cancer. One example of a strain of bacteria that can cause cancer is *Helicobacter pylori*, since infection with this bacterium increases one's risk of developing gastric cancer (Parsonnet et al., 1991, Eslick et al., 1999, Ishaq and Nunn, 2015). Viruses can also increase the risk of cancer among infected individuals. For instance, the human papilloma virus (HPV) increases the risk of cervical, breast and head and neck cancers (Boshart et al., 1984, Durst et al., 1983, Heng et al., 2009), while Hepatitis B and C both show a strong association with liver cancer development (Dane et al.,

1970, Choo et al., 1989, Bartosch, 2010). Epstein-Barr virus (EBV) is strongly correlated with Burkitt's lymphoma (Epstein et al., 1964, Brady et al., 2007) and has also shown a moderate correlation in the development of Hodgkin's lymphoma (Glaser et al., 1997, Sarwari et al., 2016). These viral and bacterial infections can disrupt the integrity of human DNA at the infection site, potentially increasing the chances of cancer initiating.

Age or the ageing process may also be associated with the likelihood of an individual developing cancer, since in ageing persons cells exhibit a decreased ability to repair the DNA abnormalities that occur during replication, particularly in response to other environmental factors, as described in the review by DePinho (2000). The transformation of a normal cell into a cancerous cell is therefore a multifactorial process that includes an accumulation of DNA damage and mutations, which over time disrupt the DNA repair and cell growth regulation system (Vijg and Suh, 2013). It is still not well known, however, whether the relationship between cancer risk and age is due to an accumulation of genetic and epigenetic mutations over time or to the high susceptibility to oncogenic mutations of elderly people (Rodriguez-Rodero et al., 2011, Lepez-Otin et al., 2013).

1.1.3 Genetic changes associated with cancer

There are different types of cytogenetic and genetic mutations that can lead to the onset of cancer. Most cancers have changes at the chromosomal level, such as the loss or gain of chromosomes (aneuploidy), or the loss or gain of part of a chromosome (Mitelman et al., 1994). In addition, chromosome translocation plays a role in initiating cancer, as has been mentioned before with respect to CML (Nowell and Hungerford, 1960). These aberrations can be detected using various cytogenetic techniques for obtaining images of clonal and non-clonal aberrations at the single cell level, such as karyotyping, fluorescence in situ hybridisation (FISH) and spectral karyotyping (SKY). Additionally, molecular cytogenetic techniques, such as array comparative genomic hybridisation (array-CGH), can be used to detect genomic amplification, deletion and information about copy number aberrations in cancer cells (Albertson and Pinkel, 2003, Evangelidou et al., 2010, Hillman et al., 2011). These molecular cytogenetic

techniques cannot detect balanced chromosomal alterations, translocations or inversions. Furthermore, these techniques do not have sufficient resolution to detect nucleotide mutations.

Two key inventions opened a new era for molecular genetics and the effective and accurate identification of point mutations in DNA. These were the development of Sanger DNA sequencing technology, which uses chain inhibitor termination to detect DNA bases and determine the sequence of the targeted DNA (Sanger et al., 1977), and the discovery of the polymerase chain reaction (PCR) process by (Mullis et al., 1986), which allowed a particular piece of DNA to generate millions of copies using an enzyme called *Taq* DNA polymerase. Furthermore, in the past decade, the field of cancer research has experienced immense developments following the completion of the human genome project by the International Human Genome Sequencing (2004). This completion has led to an improvement in the understanding of the mutational screening of regulatory genes that regulate the cell cycle and other cellular pathways, as reviewed by Stratton et al. (2009). This has revealed that some genes that can cause cancer are tumour suppressor genes in their original form, involved in DNA repair machinery and serving to control cell division when functioning normally; in their mutated state, however, they can lead to loss-of-function and the development of cancer. In addition to tumour suppressor genes, oncogenes can also cause normal cells to grow uncontrollably because of gain-of-function mutations in the normal proto-oncogene.

More recently, the introduction of next-generation sequencing (NGS) technology has revolutionised genetic research, allowing the investigation of different types of mutational, translocational and epigenetic phenomena. In addition, a previously unrecognised phenomenon of genetic instability in cancer, called chromothripsis, was discovered by Stephens et al. (2011) using microarray analysis and confirmed by NGS. This is a phenomenon where hundreds of genomic rearrangements occur in a single cellular crisis. While, surprisingly, the cell can survive this event, ultimately it stimulates cancer development.

1.2 Overview of Melanoma

Melanoma is a type of cancer that affects the melanocytes, which produce a pigment called melanin that serves to protect the human body from ultraviolet (UV)-light radiation damage. Melanocytes are found mostly in the skin and uveal tract. Although some melanomas may develop when a group of melanocytes (naevi) undergo malignant transformation, the majority of melanomas are developed without the association with naevi. Annually, there are around 300,000 new cases of cutaneous melanoma worldwide, this being the most common form of melanoma that is responsible for about 60,000 deaths annually, based on an estimate from 2018 (Bray et al., 2018). It is thus considered the fifth most frequently-diagnosed cancer in developed countries (Siegel et al., 2019).

1.3 Uveal Melanoma (UM)

Uveal melanoma (UM) is considered the most common primary intraocular malignancy among adults, accounting for 80% of all non-cutaneous melanoma (Singh et al., 2011). The incidence of UM is between 5.3 and 10.9 cases for every million individuals in the general population. While this means that UM is an uncommon disease when compared to other malignancies (Singh and Topham, 2003), it has a higher mortality rate than cutaneous melanoma (Jemal et al., 2010).

UM is a tumour that arises from neural crest-derived melanocytes, which populate the pigmented layer of the uveal tract. The uveal tract consists of two segments: the anterior segment and the posterior segment (Figure 1.1). The anterior segment contains the iris, which accounts for 10% of all UM and rarely metastasises (Shields et al., 2012). The most common form of UM, however, (90% of all cases) arises from the posterior segment, which consists of choroid tissue and the ciliary body (Damato, 2006).

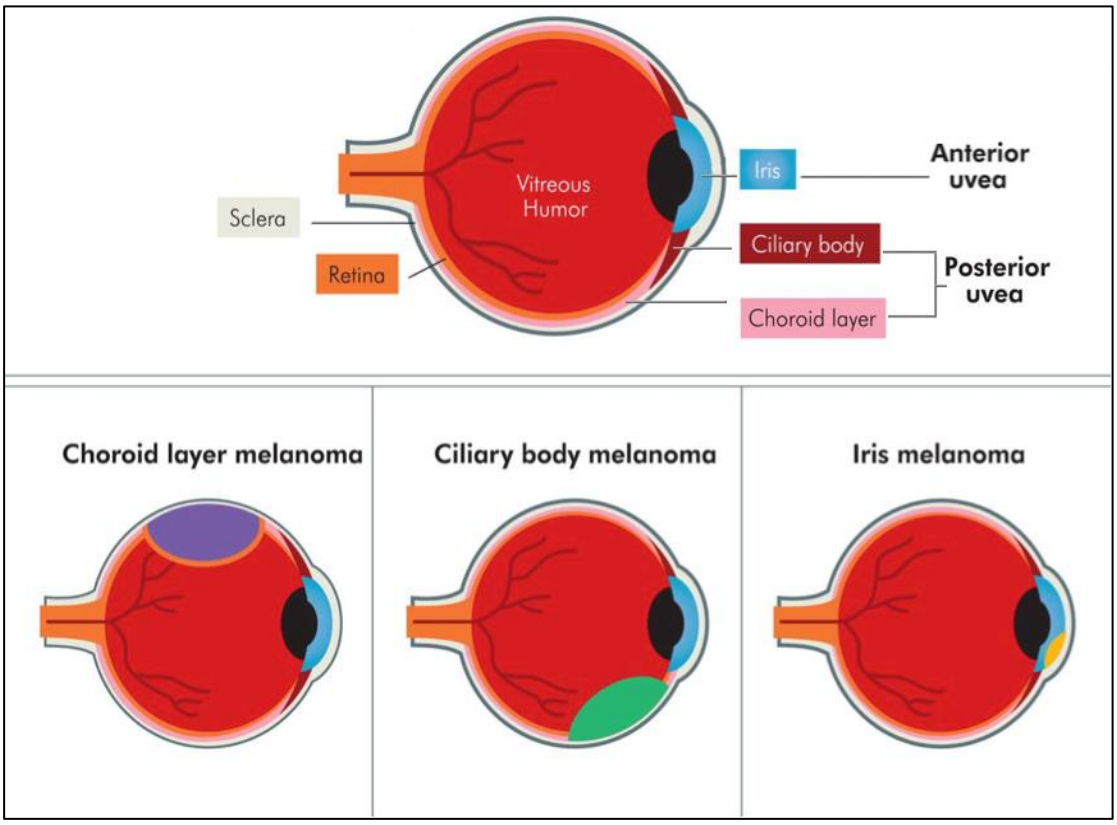

Figure 1.1. The anatomy of the eye and the origins of UM.

The eye consists of an anterior segment (iris) and a posterior segment (choroid and ciliary body). The sclera is the eye's outer membrane, while the retina is the inner membrane. The eye is filled with vitreous humour, which gives the eye its round shape. UM is dependent on the location in which it develops, such as in the choroid, ciliary body or iris. Modified from Chattopadhyay et al. (2016).

1.3.1 Risk factors of UM

There are different risk factors that can increase the incidence of melanoma disease. The primary risk factor in cutaneous melanoma, for instance, is sun exposure (UV-radiation exposure) among those with white skin pigment; as such, this cancer occurs at higher incidences among Caucasian populations who live in North America, Europe, Australia and New Zealand, and is far less common among darker-skinned populations, such as those in Africa or Asia, where the incidence of acral and mucosal melanomas is low, as reviewed by Schadendorf et al. (2015). Although exposure to UV radiation exhibits a strong association with cutaneous melanoma (IARC, 2012), extending this association to the onset of

UM is still controversial (Singh et al., 2004). For example, while some research articles correlated UV exposure to UM as a risk factor (Holly et al., 1990, Seddon et al., 1990, Vajdic et al., 2003), others showed no such correlation (Pane and Hirst, 2000, Lutz et al., 2005). In addition, cutaneous melanoma occurs in young adults and also commonly occurs in people aged between 40 to 60 (Garbe and Leiter, 2009). However, diagnoses of UM are usually made in older adults, especially those patients who are between the ages of 60 and 80 years old, with no apparent difference in incidence rates between males and females (Shields and Shields, 1992, Singh and Topham, 2003, Virgili et al., 2007).

UM is believed to be associated with ocular melanocytic lesions, including choroidal naevi and ocular melanocytosis. In addition, there are some skin disorders associated with UM, such as dysplastic nevus syndrome and the nevus of Ota (Hammer et al., 1996). A light-coloured iris, which is common in Caucasian populations, is considered to be a risk factor for the development of UM (Schmidt-Pokrzywniak et al., 2009). No association has been found, however, between UM and other environmental habits, such as smoking, alcohol consumption or dietary habits (Seddon et al., 1989).

1.3.2 Diagnosis of UM

Most UM patients present with metamorphopsia or a painless loss of vision, but larger tumours may sometimes be linked to retinal detachment, which causes photopsia (Eskelin and Kivela, 2002). Also, in some cases, patients may be entirely asymptomatic and unaware that they have UM until the tumour is identified through a routine funduscopic examination by the ophthalmologist. Most UM tumours have a very distinct dome or mushroom shape (Bedi et al., 2006). Patients who have anterior UM may notice discoloration of the iris or a permanent injection in the outer layer of the eye (episclera). The presence of sub-retinal fluid and an orange pigment are also associated with a diagnosis of UM (Melia et al., 1997). The Collaborative Ocular Melanoma Study (COMS, 1990) reported that the accuracy of a UM diagnosis is greater than 99% with enucleated eyes. The characterisation of UM is usually done by using different supportive tests such as ultrasonography, angiography, optical tomography and

autofluorescence (Shields et al., 2014). Additionally, fine-needle aspiration biopsy (FNAB) can also aid in the accurate diagnosis of UM, and this can also help the analysis of cytogenetic and gene expression to determine the prognostic factors (Char and Miller, 1995, McCannel, 2013).

1.3.3 Metastasis of UM

The prognosis with UM patients is that about 50% of them will develop metastasis to another organ within five to ten years, and when this occurs the survival rate is strikingly decreased to less than a year (Gragoudas et al., 1991, Kath et al., 1993, Diener-West et al., 2005, Rietschel et al., 2005). The most common organ that UM cells disseminate to is the liver, accounting for about 90% of cases. The survival rate after secondary metastasis of UM patients to the liver varies between six and twelve months (Diener-West et al., 2005). UM cells are disseminated directly through blood circulation due to the absence of lymph nodes in the uvea tract. Additionally, UM patients with metastasis risk may develop metastasis to other organs such as lungs, bone and, rarely, the skin and brain (The Collaborative Ocular Melanoma Study, 2001, Kujala et al., 2003, Bedikian, 2006). UM patients who experience metastasis to organs than the liver as a first site showed longer survival rate and more favourable prognosis (Kath et al., 1993).

1.3.4 Treatment of UM

Due to the poor survival rate once UM metastasises, a key aim in the treatment of UM is the prevention of the metastasis of the primary tumour. As mentioned earlier, however, half of UM cases show metastasis to the liver, with an associated reduction in the survival rate to less than a year. The main approach once UM has been diagnosed therefore is eye enucleation, as reviewed in Shields and Shields (2015). Even with eye enucleation, however, metastasis to the liver has not decreased.

In the 1970s, Zimmerman and colleagues hypothesised that eye enucleation may contribute to metastasis by releasing the tumour cells into the blood circulation (Zimmerman et al., 1978). This hypothesis was proposed around the time at

which radioactive plaque brachytherapy became available for selective UM patients (Packer and Rotman, 1980). This allowed the hypothesis to be tested in three trials that found that the survival for both medium- and large-sized UM tumours were similar after enucleation of the eye and use of brachytherapy, thus rejecting the 'Zimmerman hypothesis' (Davis et al., 1994, The Collaborative Ocular Melanoma Study, 1998, Diener-West et al., 2005). Besides surgical enucleation and radiotherapy, phototherapy using photocoagulation and transpupillary thermal therapy appear to be effective for some select small-sized UM. However, these types of therapy are associated with various side effects such as haemorrhage, occlusions of the retina and retinopathy (Singh et al., 2003, Mashayekhi et al., 2015). In addition, the use of new surgical techniques, such as stereotactic radiosurgery and proton beam therapy, appear to be effective for some UM patients with large-sized tumours and for cases that are unsuitable for plaque radiotherapy (Fakiris et al., 2007, Damato et al., 2013, Sikuade et al., 2015). These surgical techniques, however, have failed to increase the progression survival rate and overall survival for UM patients (Fabian et al., 2017). Furthermore, adjuvant therapy for UM patients using surgical techniques followed by chemo- or immunotherapy, have also failed to decrease the metastasis risk and improve the survival rate (Desjardins et al., 1998, Lane et al., 2009).

The chemotherapeutic regimens used for metastatic UM were originally adapted from cutaneous melanoma. These include dacarbazine, temozolomide, cisplatin and other combinations; however, the use of these drugs has neither led to an improvement in the survival rate nor lowered the risk of metastasis (Schmittel et al., 2006, Augsburger et al., 2009, Spagnolo et al., 2012, Spagnolo et al., 2013). In addition, several attempts have been made to use immunotherapeutic agents such as anti-CTLA-4 and anti-PD-1 on metastatic UM onsets, but the outcome remains unclear (Rodriguez et al., 2014, Kottschade et al., 2015, Zimmer et al., 2015). Recently, some molecular targeted therapies, such as mitogen-activated protein kinase (MAPK) pathway, have been tested for use in UM, however, the preliminary results showed that there was a partial response was found among UM patients (Park et al., 2020). Also, the clinical trials using epigenetic drugs are

ongoing without any result been published yet, as reviewed in Chokhachi Baradaran et al. (2020).

1.3.5 Prognosis of UM

The prognosis of UM depends on a myriad of factors, such as clinical findings, histopathology, cytogenetics and genetics. The point of origin of the tumour (the ciliary body, choroid or iris) has clinical implications for predicting the mortality rate of UM patients (Shields et al., 2001). Origin in the ciliary body usually has the worst prognosis and highest risk of metastasis, while origin in the choroid and iris suggests a good prognosis (Shields et al., 2009). Additionally, the tumour size, which is calculated from the height and base diameter of the mass, plays a role in predicting the prognosis of UM (Dienerwest et al., 1992). The large-tumour size is considered as a poor prognosis while the small-tumour size is considered as a good prognosis for UM. Moreover, a solid mushroom-shaped tumour correlates with a good prognosis while a diffuse lesion is considered as a bad prognostic marker for UM (Shields et al., 1996). Furthermore, the older patient's age is also correlated with UM poor prognosis; however, no correlations between prognosis and gender have been shown for UM (Kroll et al., 1998).

In addition to these clinical prognostic factors, the histopathology of the tumour following enucleation can be used to accurately predict a patient's survival. Callender (1931) was the first to propose a classification system for UM patients, which depended on cell type, while McLean et al. (1977) improved this system, as reviewed by Rennie (1997). McLean's classification system showed that there are three types of cells in UM, namely spindle, epithelioid and mixed cell, which combined both epithelioid and spindle cells in the same tumour. These cells are respectively associated with a good, poor and intermediate prognosis. (McLean et al., 1983). However, these clinical and histopathological parameters do not provide a conclusive determination of the prognostication risk for UM onsets. For this, there is a need to determine the effect of both cytogenetic and molecular genetic mutations of UM.

1.3.6 Chromosomal alteration in UM

Cutaneous melanoma and UM have distinctive genetic differences, despite both being considered to be melanomas. For instance, cutaneous melanoma exhibits different chromosomal and genetic aberrations that turn normal melanocyte cells into cancerous cells. The main chromosomal aberration found in cutaneous melanoma is the loss of chromosome 10 (monosomy 10), which accounts for about 60% of the cases (Bastian et al., 1998, Hoglund et al., 2004, Carless and Griffiths, 2008, Lin et al., 2008). Moreover, a recent study by Hirsch et al. (2013) using array-CGH found that the chromothripsis phenomenon occurs in malignant melanoma patients with a poor prognosis, and this result was confirmed using NGS (with paired-end sequencing) to emphasise the role of both inter- and intra-chromosomal rearrangement. Chromosomal instabilities such as the partial or complete loss of chromosomes 1p and 6q also occur in cutaneous melanoma, similar to UM, however, the cytogenetic changes in UM are not random and can in fact be characterised by key chromosomal aberrations, such as loss of chromosome 3 (monosomy 3), gain of the chromosome 8q arm and gain of chromosome 6p arm (Bastian et al., 2003, van den Bosch et al., 2010, van der Kooij et al., 2019).

The first chromosomal changes to be reported in UM were determined by Rey et al. (1985), who found abnormalities in both chromosomes 6 and 8 that are associated with increased risk of brain metastasis. Furthermore, the first two cytogenetic analyses were performed on a set of UM cases, revealing consistent abnormalities at the chromosomal level (Prescher et al., 1990, Sisley et al., 1990). These studies reported that the most frequently found abnormality was monosomy 3, while gain of chromosome 8q and deletion of the 1p arm were seen less frequently. Sisley et al. (1990) emphasised that UM originating in the ciliary body was associated with abnormalities at chromosomes 3 and 8. Detection of these anomalies was usually made by karyotyping and FISH using tumour biopsies obtained from UM patients (Sisley et al., 1990, Patel et al., 2001). Furthermore, microarray analysis using array-CGH is able to provide high-resolution evidence of chromosomal changes in UM; moreover, this method can

be used with different tissues, such as paraffin-embedded, formalin-fixed or frozen samples (Minca et al., 2014).

Monosomy 3 is associated with high rates of metastasis to the liver and is therefore also linked with a poor prognosis (Sisley et al., 1990, Prescher et al., 1996, Damato et al., 2007, Shields et al., 2007). Several studies have shown a correlation between large-size tumours, epithelioid cells and monosomy 3 with a poor overall prognosis (Prescher et al., 1996, Kilic et al., 2006, Damato et al., 2009, Shields et al., 2011, Van Beek et al., 2015). Moreover, Sisley et al. (1997) revealed that monosomy 3 and gains in chromosome 8q are associated with a poor prognosis. Additionally, the deletion of chromosome 1p and a gain of chromosome 8q are believed to be markers for a poor prognosis of UM (Aalto et al., 2001, Kilic et al., 2005). Conversely, Cross et al. (2006) and Abdel-Rahman et al. (2011) showed that the partial deletion of chromosome 3 correlated with an intermediate prognosis, while Trolet et al. (2009) reported that a normal chromosome 3 (disomy 3) is correlated with a good prognosis. In addition to disomy 3, a gain in chromosome 6p is associated with the best prognosis and non-metastatic UM (Landreville et al., 2008). The structural aberrations of chromosome 6 will be discussed in-depth in section 1.4.

Gain of chromosome 8q is usually associated with monosomy 3 and a ciliary body origin, which is correlated with poor prognosis in 50% of UM cases (Sisley et al., 1997, White et al., 1998, Singh et al., 2009). In fact, the use of more modern molecular cytogenetic technologies, such as array-CGH, has indicated the presence of monosomy 3 and gain of chromosome 8q in an even higher proportion of UM samples, between 51% and 75%, respectively (Hammond et al., 2015). Some researchers, however, have argued that the gain of chromosome 8q, either alone or with monosomy 3, is not a reliable prognostic factor to predict the outcome for UM patients (Kilic et al., 2005, Ehlers et al., 2008).

Besides these major chromosomal abnormalities in UM, there are other aberrations in chromosomes 1, 9, 11, 16 and 21. The loss of chromosome 1p arm in UM appears to be correlated with monosomy 3 and thence a poor prognosis (Naus et al., 2001, Aalto et al., 2001, Hausler et al., 2005). In addition,

loss of chromosome 9p and structural re-arrangement of chromosome 11 in UM appears to correlate with good prognosis (Speicher et al., 1994, Sisley et al., 2000, Sisley et al., 2006). Small recurrent aberrations, such as trisomy 21 and loss of chromosome 16q arm, have also been found to have a role in the UM prognosis (Horsman and White, 1993, Sisley et al., 2000, Kilic et al., 2006).

1.3.7 Mutations associated with Melanoma

Although cytogenetic analysis is able to provide a more accurate prognosis than when using clinical and histopathologic characteristics alone to assess different types of melanomas, the determination of a high or low risk for metastasis requires still more accurate information. In this regard, the main genetic mutation, accounting for more than half of melanomas, occurs in the B-Raf proto-oncogene (*BRAF*) (Davies et al., 2002), while the neuroblastoma Ras viral oncogene (*NRAS*) is responsible for around 20% of melanomas (Wilson and Nathanson, 2012). Kit proto-oncogene receptor tyrosine kinase (*KIT*) mutations commonly take place in acral and mucosal melanomas, although they rarely occur in skin cancer (Carvajal et al., 2011). While other types of melanomas, such as cutaneous, conjunctival and iris, also exhibit mutations in *BRAF* and *KIT* (Davies et al., 2002, Cohen et al., 2003, Spendlove et al., 2004, Thomas et al., 2006, Henriquez et al., 2007), they are rare or absent in cases of UM (Malaponte et al., 2006).

New technologies, however, are now identifying the unique genetic mutations in UM cells and thus a greater understanding of the associated molecular mechanisms and interactions. Genetic profiling of UM using COMS has been able to establish two classes of tumours based on the prognosis: class 1 and class 2 tumours. These respectively represent a tumour's low and high metastatic potential (Onken et al., 2010, Onken et al., 2012).

1.3.7.1 GNAQ and GNA11 mutations

Guanine nucleotide-binding protein Q polypeptide (*GNAQ*) and guanine nucleotide-binding protein alpha 11 (*GNA11*) gene mutations commonly occur in uveal melanoma patients (Onken et al., 2008, Van Raamsdonk et al., 2009, Van

Raamsdonk et al., 2010). The *GNAQ* and *GNA11* genes are located in chromosomes 9q21 and 19p13, respectively, which are found to have mutated in around 90% of UM patients (Van Raamsdonk et al., 2009, Van Raamsdonk et al., 2010, Koopmans et al., 2013). These mutated genes also tend to be found mutated in more than half of those patients with blue naevi (Van Raamsdonk et al., 2010, Sisley et al., 2011). Most of the *GNAQ* and *GNA11* mutations are found in codon Q209 of exon 5, although some are also found in codon R183 of exon 4. Furthermore, GNAQ and GNA11 mutations appeared to occur in early tumourigenesis in UM; these mutations have also been observed throughout all tumour progression processes. *GNAQ* and *GNA11* play a role in oncogenic behaviour because they encode G-proteins, meaning that their mutation can lead to G-proteins becoming constitutively active, upregulating the MAPK pathway. Recently, cases with mutations in *GNAQ* and *GNA11* have showed activation of the yes-associated protein (YAP), an effector on the Hippo tumour-suppressor pathway, which may enhance the oncogenic properties of these genes (Feng et al., 2014, Yu et al., 2014). Although *GNAQ* and *GNA11* are important because they are a driver mutations for melanocytic transformation, these genes do not have an impact on the prognosis for UM because they are found in early stages of UM, including in benign lesions, as well as in all further stages of progression (Dhillon et al., 2007, Bauer et al., 2009, Kim and Choi, 2010).

There are other genetic mutations besides *GNAQ* and *GNA11* that correlate with the development of UM. For instance, cysteinyl-leukotriene receptor 2 (*CYSLTR2*) which is a member of the G-protein family, similar to *GNAQ* and *GNA11* (Moore et al., 2016). In addition, phospholipase C Beta 4 (*PLCB4*) has been found to be mutated in UM, apparently activated by its interaction with *GNAQ* (Johansson et al., 2016). The mutations of *CYSLTR2* and *PLCB4* account for around 5% of UM, yet these mutations appear to be mutually exclusive from mutations of *GNAQ* and *GNA11* (Robertson et al., 2017). Although these newly identified gene mutations seem to have a similar functional effect on UM development as the *GNAQ* and *GNA11* mutations, their effect on the progression of UM is still undetermined.

1.3.7.2 BAP1 mutations

Harbour et al. (2010) were the first to describe the inactivation of a mutated BRCA1-associated protein 1 (*BAP1*) gene in more than 80% of UM cases exhibiting tumour metastasis. This gene is interestingly located in chromosome 3p21, which is an area that is frequently lost in metastatic UM. Mutations in the *BAP1* gene can terminate the BAP1 premature protein and some of these mutations can affect the ubiquitin carboxyl-terminal hydrolase domain which alter its deubiquitinase activity (Jensen et al., 1998). Pan et al. (2015) showed that the BAP1 protein may interact with the promoters that regulate E2F transcription factor 1 (*E2F1*), which may in turn have an effect on those genes involved in cell cycle progression that are controlled by the E2F family. In addition, the dysfunction of BAP1 protein has implications on cell pluripotency (Moon et al., 2017). Although the genetic mutations of *BAP1* appear to be correlated with the dysregulated expression of BAP1 protein, immunohistochemical assessment of the protein is more reliable than genetic mutational analysis (Kalirai et al., 2014). Furthermore, *BAP1* has been described in germline mutations among younger patients with UM, which suggests that it may be a predisposing gene among hereditary UM patients (Singh et al., 1996a, Singh et al., 1996b, Aoude et al., 2013, Cebulla et al., 2015). When *BAP1* mutations are found in UM, they are considered class 2 tumours (i.e. they are associated with a high risk of metastasis and a poor prognosis) (Harbour et al., 2013, Martin et al., 2013). The complete role of the dysregulation of BAP1 protein in UM is still unclear, however, and BAP1 dysregulation alone does not predict poor prognosis in UM cases (Harbour et al., 2010, Abdel-Rahman et al., 2011, Robertson et al., 2017).

1.3.7.3 SF3B1 mutations

The splicing factor 3B subunit 1 (*SF3B1*) gene is located in chromosome 2q33. It is a component of the spliceosome, which is a large and complex intracellular machine that processes precursor messenger RNA (pre-mRNA) into the mature transcript (Alsafadi et al., 2016). The mutation of this gene is responsible for different alternative splicing events, such as alternative terminal exon usage, intron retention and cryptic splicing within exons, for both protein coding and non-coding genes (Furney et al., 2013). Intriguingly, mutations in *SF3B1* have been

reported in different types of cancers, such as blood, breast and pancreatic cancer, where the predominant mutation hotspot in these cancers is in codon K700 (Malcovati et al., 2011, Wang et al., 2011, Biankin et al., 2012, Cancer Genome Atlas, 2012). The most common mutation hotspot of this gene in UM, however, is found in codon R625 of exon 14, occurring in between 10 and 20% of UM cases without the complete or partial loss of chromosome 3 (Furney et al., 2013, Harbour et al., 2013, Martin et al., 2013). In contrast, mutations in *SF3B1* occur only rarely in cutaneous melanoma (1% of cases) (Kong et al., 2014). Mutations in *SF3B1* gene are associated with a good UM prognosis, and are almost completely exclusive of mutations in *BAP1* (Harbour et al., 2013). A recent report by Luscan et al. (2015), however, revealed that some UM cells with mutations in the *SF3B1* gene can be observed in UM cases featuring liver metastasis. In addition, Yavuzyigitoglu et al. (2016b) showed that 79% of UM patients with mutated *SF3B1* exhibited late metastasis, although those patients were disomy 3. They emphasised that mutations of *SF3B1* in UM were likely to be correlated with gain of chromosome 6p, possibly indicating a role for chromosome 6 in terms of predicting the UM prognosis. Furthermore, this may be because of the partial gain of chromosome 8q in UM that appears to correlate with the poor prognosis (Sisley et al., 1997, Hammond et al., 2015, Robertson et al., 2017). Although it has been shown that *SF3B1* mutations in leukaemia lead to the accumulation of DNA damage by altering the DNA damage response (Te Raa et al., 2015), the biological role of splicing genes by mutated *SF3B1* in UM remains unclear (Furney et al., 2013, DeBoever et al., 2015).

1.3.7.4 EIF1AX mutations

Eukaryotic translation initiation factor 1A, X-linked (*EIF1AX*), which is located in chromosome Xp22, encodes for a protein that plays an essential role in both the recognition of the target mRNA start codon and mRNA translation (Chaudhuri et al., 1997). The use of new technologies, such as whole exome sequencing (WES), has revealed that 13% of UM with disomy 3 demonstrates mutations in *EIF1AX* exons 1 and 2 (Martin et al., 2013). Mutations in this gene are uncommon in UM patients with monosomy 3 and it appears to be mutually exclusive to *SF3B1*, which emphasises the rarity of mutated *EIF1AX* in metastasis to the liver.

Similar to *SF3B1*, mutations of *EIF1AX* in UM appear also to be correlated with the gain of chromosome 6p (Yavuzyigitoglu et al., 2016a). This is another gene that has recently been shown to be associated with UM prognosis when it is mutated. *EIF1AX* mutations are therefore considered class 1 tumours (at low risk of metastasis) and are associated with a good prognosis (Harbour et al., 2013, Decatur et al., 2016, Robertson et al., 2017). In addition, about 42% of *EIF1AX* mutations occur in iris melanoma cases, while mutations in other types of UM, such as ciliary body and choroidal, accounted for only 13% (Scholz et al., 2017). In a recent study Johnson et al. (2017) performed analyses on EIF1AX aiming to understand its function in UM cells. They found that UM cells with mutated EIF1AX have a deviant translational regulation in comparison with the normal EIF1AX, and they suggest that this may explain the selective advantage of mutant EIF1AX in UM.

1.3.7.5 TERTp mutations

The telomerase reverse transcriptase (*TERT*) gene is located in chromosome 5p15, where it encodes the catalytic reverse transcriptase subunit of telomerase, which is part of the ribonucleoprotein complex that maintains the telomere length (Cesare and Reddel, 2010, Horn et al., 2013). Telomerase activity has been found to be present in more than 90% of somatic cancer cells, but is absent in normal human cells (Shay and Bacchetti, 1997). Telomere maintenance is not TERT's only function: it is also involved in regulation of gene expression, cellular signalling, cell cycle and DNA damage response, apoptosis inhibition and maintenance of mitochondria DNA (mtDNA), as reviewed in Wu et al. (2013). These diverse functions indicate that the disruption of this protein may increase the cellular instability and thus tumourgenesis. Mutations in TERT promoter (*TERTp*) create a new binding motif for E-twenty-six (ETS) transcription factors and upregulate the expression of TERT (Huang et al., 2013). Interestingly, *TERTp* mutations have been shown to be a good prognostic marker in various cancers such as melanoma, thyroid, lung, liver and glioma (Yuan et al., 2016). Only two studies, however, have found mutations in *TERTp* gene in UM (one UM case in each study), which indicates the rarity of mutated *TERTp* mutations for UM cells (Dono et al., 2014, Koopmans et al., 2014a). The prognostic effect of

TERTp mutations for UM cells has been found to be similar to patients with good prognosis. Although the *TERTp* mutations are more common in other types of melanomas, such as cutaneous (Horn et al., 2013, Huang et al., 2013) and conjunctival melanomas (Griewank et al., 2013) than in UM, the discovery that they do appear in UM cells may provide a new insight into the role of *TERTp* in UM.

1.4 Ambiguity of chromosome 6 changes in UM

While structural aberrations of chromosome 6 have often been observed in UM, such as gain of 6p only, or loss of chromosome 6q and gain of 6p (isochromosome 6p), little is known about the implications of this chromosome and the involvement of genes in this chromosome. Chromosome 6 aberrations in other types of cancer, such as cutaneous melanoma, retinoblastoma and osteosarcoma, are correlated with poor prognosis (Ozaki et al., 2002, Bastian et al., 2003, Namiki et al., 2005, Zielinski et al., 2005, Gerami et al., 2010, Martin et al., 2012, Theriault et al., 2014) but in UM the gain of chromosome 6p is correlated with good prognosis and favourable outcomes (Aalto et al., 2001, Onken et al., 2004). Although some studies have argued that the gain of chromosome 6p is unlikely to be correlated with monosomy 3 in UM and thus the outcome is good prognosis (Prescher et al., 1995, Parrella et al., 1999, Ehlers et al., 2008, Landreville et al., 2008), other studies have showed that monosomy 3 occurs with gain of chromosome 6p in the same UM tumour (Sisley et al., 2000, Aalto et al., 2001).

The deletion of chromosome 6q has also been reported in different cancer types such as cutaneous melanoma, prostate cancer and acute lymphoblastic leukaemia, and correlates with a poor outcome (Healy et al., 1998, Nupponen et al., 1998, Mancini et al., 2002). The change in UM for chromosome 6q is usually correlated with gain of 6p to form an isochromosome 6p, which is correlated with monosomy 3, gain of chromosome 8q and poor prognosis (Sisley et al., 2000, Aalto et al., 2001, Kilic et al., 2006, Damato et al., 2009). Little is known, however, about the effect of the loss of chromosome 6q in UM because it is believed that this aberration is a late event resulting from the progression of the cancer

(Prescher et al., 1990, Gordon et al., 1994, White et al., 1998). Sisley et al. (2006) rationalised that structural aberrations and translocation events for chromosome 6 been found in around 70% of the UM cases. This finding may indicate that structural aberrations of chromosome 6 have a role in the prognosis of the UM.

Parrella et al. proposed a bifurcated pathway for UM tumour prognosis describing the chromosomal alteration events in which monosomy 3 and gain of chromosome 6p were mutually exclusive and then both advanced to gain of chromosome 8q that indicates a poor prognosis (Parrella et al., 1999). In an extension of this proposal, Sisley (2015) proposed an alternative pathway that include aberrations in chromosome 3 and chromosome 6 as an initiative pathway for UM progression and one correlated with the tumour origin, as seen in Figure 1.2. These genetic pathways for UM may therefore indicate the role of those aberrant chromosomes and determine their effect on UM development and progression. Generally, different research groups have come up with different results regarding the alterations of chromosome 6 in UM, making this chromosome a priority for further studies and gene exploration to clarify its role in both the development and progression of UM.

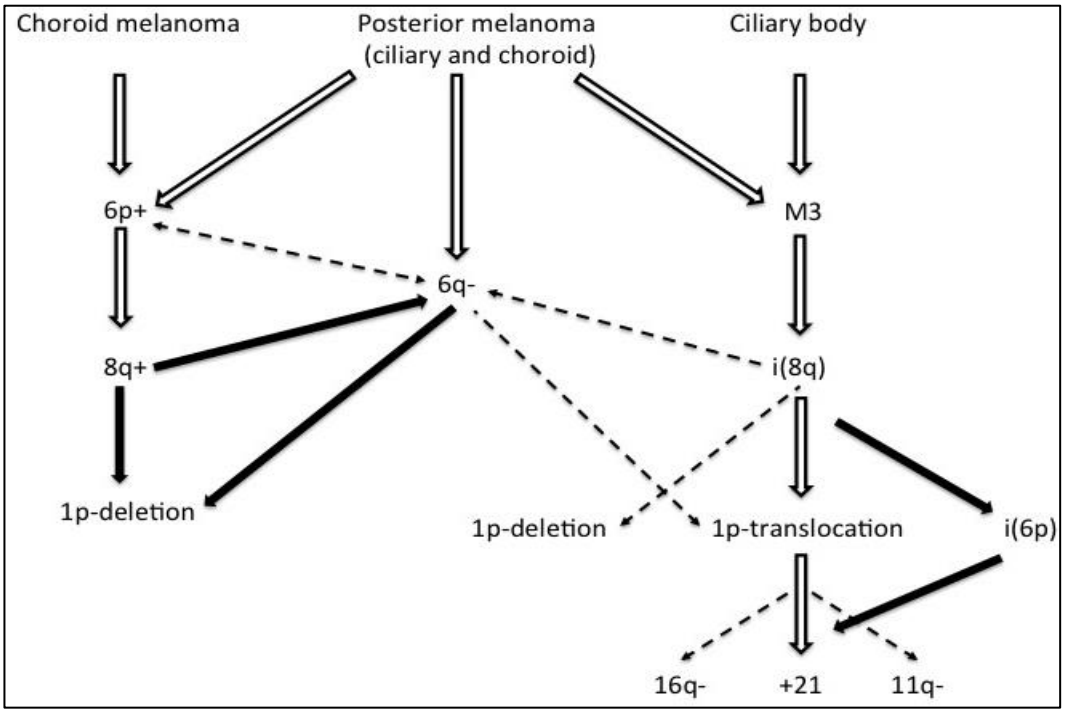

Figure 1.2. The chromosomal changes that occur in UM cells.

The figure indicates the tumour's origin (ciliary or choroid) then these cells develop to gain of 6p, loss of 6q or monosomy 3 (M3) that determine a patient's prognosis. The dashed lines indicate that these changes are possible, albeit this finding is not yet well established. Adapted from Sisley (2015).

1.5 Summary

In summary, the prognosis of UM depends on different clinical and cellular characteristics. An increasingly important area of research over the last twenty years has been the association of chromosomes 1, 3, 6 and 8 in predicting the prognosis of UM patients. Little is known, however, about the effect of chromosome 6 alterations on the progression of UM and thus it is necessary to identify genes in chromosome 6 and determine their effect on UM development and progression. Moreover, the last ten years have witnessed an increase in the identification of specific mutations in genes such as *GNAQ* and *GNA11* which have an association with the development of UM; while mutations in *SF3B1*, *EIF1AX* and *TERTp* have showed some association with the prognosis of UM; as summarised in Figure 1.3 (Doherty et al., 2018).

This introduction has emphasised the role of both chromosomal and genetic alterations in UM cells that can lead to an increase or decrease in metastasis to the liver. Although a number of studies have reported associations between chromosomal and genetic mutations and the development and progression of UM, some of these studies are fairly preliminary, and data on long-term follow up is not yet available, meaning that the evidence is not yet strong enough to validate their claims. Moreover, these genetic mutations do not seem to provide a clear indication of the way UM patients are going to behave, and instead the best information still comes from the actual chromosomal imbalances.

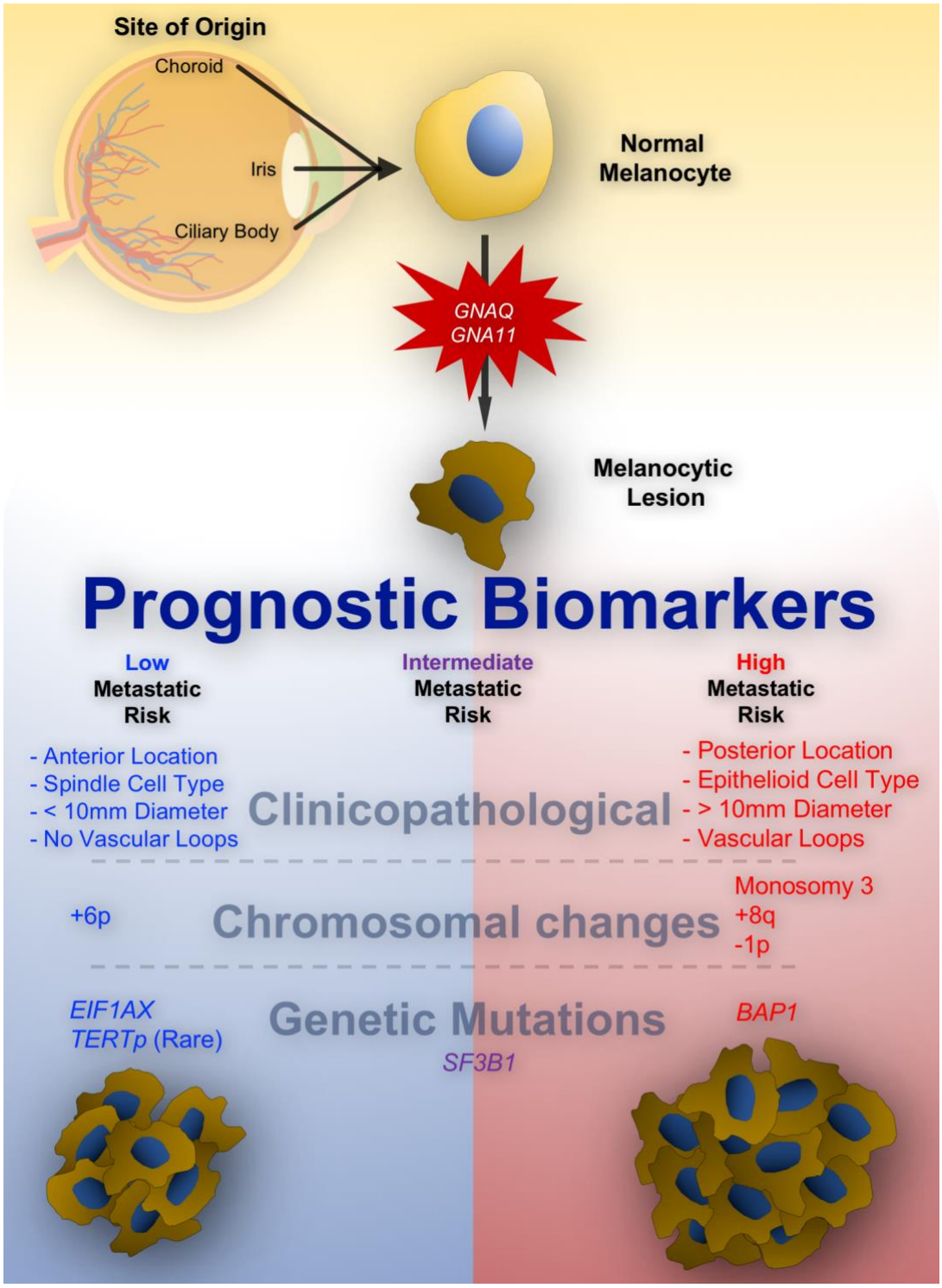

Figure 1.3. The correlation of prognostic biomarkers in UM with different clinical, histological, chromosomal and genetic changes.

This simple model elucidates the tumour progression in UM from a normal melanocyte to the mutations in *GNAQ* and *GNA11* that transformed it into a malignant melanocyte. Clinicopathological considerations then determine the progression of UM, along with changes in chromosomes such as chromosomes 1, 3, 6 and 8; and the effect of genetic mutations in *BAP1*, *SF3B1*, *EIF1AX*, and *TERTp* on the prognosis of UM.

1.6 Hypothesis and aims of the study

UM is an aggressive disease and there is not yet an effective therapeutic approach for secondary disease (Violanti et al., 2019). Genetic biomarkers of UM can successfully indicate prognosis, yet there is some debate over the importance and implications of changes in chromosome 6 aberrations. Furthermore, the genes involved in chromomere 6 are not yet identified. Therefore, the hypothesis is that:

Chromosome 6 aberrations can affect UM prognosis and there are genes on both arms which contribute to the development, prognosis and metastasis of UM.

This present study aims to continue the investigation initiated previously for a PhD study by Nawal Alshammari (Alshammari, 2017), which found candidate genes in chromosomes 6p and 6q that are relevant to the prognosis of UM using high-resolution array-CGH.

- The present study will continue this investigation to cover in more detail the cytogenetic changes effect of chromosome 6 aberrations associated with known genetic mutations.
- This study will then use high-resolution array-CGH to further assess other implicated regions of chromosomes 6p and 6q in respect the prognosis of UM.
- This study will also determine some of the underlying genetic abnormalities in those regions and explore the effect of targeting, using various techniques.

Chapter 2: Materials and Methods

2.1 Materials

2.1.1 General reagents and consumables

Reagents

Reagent	Supplier	Reagent	Supplier
Agarose	Fisher Scientific™	Glycerol	Fisher Scientific™
Bromophenol blue	Sigma™	Glycine	Sigma™
Deionised H_2O	Millipore™	Hydrogen Peroxide (H_2O_2)	Sigma™
DPX	Sigma™	Methanol	Fisher Scientific™
EDTA	Fisher Scientific™	Nuclease Free H_2O	Invitrogen™
Ethanol (EtOH)	Fisher Scientific™	Sterile phosphate buffered saline (PBS)	Fisher Scientific™
Ethidium Bromide (EtBr)	Sigma™	Tris base	Fluorochem®
Gill's haematoxylin	Fisher Scientific™	Tween-20	Sigma™
Glacial acetic acid	Fisher Scientific™	Xylene	Fisher Scientific™

Consumables

Reagent	Supplier	Reagent	Supplier
Centrifuge tubes (15, 25 and 50ml)	Starstedt™	Sterile filter pipette tips (10, 20, 200 and 1000µl)	StarLab™
Coverslips (22 x 22mm and 22 x 30mm)	VWR™	Sterile needles (20G and 31G)	Becton Dickinson (BD™)
Eppendorf microfuge tubes (0.2, 0.5, 1.5 and 2.0ml)	Starstedt™	Sterile plastic syringes	Becton Dickinson (BD™)
Nitrile examination gloves	StarLab™	Sterile pipette tips (10, 20, 200 and 1000µl)	StarLab™
Serological pipettes (5ml, 10ml and 25ml)	Corning®	Tissue culture flasks (T25 and T75)	Nunc®
Sterile petri dishes	Nunc®	Tissue culture plates (6, 12, 24, 48 and 96 wells)	Nunc®
Sterile scalpels	Swann Morton™		

2.1.2 Sample collection

Tumour tissue from 30 patients who were diagnosed with primary UM and who had undergone enucleation between 1994 and 2016, was instantly snap frozen and stored at -80 °C until DNA extraction (the Ocular Oncology Unit at the Royal Hallamshire Hospital, Sheffield, UK). Some of genomic DNA (gDNA) was previously extracted from the same patients' whole blood using standard extraction methods and was available for the archived samples. Ethical approval and patient consent were obtained from the Central Research Ethics Committee for research purposes (SSREC 94/247 and 09/H1008/141).

2.1.3 Cell lines

In this study, four cell lines were used as disease models. The cell lines were derived at the University of Sheffield from tumours that were diagnosed as UM and collected between 2009 and 2017 by Dr. Karen Sisley. These cell lines were given a laboratory designation numbers of MEL-577, MEL-585, MEL-627 and MEL-644. All these cell lines were phenotypically and genetically examined and correlated with their parent tumours by Dr. Karen Sisley. The HepG2 cell line (supplied by Dr. Nigel Bird) was used as a biological positive control for both immunocytochemistry and western blot (WB) experiments, following the manufacturer's recommended protocol.

2.1.4 DNA extraction from patients' blood and frozen tumour tissue samples

Patients' whole blood DNA extraction was prepared using QIAamp® DNA blood midi kit (QIAGEN®). Reagents that were used contained:

- QIAGEN® Protease.
- Lysis buffer (Buffer AL).
- Washing buffers (Buffer AW1 and AW2) after an addition of the appropriate volumes of absolute ethanol.
- Elution buffer (Buffer AE).
- QIAamp® midi columns and collection tubes.

DNA extraction for patients' snap-frozen tumour tissue was prepared using DNeasy® blood and tissue kit (QIAGEN®). Reagents that were used contained:

- QIAGEN® proteinase K.
- Tissue lysis buffer (Buffer ATL).
- RNase A
- Lysis buffer (Buffer AL).
- Washing buffers (Buffers AW1 and AW2) after an addition of the appropriate volumes of absolute ethanol.
- Elution buffer (Buffer AE)
- DNeasy® mini spin columns and collection tubes.

2.1.5 Primer design for GNAQ, GNA11, SF3B1, EIF1AX and TERTp

Forward and reverse primers for *GNAQ* and *GNA11* were previously designed by Onken et al. (2008) and Van Raamsdonk et al. (2010) (Table 2.1). Forward and reverse primers for *SF3B1*, *EIF1AX* and *TERTp* were also designed by Dono et al. (2014). In this study, these primers were confirmed using primer-BLAST website (www.ncbi.nlm.nih.gov/tools/primer-blast) to determine their specificity for the targeted genes. These primers were supplied lyophilised from (Eurofins Genomics) and were re-concentrated with nuclease free H_2O to a concentration of 100 pmol/µl and stored at -20 °C.

Table 2.1: Primer design for *GNAQ*, *GNA11*, *SF3B1*, *EIF1AX*, and *TERTp*.

Gene	Exon	Primer Direction	Primer sequence (5'->3')	Length (mer)	Tm (°C)	Product size (bp)
GNAQ	4	Forward	TCTTTTTCTCCCACCCCTTGC	21	60.0	509
		Reverse	TTGTTTTGAAGCCTACACATGATTCC	26	57.2	
	5	Forward	AGAAGTAAGTTCACTCCATTCCC	23	56.0	317
		Reverse	TTCCCTAAGTTTGTAAGTAGTGC	23	54.2	
GNA11	4	Forward	GTGCTGTGTCCCTGTCCTG	15	60.1	249
		Reverse	GGCAAATGAGCCTCTCAGTG	20	58.2	
	5	Forward	CGCTGTGTCCTTTCAGGATG	20	58.3	147
		Reverse	CCTCGTTGTCCGACT	15	52.5	
SF3B1	14	Forward	TGATTATGGAAAGAAATGGTTGAAG	25	56.0	343
		Reverse	CATGTTCAATGATTTCAACTAAACTTC	27	56.5	
EIF1AX	1	Forward	GAAAAGCGACGCAAAGAGTC	20	58.0	320
		Reverse	CTGGGTGACCTGCAATCTAC	20	57.9	
	2	Forward	GGGTAGGGAGGTGATAATGTG	21	57.2	406
		Reverse	CTGTAATCGTGCCACCACAC	20	59.2	
TERTp	Promoter	Forward	GTCCTGCCCCTTCACCTT	18	58.8	187
		Reverse	GCTTCCCACGTGCGCA	16	60.7	

2.1.6 Polymerase chain reaction (PCR)

For all PCR reactions, IMMOLASE™ DNA polymerase kit (BIOLINE, London, UK) was used and stored at -20 °C. The kit contained:

- 10× ImmunoBuffer.
- 50 mM $MgCl_2$ solution.
- IMMOLASE™ DNA polymerase.

Deoxyribonucleotide triphosphates (dNTPs): dNTPs set (BIOLINE™) containing dATP, dCTP, dGTP, and dTTP (100 mM). To make the working concentration of 50 mM of dNTPs, 25 µl of each was added to 100 µl of dH_2O.

Thermal cycler: Mastercycler® nexus gradient (Eppendorf).

Running buffer: 50× Tris-Acetate-EDTA (TAE) stock solution, prepared in 1000 ml of dH_2O as followed:

- 242 g tris base.
- 57.1 ml glacial acetic acid.
- 18.6 g EDTA.

Storage was at room temperature and was diluted to 1× for use.

Electrophoresis unit: Multi sub-choice electrophoresis unit (Geneflow), comprising:

- Gel casting tray (15 × 15 cm).
- Sample comb (20 samples).
- Electrophoresis tank.

Power source: Power-Pac 3000 basic power supply for electrophoresis (Biorad).

Ethidium bromide: Ready-to-use 20 mg/ml ethidium bromide (Sigma™) and stored at room temperature.

DNA ladder: 100 bp ladder (Promega™) stored at 4 °C.

Loading buffer: 6× loading buffer 0.25% (w/v) bromophenol blue and 30% (v/v) glycerol prepared by adding 25 mg bromophenol blue to 3 ml glycerol and made up to 10 ml using dH_2O and stored at 4 °C.

Gel documentation: Gel Doc™ EZ imager (Biorad).

2.1.7 Array-comparative genomic hybridisation (array-CGH)

Restriction digestion enzymes (Promega™) were stored -20 °C and contained:

- 10× Buffer C.
- Alu1 (10U/μl).
- Rsa1 (10U/μl).
- Acetylated bovine serum albumin (10μg/ml).

Genomic DNA enzymatic labelling kit (Agilent™) was stored at -20 °C containing:

- Random primers.
- 5× Buffer.
- 10× dNTPs.
- Cyanine 3-dUTP (Cy3) (1.0 mM).
- Cyanine 5-dUTP (Cy5) (1.0 mM).
- Exo-Klenow fragment.

Amicon® 30 kDA filters and 1× TE buffer for labelling DNA purification stored at room temperature.

Human Cot-1 DNA™ (Invitrogen™).

Oligo array-CGH Hybridisation kit (Agilent™) containing:

- Agilent 2× Hi-RPM hybridisation buffer stored at room temperature.
- Agilent 10× Blocking agent.

Microarray Hybridisation Assembly (Agilent™) containing:

- SurePrint® G3 Human CGH Microarray Slide 4×180K.
- Hybridisation gasket slide.
- Hybridisation champer kit-SureHyb® enabled, stainless steel.

Microarray hybridisation oven (Agilent™) fitted out with removable rotator rack.

Washing buffer kit: oligo array-CGH/ChIP-on chip wash buffer kit containing:

- Oligo array-CGH wash buffer 1.
- Oligo array-CGH wash buffer 2.

Microarray slide scanner system (G2565CA) (Aglient™).

2.1.8 Immunochemistry

Phosphate Buffered Saline (PBS): 10 tablets of PBS (Oxiod) dissolved into 1 L of H_2O.

Phosphate Buffered Saline with TWEEN 20 (PBST): 10 tablets of PBS dissolved into 1 L of H_2O with 0.1% of TWEEN 20® (1ml) (Sigma™).

Peroxidase quenching solution: 3% of hydrogen peroxide (H_2O_2) (Sigma™) in Methanol (Fisher Scientific™) prepared freshly by adding 30 ml of 30% H_2O_2 into 270 ml absolute methanol.

Melanin bleaching: 1.5% of H_2O_2 (Sigma™) in PBS prepared freshly by adding 15 ml of H_2O_2 into 285 ml of PBS.

Target retrieval solution (10×): 1:10 working solution prepared by adding 10 ml of DAKO (DAKO™) into 90 ml of deionised H_2O adjusted to pH 6.0.

Antigen retrieval instrument: 2100 Antigen Retriever (Aptum®)

Blocking kit: Consisting of two solutions: solution A (Avidin) and B (Biotin) (Vector Laboratories).

Blocking serum: Normal goat serum (Vector Laboratories) was stored at 4 °C and diluted in PBS with 10× casein solution (Vector Laboratories) to give a 10% working solution.

Primary antibodies: All primary antibodies were provided by (Abcam), and were stored at -20 °C, and diluted in 2% normal goat serum prior to use (Table 2.2).

Table 2.2: Summary of primary antibodies and their conditions.

Antibodies	Type	Source	Class	Control Tissue	Dilution and conditions
Anti-FARS2	Polyclonal	Rabbit	IgG	Human colon tissue	1:400 Overnight at 4°C
Anti-FOXQ1	Polyclonal	Rabbit	IgG	Human kidney tissue	1:200 Overnight at 4°C
Anti-AMD1	Polyclonal	Rabbit	IgG	Human mammary tissue	1:500 Overnight at 4°C

Secondary antibody: Made from goat anti-rabbit, biotinylated IgG (Vector Laboratories) was stored at 4 °C and diluted 1:200 in 2% blocking serum.

Avidin/Biotin peroxidase kit: VECTASTAIN® Avidin-biotin complex (ABC) kit stored at 4°C and used according to the manufacturer's instructions.

Peroxidase Substrate Kit: 3,3'-dianimobenzidine (DAB) peroxidase (HRP) substrate kit (with Nickel) (VECTASTAIN®) stored at 4 °C and used according to the manufacturer's instructions.

Mounting media: DPX mountant, a mixture of Distyrene, a Plasticiser, and Xylene; stored in the fume hood to preserve the tissue after staining.

2.1.9 Tissue culture

Culture medium: RPMI-1640 culture medium (Lonza™) was used and supplemented with 10% foetal bovine serum (Lonza™), 1% L-Glutamine (200mM in 0.85% NaCl; Lonza™), 1% Penicillin/streptomycin (10kU/ml; Lonza™) and 0.4% D-glucose (45% solution, Sigma™) in order to maintain UM cell lines; the media was then stored at 4 °C and warmed to 37 °C prior to use.

Trypsin-EDTA: 0.4% Trypsin-EDTA solution (Lonza™) was stored -20 °C and warmed to 37 °C prior to use.

Dulbecco's phosphate buffer saline (DPBS): 1× of DPBS that contains 9.5 mM PO_4 without Calcium and Magnesium, 500 ml (Lonza™).

2.1.10 Western blot (WB)

Lysis buffer: Radioimmunoprecipitation assay (RIPA) buffer is a ready-to-use reagent containing 150 mM of NaCl, 1.0% IGEPAL® CA-630, 0.5% sodium deoxycholate, 0.1% SDS, 50 mM Tris, pH 8.0. Stored at 4 °C (Sigma™)

Protease and phosphatase inhibitor: Ready-to-use cocktail stored at -20 °C (Sigma-Aldrich™).

Bradford protein assay: BCA protein assay Dye reagent (Biorad).

Filter paper: Whatman® qualitative filter paper, grade 1 (Sigma™).

Protein standard: Measuring 1 mg of BSA (Fisher Scientific™) and diluted with 1 ml of deionised H_2O.

Spectrophotometer reader: Multiskan™ microplate photometer (Thermo Scientific™).

Sample Loading buffer: NuPAGE® 4× lithium dodecyl sulphate (LDS) (Thermofisher™).

Reducing buffer: NuPAGE® 10× reducing agent (Thermofisher™).

Protein marker standard: Precision plus protein™, dual colour standards (Biorad).

Running buffer: For 10× buffer, 250 mM Tris-base (30.3 g) (Fluorochem) with 1.9M Glycine (Sigma™) (144 g) and 50 ml of 20% Sodium dodecyl sulphate (SDS) (Fisher Scientific™) with the volume being brought up to 1 L with H_2O**.**

Precast gel: 4-15% mini-PROTEAN® TGX™ precast protein gel (Biorad).

Electrophoresis chamber: Mini-PROREAN® tetra vertical electrophoresis cell **(**Bio-rad)

Transfer buffer: For 1× buffer, measuring 25 mM of Tris-base (Fluorochem) (3.03 g) with 192 mM Glycine (Sigma™) (14.4 g) and 20% of methanol (Fisher Scientific™) (200 ml), with the volume being brought up to 1 L with H_2O**.**

Filter papers: Whatman® gel blotting paper 30 × 60 cm (Sigma Aldrich™).

Polyvinylidene difluoride (PVDF) membrane: Immobilon-P PVDF membrane (Millipore™) 1 roll, 26.5 cm × 3.75 m, 0.45 µm pore size.

Semi-dry transfer system: Transblot® turbo™ transfer system (Biorad).

PBST: 1× phosphate buffer saline (PBS) with 0.1% TWEEN® 20 (Fisher Scientific™).

TBST: Supplied in a powder pouch containing (0.05M Tris-buffered saline (0.138M NaCl; 0.0027M KCl); 0.1% TWEEN® 20, pH 8.0) (Sigma™) and dissolved in 1 L of H_2O.

Blocking reagent: 5% non-fat dry milk diluted in PBST or TBST.

Primary antibody: Anti-AMD1 polyclonal rabbit antibody was provided by (Proteintech), stored at -20 °C and diluted to 1:300 with blocking solution prior to use.

Secondary antibody: Goat anti-rabbit IgG antibody conjugated to horseradish peroxidase (HRP) (Cell signalling Technology®) stored at -20 °C and diluted to 1:2000 with blocking solution prior to use.

Stripping buffer: Restore™ western blot stripping buffer (Thermofisher Scientific™).

Housekeeping antibody: Anti-beta tubulin antibody was provided by (Abcam), stored at -20 °C and diluted 1:5000 with blocking solution prior to use.

Detection reagent: Amersham™ Enhanced Chemiluminescence (ECL) western blotting detection reagent consist of two reagents, reagent A: luminol solution and reagent B: peroxide solution (GE healthcare).

Detection instrument: ChemiDoc™ MP (Biorad) imaging System.

2.1.11 CRISPR knockout

Single-guide RNA (sgRNA): TrueGuide™ Modified Synthetic sgRNA for AMD1 (ID: CRISPR843561_SGM), sequence (5'CCGACGCAAACCAAGGATCT'3) (Invitrogen™).

Cas9 protein: GeneArt™ TrueCut™ Cas9 Protein v2, 1µg/µl, (Invitrogen™).

Lipofectamine: Lipofectamine CRISPRMAX Transfection Kit (Invitrogen™) containing the following:

- Lipofectamine CRISPRMAX Transfection reagent.
- Lipofectamine™ Cas9 Plus™ reagent.

Serum-free media: Opti-MEM™ I Reduced serum media (Gibco™).

Full growth media: RPMI-1640 complete growth media (Lonza™).

Genomic cleavage detection (GCD): GeneArt™ Genomic Cleavage Detection Kit, containing the following:

- Cell lysis buffer, 1 ml.
- Protein degrader, 96 µl.

- AmpliTaq Gold™ 360 master mix, 1 ml.
- Water, 1 ml.
- Detection enzyme, 20 µl.
- 10× Detection reaction buffer, 40 µl.
- Control template and primers, 10 µl.

2.1.12 MTT proliferation assay

Tetrazolium reagent (Sigma™): (3-(4, 5-Dimethylthiazol-2-yl)-2, 5-diphenyltetrazolium bromide) (MTT) was dissolved to 5mg/ml stock concentration in sterile PBS and stored at 4 °C.

Cell counter: TC20™ automated cell counter (Biorad).

Dimethyl sulfoxide (DMSO): (Sigma™).

2.2 Methods

The laboratory work was done according to the health and safety measures. All Chemicals were used according to the Control of Substances Hazardous to Health (COSHH) guidelines.

2.2.1 DNA isolation and purification

2.2.1.1 Whole blood DNA isolation and purification

Patients' peripheral blood was collected into both purple ethylenediaminetetraacetic acid (EDTA) and light blue (sodium citrate) bottles provided by BD™ Vacutainer® to avoid blood clotting. Then, 200 μl of protease was added into a 15 ml centrifuge tube and 2 ml of whole blood were added to the same tube. After shaking and mixing several times, 2.4 ml of Buffer AL was added to the tube with another shaking and mixing step for the tube. The mixture was then incubated at 70 °C for 10 minutes. After incubation, 2 ml of absolute ethanol were added to the mixture with subsequent vigorous shaking and inverting. Following the addition of absolute ethanol, half of the mixture (around 3 ml) was transferred to a QIAamp® midi column (provided by the kit) and the tube were centrifuged at 1850×g for three minutes. The filtrate was then discarded. This prior step was repeated again with the remaining (around 3 ml) of the mixture, again with centrifuging at 1850×g for three minutes and discarding of the filtrate. 2 ml of Buffer AW1 was then added to the column and centrifuged at 3,500×g for one minute. 2 ml of Buffer AW2 was added to the column and centrifuged at 3,500×g for 15 minutes; the tube was discarded and a new 15 ml collection tube was used. The column was incubated at 70 °C for ten minutes to remove any ethanol residue. Finally, 300 μl of Buffer AE was added to the column, incubated for five minutes at room temperature and centrifuged at 3,500×g for two minutes; and this step was repeated again to gain a higher concentration of DNA.

2.2.1.2 DNA isolation and purification from frozen tumour tissue

Frozen tumour tissue that been stored at -80 °C was transferred into a 1.5 ml centrifuge tube and cut into small pieces using a sterile 32G needle (BD™). Then, 180 µl of Buffer ATL and 20 µl of proteinase K were added to the sliced tumour tissue; and the sample was incubated overnight at 56 °C to homogenise the solid tissue. After the incubation, 4 µl of RNase A was added to the sample which was vortexed for 15 seconds and incubated at room temperature for one minute. Afterwards, 200 µl of Buffer AL and 200 µl absolute ethanol were added to the sample and vortexed. The whole mixture was then transferred to a DNeasy® mini spin column (provided by the kit) and was centrifuged at 6,000×g for one minute. The column was then transferred to a new collection tube and 500 µl of Buffer AW1 was added to the column and centrifuged at 6,000×g for one minute; the flow-through was discarded. The column was transferred again to a new collection tube and 500 µl of Buffer AW2 was added to the column and centrifuged at 16,100×g for three minutes. The spin column was transferred after the centrifugation to a new-clean 1.5 ml collection tube and 200 µl of Buffer AE was added and incubated at room temperature for one minute. The sample was finally centrifuged at 6,000×g for one minute; the last step was repeated again in another new and clean 1.5 ml collection tube to have a higher quantity of DNA.

2.2.1.3 Genomic DNA quantification and purity assessment

The DNA extracted and purified from both the blood and frozen tumour samples was measured to establish its concentration in ng/µl using UV-VIS spectrophotometry NanoDrop® ND-1000 (Fisher Scientific™). The DNA absorbance at a wavelength of 260 nm was used to determine the amount of nucleic acid in the solution. The determination of DNA purity was measured using the ratio of absorbance 260/280 nm, which indicates any protein contamination at 280 nm while the ratio of absorbance 260/230nm indicates any contamination from other organic compounds such as phenol, EDTA and carbohydrates, which usually absorbed at a wavelength of 230 nm.

To operate the NanoDrop® ND-1000, the lens was first wiped with Kimwipes® and 2 μl of nuclease-free H_2O was added to initialise the instrument. A similar volume of Buffer AE was added to serve as a blank solution. After that, 2 μl of the DNA sample was applied into the cleaned lens and the concentration of DNA was recorded in ng/μl, as well as the absorbance at both 260/280 nm and 260/230 nm, where an acceptable range was considered to be between 1.8 and 2.

2.2.2 Sequencing analysis for GNAQ, GNA11, SF3B1, EIF1AX and TERTp

2.2.2.1 Standard PCR

Standard PCR was used to amplify a specific DNA fragment based on three main steps: denaturation, annealing and extension. Denaturation means the double strand DNA was separated at 95 °C; annealing allows the primers to bind to a specific location on the DNA; where the annealing temperature varies between 50 and 65 °C. The final step of PCR is primer extension when the *Taq* polymerase together with dNTPs copies the original strand. These three steps are repeated across 25 to 30 cycles so as to produce an exponential amount of the specific product. Table 2.3 specifies each component and the amount that was added to attain 23 μl of master mix. Then, 2 μl of DNA (25 ng/μl) was added to the sample in addition to a negative control to check for any contamination that may occur during the protocol. Afterwards, PCR reaction tubes were transferred to the thermocycler using either three-step PCR, touchdown PCR or modified touchdown PCR as set out in Tables 2.4, 2.5, 2.6, 2.7, 2.8, 2.9 and 2.10.

Table 2.3: PCR master mix for *GNAQ*, *GNA11*, *SF3B1*, *EIF1AX*, and *TERTp*.

***GNAQ* exons 4, 5 and *EIF1AX* exon 1**

Component		Per sample
Immunobuffer	10X	2.5µl
$MgCl_2$	50mM	0.75µl
dNTPs	50mM	0.5µl
Forward Primer	10pmol/µl	1µl
Reverse Primer	10pmol/µl	1µl
Immolase	250U	0.5µl
H_2O		16.75µl
Amount of DNA	50ng	2µl

***SF3B1* exon 14**

Component		Per sample
Immunobuffer	10X	2.5µl
$MgCl_2$	50mM	0.75µl
dNTPs	50mM	0.5µl
Forward Primer	10pmol/µl	1µl
Reverse Primer	10pmol/µl	1µl
Immolase	250U	0.5µl
H_2O		16.75µl
Amount of DNA	50ng	2µl

***GNA11* exon 4 and *EIF1AX* exon 2**

Component		Per sample
Immunobuffer	10X	2.5µl
$MgCl_2$	50 mM	0.375µl
dNTPs	50 mM	0.5µl
Forward Primer	10pmol/µl	1µl
Reverse Primer	10pmol/µl	1µl
Immolase	250U	0.5µl
H_2O		17.125µl
Amount of DNA	50ng	2µl

GNA11* exon 5 and *TERTp

Component		Per sample
Immunobuffer	10X	2.5µl
$MgCl_2$	50mM	0.25µl
dNTPs	50mM	0.5µl
Forward Primer	10pmol/µl	1µl
Reverse Primer	10pmol/µl	1µl
Immolase	250U	0.5µl
H_2O		17.25µl
Amount of DNA	50ng	2µl

Table 2.4: 3-step PCR conditions for *GNAQ* exon 4

Stage	Temperature	Time	Cycles	Comment
Activation	95 °C	10 min	1X	
Denature	95 °C	30 sec	30X	
Anneal	53 °C	30 sec		
Extension	72 °C	60 sec		
Hold	4 °C	∞		

Table 2.5: 3-step PCR conditions for *GNAQ* exon 5

Stage	Temperature	Time	Cycles	Comment
Activation	95 °C	10 min	1X	
Denature	95 °C	30 sec	30X	
Anneal	60 °C	30 sec		
Extension	72 °C	60 sec		
Hold	4 °C	∞		

Table 2.6: 3-Step PCR conditions for *SF3B1* exon 14 and *EIF1AX* exon 1.

Stage	Temperature	Time	Cycles	Comment
Activation	95 °C	10 min	1X	
Denature	95 °C	30 sec	30X	
Anneal	61 °C	30 sec		
Extension	72 °C	90 sec		
Final extension	72 °C	5 min	1X	
Hold	4 °C	∞		

Table 2.7: Touchdown PCR conditions for *EIF1AX* exon 2

Stage	Temperature	Time	Cycles	Comment
Activation	95 °C	10 min	1X	
Denature	95 °C	30 sec	10X	-1°C increment each cycle
Anneal	64 °C	30 sec		
Extension	72 °C	90 sec		
Denature	95 °C	30 sec	30X	
Anneal	60 °C	30 sec		
Extension	72 °C	90 sec		
Final extension	72 °C	5 min	1X	
Hold	4 °C	∞		

Table 2.8: Touchdown PCR conditions for *TERTp*.

Stage	Temperature	Time	Cycles	Comment
Activation	95 °C	10 min	1X	
Denature	95 °C	30 sec	10X	-1°C increment each cycle
Anneal	61 °C	30 sec		
Extension	72 °C	90 sec		
Denature	95 °C	30 sec	30X	
Anneal	56 °C	30 sec		
Extension	72 °C	90 sec		
Final extension	72 °C	5 min	1X	
Hold	4 °C	∞		

Table 2.9: Modified Touchdown PCR conditions for *GNA11* exon 4.

Stage	Temperature	Time	Cycles	Comment
Activation	95 °C	10 min	1X	
Denature	95 °C	30 sec	3X	
Anneal	64 °C	30 sec		
Extension	72 °C	60 sec		
Denature	95 °C	30 sec	3X	
Anneal	62 °C	30 sec		
Extension	72 °C	60 sec		
Denature	95 °C	30 sec	3X	
Anneal	59 °C	30 sec		
Extension	72 °C	60 sec		
Denature	95 °C	30 sec	30X	
Anneal	56 °C	30 sec		
Extension	72 °C	60 sec		
Hold	4 °C	∞		

Table 2.10: Modified Touchdown PCR for *GNA11* exon 5.

Stage	Temperature	Time	Cycles	Comment
Activation	95 °C	10 min	1X	
Denature	95 °C	30 sec	3X	
Anneal	62 °C	30 sec		
Extension	72 °C	60 sec		
Denature	95 °C	30 sec	3X	
Anneal	59 °C	30 sec		
Extension	72 °C	60 sec		
Denature	95 °C	30 sec	3X	
Anneal	56 °C	30 sec		
Extension	72 °C	60 sec		
Denature	95 °C	30 sec	30X	
Anneal	53 °C	30 sec		
Extension	72 °C	60 sec		
Hold	4 °C	∞		

2.2.2.2 Agarose gel electrophoresis

Agarose gel was prepared in 1.8% by dissolving 2.7 g of agarose into 150 ml of 1X TAE buffer in a flask. The mixture was then heated in a microwave at high power to have a clear solution without any residue of undissolved agarose. The solution was cooled to be warm and 10 µl of EtBr was added to the solution, which was then poured into the gel tray with a comb and left for around twenty minutes to solidify. After gel solidification, the rubber around the tray was

removed and the gel tray was put into a gel tank prefilled with 1X TAE buffer. Then, 5 μl of the sample was mixed with 1 μl of 6× loading dye and pipetted into the well. Also, 5 μl of 100 bp standard size marker was applied into the well to determine the actual size of the product. The power source was turn on at 120V for 40 minutes; and then the gel was visualised using a UV trans-illuminator gel documentation instrument (Biorad) and it was photographed.

2.2.2.3 DNA sequencing

DNA sequencing of the PCR products was achieved using the Sanger sequencing method. The aim of this procedure is to identify any insertion, deletion or substitution within the targeted gene. The DNA sequencing for all samples was carried out by the sequencing core facility at University of Sheffield, Medical School, UK. Briefly, the PCR product that was generated previously was added with one primer direction (forward or reverse) together with DNA polymerase and a fluorescent dideoxyribonucleotide triphosphate (ddNTPs) in a programmed thermocycler. The ddNTPs is similar to the dNTPs used for PCR except lacking the 3' hydroxyl group that allows the nucleotide synthesis to terminate for the next nucleotide binding. These ddNTPs were randomly incorporated with the PCR product on different sizes. Thus, unique nucleotide sequences of A, T, C, G were generated based on the size of each incorporated ddNTPs after running the sample in a capillary gel which was then detected by laser camera using API 3730xl (Applied Biosystems™).

2.2.2.4 Sequencing analysis

FinchTV sequence analysis software (Geospiza) was used to visualise the generated sequence data. The sequences were screened in comparison to reference sequences for *GNAQ*, *GNA11*, *SF3B1*, *EIF1AX* and *TERTp* in order to identify any mutations in those genes.

2.2.3 Genomic-wide analysis using array-CGH

2.2.3.1 Array-CGH concept

This recently developed molecular cytogenetic technique is used to study whole gDNA to detect copy number aberrations (CNAs). The gDNA isolated from tumour and blood samples of the same patient were labelled with two different fluorescent dyes, Cyanine-5 (Cy5) and Cyanine-3 (Cy3). The Agilent™ labelling system uses random priming with *exo*-klenow DNA polymerase (enzymatic method) to label the gDNA; and this method uses Human Cot-1 DNA (Invitrogen™) to block the binding of repetitive elements prior to hybridisation. The labelled gDNA was then hybridised to a customised microarray slide specifically designed for UM (4×180K probes) (Hammond et al., 2015), and focused on specific areas of the genome such as chromosomes 1, 3, 6, 8 and 11. For example, the probes in chromosome 6 had a spacing mean of 14.5 kb compared to the off-shelf array that had a mean probe spacing of 36.6 kb. This customised microarray slide helps to uncover regions of chromosomal gain and loss which may contain oncogenes and tumour suppressor genes. The array was then washed and scanned, whereby the differential intensity of the fluorescent dyes at each probe served as a surrogate for the ratio of copy numbers of the probe sequence in the tumour versus the reference genome, as shown in Figure 2.1 below. In the figure, the red spots specify a duplicate region in the genome of the patient's DNA whereas the green spots specify the missing regions in the patient's genome compared to the reference genome; consequently, chromosomal aberration is shown as amplification and deletion.

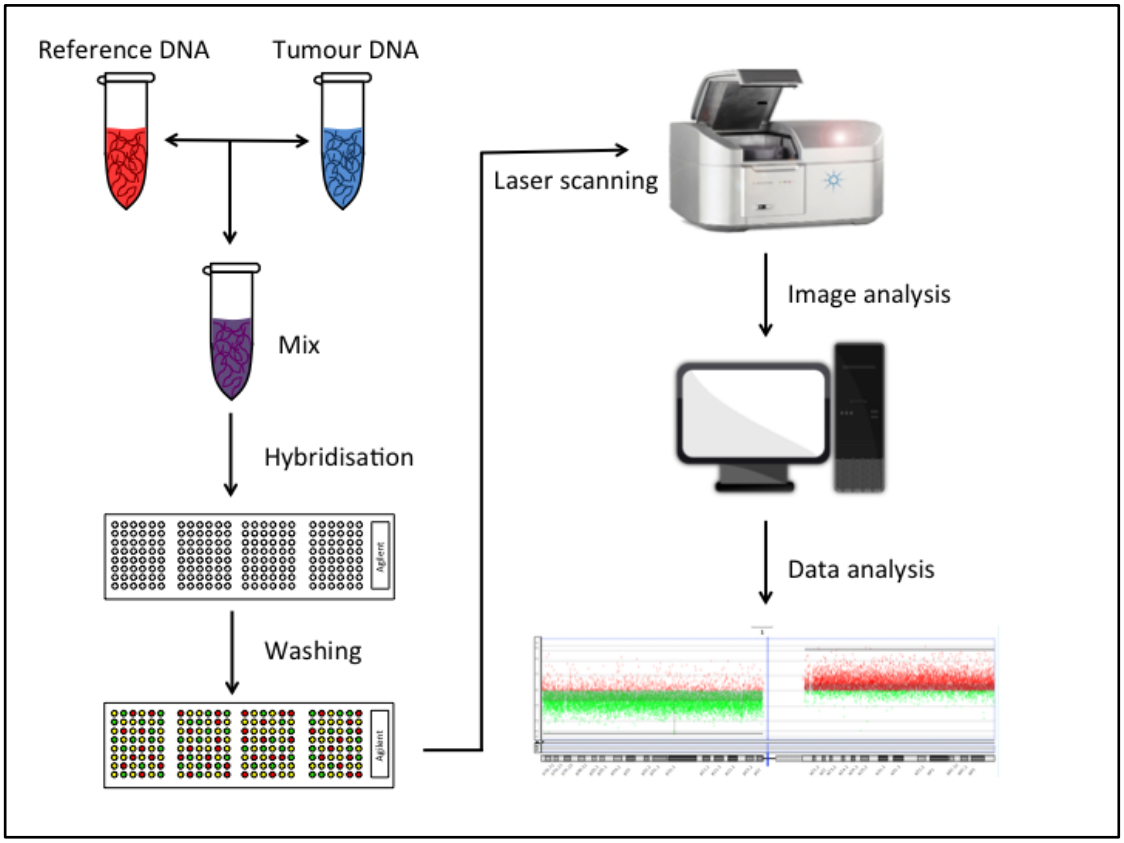

Figure 2.1: Flowchart of the array-CGH protocol.

The experiment starts by labelling and mixing Cy3-reference DNA with Cy5-tumour DNA and hybridising them on an Agilent™ slide. The slide then was incubated for 24 hours at 65 °C followed by washing steps. Directly, the slide was scanned so as to produces an image that will be analysed using the software. The image of the microarray laser scanner was adapted from www.biocompare.com.

2.2.3.2 Array-CGH protocol

DNA digestion

A gDNA input of between 0.5-1.0 μg for each sample was required and the DNA digestion for both patient and control samples was carried out by adding two restriction enzymes, Alu1 and Rsa1, to digest the DNA into smaller strands of random size; a digestion master mix was prepared for nine samples (four reference DNA and four tumour DNA with one dead volume), as shown in Table 2.11. Then, 5.8 μl of the digestion master mix was added to each tube containing 20.2 μl of gDNA to make a total volume of 26 μl. Tubes were transferred to a thermocycler with the heated lid programmed for incubation at 37 °C for two

hours, then turned up to 65 °C for 20 minutes. The samples were then held at 4 °C.

Table 2.11: Digestion master mix components.

Component	Per tube (μl)	For 9 tubes (μl)
Nuclease-free H_2O	2.0	18
10X buffer	2.6	23.4
Acetylated BSA (10 μg/μl)	0.2	1.8
Alu1 (10 μg/μl)	0.5	4.5
Rsa1 (10 μg/μl)	0.5	4.5
Total	5.8	52.2

DNA labelling and purification

The digested gDNA was then labelled by two fluorescent dyes using the Agilent® labelling kit; 5 μl of random primers were added to each reaction tube, the DNA was denatured and the primers were annealed at 95 °C for three minutes. A total of 19 μl of labelling master mix was made of the components illustrated in Table 2.12 with 3 μl of Cy3-dUTP (1.0 mM) being added to each control sample and a similar labelling master mix with 3 μl of Cy5-dUTP (1.0 mM) being added to each tumour sample with an extra tube for dead volume; reaction tubes were then transferred to thermocycler and incubated for two hours at 37 °C, then at 65 °C for ten minutes. The samples were then held at 4 °C.

The labelled gDNA was purified using Amicon® 30 kDA filters that trapped the labelled gDNA based on their size. Firstly, the samples were centrifuged at 6,000×g for one minute. Then, each sample was mixed by adding 430 μl of 1×

TE buffer and transferred to Amicon® 30 kDA filters that were placed in a 1.5 ml collection tube and centrifuged at 14,000×g for ten minutes. The flow-through was discarded and the wash repeated again by adding 480 µl 1× TE buffer to each sample and centrifuged at 14,000×g for ten minutes. The flow-through and collection tubes were discarded, and the filter was inverted into a fresh collection tube and centrifuged at 1,000×g for one minute. The final volume expected in the collection tube was around 21 µl of clean, labelled DNA.

Table 2.12: Components of labelling master mix.

Component	Per tube (µl)	For 5 tubes (µl)
5X buffer	10.0	50.0
10X dNTPs	5.0	25.0
Cy3-dUTP or Cy5-dUTP	3.0	15.0
***Exo-klenow* fragment**	1.0	5.0
Total	19.0	95.0

The total mixture volume of each sample was measured after purification, and the clean, labelled gDNA was used to quantifiy the concentrations of Cy3 at 550 m and Cy5 at 650 nm using NanoDrop® with 1× TE buffer as a blank. These values were used to determine the yield of gDNA and the dye specific activity of the labelled DNA. The calculation methods for these parameters are shown below, with a normal range for the DNA yield being between 8 and 11 µg, and the normal range for Cy3 and Cy5 specific activity varying between 20 and 35 pmol/µg, and 20 and 30 pmol/µg, respectively. Samples within the optimum range were then hybridised or stored at -20 °C in the dark.

$$\textbf{Dye specific Activity } (\textbf{pmol}/\mu\textbf{g}) = \frac{\textbf{dye concentration } (\textbf{pmol}/\mu\textbf{l})}{\textbf{DNA concentration } (\mu\textbf{g}/\mu\textbf{l})}$$

$$\textbf{DNA yield } (\mu\textbf{g}) = \textbf{DNA concentration}(\mu\textbf{g}/\mu\textbf{l}) \times \textbf{volume}(\mu\textbf{l})$$

Microarray hybridisation and assembly

The optimum range of labelled gDNA for both the tumour and the reference were mixed together by taking 19.5 μl of each of them and mixing in a 0.5 ml microfuge tube. The hybridisation master mix was prepared as shown in Table 2.13; and 71 μl of this master mix was added to each sample with an extra tube for dead volume. Then, the reaction tube was transferred to the thermocycler at 95 °C for three minutes, and 37 °C for thirty minutes. The samples were then immediately centrifuged at 16,100×g for one minute to pull the mixture down. Finally, 100 μl of the mixture was added to a gasket slide and sandwiched with the active side of the Agilent™ SurePrint® G3 human microarray slide 4×180K and placed into a clamped chamber; the assembled slide chamber was placed into the rotator rack in the hybridisation oven set at 65 °C and 20 rpm for 24 hours.

Table 2.13: Components of the hybridisation master mix.

Component	Per tube (μl)	For 5 tubes (μl)
Human Cot-1 DNA	5.0	25.0
10× Blocking agent	11.0	55.0
2× Hi-RPM buffer	55.0	275.0
Total	71.0	355.0

Microarray washing and scanning

Oligo array-CGH Wash Buffer 2 with a slide-staining dish 3 was pre-warmed at 37 °C overnight for optimal performance. A slide-staining dish 1 with an Oligo array-CGH wash buffer 1 was used to detach the array-gasket sandwich so as to obtain the array slide after being removed from the hybridisation oven. After that, the slide rack was placed into the slide dish with washing buffer 1 for five minutes at room temperature, and then into wash buffer 2 (37 °C) for one minute, the slide rack was removed slowly in order to minimise the number of droplets left on the slides. The microarray slide was then scanned directly using an Agilent™ DNA Microarray scanner with Sure-scan® high-resolution technology. The scanned images were saved in a *.tiff format to evaluate any microarray damage or hybridisation artefacts.

Array quality assessment

The scanned images were analysed with Agilent™ feature extraction (FE) software (version 11.0.1.1). The software normalises the intensity of both fluorescents (red and green) and calculates the ratio for each probe. It expresses the probe intensity on a logarithmic scale (log ratio), which is then exported as a *.txt file. Then, the FE software produces an image processing quality control (QC) report that assess the reliability and reproducibility of the experiment, including the background noise (BGNoise), signal to noise ratio (SNR) of the array and the derivative log ratio spread (DLRS) (Table 2.14). The DLRS is the standard deviation of the log ratio difference between consecutive probes, where this algorithm estimates the noise from the array only. This ratio is necessary if amplification or deletion is to be detected reliably.

Table 2.14: Quality control metric to assess the array performance.

Background noise (BGNoise)	This metric is calculated as the standard deviation of the signals on the negative control probes after rejecting the outlier features.	Excellent: <5 Good: 5-10 Evaluate: >10
Signal to noise ratio (SNR)	This metric calculates the ratio signal to noise ratio by dividing the signal intensity by BGNoise. It is used to distinguish the real signal from the signals obtained due to the experimental variation,	Excellent: >100 Good: 30-100 Evaluate: <30
Derivative Log ratio spread (DLRSD)	This metric calculates the standard deviation of the log ratio differences between consecutive probes, so as to smooth the data and estimate the measure of the noise of an array.	Excellent: <0.2 Good: 0.2-0.3 Evaluate: >0.3

Microarray analysis using Agilent Genomic Workbench

Agilent Genomic Workbench (Version 7.0.4.0) analysis software with an array-CGH licence obtained from http://www.genomics.agilent.com was used to analyse, visualise and detect any chromosomal aberration from the microarray profiles. The Agilent Genomic Workbench software requires a design file matched to the feature extraction files; thus, Agilent GEML-based (*.xml) array design files were imported prior to any FE data. The Agilent Feature Extraction (*.txt) data files from each experiment were imported into the software and a new experiment was created for the FE files. A centralisation algorithm was applied to centre the log ratio after applying preselected filters. Afterwards, the data were analysed by applying the Aberration Detection Method-2 (ADM-2) algorithm, which incorporates quality information for each log ratio value, with the threshold adjusted to 6.0, as recommended by the manufacture. In addition, fuzzy zero was used with ADM-2 to identify extended aberrant segments with a low mean ratio. The genomic viewer was used to display the data alongside chromosome ideograms.

2.2.4 Tissue culture

The procedure was carried out under the class II biological hood. Cells were sub-cultured when they reached 80-90% confluence by checking the flask under the inverted microscope (4× magnification) prior to the sub-culture for any noted changes. Afterwards, culture media was carefully removed, and cells were washed twice with DPBS. Trypsin-EDTA was added (2 ml for T25 and 4 ml for T75) and cells were incubated for 1-3 minutes in a humidified incubator at 37 °C and 5% CO_2. Then, cells were monitored under an inverted microscope until the cells detached. The trypsinisation was then stopped by adding an equivalent volume of fresh culture media. The cell suspension was mixed up and down several times to recover any residual cells. Afterwards, the cell suspension was transferred into a 15 ml conical tube and spun down at 1,000×g for five minutes at room temperature and the supernatant was discarded. Cells were then resuspended in a fresh culture media and were split into an appropriate number of flasks. The new flasks were then incubated in the humidified incubator at 37 °C and 5% CO_2.

2.2.5 Immunochemistry

Cultured cells fixed on glass slides were used for Immunocytochemistry (ICC) while FFPE sections (0.45 μm thickness) were used for immunohistochemistry (IHC) experiments. These experiments were done at the histopathology core facility laboratory at The University of Sheffield Medical School with help of (lead technician Mrs. Maggie Glover).

This experiment used a modified Avidin-Biotin-Peroxidase complex (ABC) method, as described by Hsu et al. (1981). A melanin removal step was also used, because the UM tissue sections were highly melanotic. This step was adapted from Sheffield Teaching Hospital, UK.

To summarise the experiment, tissue sections were processed to remove the melanin because UM sections were highly melanotic. This served to expose the relevant antigen and to block any non-specific antibody binding by incubating these sections in 10% species-specific relevant normal serum. The tissue

sections were then incubated overnight with the specific primary antibody at its optimum dilution. The next day, these tissue sections were washed and a relevant biotinylated secondary antibody was added, which binds to the F_C portion of any bound primary antibody. Then, a colorimetric reaction was used in forms of complexes of avidin molecules linked to an enzyme reporter system and bound to the secondary antibody.

Negative control tissues were incubated in the absence of the primary antibody; however, both positive control tissues and test tissue samples were incubated with primary antibody diluted in blocking serum, and these controls were included in every run.

2.2.5.1 Antibody optimisation

All antibodies used in this study were optimised prior to staining. The manufacturer's recommended conditions were used as a guide, with a range of antibody dilutions. In this study, three independent observers (Mohammed Alfawaz (MA), Ahmad Alshammari (AA) and Dr. Karen Sisley (KS)) assessed the specific antibody staining with minimal non-specific background staining, and identified the optimal antibody conditions, as summarised earlier in Table 2.2.

2.2.5.2 Formalin fixed paraffin-embedded (FFPE) tissue preparation

The FFPE tissues were cut into pieces 0.45 μm thick and were collected onto positively charged slides that had been dried in an oven overnight at 37 °C. The tissue cutting and preparation was conducted by Mrs. Maggie Glover.

Prior to staining, tissue sections were dewaxed by placing them into two consecutive xylenes for ten minutes and five minutes, respectively. They were then hydrated in a graded series of EtOH (100% EtOH for five minutes, 100% EtOH for five minutes, and 95% EtOH for three minutes). The endogenous peroxidase was then blocked by placing the tissue sections in a freshly prepared 3% H_2O_2/methanol for thirty minutes at room temperature, which then subsequently washed for five minutes under running tap water.

2.2.5.3 Melanin bleaching

The melanin removal or bleaching was done by preparing 1.5% of H_2O_2/PBS into a staining dish and the tissue sections were incubated in the dark overnight at room temperature. The next day, the tissue sections were washed for five minutes under running tap water.

2.2.5.4 Antigen retrieval treatment for IHC

Antigen retrieval treatment was an essential step for the preparation of FFPE tissue sections for staining. It was carried out by immersing the tissue sections in target retrieval solution, so as to detach the protein cross-links cluster formed from formalin particles on the tissues' antigen binding sites. The complexity of this cluster increased in the tissue with longer formalin embedding time; therefore, inadequate antigen retrieval treatment risks leaving some clusters that may shield the antigen binding site from antibody attachment. Many antigen retrieval methods are available in the laboratory. The method applied in this study started by immersing the tissue sections in a pressure cooker in 0.01M DAKO (PH 6.0) for twenty minutes. Then, the tissue sections were allowed to cool down in the same buffer for approximately two hours. This was followed by rinsing with PBST and washing twice for five minutes, before the remaining staining steps were completed.

2.2.5.5 Slide preparation of ICC

For the ICC, glass slides were cleaned by immersion in absolute methanol for at least 24 hours at room temperature; left to dry under a laminar flow hood for at least ten minutes and arranged in a single layer in a sterile petri dish (145/20 mm). Cells were trypsinised and dissociated from the flask as described in Section 2.2.4, and then suspended in fresh media and counted (12,000 cells per 0.5 ml). After counting, cells were seeded onto a glass slide that been put onto the petri dish lengthways to ensure even distribution. The petri dish was carefully placed in the humidifier incubator at 37 °C and 5% CO_2 for three hours to allow the cells to adhere to the slide. Then, 30 ml of prewarmed fresh media was added to the petri dish and incubated at 37 °C and 5% CO_2 for 48 hours. The slides were then

washed four times with PBS and slides were immersed and fixed by incubation on 1:1 ice-cold methanol/acetone for ten minutes. The slides were left to dry under the laminar flow hood for ten minutes before use or stored at -20 °C until needed. The cells on slides were then treated similar to tissue sections for blocking, antibody incubation, counter staining and mounting.

2.2.5.6 Blocking and primary antibody incubation for immunochemistry

An ImmEdge™ hydrophobic Barrier Pen was used to outline the relevant area of tissue sections. Afterwards, a blocking step was conducted using an avidin/biotin blocking kit. Solution A from the kit was applied to the tissue sections and incubated for fifteen minutes at room temperature. This was then washed by PBST and then the solution B from the blocking kit was applied to the tissue sections, which were again washed subsequently by PBST. In addition, another blocking step was done by applying 10% of appropriate blocking serum (normal goat serum and casein) before incubation at room temperature for thirty minutes. These blocking steps were done to eliminate any non-specific binding substances present in the tissue sections. After incubation for thirty minutes with 10% blocking serum, it was removed by tapping the slide only. Next, the primary antibody was diluted in 2% blocking serum and applied to the positive control and the tissue sections. In addition, 2% blocking serum (without antibody) was applied to the negative control. These slides were subsequently incubated overnight at 4 °C.

2.2.5.7 Secondary antibody incubation and immunoreactivity

The next day, the tissue sections were rinsed and washed twice in PBST for five minutes each, and the appropriate Secondary Antibody (goat anti-rabbit, Biotinylated IgG), diluted in 2% blocking serum, was applied on all tissue sections and incubated at room temperature for one hour. During the secondary antibody incubation, ABC reagent was prepared and allowed to stand at room temperature for thirty minutes. The tissue sections were then rinsed and washed twice with PBST for five minutes each, and the ABC reagent was applied and incubated at room temperature for thirty minutes. This was followed by rinsing and washing

twice with PBST for five minutes each. During the last wash, the peroxidase enzyme substrate (DAB) was freshly prepared, and this was then applied on the tissue sections after the last wash and incubated at room temperature for up to ten minutes so as to allow the stain to develop until the desired brown stain intensity was reached. At this point, the reaction was stopped by washing the stained tissue sections with deionised H_2O.

2.2.5.8 Counterstaining and mounting

The tissue sections were washed under running tap water for five minutes, and these sections were counterstained in Gill's haematoxylin for 60 seconds and washed again under running tap water for five minutes. The stained tissue sections were then dehydrated with graded series of EtOH (70%, 90%, 95%, 100% and 100%) for three minutes each. Afterwards, the stained sections were cleared two consecutive incubations in xylene for three minutes each, under a fume hood. Finally, while the stained sections were wet with xylene, they were mounted with DPX and covered with 22 mm × 32 mm coverslips, and then allowed to dry overnight at room temperature. The ICC was analysed using a light microscope at 40× magnification, while the tissue slides were examined using an automated slide scanner (3DHISTECH, Panoramic 250 Flash III).

2.2.6 Western blot

2.2.6.1 Protein extraction

To get a cell lysate, cells were grown in a T75 flask until they reached a confluence of 80-90% and being checked under the inverted microscope (4× magnification) prior to the extraction for any noted changes. This procedure was carried out under a class II biological hood. The media in the T75 flask was carefully removed and discarded and cells were washed twice with 4 ml of DPBS. 4 ml of Trypsin-EDTA was added to the flask and incubated in a humidified incubator at 37 °C and 5% CO_2 for 1-3 minutes in order to detach the cells from the surface of the flask. The cells were checked under 4× magnification to check whether any cells remained adherent to the flask's wall. The trypsinisation was stopped by adding an equivalent amount of fresh culture media. The cell

suspension was mixed up and down several times to recover any residual cells. Afterwards, the cell suspension was transferred into a 15 ml conical tube and spun down at 1000×g for five minutes at room temperature and the supernatant was discarded. Next, 5 ml of ice-cold DPBS was added to the cells and mixed up and down several times to wash them before being centrifuged at 1,000×g for five minutes at 4 °C. This step was repeated twice. After the supernatant was discarded, 100 µl of (RIPA) lysis buffer and 1 µl of protease and phosphatase inhibitor was freshly prepared (1% final concentration v/v) and were added to the cell pellet. The cells were then transferred to a 1.5 ml micro-centrifuge tube and incubated on ice for thirty minutes, the tube was vortexed every ten minutes. The cells were passed through a 20G needle up and down ten times. Then, the extract was centrifuged at 16,000×g for twenty minutes at 4 °C and the supernatant was transferred and aliquoted to a new 1.5 ml micro-centrifuges and stored at -80 °C.

2.2.6.2 Protein quantification

To measure the protein concentration, the stock protein standards were prepared by measuring 1 mg of BSA and dissolving it into 1 ml of deionised water. The dye reagent was prepared by diluting 1:4 with deionised water and the mixture was filtered using Whatman® grade 1 filter paper. 200 µl of the filtered dye reagent was applied into the 96-well plate. Then, six protein standards were prepared in serial dilutions (1 mg/ml, 0.5 mg/ml, 0.25 mg/ml, 0.125 mg/ml, 0.0625 mg/ml and 0.0312 mg/ml). The cell lysate was aliquoted and diluted 1:50 and 1:100 to have an accurate reading. Afterwards, 10 µl of each standard and the test sample were added to the filtered dye reagent in triplicate, after vortexing each sample. All wells were mixed up and down several times and incubated at room temperature for between five minutes to one hour. The absorbance was measured using the spectrophotometer at 595 nm. The background absorbance was eliminated to calculate the actual protein concentration by subtracting the control well absorbance, which has only 200 µl of filtered dye reagent, from each test well absorbance. The results of the absorbances reading were then plotted using GraphPad Prism 8 (GraphPad Software, Inc.) to produce a standard curve and to calculate the protein concentration of the cell lysate (Figure 2.2).

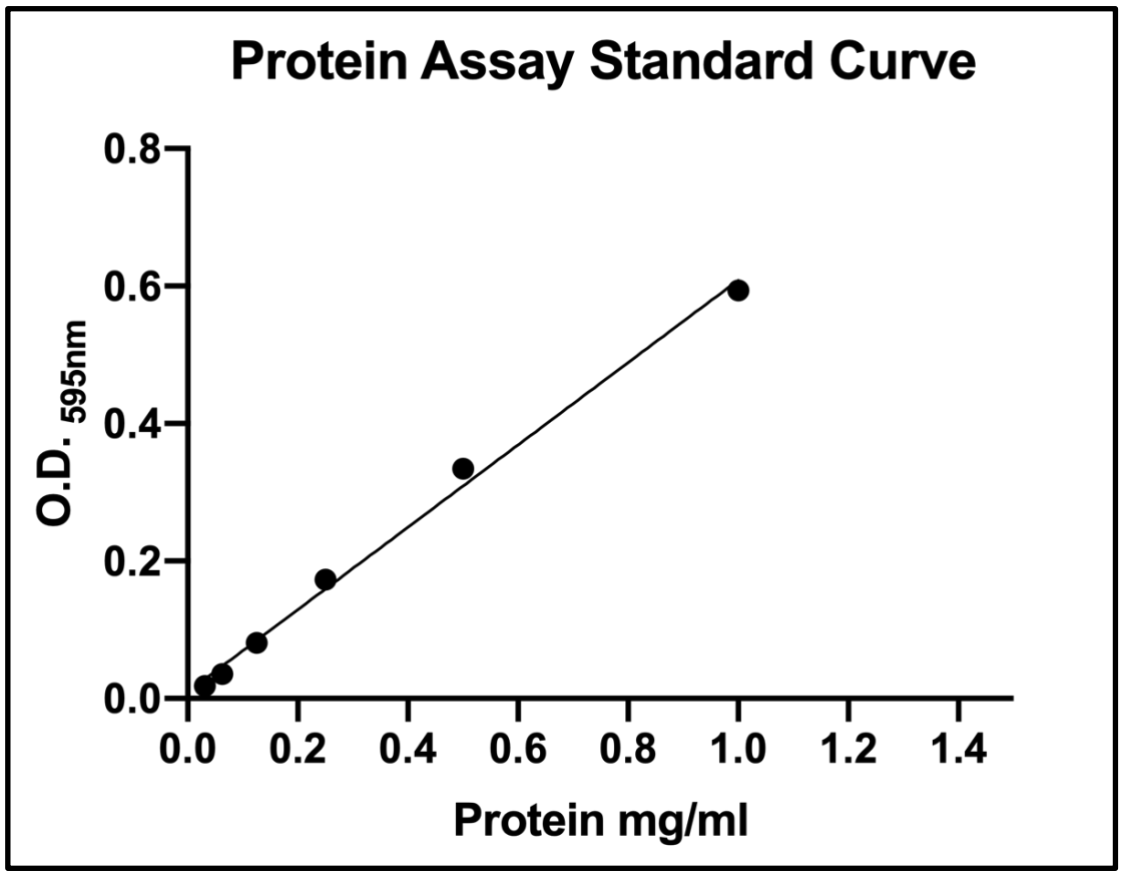

Figure 2.2: The standard curve for the Biorad protein assay.

This shows the protein standard plotted against the O.D.595 nm with R^2: 0.9909.

2.2.6.3 Sodium dodecyl sulphate-polyacrylamide gel electrophoresis (SDS-PAGE)

After the determination of the protein concentration, the protein extracts were diluted with RIPA buffer to reach 30 µg of protein in a new 1.5 ml micro-centrifuge tube. Then, 10 µl of 4× sample loading buffer and 4 µl of 10× reducing agent were added to the micro-centrifuge tube and the volume was made up to 40 µl using RIPA buffer. The samples were then heated at 95 °C for five minutes and put on ice to cool down. Samples were loaded together with the protein marker standard onto the precast gel that the tank been filled with 1× running buffer (100 ml of 10× running buffer with 900 ml of H_2O) and run at 80 V for thirty minutes for the stacking gel and the voltage was increased to 120 V for the separation gel till the end.

2.2.6.4 Protein blotting and visualisation

When the SDS-PAGE run finished, the precast gel was disassembled and blotted onto the ethanol-activated PVDF membrane using two types of transfer system: semi-dry and wet transfer. The semi-dry transfer was done by making a sandwich that consisted of, from cathode to anode: filter papers merged into the transfer buffer, the SDS-PAGE gel, the PVDF membrane and more filter papers (Figure 2.3 A). Then, the sandwich was placed onto the Transblot® turbo™ transfer system and run for seven minutes at 25 V. Wet transfer, meanwhile, entailed making a sandwich that consisted of, from anode to cathode: sponge, filter papers, PVDF membrane, SDS-PAGE gel, filter papers and sponge (Figure 2.3 B). After the sandwich had been assembled and no bubbles were present, the tank was filled with cold transfer buffer and with an ice pack, to keep the transfer cold. Then, the wet transfer system was run at 180 mA for ninety minutes.

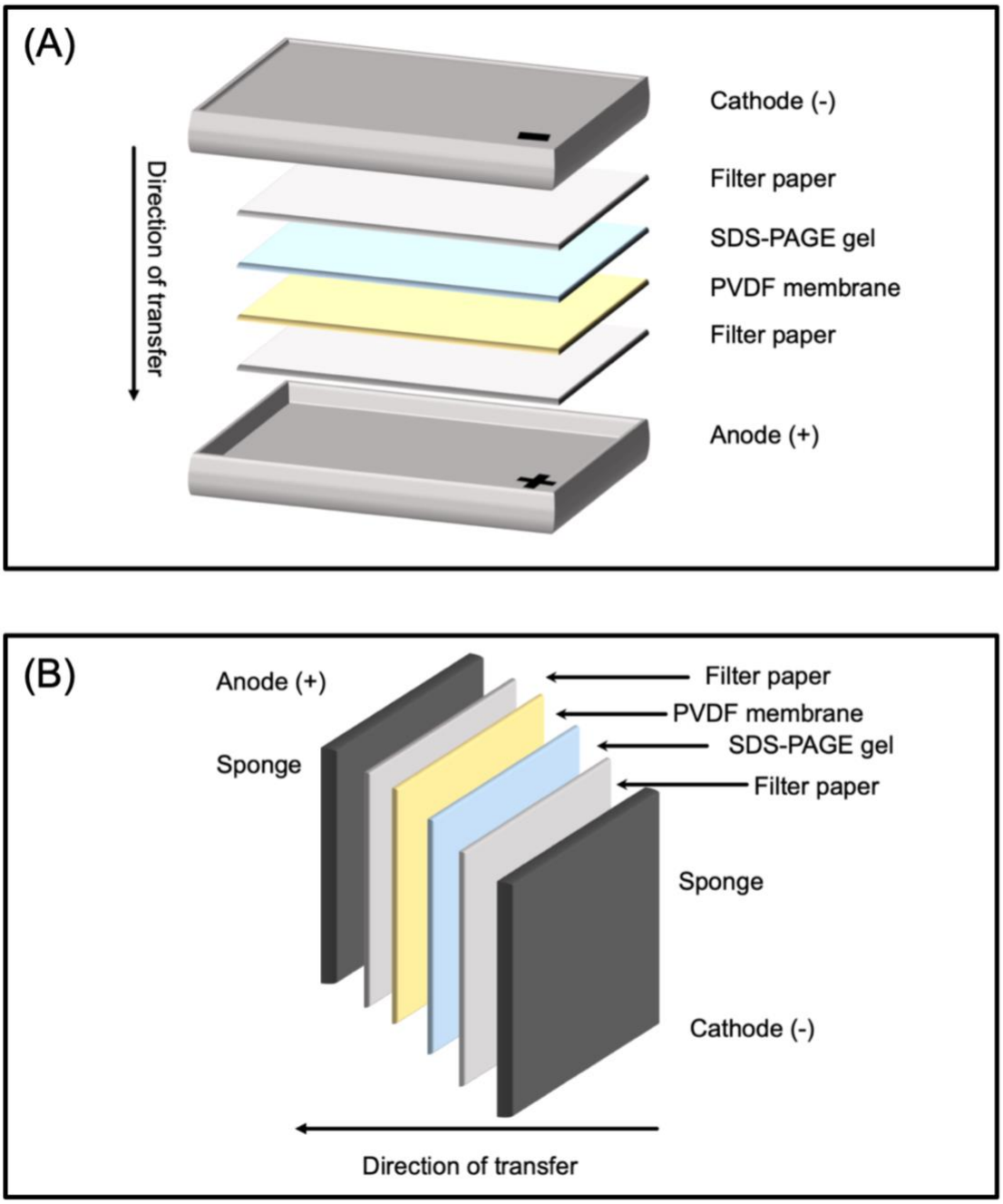

Figure 2.3: The transfer methods for protein from SDS-PAGE gel to PVDF membrane.

(A) the semi-dry transfer method showing the assembly of filter papers, SDS-PAGE gel and PVDF membrane from cathode to anode; **(B)** the wet transfer method, showing the assembly of sponge, filter papers, SDS-PAGE gel, PVDF membrane, filter papers and sponge from cathode to anode for the protein transfer. The direction of transfer is the same for both systems, i.e. from cathode to anode.

The membrane was washed twice with H_2O and blocked with blocking reagent (5% non-fat dry milk in PBST or TBST) for one hour. Afterwards, the primary antibody (AMD1) was diluted 1:300 in blocking reagent and added to the membrane and incubated overnight at 4 °C. The next day, the membrane was washed using PBST or TBST three times for five minutes each. Then, the HRP-conjugated secondary antibody was diluted 1:2000 using the blocking reagent and added to the membrane and incubated for one hour at room temperature. The membrane was washed three times for five minutes each using PBST or TBST. All incubations and washings were carried out on an orbital shaker. For the detection of protein bands, Amersham™ ECL detection reagent was used on the membrane according to the manufacturer's instructions. The membrane imaging was done using the ChemiDoc™ MP imaging system to visualise the detected bands.

To incubate the same membrane with the housekeeping antibody (Beta-tubulin), the membrane was washed three times with PBST or TBST for ten minutes each and the membrane was incubated with stripping buffer for fifteen minutes followed by another three times washing for thirty minutes. Then, the membrane was blocked using the blocking reagent, as mentioned above. The housekeeping antibody was diluted 1:5000 using the blocking reagent and added to the membrane and incubated overnight at 4 °C. The membrane was treated again the next day similar to the procedure described above.

2.2.7 AMD1 knockout using CRISPR

2.2.7.1 CRISPR overview

Clustered Regularly Interspaced Short Palindromic Repeats (CRISPR) is a new technology that allows human DNA to be edited, creating stable deletions, insertions and modifications. Basically, the CRISPR technology consists of two main components: single guide RNA (sgRNA) and CRIPSR associated endonuclease protein (Cas9), which together form a ribonucleoprotein (RNP) complex.

SgRNA consists of two segments CRISPR RNA (crRNA) and transactivating CRISPR RNA (tracrRNA) (Jinek et al., 2012). The crRNA contains a specific sequence of twenty nucleotides that complements the targeted DNA and preceded by three nucleotides (5'NGG'3 sequence) called protospacer adjacent motif (PAM) sequence (Sternberg et al., 2014). The PAM sequence is a short nucleotide sequence that is important to be present in the targeted DNA to allow the Cas9 to bind at the specific DNA site. In addition, the tracrRNA activates and guide the Cas9 protein to bind with the foreign DNA. Thus, the sgRNA basically bind to its target site and the Cas9 nuclease specifically cleaves the targeted DNA about three nucleotides after the PAM sequence.

2.2.7.2 Design the sgRNA

The sgRNA was designed using ThermoFisher™ software and was confirmed using the Synthego™ website (http://www.synthego.com) for any mismatches (Figure 2.4). The target has a minimal target-mismatch and is located in a common exon with high activity, based on Doneach et al.'s (2016) scoring system.

In addition, the forward primer 5'ACAGTATGGCCGGCGACATT'3 and reverse 5'GGAGAGCGGCCATGTCCA'3 were designed using ThermoFisher™ software around the area of knockout area to detect the efficiency of the transfection using GCD assay and sequencing analysis (Figure 2.5).

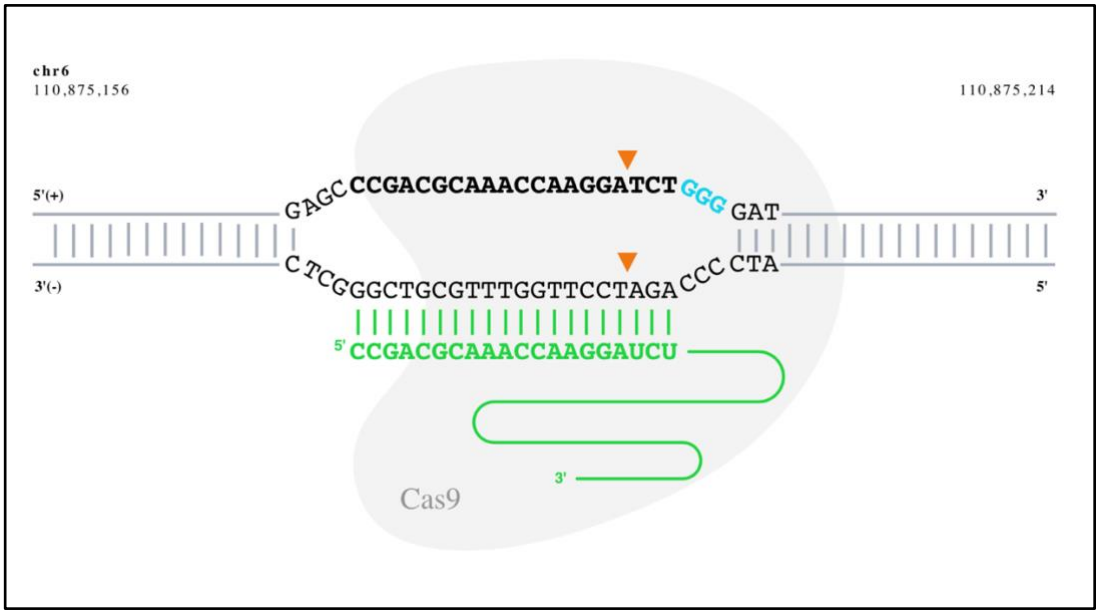

Figure 2.4: The area where gRNA binds and Cas9 will cut.

The light blue (GGG) is PAM sequence and the green is the designed gRNA together with trcrRNA. The orange arrow indicates where the site of cut that will happen. Image was adapted from www.synthego.com.

>chromosome:GRCh38:6:110874170:110896313:1

GTGGGACGATGCGTCACTTCCTGGTCTTTTGGGGGGAGCCGGGATATATAAGGGCGGTGC
TCACGCAGCGCTCTCGCTTACACAGTATGGCCGGCGACATTAGCTAGCGCTCGCTCTACT
CTCTCTAACGGGAAAGCAGCGGAATACAAGAGACTGAACTGTATCTGCCTCTATTTCCAA
AAGACTCACGTTCAACTTTCGCTCACACAAAGCCGGGAAAATTTTATTAGTCCTTTTTTT
AAAAAAAGTTAATATAAAATTATAGCAAAAAAAAAAAGGAACCTGAACTTTAGTAACACA
GCTGGAACAATCCGCAGCGGCGGCGGCAGCGGCGGGAGAAGAGGTTTAATTTAGTTGATT
TTCTGTGGTTGTTGGTTGTTCGCTAGTCTCACGGTGATGGAAGCTGCACATTTTTTCGAA
GGGACCGAGAAGCTGCTGGAGGTTTGGTTCTCCCGGCAGCAGCCCGACGCAAACCAAGGA
TCTGGGGATCTTCGCACTATCCCAAGGTGGGTCCCCGGGGCGCTCGCTGACATCCGGGCC
TGGGGGCTGTCGCCGCCGCCGAGGCACCAGCCACGGGTGGAGCCCGAGTTCCCTCAGCTT
TCAGTTGGGGGCAAGTCTGCGGCCTGGGGTCGCTTCGGCGGCCTTGGAAGGTGCGCGGTT
TGGGGGAGAGCGGCCATGTCCACGCGGGCCGGAGCCGGCTTCTCCCGCCGTGGTTGCCGC

Figure 2.5: The FASTA file for AMD1 exon 1.

The figure shows the gRNA (green) with PAM sequence (GGG) (pink) and the forward and reverse primers (red) around the area of knock-out (600 bp).

2.2.7.3 Lipid-based transfection of synthetic gRNA and Cas9 nuclease

UM cells were seeded, the day before transfection, into a 24-well plate at 90,000 cells per 0.5 ml of RPMI-1640 media and the plate was incubated in a humidified incubator at 37 °C and 5% CO_2. The next day, cells were checked under an inverted microscope (4× magnification) to ensure cell adherence. Then, the lipid complexing was prepared for transfection together with the negative control, as shown in Table 2.15. It is important to note that the Cas9 plus reagent was added last. These components were mixed by vortexing and then incubated on ice. In another sterile tube, 7.5 µl of lipofectamine CRISPRMAX transfection reagent was diluted onto 125 µl of Opti-MEM™I Reduced serum media and then mixed and incubated at room temperature for one minute.

Table 2.15: gRNA complex with Cas9 in Opti-MEM I media.

Volumes are for 2 reactions	Tube 1 Cas9 + AMD1 gRNA	Tube 2 Reagent only Control
Opti-MEM™I Reduced serum media	50 µl	50 µl
TrueCut™ Cas9 Protein	2.5 µl (2.5 µg)	-
gRNA	2 µl (480 ng)	-
Cas9 Plus Reagent	5.0 µl	5.0 µl

Afterwards, 50 µl of the diluted CRISPRMAX reagent was added to both tubes and mixed up and down without any vortexing and incubated at room temperature for fifteen minutes to allow the CRISPR/lipid complexes to form. Finally, 50 µl of the complex was added to each well of the plate in duplicate. The

plate was then incubated in a humidified incubator 37 °C and 5% CO_2 for 48 hours.

2.2.7.4 Genomic cleavage detection (GCD) assay

Cell harvesting and lysis

The cells that had been transfected with CRISPR were harvested after 48 hours. The plate was examined under an inverted microscope to note any changes. Then, the media was aspirated and 100 µl of Trypsin-EDTA was added to each well. The plate was incubated in the humidified incubator at 37 °C and 5% CO_2 for three minutes and the cells were checked under the inverted microscope to confirm that all cells were detached. Immediately, 500 µl of RPMI-1640 media was added to each well to stop the trypsinisation reaction, and the cells were transferred to a new 1.5 ml micro-centrifuge tube. The tubes were centrifuged at 1,000Xg for ten minutes and the supernatant was discarded. Next, 50 µl of lysis buffer and 2 µl of protein degrader were mixed by vortexing and added to each tube, the suspension was transferred to a new 0.2 ml PCR and these steps were performed for all wells. The PCR tubes were then placed onto the thermocycler for cell lysis, as described in Table 2.16.

Table 2.16: Thermocycler condition for cell lysis.

Temperature	Time
68 °C	15 min
95 °C	10 min
4 °C	∞ (Hold)

PCR amplification

The samples were vortexed briefly after the lysis, and the PCR reaction was prepared as described in Table 2.17. Then, the tubes were mixed and spun down using a mini-centrifuge after adding all components; and the tubes were placed onto a thermocycler for PCR amplification, as shown in Table 2.18. The PCR products were then examined on 1.8% agarose gel at 120 V for 45 minutes, as previously described in Section 2.2.2.

Table 2.17: components for CRISPR PCR amplification.

	Samples		
Component	**GCD Kit positive control**	**Cells negative control**	**Lipid gRNA1**
Cell Lysate	-	2 µl	2 µl
Target specific 10µM F and R GCD primers	1 µl (Kit primers + template)	1 µl (use gRNA1)	1 µl
AmpliTaq Gold 360 master mix	25 µl	25 µl	25 µl
Water	24 µl	22 µl	22 µl
Total	**50 µl**	**50 µl**	**50 µl**

Table 2.18: Thermocycler conditions for CRISPR PCR amplification.

Stage	Temperature	Time	Cycles	Comment
Activation	95 °C	10 min	1 X	
Denature	95 °C	30 sec	10 X	-1°C increment each cycle
Anneal	61 °C	30 sec		
Extension	72 °C	30 sec		
Denature	95 °C	30 sec	30 X	
Anneal	58 °C	30 sec		
Extension	72 °C	30 sec		
Final extension	72 °C	5 min	1 X	
Hold	4 °C	∞	1 X	

Mismatch digestion

The mismatch digestion was bone by denaturing and randomly re-annealing the PCR fragments so that some strands for edited samples would anneal with wild-type strands to form a heterogenous DNA duplex. Accordingly, 2 µl of the PCR product was added together with 1 µl of 10X detection reaction buffer and the volume was made up to 10 µl by nuclease-free H_2O in new 0.2 ml PCR tubes. The solution was mixed and spun-down using a mini-centrifuge; and the tubes were added onto the thermocycle (Table 2.19). After the program was completed, 1 µl of detection enzyme was added to all transfected samples and placed onto the thermocycler at 37 °C for one hour. Finally, the samples were examined again using 1.8% agarose gel, as previously described in Section 2.2.2, so as to detect the digestion site and determine the knock-out efficiency using Image Lab software (Version 6.0.1) (Biorad).

Table 2.19: Thermocycler condition for mismatch digestion.

Stage	Temperature	Time	Ramp rate °C temp/time
1	95 °C	5 min	3 °C
2	85 °C	0 sec	2 °C
3	25 °C	0 sec	0.1 °C/1 second
4	4 °C	∞	3 °C

2.2.8 MTT proliferation assay

This experiment was kindly done by Mr. Ahamd Alshammari, a fellow PhD student in the RTRG group, as he was very experienced with the methodology and time limitations were restrictive. This procedure done to find any differences in proliferation between the normal cell lines and the knocked-out cell lines. Cells were therefore dissociated with trypsin, as described in Section 2.2.4. Cells were counted by adding an equivalent volume of cell suspension to trypan blue which was then applied to the cell counter to count the live compared to dead cell. Then, cells were seeded at a density of 2000 cells in 100 µl of culture media to each well of a 96-well plate and incubated in a humidified incubator at 37 °C and 5% CO_2. Control wells contained only the media without cells being added. Four plates were set up to measure the cells' growth over four days at 24-hour intervals.

At each time point, 10 µl of MTT solution (5 mg/ml dissolved in PBS) was added to each well, including the controls, and the plate was returned to the humidified incubator at 37 °C and 5% CO_2 for three hours. Media were then removed and replaced with 100 µl DMSO and incubated again for thirty minutes. A Multiskan™ spectrophotometer reader was used to measure the optical density at 570 nm. The background absorbance was eliminated to estimate the MTT activity by subtracting the control well absorbance from each test well absorbance. The MTT activity was then plotted against the time points and standard error of the mean (SEM) was calculated using GraphPad® Prism software (Version 8). Using the software, the exponential growth equation was used to calculate the doubling time and indicative of the proliferation rate.

Chapter 3: Correlation of chromosome 6 aberrations with other genetic alterations

3.1 Introduction

UMs are considered relatively free of high genetic instability unlike other solid tumours (Cross et al., 2003). Different technologies such as FISH, CGH, microsatellite analysis (MSA), multiple ligation-dependent probe amplification (MLPA) and array-CGH have been used to study the well-known changes of chromosomes 1, 3, 6 and 8 (Horsman and White, 1993, Gordon et al., 1993, Speicher et al., 1994, Sisley et al., 2000, Kilic et al., 2006, Aronow et al., 2012, Cassoux et al., 2014). These studies however provided different frequencies for these changes and can still underestimate the effect on the prognosis of UM.

Thus, the prognosis of UM is still usually linked to changes in chromosomes 3 and 8, whilst deletion of chromosome 1p is an indicator for poor outcome, but the relevance of chromosome 6 aberrations to the prognosis of UM remains unclear (Prescher et al., 1996, Sisley et al., 1997, White et al., 1998, Sisley et al., 2000, Aalto et al., 2001, Damato, 2010, Hammond et al., 2015, Jager et al., 2018, Shain et al., 2019). A large study conducted by Cassoux et al., analysed 338 UM samples using array-CGH to confirm that monosomy 3 with chromosome 8q gain presents the highest risk, but the role of chromosome 6 in prognosis was not described (Cassoux et al., 2014). Other studies have also confirmed that the greatest risk is associated to monosomy 3 and more copies of 8q gain (Sisley et al., 1997, White et al., 1998, Singh et al., 2009). Most investigations, including those using array-CGH, did not specifically emphasize the role of chromosome 6 alterations in UM cases (Damato et al., 2007, Damato, 2010, Hammond et al., 2015).

Chromosome 6 alterations in UM usually occur as a gain of chromosome 6p with disomy 3, or as an isochromosome 6p associated with monosomy 3, gain of chromosome 8q and loss of chromosome 1p (Aalto et al., 2001, Naus et al., 2001, Hausler et al., 2005, Kilic et al., 2005). Additionally, UM patients with gain of chromosome 6p only are proposed to be in a separate group associated with disomy 3 and having a better prognosis (Prescher et al., 1995, Sisley et al., 1997, Parrella et al., 1999, Landreville et al., 2008, Robertson et al., 2017, Drabarek et al., 2019). Sisley et al. (2006) indicated that aberrations of chromosome 6 in UM

were however likely to be underestimated, depending on the methodology used, and more recent studies have confirmed these observations (Cassoux et al., 2014, Hammond et al., 2015). Although few articles specifically mention the loss of chromosome 6q, there may be an association with metastasis; the majority of studies emphasize the relationship of gain of chromosome 6p with good prognosis (Prescher et al., 1990, Speicher et al., 1994, White et al., 1998, Sisley et al., 2000, Kilic et al., 2006, Damato et al., 2007).

More recently, mutational analysis has identified specific mutations in UM, as mentioned in section 1.3.7, but only *SF3B1* and *EFI1AX* are relevant for the prognosis of UM (Harbour et al., 2013, Martin et al., 2013, Dono et al., 2014, Koopmans et al., 2014a, Luscan et al., 2015, Yavuzyigitoglu et al., 2016b). As most mutational changes found in UM do not clearly indicate the way UM patients are going to behave, reliance is still placed on chromosomal imbalances (Robertson et al., 2017, Shields et al., 2019). Therefore, it is necessary to further study known mutations together with chromosomal aberrations, and to seek to identify specific genes on these prognostically relevant chromosomes.

The use of a high-resolution array-CGH specifically designed for UM found detailed information about CNA of commonly altered chromosomes such as chromosomes 1, 3, 6 and 8 (Hammond et al., 2015). This specifically designed array-CGH for UM has more probes on the commonly altered chromosomes, including chromosome 6. More detailed information about chromosome 6 allows a more in-depth analysis of the relevant changes and relationship to other alterations of UM. Previously, the array designed by Dr. Hammond had been used to analyse 137 cases (Alshammari, 2017). In this study, a further 22 UM cases were analysed by array-CGH to consolidate the dataset, and mutational analysis was undertaken specifically on these cases.

3.2 Results

3.2.1 Sample collection and preparation

The mutation analysis for 28 primary UMs for *SF3B1* exon 14, *EIF1AX* exons 1 and 2 and *TERTp* was initially worked up and performed. In addition, two samples, MEL-312 and MEL-352, were included in the series as internal controls, because they were metastatic samples from another organ to the eye. Therefore, the total collection was 30 samples for mutational analysis screening. Later in this study, mutational screening been done for *GNAQ* and *GNA11* exons 4 and 5 for the same series, however, MEL-672 did not have sufficient DNA and there was not enough frozen tissue to re-extract the DNA.

3.2.2 PCR and gel electrophoresis optimisation

The PCR was optimised for *SF3B1* exon 14, *EIF1AX* exons 1 and 2 and *TERTp* using different methods such as gradient, touchdown and modified touchdown. However, *GNAQ* and *GNA11* exons 4 and 5 had been previously optimised within the research group as a 3-step PCR and modified touchdown. To optimise, a single blood DNA sample was used to determine the optimum annealing temperature for all of these genes and was then used for all UM patients' DNA samples. After optimising all genes, gel electrophoresis was used to visualise the amplified product under UV-light, as mentioned in section 2.2.2. All amplified products were then sent for Sanger sequencing to obtain detailed information and screening for any mutations in those genes.

3.2.3 Mutational screening for GNAQ and GNA11

The main mutation for these genes occurs in exon 5; a single substitution mutation that changes the amino acid glutamine (Q) into a different amino acid. Sanger sequencing was therefore done on 27 primary UMs and 2 metastases to the eye to confirm that cases were indeed UM (Figures 3.1 and 3.2).

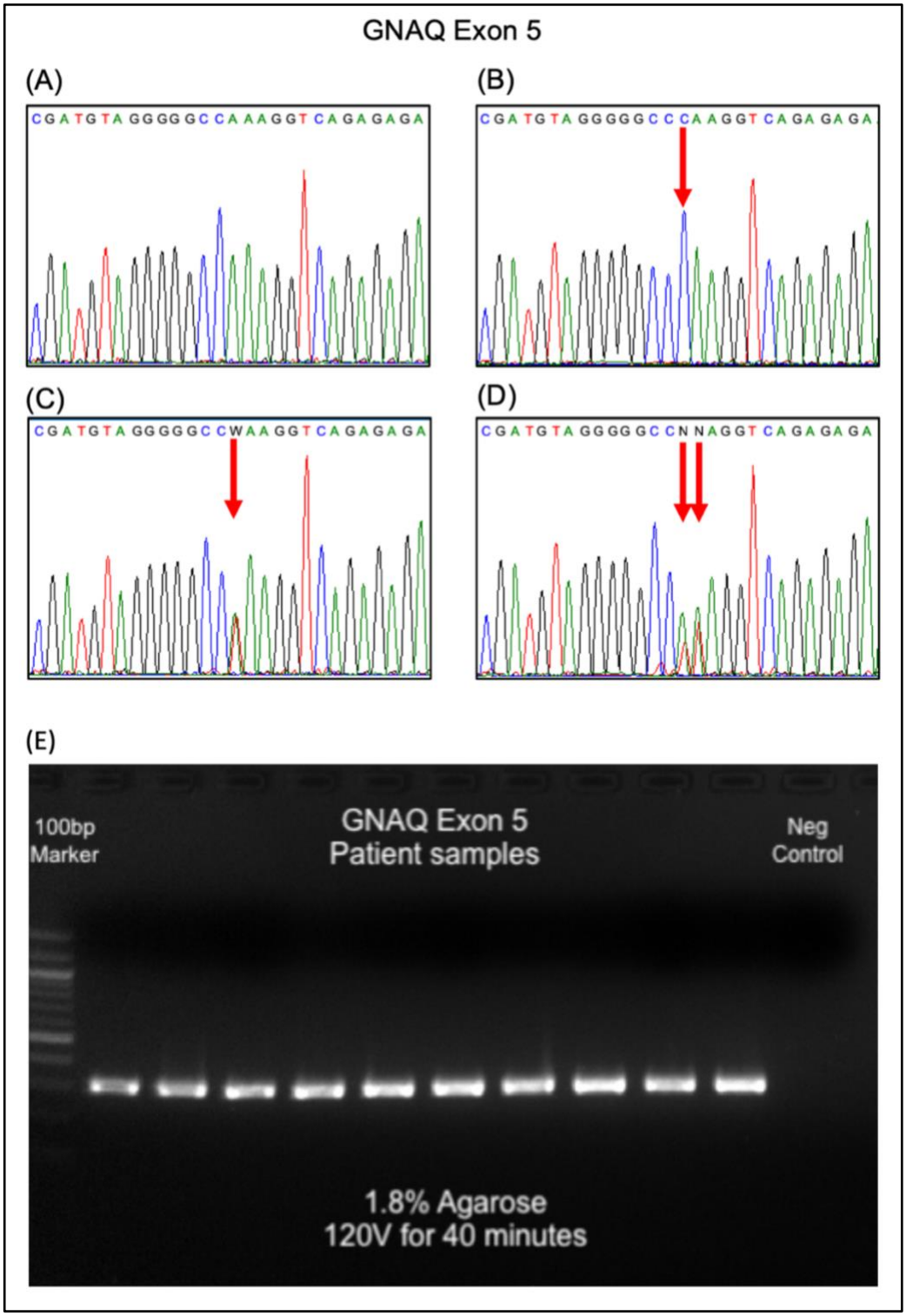

Figure 3.1: The Sanger sequencing chromatogram and gel electrophoresis for *GNAQ* exon 5.

(A) The chromatogram for the wild type (WT) of *GNAQ* exon 5, **(B)** the red arrow shows a homozygous substitution mutation of A>C, **(C)** shows the heterozygous mutation from A>T and **(D)** shows the substitution mutation of two nucleotides AA>TT which is the same amino acid change p.Q209L. **(E)** The gel electrophoresis of *GNAQ* exon 5 that indicates that all bands are amplified on 317 bp.

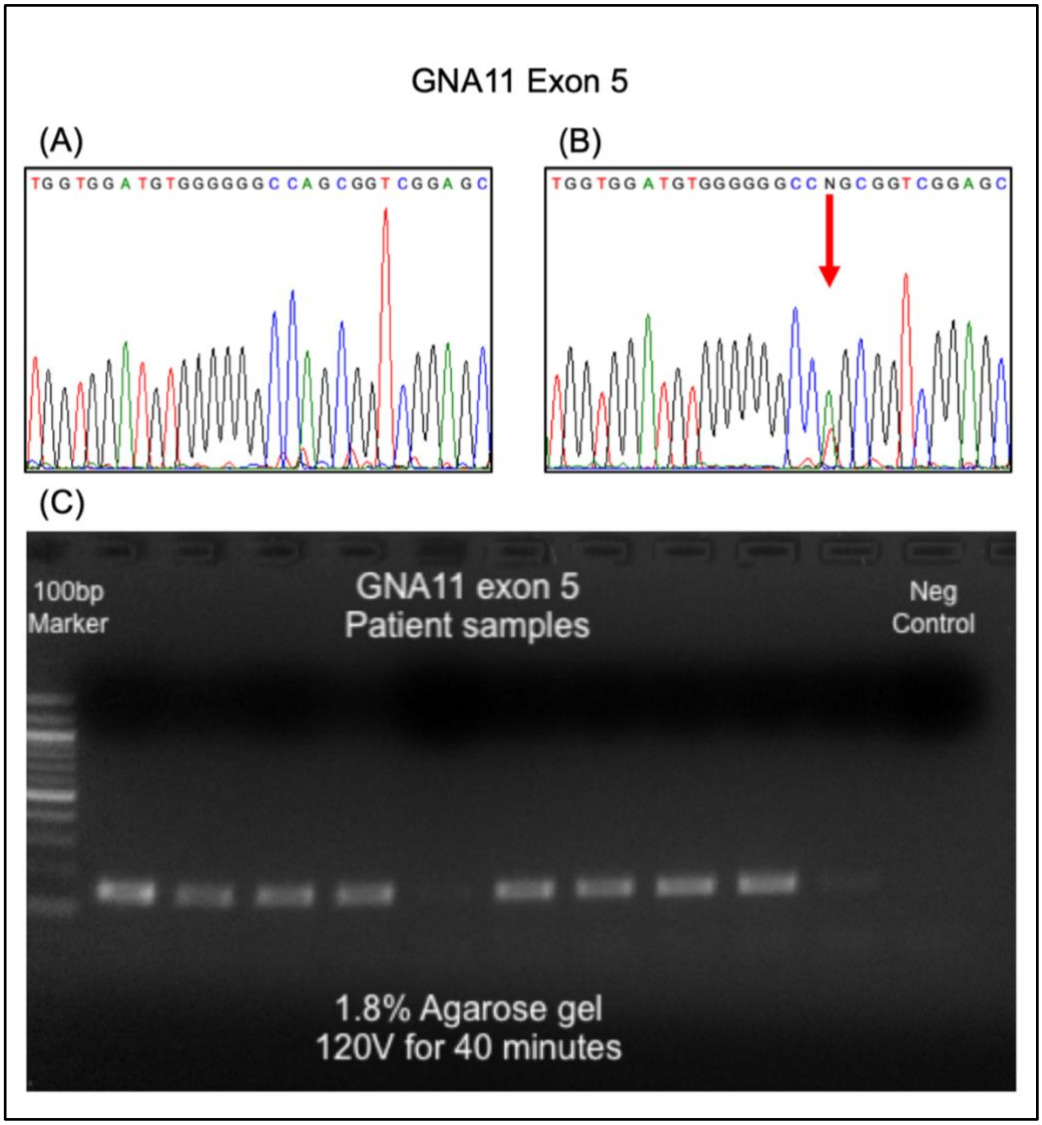

Figure 3.2: The Sanger sequencing chromatogram and gel electrophoresis of *GNA11* exon 5.

(A) shows the WT sequence of *GNA11* exon 5 while in **(B)** the red arrow shows the substitution mutation of A>T. **(C)** The gel image of *GNA11* exon 5 that indicate all bands are amplified on 147bp.

It was found that about 93% of the samples (25 of 27) had mutations in either *GNAQ* or *GNA11* exon 5. However, two samples, MEL-665 and MEL-491, did not harbour any mutations for *GNAQ* or *GNA11* exons 4 and 5, as well as the control metastatic samples (MEL-312 and MEL-352). In this series, the most common mutation for *GNAQ* and *GNA11* exon 5 was a single substitution mutation of the amino acid (Q) to leucine (L) [c.626A>T;p.Q209L]. *GNA11* exon 5 was mutated at around 52% (14 of 27 cases), and around 15% of cases (4 of 27) had mutations of *GNAQ* exon 5. Additionally, *GNAQ* exon 5 had a single substitution mutation on the amino acid (Q) that changed to proline (P)

[c.626A>C;p.Q209P], which accounted for around 26% (7 out of 27) of all UM samples. However, no mutations were detected for exon 4 of *GNAQ* and *GNA11* after analysing 27 primary UM samples.

3.2.4 Mutational screening for SF3B1, EIF1AX and TERTp

The main mutation of the *SF3B1* gene in patients with UM usually occurs in exon 14, with a single substitution mutation that changes the amino acid arginine (R) into a different amino acid. Thus, mutational analysis using Sanger sequencing was done on 30 frozen tissue samples (Figure 3.3).

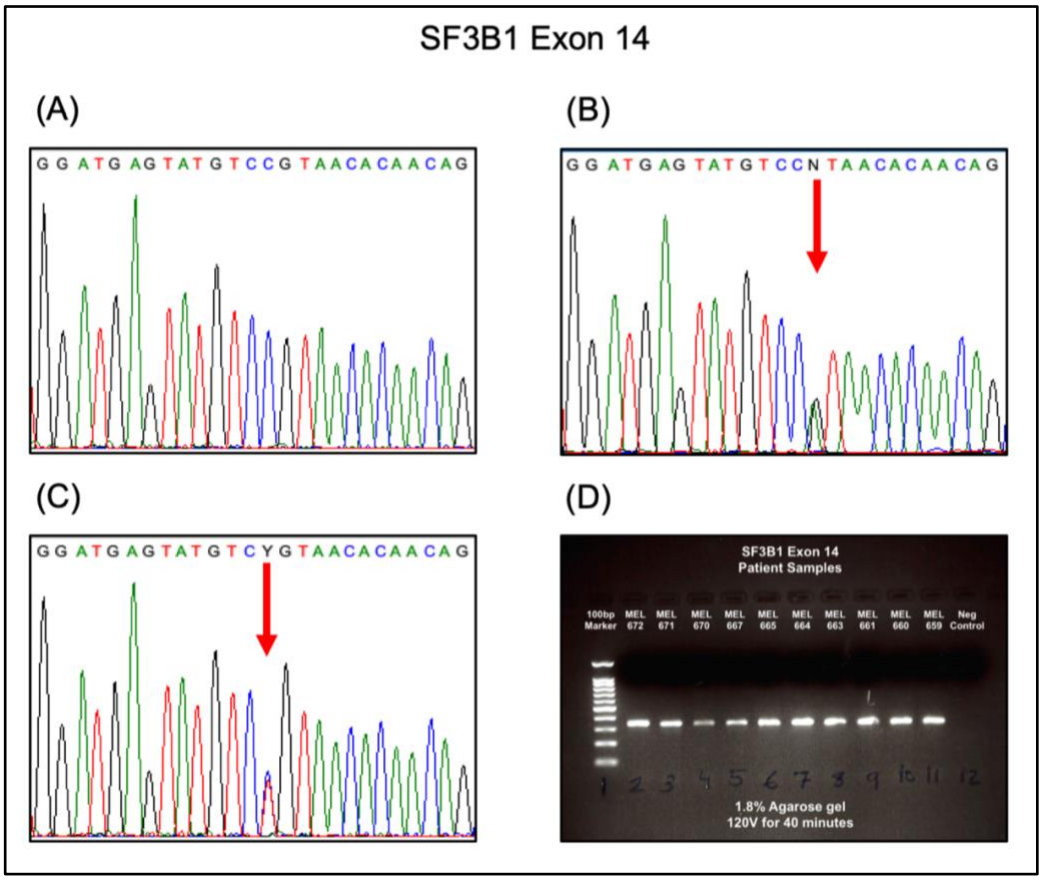

Figure 3.3: The Sanger sequencing chromatogram and gel electrophoresis of *SF3B1* exon 14.

(A) shows the WT sequence of *SF3B1* exon 14, **(B)** the red arrow shows the point mutation of G>A, **(C)** another point mutation for the same nucleotide from C>T and **(D)** shows the gel image of *SF3B1* exon 14 indicates that all bands were amplified at 343 bp.

It was found that four out of the 30 analysed samples had a mutation in *SF3B1* exon 14. Two UM samples had a mutation that changes the amino acid (R) into cysteine (C) [c.1873C>T;p.R625C], while the other two had a mutation at the same spot that changes the amino acid (R) into histidine (H) [c.1874G>A;p.R625H]. The results of *SF3B1* exon accounts for around 14%, which was consistent with previous reports (Harbour et al., 2013, Furney et al., 2013, Dono et al., 2014).

Mutations in the *EIF1AX* gene vary in different codons, but they occur mostly at codons 2, 3 and 4. Therefore, two exons were used to screen for genetic mutations in the 30 tissue samples. In *EIF1AX* exon 1, only one sample was found to be mutated at the same hotspot that usually had a mutation, but it had an interesting insertion of six nucleotides (TCTTGC) (Figure 3.4).

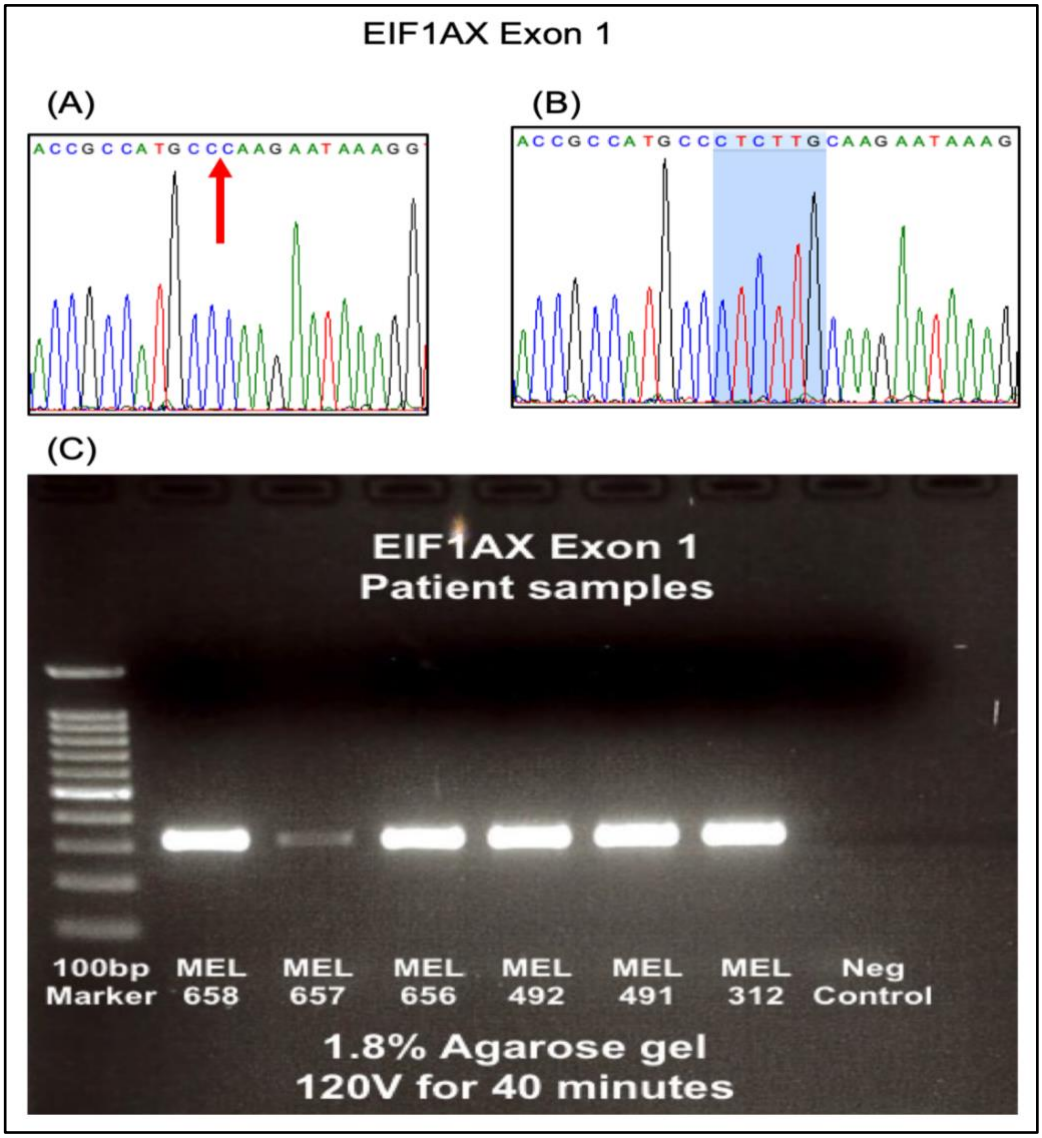

Figure 3.4: The Sanger sequencing chromatogram and gel electrophoresis for *EIF1AX* exon 1.

(A) The chromatogram shows the WT *EIF1AX* exon 1 and the red arrow indicates the area in which six nucleotides (TCTTGC) were inserted as shown further in **(B)**. **(C)** The gel image of *EIF1AX* exon 1 that indicated all bands were amplified at 320 bp.

Besides *EIF1AX* exon 1, a mutation in codon 3, lysine (K) to glutamate (E), was found in only one sample with the *EIF1AX* exon 2, where the mutation was [c.7A>G;p.K3E] (Figure 3.5), which was similar to previous findings (Martin et al., 2013, Dono et al., 2014). However, the frequencies detected in the samples analysed were about 7% which is broadly consistent with the frequencies in other articles (Martin et al., 2013, Yavuzyigitoglu et al., 2016a).

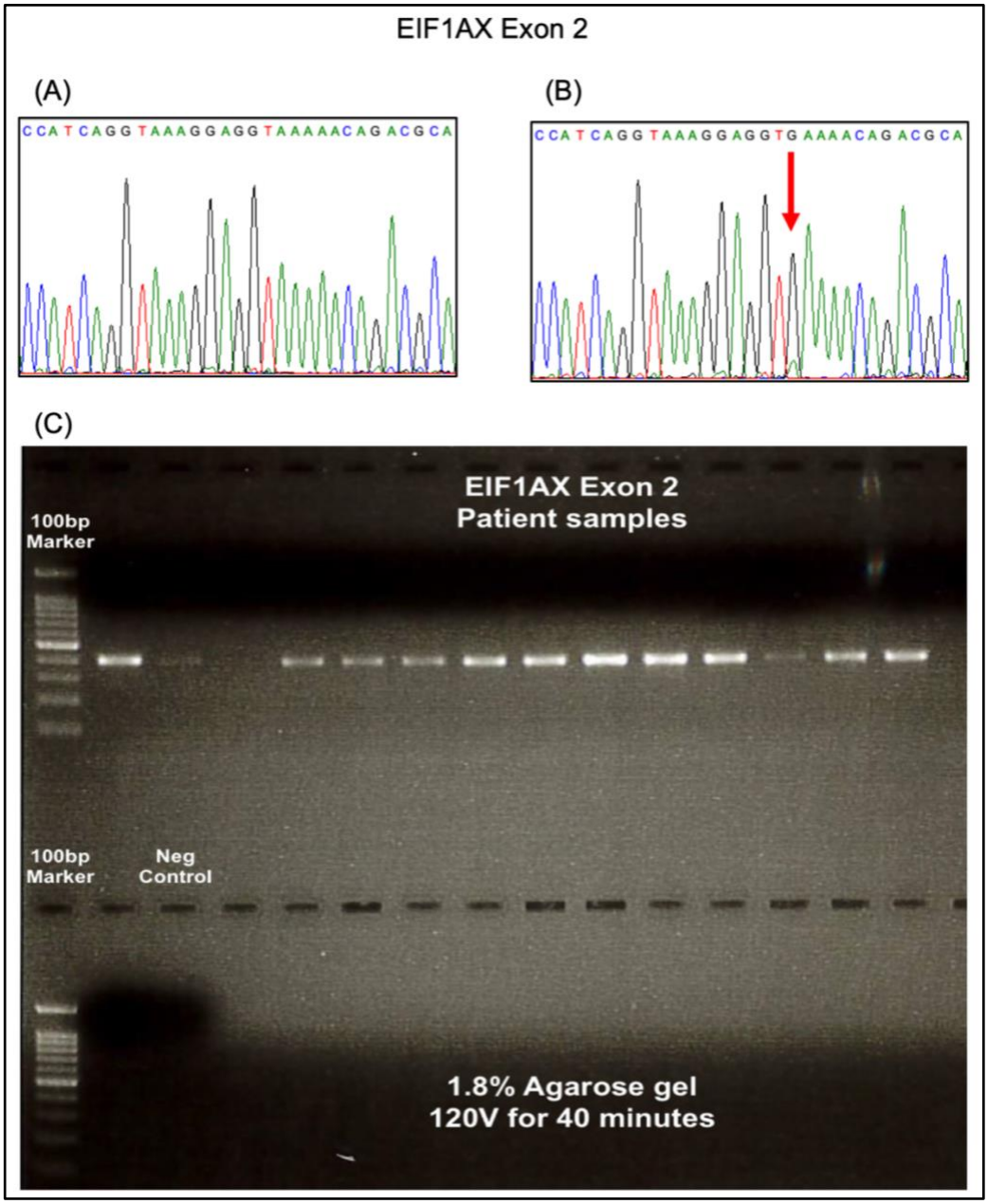

Figure 3.5: The Sanger sequencing chromatogram and gel electrophoresis for *EIF1AX* exon 2.

(A) The chromatogram shows the WT of *EIF1AX* exon 2 and **(B)** the red arrow shows the point mutation of A>G. **(C)** The gel image of *EIF1AX* exon 2 indicates that all bands were amplified at 406bp.

For the *TERTp* gene, however, after amplifying and analysing 30 tissue samples, there was no mutation detected, which previous reports concluded that mutations of *TERTp* gene are rarely found in UM cells (Dono et al., 2014, Koopmans et al., 2014a). Thus, the results of all mutational screening are presented in Table 3.1, which shows all samples that were analysed for all with their genetic mutations.

Table 3.1: The mutational analysis for the 30 UM patient samples and the distribution of mutations.

Sample Number	GNAQ Ex.4	GNAQ Ex.5	GNA11 Ex.4	GNA11 Ex.5	SF3B1 Ex.14	EIF1AX Ex.1	EIF1AX Ex.2	TERTp
MEL-672	FAILED	FAILED	FAILED	FAILED	WT	WT	WT	WT
MEL-671	WT	A>T (Q209L)	WT	WT	WT	WT	WT	WT
MEL-670	WT	WT	WT	A>T (Q209L)	WT	WT	WT	WT
MEL-667	WT	WT	WT	A>T (Q209L)	WT	WT	WT	WT
MEL-665	WT	WT	WT	WT	WT	WT	WT	WT
MEL-664	WT	AA>TT (Q209L)	WT	WT	WT	WT	WT	WT
MEL-663	WT	WT	WT	A>T (Q209L)	WT	WT	WT	WT
MEL-661	WT	A>T (Q209L)	WT	WT	WT	WT	WT	WT
MEL-660	WT	WT	WT	A>T (Q209L)	WT	WT	WT	WT
MEL-659	WT	WT	WT	A>T (Q209L)	C>T (R625C)	WT	WT	WT
MEL-658	WT	WT	WT	A>T (Q209L)	WT	WT	A>G (K3E)	WT
MEL-657	WT	WT	WT	A>T (Q209L)	WT	WT	WT	WT
MEL-656	WT	WT	WT	A>T (Q209L)	WT	WT	WT	WT
MEL-655	WT	WT	WT	A>T (Q209L)	WT	WT	WT	WT
MEL-654	WT	WT	WT	A>T (Q209L)	WT	WT	WT	WT
MEL-652	WT	A>C (Q209P)	WT	WT	WT	Ins (CTCTTG)	WT	WT
MEL-530	WT	WT	WT	A>T (Q209L)	C>T (R625C)	WT	WT	WT
MEL-529	WT	A>C (Q209P)	WT	WT	WT	WT	WT	WT
MEL-528	WT	WT	WT	A>T (Q209L)	WT	WT	WT	WT
MEL-524	WT	A>C (Q209P)	WT	WT	WT	WT	WT	WT
MEL-523	WT	A>C (Q209P)	WT	WT	WT	WT	WT	WT
MEL-522	WT	A>C (Q209P)	WT	WT	WT	WT	WT	WT
MEL-521	WT	A>T (Q209L)	WT	WT	WT	WT	WT	WT
MEL-492	WT	A>C (Q209P)	WT	WT	WT	WT	WT	WT
MEL-491	WT	WT	WT	WT	WT	WT	WT	WT
MEL-489	WT	A>C (Q209P)	WT	WT	G>A (R625H)	WT	WT	WT
MEL-486	WT	WT	WT	A>T (Q209L)	G>A (R625H)	WT	WT	WT
MEL-485	WT	WT	WT	A>T (Q209L)	WT	WT	WT	WT
MEL-352	WT	WT	WT	WT	WT	WT	WT	WT
MEL-312	WT	WT	WT	WT	WT	WT	WT	WT

WT= Wild type; MEL-672 did not have enough DNA for *GNAQ* and *GNA11* mutation analysis; MEL-665 and MEL-491 did not harbour any mutations for all tested genes; MEL-312 and MEL-352 were metastatic from another organ to the eye and used as internal controls.

3.2.4 Array-CGH

This study was carried out with array-CGH for 22 primary UM tissue samples to investigate any somatic copy number aberrations (SCNAs), as mentioned in section 2.2.3. The gDNA were extracted from primary UM frozen tissue and compared with the patient's normal blood gDNA as a reference DNA. The tumour and blood gDNA were labelled and hybridised onto a microarray slide comprised of 180,000 probes, which was specially designed for UM by Dr. David Hammond, Rare Tumour Research Group (RTRG), University of Sheffield. Subsequently, the analysis of these samples was done with Agilent Genomic Workbench software (Version 7.0.4.0) using ADM-2 algorithm, as shown in Table 3.2. The ADM-2 algorithm was based on the probes distribution with a threshold of 6.0. The software is validated log ratio using ADM-2 algorithm by having the log ratio of amplification of >0.6 and the deletion of ≤–1.0, which appeared as red and green, respectively.

Table 3.2: Default Agilent Genomic Workbench software preferences.

Genome	**hg18**
Aberration algorithm	ADM-2 (Threshold: 6.0, Fuzzy zero: ON)
GC correction	ON (window size: 2kb)
Centralisation (legacy)	OFF
Combine replicates (IntraArray)	ON
Array level filter	NONE
Aberration filter	DefaultAberrationFilter_V2

After analysing the 22 primary UM tissue samples, the results showed that partial or complete gain of chromosome 8q arm was the most detected chromosomal aberration, which varied between 60% to 80% depending on whether the aberration was a complete or partial gain of chromosome 8q (Figure 3.6). Also, monosomy 3 was found in around 60% of all primary UM tissue samples. The gain of the chromosome 6p and deletion 6q appeared in around 45% and 32%, respectively. Additionally, aberrations in chromosome 1, such as the loss of 1p and gain of 1q, were found in around 20% of all samples. However, aberrations in other chromosomes did not reach 10%, except for the chromosome 16p and 19, which showed a deletion in 30% to 35% of the samples, respectively.

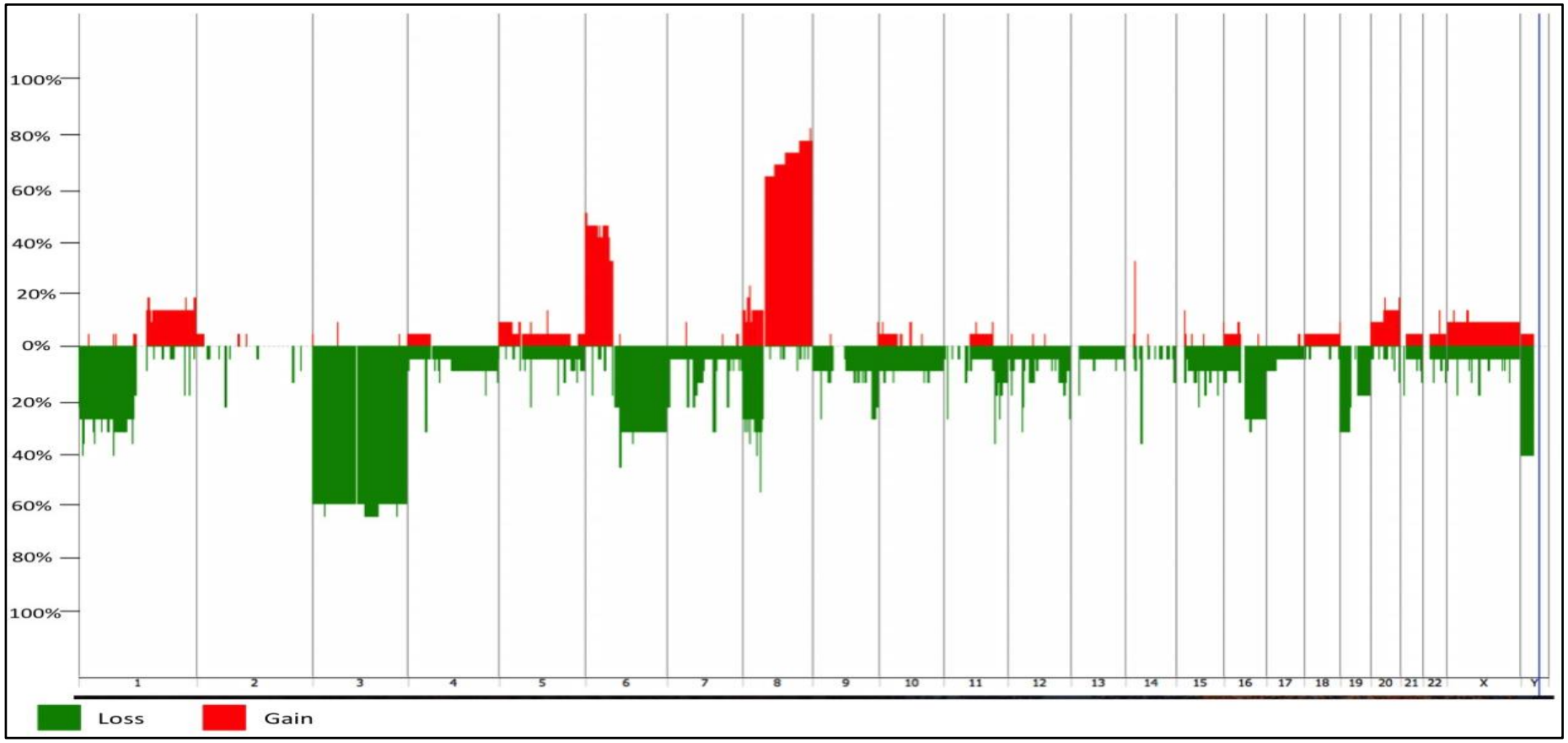

Figure 3.6: Total percentage of gain and loss in each chromosome among all the primary UM tissue samples.

The red shows the percentage of gain among the chromosomes, showing chromosome 8q to be the most common gain. The green shows the losses, with a loss in chromosome 3 being the most common. Images output from Agilent Genomic Workbench software v7.0.4.0. The ADM-2 algorithm was used to detect all the aberrations.

In addition, these results demonstrated that there was a correlation between the complete loss of chromosome 3, the amplification of chromosome 8q and the gain of chromosome 6p and loss of 6q (Figure 3.7). The amplification of 6p only was found in around 13% of the samples while the gain of chromosome 6p and deletion of 6q (isochromosome 6p) was found in around 32% of the samples. Furthermore, all the samples with amplification of chromosome 6p only had disomy 3 and no gain in chromosome 8q arm.

There were only two of the samples found to have an isochromosome 6p together with a complete loss of chromosome 3 and gain of chromosome 8q. However, four samples showed isochromosome 6p, but they had disomy 3. Only one sample that showed isochromosome 6p that have partial deletion of chromosome 3p and complete gain of chromosome 8.

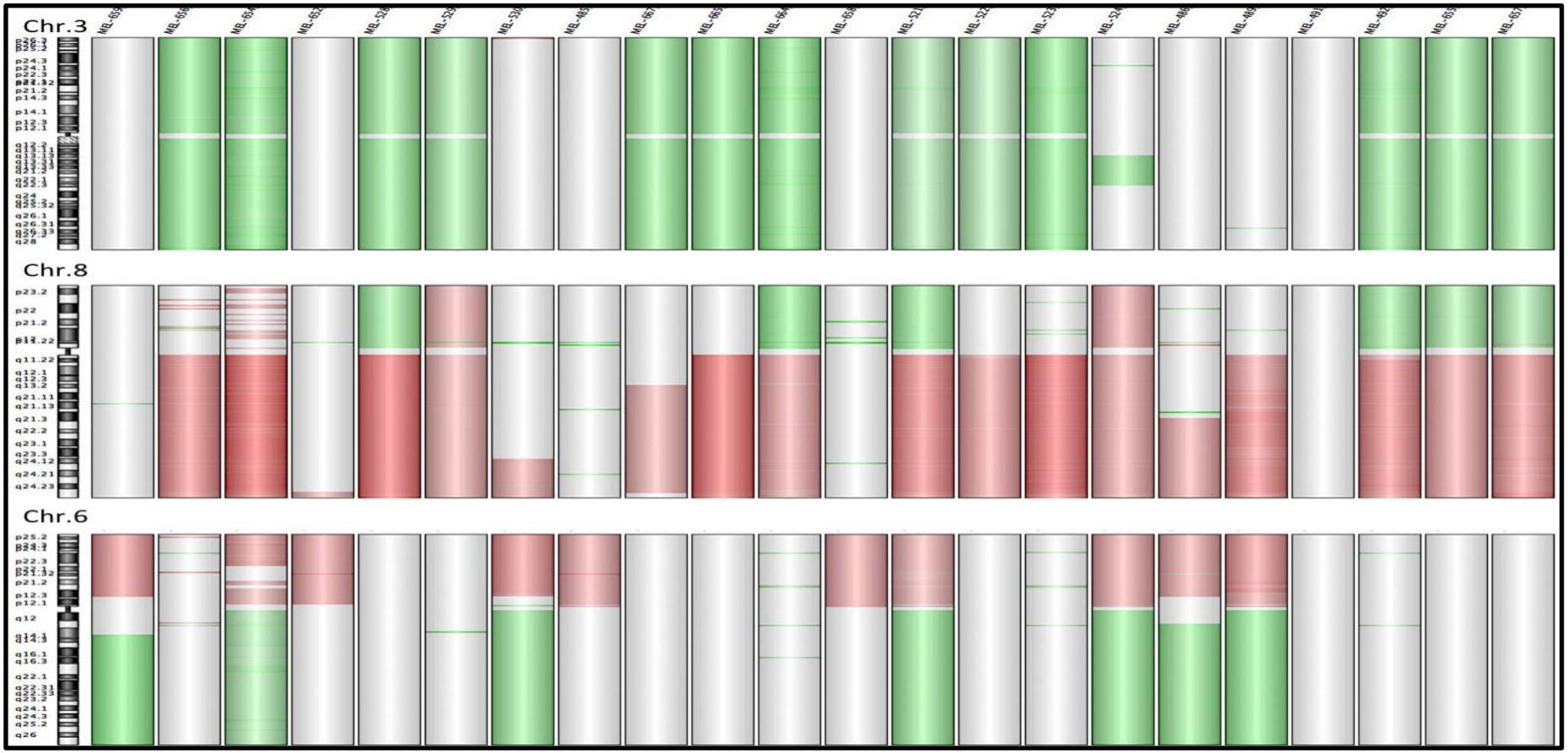

Figure 3.7: Comparison between chromosomes 3, 8 and 6 deletion and amplification.

The figure shows all UM patient samples that were analysed using array-CGH to compare the gain and loss among the most recurrent aberrations in these chromosomes. The green shows losses while red shows gains. Images output from Agilent Genomic Workbench software v7.0.4.0. The ADM-2 algorithm was used to detect all the aberrations.

In addition, one primary UM had greater instability with a much higher level of SCNA, and one sample had no SCNA at all (Figure 3.8). The UM that did not show any apparent chromosomal aberrations, also had no mutations amongst the genes that were screened.

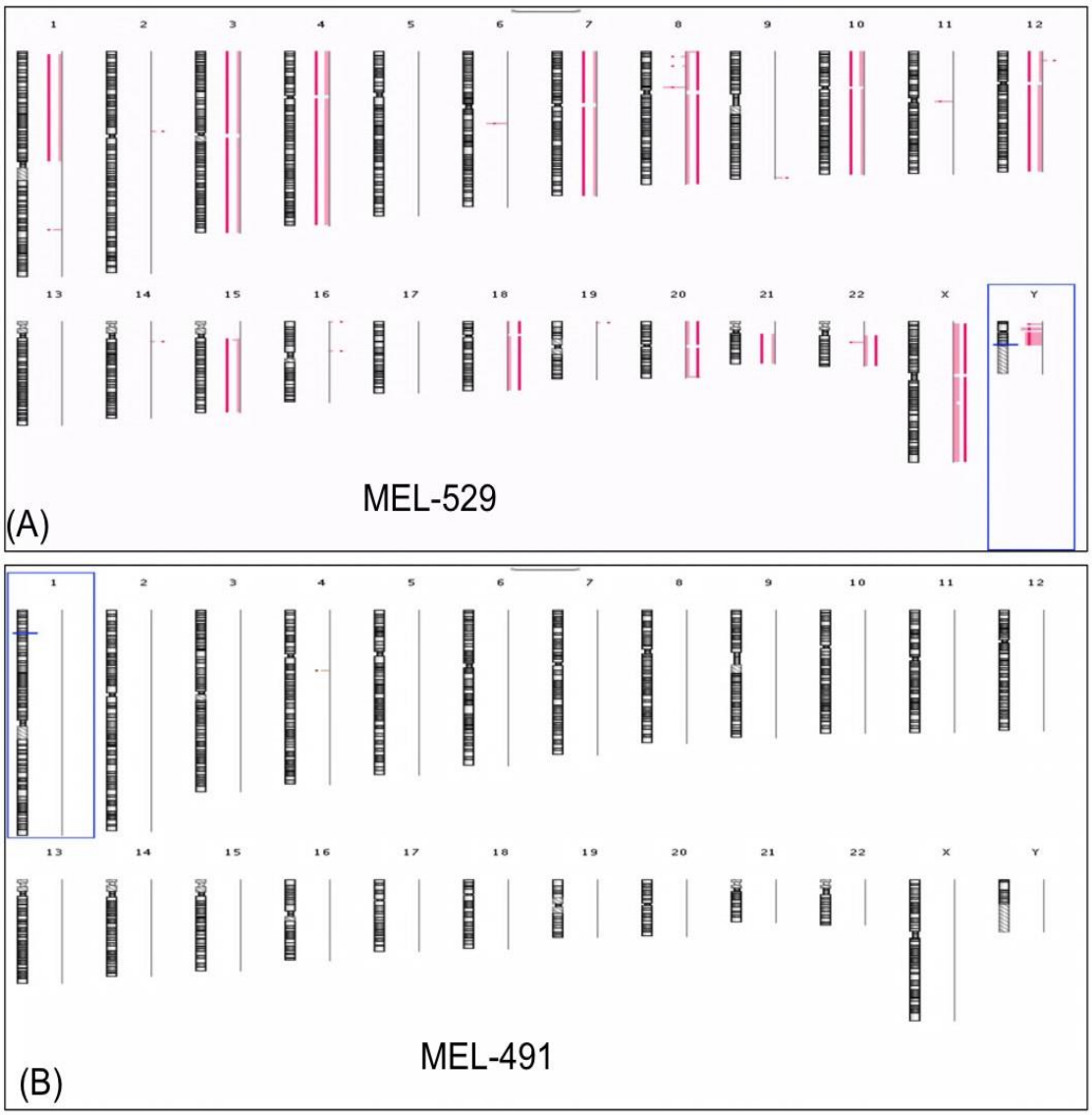

Figure 3.8: Array-CGH for the highest and lowest number of chromosomal aberrations.

Array-CGH ideogram showing: **(A)** a sample with a deletion of chromosomes 1p, 3, 4, 7, 10, 12, 15 and 21, and a gain of chromosomes 8, 18, 20 and 22; **(B)** a sample with no chromosomal aberration detected.
Images output from Agilent Genomic Workbench software v7.0.4.0. The ADM-2 algorithm was used to detect all the aberrations.

3.2.5 The correlation between genetic mutations and chromosomal aberrations

An observation comparison between the samples that were found to have mutations for genes *SF3B1* and *EIF1AX* and chromosomal aberrations showed some interesting results. Specifically, all the samples that had a mutated *SF3B1* gene showed no deletion in chromosome 3; however, all of those mutated samples showed an isochromosome 6p (Figure 3.9). Furthermore, two samples showed partial gain of chromosome 8q and one sample showed a complete amplification of chromosome 8q, while only one sample (MEL-659) did not have any alterations for chromosome 8q. In addition, three out of four samples showed a focal deletion of chromosome 11q.

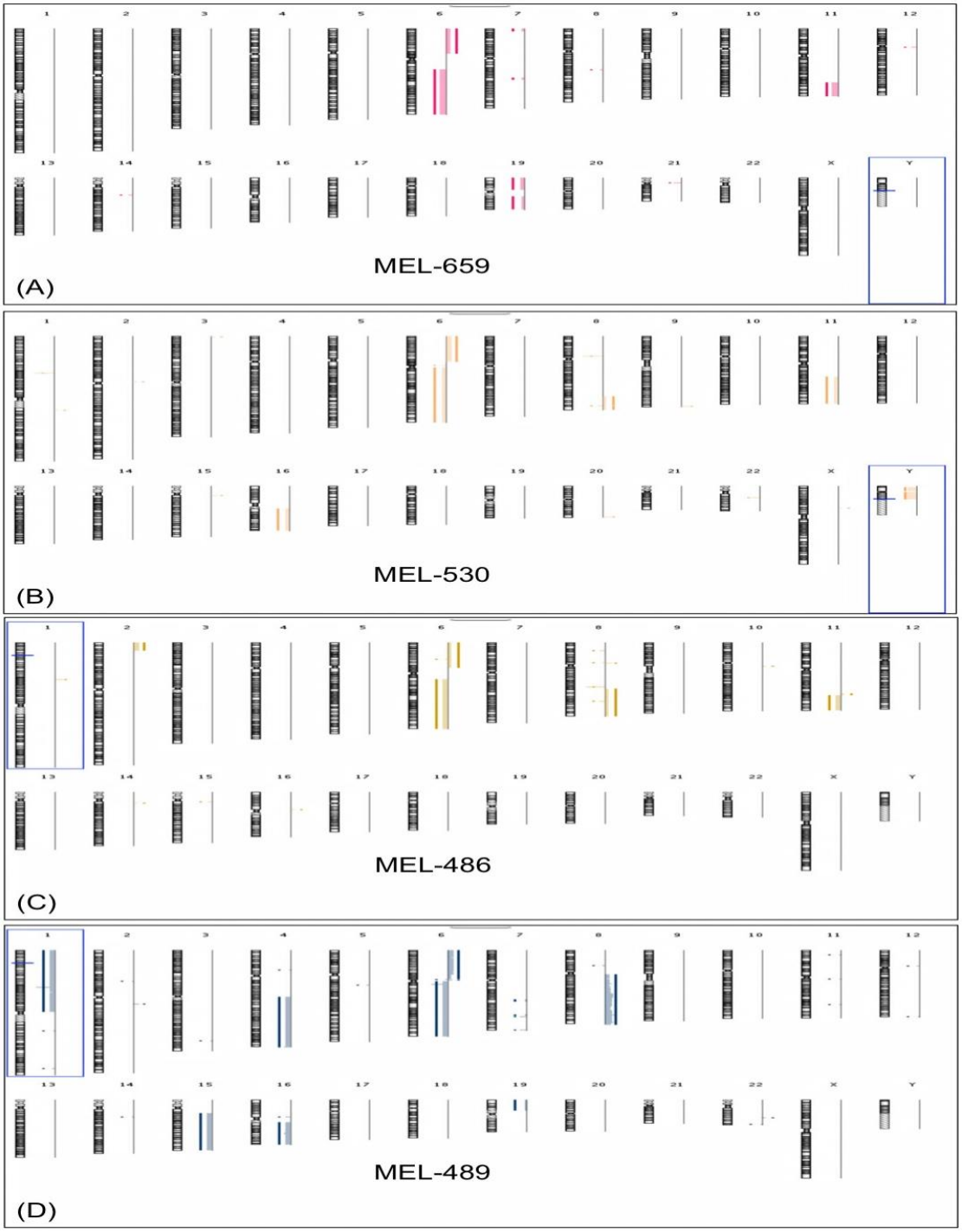

Figure 3.9: Ideograms for the samples with a mutation of the for *SF3B1* gene.

All samples showed a gain of chromosome 6p and loss of 6q (isochromosome 6p). **(A)** The sample showed a partial loss of the bottom chromosome 11q and a complete loss of chromosome 19. **(B)** The sample showed a gain in part of chromosome 8q, partial loss of 11q and loss of the chromosome 16q arm. **(C)** The ideogram shows a partial gain of chromosome 8q with a focal deletion in chromosome 11q. **(D)** The ideogram shows a gain in chromosome 8q, deletion in chromosome 1p, and a partial deletion of chromosomes 4q, 15q 16q, and 19p arm.
Images output from Agilent Genomic Workbench software v7.0.4.0. The ADM-2 algorithm was used to detect all the aberrations.

In addition to the *SF3B1* mutations and their correlation with chromosome 6, chromosomal aberrations in the *EIF1AX* gene showed that they consisted mainly of an amplification in chromosome 6p only (Figure 3.10).

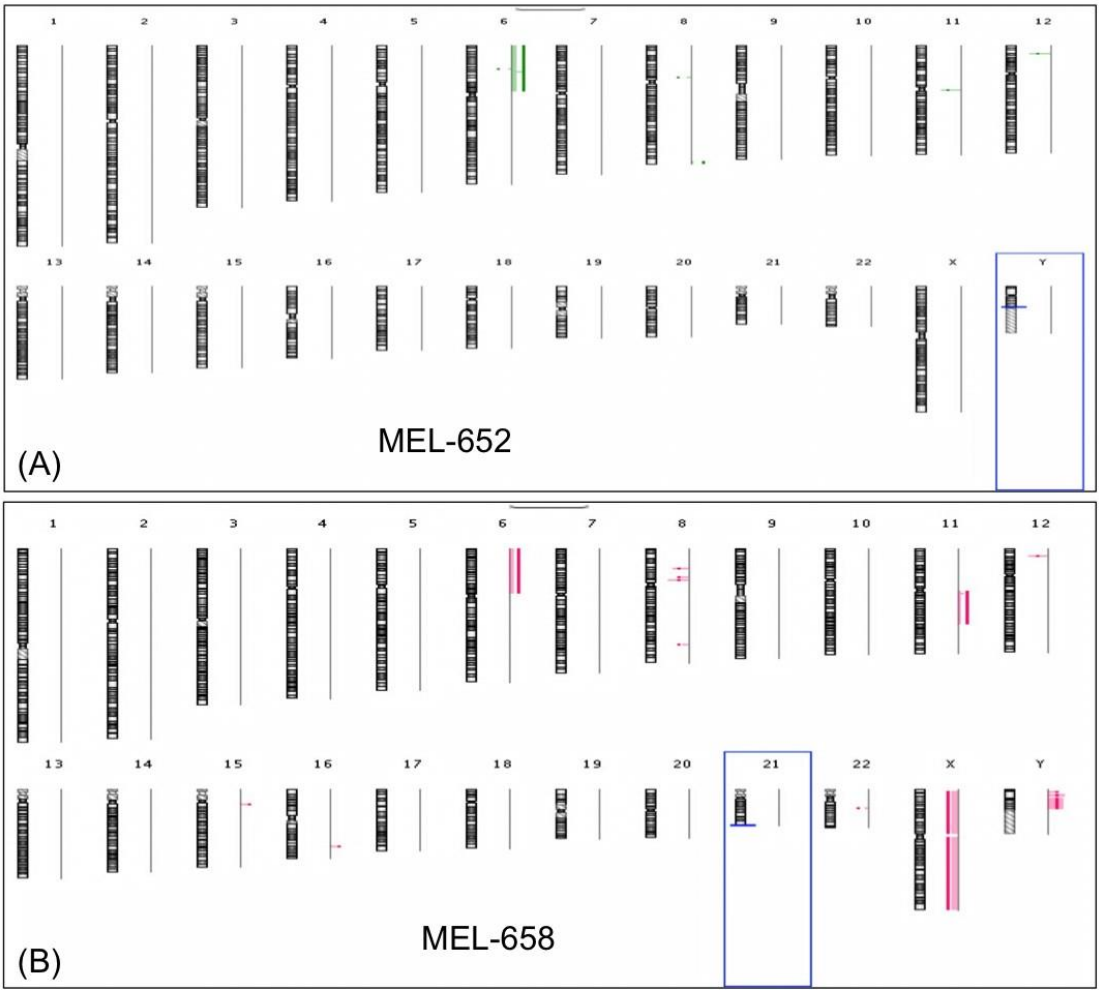

Figure 3.10: Ideograms for the samples with a mutated *EIF1AX* gene.

(A) shows a gain in chromosome 6p arm and similarly **(B)** shows the same amplification of chromosome 6p but there is an addition of a small amplification in the chromosome 11q.
Images output from Agilent Genomic Workbench software v7.0.4.0. The ADM-2 algorithm was used to detect all the aberrations.

3.3 Discussion

The assessment of prognosis by genetic markers for UM has gone through different stages of cytogenetic and genetic classifications over the last two decades, such as the chromosomal classification (Prescher et al., 1996, Sisley et al., 1997), and genetic profiling class 1 and 2 (Onken et al., 2004). However, some high-risk UM patients are still misclassified (Field et al., 2016).

In this study, the SCNA for chromosome 8q (80%) was the most frequent chromosome change, followed by monosomy 3 (60%) and abnormalities of chromosome 6 (45%). These findings together with other chromosomal aberrations of chromosomes 1, 16, and 19 are in agreement with previous reports (Sisley et al., 1990, Sisley et al., 1997, Aalto et al., 2001, Kilic et al., 2005, Cassoux et al., 2014, Hammond et al., 2015). Activating mutations in UM are in *GNAQ* and *GNA11* which occur in a mutually exclusive pattern (Van Raamsdonk et al., 2009, Van Raamsdonk et al., 2010, Sisley et al., 2011) and are found in around 90% of UM cases that are considered as early progression events of UM (Onken et al., 2008, Bauer et al., 2009). In this current study about 93% of the UM samples (25 out 27) were *GNAQ* and *GNA11* mutated, similar to previously mentioned reports. One UM sample had no SCNA and also had no mutations. However, these mutations are not predictive of UM prognosis in comparison to monosomy 3, gain of chromosome 8q and gain of chromosome 6p. Mutations of potential relevance to prognosis (*SF3B1* and *EIF1AX*) were also broadly consistent with previous studies (Furney et al., 2013, Harbour et al., 2013, Martin et al., 2013, Dono et al., 2014, Yavuzyigitoglu et al., 2016b).

3.3.1 Correlation of genetic changes with clinical features

The involvement of ciliary body is usually indicative of a worse prognosis in UM (Kaliki et al., 2015). Monosomy 3 is consistently reported to correlate with ciliary body melanomas (Prescher et al., 1996, Scholes et al., 2003, Kilic et al., 2005, Damato et al., 2007). Furthermore, mutation frequencies for *SF3B1* and *EIF1AX* and ciliary body involvement in UM have been reported for a number of studies

(Table 3.3). Overall mutated *SF3B1* is more often correlated with ciliary body than *EIF1AX* mutations.

Table 3.3: Mutation frequency for both *SF3B1* and *EIF1AX* and ciliary body.

SF3B1	No. of samples	Mutation frequency	Ciliary body involvement
(Harbour et al., 2013)	102	19 (18.6%)	47%
(Martin et al., 2013)	111	23 (20.7%)	48%
(Yavuzyigitoglu et al., 2016a)	133	31 (25.6%)	8 (25.8%)
EIF1AX	**No. of samples**	**Mutation frequency**	**Ciliary body involvement**
(Martin et al., 2013)	111	20 (18%)	30%
(Yavuzyigitoglu et al., 2016a)	133	28 (21%)	4 (14.4%)

3.3.2 What other correlations do mutations of SF3B1 and EIF1AX have?

The data in this study indicates that most of the cases of disomy 3 (except for MEL- 491) also had gain of 6p and mutations in either *SF3B1* or *EIF1AX*. Disomy 3 and gain of 6p are well known to be associated with favourable prognosis (Parrella et al., 1999). Correlation between chromosome 6 alterations and mutations of *SF3B1* and *EIF1AX* have also been related previously (Yavuzyigitoglu et al., 2016a). They found that the mutant samples with *SF3B1* harboured a gain of chromosome 6p in more than 80% of their samples, while the loss of chromosome 6q was found in about half of the analysed samples. They also mentioned that the role of *SF3B1* mutations in disomy 3 may have a late metastatic risk; and the findings have also been confirmed in more recent investigations (Robertson et al., 2017). The results of this current study can qualify these observations to some extent. Specifically, cases of UM with disomy 3 could be further subdivided on the basis of mutational profile and the type of chromosome 6 abnormality. Most disomy 3 cases with chromosome 6p gain only

had mutations of *E1FAX* (MEL-652 and MEL-658, Figure 3.10). Disomy 3 cases with both gain of chromosome 6p and loss of 6q (or an effective isochromosome 6p) had mutations of *SF3B1*. Given that *SF3B1* mutations may indicate later risk of metastasis, it is interesting that isochromosome 6p occurs as a potentially later event for monosomy 3 cases after gain of chromosome 8q, and the findings were again seen for cases in Figure 3.9. The findings of this study are slightly at odds with those of Yavuzyigitoglu et al. (2016a), which did not indicate whether there is a risk of metastasis or not for UM patients with mutated *SF3B1* and *EIF1AX,* because there was no long follow-up for those UM patients in this series.

A limited number of research studies found deletions on chromosome 11 in UM cells (Sisley et al., 2000, Kilic et al., 2006, White et al., 2006, Drabarek et al., 2019). Sisley et al. (2000) highlighted that aberrations of chromosome 6 and deletion of chromosome 11q25 in UM are frequent and associated with choroid origin. Moreover, it was found recently that isochromosome 6p is associated with gain of chromosome 8q and loss of chromosome 11q in UM (Drabarek et al., 2019). Remarkably, this study showed that focal deletion of chromosome 11q appeared in 3 out of 22 UM samples and were correlated with mutations in *SF3B1* and isochromosome 6p (Figure 3.9). This outcome emphasises that loss of chromosome 11q may follow isochromosome 6p in indicating the prognosis of UM.

3.3.3 What is the sequence of genetic progression for UM?

Robertson et al. (2017) clustered the metastatic risk of UM into four distinctive groups based on the chromosomal aberrations and concurrent mutations of *EIF1AX* and *SF3B1*. However, they only considered the role of gain of chromosome 6p with disomy 3 and gain of chromosome 8q with the low and medium risk of metastasis, respectively. In addition, they proposed a sequence of events for UM metastasis which it started with monosomy 3, *BAP1* mutation, whole genome doubling and then gain of chromosome 8q.

However, based on Figure 3.7, this study is proposing an alternative sequence of events for UM progression based on the results presented. 1) Starting with

mutations in *GNAQ* and *GNA11*, which one case of this current study did not have a mutation of these genes. Therefore, an alternative pathway may exist, or more likely as has been reported previously mutations in other genes affecting the same pathway may be implicated such as *CYSTLR2* or *PLCB4*. 2) UM cases subdivide on the basis of whether they acquire monosomy 3 or not. 3A) For those UM with monosomy 3 the sequence follows as reported in the literature, gain of chromosome 8q, loss of chromosome 1p and isochromosome 6p, and no mutations of *SF3B1* or *EIF1AX*. 3B) UM cases with disomy 3 and gain of chromosome 6p only, then have mutations of *EIF1AX*. Alternatively, disomy 3 cases can acquire isochromosome 6p followed by mutations in *SF3B1* and then partial or complete gain of chromosome 8q. This proposed sequence of events highlights the importance of the isochromosome 6p in the prognosis of UM, which was ignored by previous reports. In a recent report by Drabarek and colleagues, they supported the proposed idea that isochromosome 6p should be in a separate group with disomy 3 (Drabarek et al., 2019).

In summary, this study performed 22 array-CGH analyses out of 28 cases in order to obtain a detailed information about the SCNA of UM. The study applied mutational screening for *SF3B1*, *EIF1AX* and *TERTp*. The finding of apparent associations between mutated *SF3B1* and *EIF1AX* genes with different abnormalities in chromosome 6 is an interesting, and qualified some of the subgrouping of UM and has potential implications for prognosis. Thus, detailed analysis of chromosome 6 aberrations may help identify candidate genes of relevance and improve the understanding of the progression of UM.

Chapter 4: Analysis of chromosome 6 using array-CGH to determine candidate genes in UM

4.1 Introduction

In the previous chapter, the correlation between chromosome 6 aberrations with other genetic alterations in UM was examined. This correlation highlighted the importance of the recurrent abnormalities of chromosome 6 in UM such as gain of chromosome 6p only and isochromosome 6p, and how the relationship with other chromosomes and mutational changes can be used to further subdivide UM.

Beroukhim et al., meanwhile found most cancers that have SCNA of whole chromosome length or arm length are more frequent than the focal SCNA (Beroukhim et al., 2010). They also highlighted that focal SCNA were more likely to have a potential target gene or genes than whole arm SCNA in different cancers, as it is easier to identify those potential genes if the region of aberration is smaller. Previous studies using SKY, CGH or bacterial artificial chromosome (BAC) arrays may have missed these small focal SCNA due to the limited resolution (Speicher et al., 1994, Naus et al., 2001, Sisley et al., 2006, Ehlers et al., 2008). Therefore, the goal of using a high-resolution array-CGH technology is to accurately access these SCNAs, that may help identifying the location of novel oncogenes or tumour suppressor genes. For instance, the use of high-resolution array-CGH helped to identify novel target genes in different tumours such as breast and ovarian cancers, lymphomas and oral cancer (Cheng et al., 2004, Tagawa et al., 2005, Nakaya et al., 2007).

Although there have been some attempts to identify focal SCNA on the chromosome arms implicated in UM (Parrella et al., 2001, Tschentscher et al., 2001, Cross et al., 2003, Parrella et al., 2003, Ehlers and Harbour, 2005, Ehlers et al., 2005, van Gils et al., 2008), for the most part these have failed to identify strong candidates. For example, candidate genes within the recurrent abnormal chromosomes, such as gain of chromosome 8q, have been investigated in UM, with mixed results (Parrella et al., 2001, Ehlers and Harbour, 2005, Ehlers et al., 2005). It was found that the amplification of the *c-Myc* oncogene is associated with gain of chromosome 8q, however, the expression of *c-Myc* was significantly upregulated followed monosomy 3 instead of gain of chromosome 8q (Royds et

al., 1992, Parrella et al., 2001). Furthermore, UM frequently have monosomy of chromosome 3 and mutations of *BAP1* located on chromosome 3p21 are of relevance (Harbour et al., 2010). More specifically, the nuclear protein expression of BAP1 in UM is considered as a poor prognostic marker using IHC with monosomy 3 rather than the mutational status of *BAP1*, mainly because there is not a specific point mutation to correlate with the prognosis (Koopmans et al., 2014b, van de Nes et al., 2016, Field et al., 2018). There are also indications that other genes on chromosome 3 may also be implicated, but there was no strong association with the prognosis of UM (Tschentscher et al., 2001, Parrella et al., 2003, van Gils et al., 2008). As previously stated, the impact of chromosome 6 aberrations and relationships to prognosis of UM is unclear. There have been a number of studies proposing target genes on chromosome 6 (Millikin et al., 1991, Hijiya et al., 1994, Ogino et al., 2006, Gautrey et al., 2015, Shukla et al., 2015), but no strong candidates have immerged for UM. A recent study however found that there is a gene called *PHF10* in the aberrant chromosome 6q27 may have a role in UM development and adhesion (Anbunathan et al., 2019).

Previously, a specifically designed high-resolution array-CGH for UM by (Hammond et al., 2015), and used to study 137 UM samples as part of combined research group and PhD project (Alshammari, 2017). Preliminary analysis using Nexus software (BioDiscovery) identified regions on chromosome 6p and 6q that were preferentially amplified and deleted, respectively. Those genes on chromosome 6p are forkhead box Q1 (*FOXQ1*) and phenylalanyl-tRNA synthetase (*FARS2*); and the gene implicated on chromosome 6q is adenosylmethionine decarboxylase 1 (*AMD1*). An attempt to validate the expression of these target genes using IHC, was performed by Alshammari (2017), the results however were inconclusive, and the sample size was too small to validate.

In this study, array-CGH was previously performed on 22 UM (Figure 3.6). This series acted as a small independent cohort and was analysed separately using different software, to confirm and validate the previous observations, and IHC was performed on a larger set of UMs to explore the expression of these target genes.

4.2 Results

4.2.1 The classification of chromosome 6

Of 22 cases of UM, 10 had abnormalities of chromosome 6 in this study (section 3.2.4, Figure 3.7). This study, as mentioned in the previous chapter, had 10 UM samples with aberrations of chromosome 6 out of 22 and that counts for around 45%, which is similar to previous reports (Prescher et al., 1996, Sisley et al., 1997, White et al., 1998, Sisley et al., 2000, Aalto et al., 2001, Damato et al., 2010). The aberrations of chromosome 6 were divided into 4 groups, independent of other common aberrations, such as loss of chromosome 1p, monosomy 3 and gain of chromosome 8q (Figure 4.1).

The first group consists of just chromosome 6p amplification located from 6pter-6p12.1, creating chromosome 6p trisomy, as represented in Figure 4.1 A. There were three UM samples which accounted for around 14% of the total samples is in the first group. The second group consists of the gain of chromosome 6p arm and the loss of chromosome 6q arm (isochromosome 6p or pseudo-isochromosome 6p). The aberrations of this group consist of gains spanning from 6pter-6p12.1 and losses spanning from 6qter-6q12 with a breakpoint near the centromere (Figure 4.1 B). There were seven UM samples which accounted for around 32% of the total samples in this group. The third group covers any other aberrations for chromosome 6, either the gain or loss of the whole chromosome or any other partial deletions or gains (Figure 4.1 C). However, the collection of this present study did not have any UM to fit in this group. The fourth group covers examples where there were no aberrations of chromosome 6, as represented in Figure 4.1 D, which were 12 UM samples that accounted for 54% of the total samples.

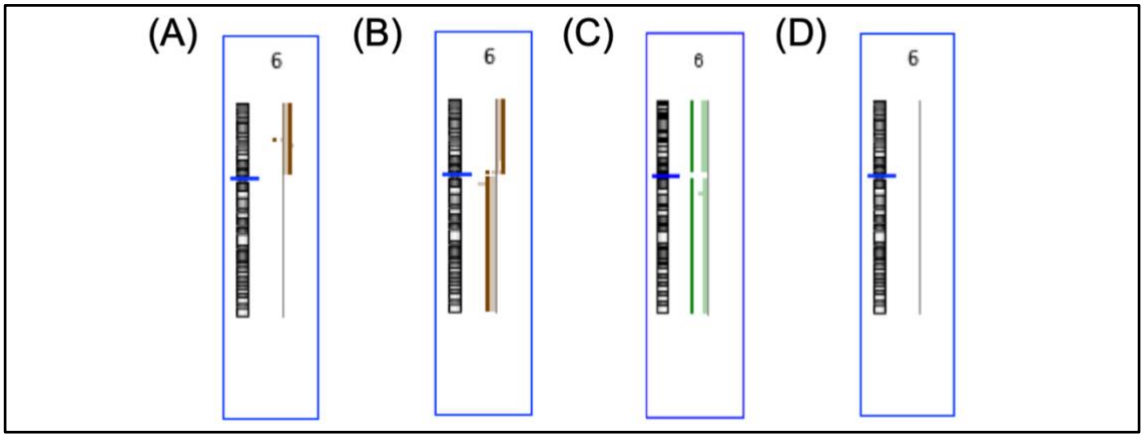

Figure 4.1: Groups classification of different gain and loss of chromosome 6 in UM.

The figure shows the types of aberrations of chromosome 6. The grey line in the middle represents zero line with gains on the right and losses on the left. **(A)** The amplification of chromosome 6p only, **(B)** gain of chromosome 6p and loss of 6q to form (isochromosome 6p). **(C)** An example of different aberrations of chromosome 6 either loss of whole chromosome 6 as seen or any other type of aberrations that does not follow groups **(A)** or **(B)**. This image was adapted from Dr. Alshammari's thesis (Alshammari, 2017). **(D)** The last group where no changes in chromosome 6 was identified. Images output for ideograms were taken from Agilent Genomic Workbench software v7.0.4.0. The ADM-2 algorithm was used to detect all the aberrations.

4.2.2 Confirmation of target genes on chromosome 6

In Dr. Alshammari's thesis, three potential genes *FOXQ1*, *FARS2* and *AMD1* were implicated in UM (Alshammari, 2017). Therefore, this study tried to confirm these findings by analysing a small independent cohort (22 UM samples). Furthermore, as the Nexus software (BioDiscovery) was unavailable, a different software (Agilent Genomic Workbench software) was used to independently confirm previous findings.

After searching for genes in group 1 (the gain of chromosome 6p only) (Figure 4.2 A), the results showed that the Agilent Genomic Workbench software called for more than 100 genes within the region. These genes included the *FARS2* gene that located at chr.6p25.1, but not *FOXQ1*. In addition, for group 2 (isochromosome 6p) more than 200 genes were called, but neither *FARS2* nor *FOXQ1* were called. However, it been found in group 2 that *AMD1* gene was called and this gene is located on chromosome 6q21 (Figure 4.2 B). Because the

software did not call for *FOXQ1*, which is located on 6p25.3, for the samples within groups 1 and 2, due to limitation in statistical tools, it was manually pointed out for illustration (Figure 4.2 C). Even though this outcome is not as reliable, the information broadly confirmed the previous findings which suggest these target genes are of interest for further study in UM.

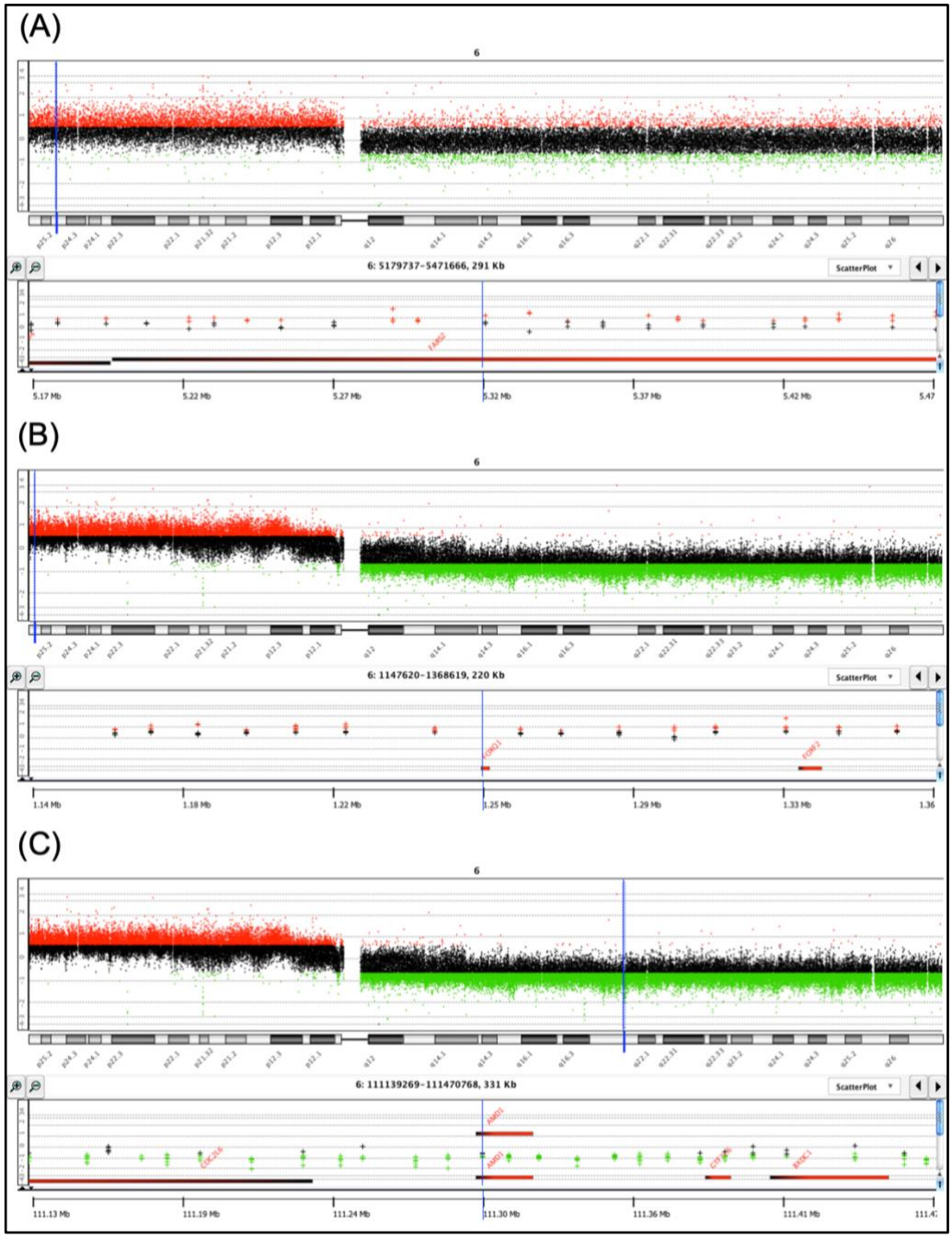

Figure 4.2: A high-resolution view of the gain of chromosome 6p and 6q with gene view.

The figure shows a high-resolution view with gene view in the Agilent Workbench Software shows the red dots represent the gain where the green dots represent the loss, the black dots in the middle represent the log ratio that been calculated for gain and loss (≤–0.1->0.6). **(A)** The call for *FARS2* gene in the gain of chromosome 6p only, evident in three UM samples. **(B)** The software also the call for *AMD1* gene in the isochromosome 6p, evident in seven UM samples. However, **(C)** the *FOXQ1* gene was pointed out for the isochromosome 6p, evident in seven UM samples. Images output for ideograms were taken from Agilent Genomic Workbench software v7.0.4.0. The ADM-2 algorithm was used to detect all the aberrations.

4.2.3 Clinicopathological details for UM data set

In the next stage, a larger group of UM samples were studied for the expression of the target genes. For this part of the study, a total of 80 UM had both array-CGH analyses and also available tissue sections for IHC. Unfortunately, the clinicopathological data was not always complete for all patients, due to patients becoming lost to follow up,

Thus, the range of UM patients' ages in this series between 13 and 89 years old with a median of 62, and the UM tumours' mean diameter ranged between 7.58 to 22.15 mm. In addition, the follow-up of this series ranged between 6 to 187 months with an average of 54.6 months. The follow up of patients with liver metastasis ranged between 7 to 131 months with an average of 33.5 months. In addition, the metastasis to other organs for UM patients other than liver ranged between 11 and 123 months with an average of 49.1 months. Three UM patients were lost to follow-up where there were 10 patients died from unknown causes and 4 patients died as a result of unrelated causes. Based on this clinical data, about 54% of male in this study have UM while female was accounted for around 46% of the cases. Thus, there were no statistical differences between males and females for the tumour distribution (Figure 4.3 A).

About 62% of the UM tumours in this study were choroid, and these correlated with good prognosis while 19% involved the ciliary body and were associated with poor prognosis (Figure 4.3 B). The inclusion of choroidal and ciliary body tumours comprised about 17% of all cases and were also associated with poor prognosis. One sample involved a tumour encompassing the choroid, ciliary body and iris. Besides the location, more than 45% of the tumours had a spindle cell, 10% epithelioid and around 44% have mixed cells morphology (Figure 4.3 C). A spindle cells morphology was correlated with better prognosis than epithelioid and mixed cells. The survival for UM patients with metastasis to the liver or other organs was lower compared to other UM patients (Figure 4.3 D). About 40% of patients with UM in this series had a low survival, while more than 17% died for reason unrelated to metastasis. About 33% of patients had metastasis to the liver and more than 11% to other organs.

The outcomes of this current clinical data for UM patients based on sex, age, tumour location, cell type and metastasis were comparable with previous reported studies (Mooy and De Jong, 1996, Kujala et al., 2003, Kaliki et al., 2015). In addition, this suggest that the clinicopathological data for UM in this study is representative, and this study has no selection bias.

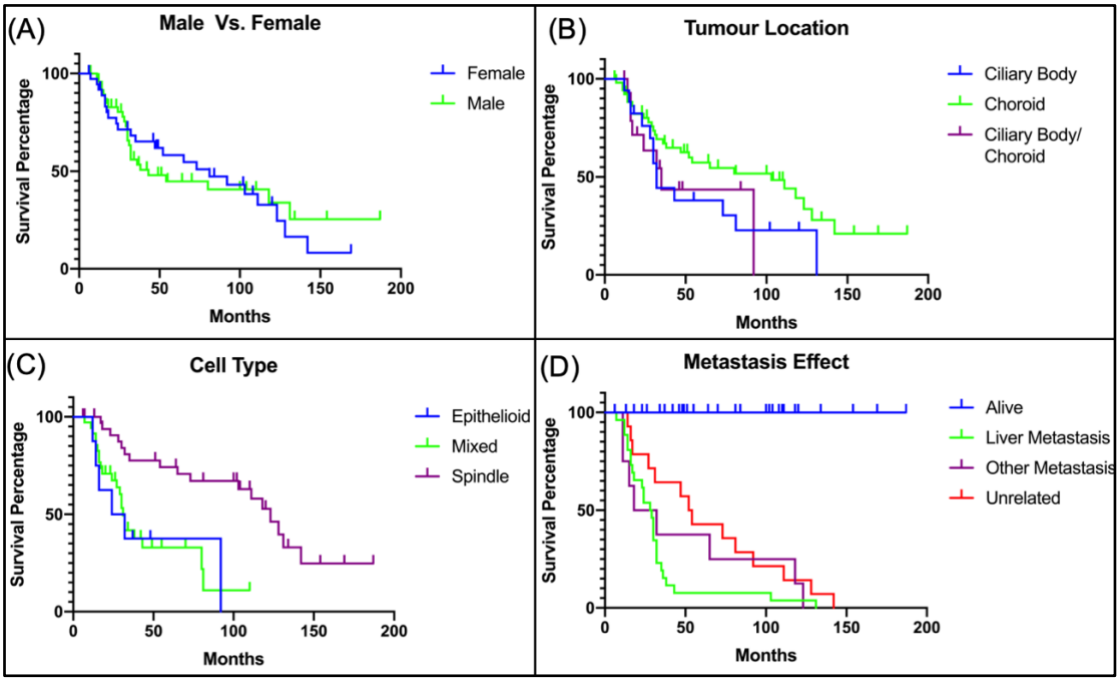

Figure 4.3: Kaplan-Meier analysis of patients' mortality based on sex, tumour location and cell type.

The Kaplan-Meier analysis of UM showed that the X-axis represents the survival time in months and the Y-axis represents the percentage of survival among UM patients. **(A)** Survival based on sex, indicating no significant difference. **(B)** Survival based on the location of the UM with ciliary body and ciliary body/choroid location having a poor prognosis than a choroid location only. **(C)** Survival according to cell type: a spindle cell types suggest longer survival than epithelioid and mixed cell morphology. **(D)** Survival according to metastasis: liver metastasis was associated with a poor prognosis, while metastasis to other organs showed a slightly better than liver metastasis. The unrelated deaths for UM patients were considered a separate event unrelated to UM prognosis. All figures output was produced and calculated using GraphPad Prism (v 8.0).

4.2.3.1 Survival analysis based on chromosome 6 groups

In respect to the groups that were used to categorise chromosome 6 alterations group 1 (gain of chromosome 6p arm only) comprised 20% of the series (16 out 80), group 2 (isochromosome 6p) around 21% (17 out of 80), group 3 (different chromosome 6 aberrations) around 19% (15 out of 80) and group 4 (no chromosome 6 changes) comprised 40% (32 out of 80) of all cases.

Survival analysis was undertaken to establish the effect of different chromosome 6 alterations and relationship to prognosis. For overall survival, group 1 have a better survival than the other three groups. Nonetheless, group 2 had poorer survival rate than group 1, but better than groups 3 and 4 (Figure 4.4 A).

Liver metastasis is the most common site for UM patient compared to other organs and it showed the worst overall survival, as seen earlier in Figure 4.3 D. The comparison of chromosome 6 groups in respect to liver metastasis identified that those with group 1 aberrations survived longer than in those other groups, while group 3 showed the worst survival rate. (Figure 4.4 B). This is because there are differences based on the type of chromosome 6 changes only and excluded the classical chromosomal aberrations in UM such as monosomy 3, loss of chromosome 1p and gain of chromosome 8q.

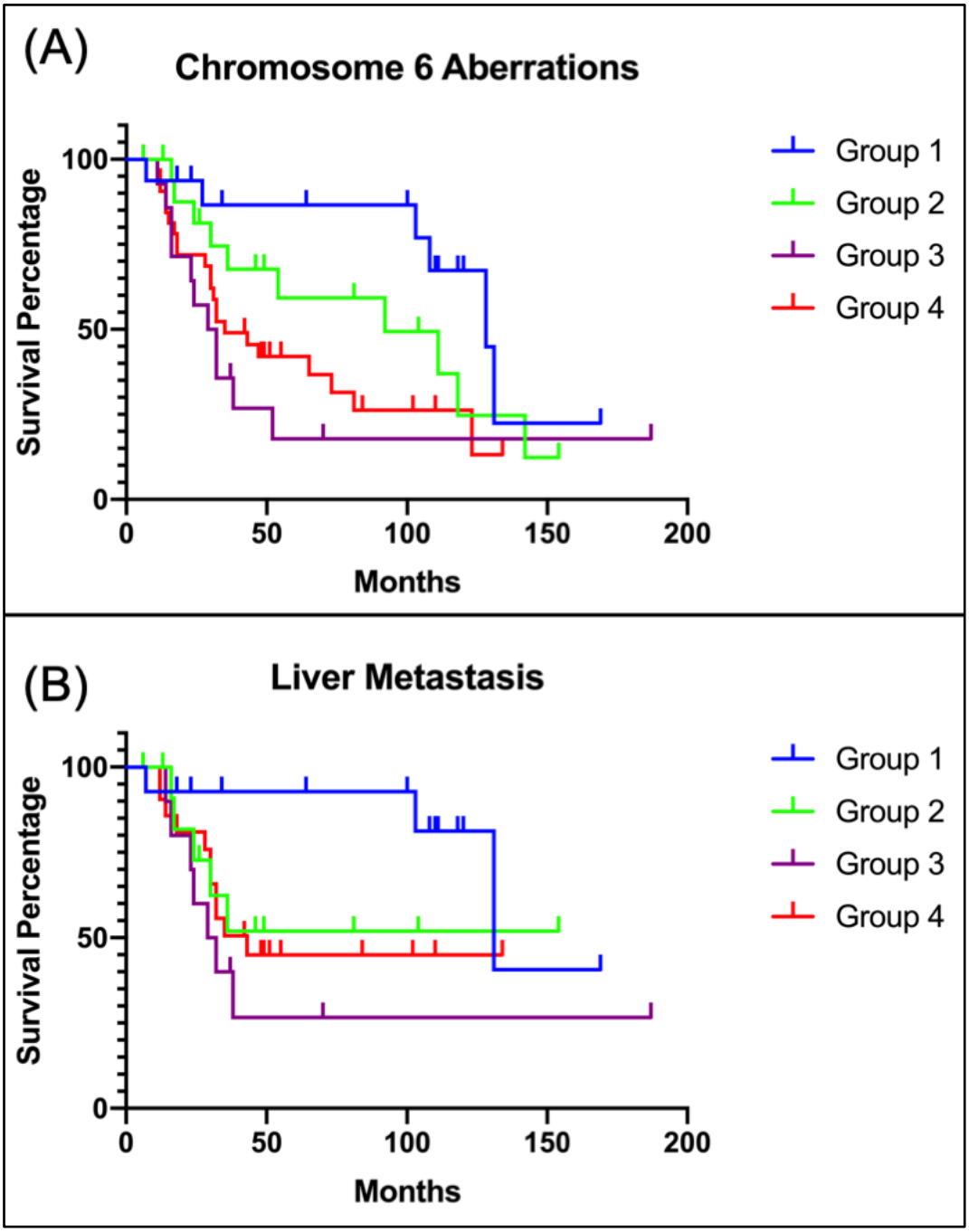

Figure 4.4: Kaplan-Meier analysis of the patients' mortality based on groups of altered chromosome 6.

The Kaplan-Meier analysis showed the X-axis represents the survival time in months and the Y-axis represents the percentage of survival among UM patients. **(A)** The overall survival rate based on chromosome 6 aberrations, showing that group 1 (gain of chromosome 6p only) had a better prognosis than groups 3 and 4 (different aberration on chromosome 6 and no chromosome 6 aberrations, respectively). Group 2 (isochromosome 6p) showed an intermediate survival rate in comparison with other groups. **(B)** In respect to liver metastasis only, group 1 had a better survival than other groups while group 3 had the worst survival, (n=56). These graphs were designed and calculated using GraphPad Prism (v 8.0).

4.2.4 IHC analysis for FOXQ1, FARS2 and AMD1

The total number of samples used for IHC in this study is 80 FFPE UM tissue sections, all with matched array-CGH to compare the subdivision of changes of chromosome 6 with survival. This number expanded the pilot study initially undertaken in Dr. Alshammari's thesis where there was also an issue with melanin pigmentation.

In this study, the optimisation of FOXQ1, FARS2 and AMD1 antibodies was done to determine the optimum staining of those proteins. Additionally, a melanin removal step was applied to enhance the quality of the tissue and decrease the melanin pigmentation in the UM tissues by incubating the slides with 1.5% of H_2O_2/PBS in the dark for overnight. This melanin removal technique was recommended by the Department of Pathology at Hallamshire Teaching Hospital in Sheffield UK, and enhanced the results. There was another issue with staining the negative controls at the beginning of the optimisation, however, it showed positive results although no primary antibody was added to those negative controls. To overcome this issue, an extra blocking step using an avidin/biotin blocking kit was added to the protocol before the addition of the primary antibody to avoid any endogenous biotin or non-specific binding present in the section. This was done to increase the specificity of the IHC and to eliminate any false positives appearing in the negative controls and UM tissue sections.

All of these tissue sections were treated the same with an addition of negative and positive control to each run to confirm findings. The slides were scanned using the automated slide scanner (Panoramic 350 Flash III) and were then stored as a digital image. The image was then viewed and analysed using Qupath software (Version 0.1.0) to visualise and zoom in and out for the whole of the tissue section.

4.2.4.1 Allred scoring system

The scoring system that was used for analysing those tissue sections was the Allred scoring system (Allred et al., 1998, Harvey et al., 1999). This system is a semi-quantitative assessment of the staining based on a proportion score (PS)

from 0 to 5 and an intensity score of the staining (IS) is from 0 to 3, which are added together to form a total score (PS+IS=TS) out of 8. The PS score is a six score system 0= no stain, 1=≤0.1% of the cells stained, 2=≤10% of the cells stained, 3=≤33% of the cells stained, 4=≤67% of the cells stained and 5= all the cells stained. The IS score depends on the four categories 0=no stain, 1= weak, 2= moderate and 3= high stain. This scoring is applied for both the nucleus and the cytoplasm. The assessment of this scoring system was by three independent scorers (MA, AA) and overview by KS, which show a good agreement for the outcome. Finally, all data were analysed using non-parametric one-way ANNOVA with SEM by GraphPad Prism (Version 8.0) software as a statistical calculation for the scoring of the analysed tissue.

4.2.4.2 FOXQ1 protein expression

The FOXQ1 protein is mainly expressed in the nucleus. Thus, the IHC was used to assess the FOXQ1 protein expression in 80 UM tissue sections. The control used to evaluate the protein expression of FOXQ1 was normal kidney tissue. This showed that there was staining in the renal tubules which varies between moderate and strong, in comparison with the negative normal kidney tissue control (Figure 4.5 A and B).

The 80 UM FFPE tissue sections were stained with FOXQ1 antibody with the extent of staining varying from one tissue to another, regardless to their groups. Some UM tissue samples showed low nuclear staining for FOXQ1 protein, as seen in Figure 4.5 C. In addition, some of the UM samples had a high FOXQ1 staining in both the cytoplasm and the nucleus (Figure 4.5 D) while other UM samples showed a mixed staining from cell to cell between low to moderate, as appeared in Figure 4.5 E. The UM samples showed more staining of the nucleus than of the cytoplasm, which is consistent with the reported staining.

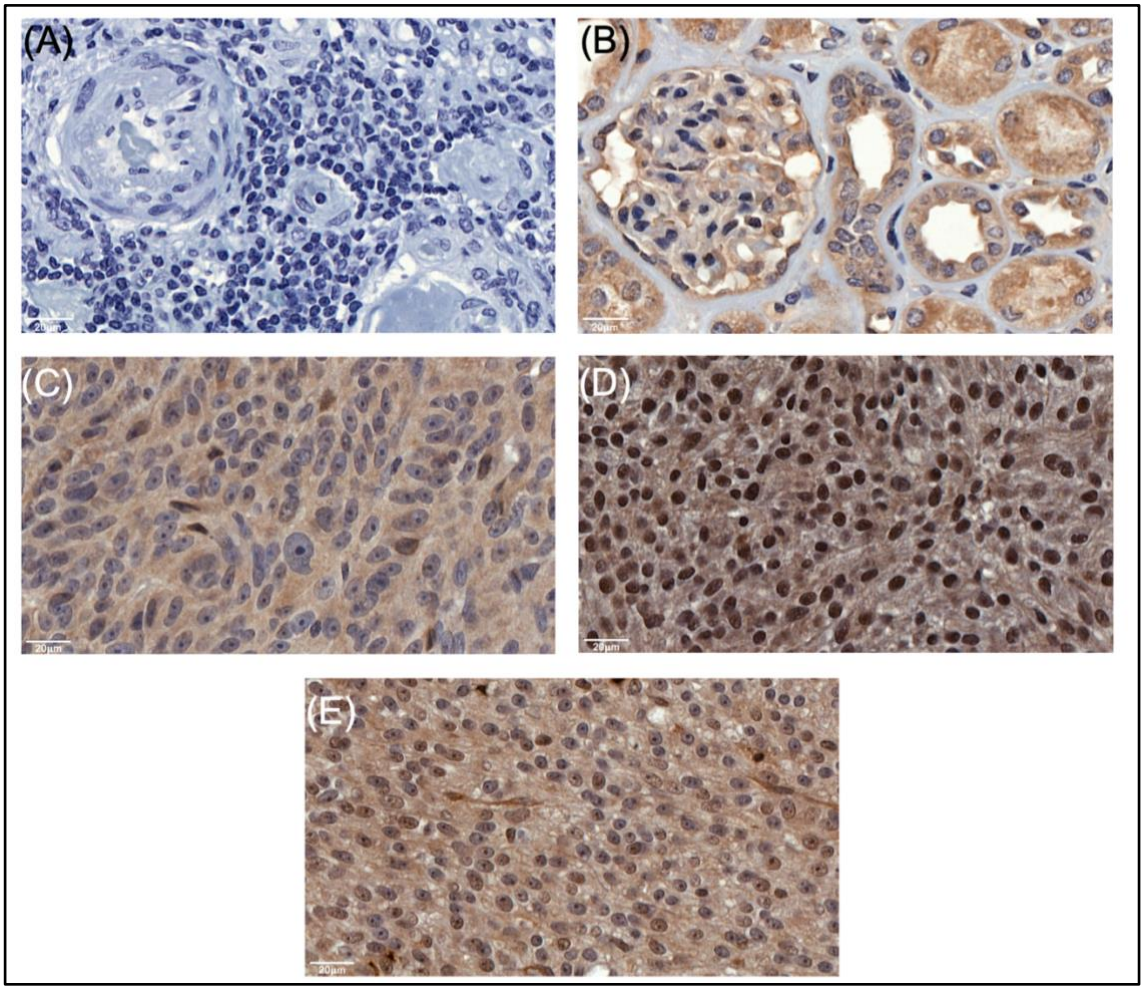

Figure 4.5: The expression of FOXQ1 protein in UM tissue sections using IHC.

(A) Negative control of normal kidney FFPE tissue section without any FOXQ1 primary antibody and only haematoxylin counter staining. **(B)** Same normal kidney FFPE tissue section with FOXQ1 primary antibody, immune staining mainly in the renal tubules (brown) rather than the nucleus (blue), varying between moderate to strong, as recommended by the manufacturer. **(C)** The staining of FOXQ1 was mainly low for both the cytoplasm and nucleus with exception of a few cells. **(D)** In contrast, the staining of FOXQ1 was high in the cytoplasm encompassing the area of nucleus. **(E)** Represents the moderate nucleus staining of FOXQ1 that appears to vary between cells. All images were taken using Qupath software (v 0.1.0).

The analysis of FOXQ1 protein expression using Allred scoring system resulted in all groups having the staining in the nucleus more than cytoplasm (Figure 4.6 A). Based on the Allred scoring system, there was no significant difference between groups 1, 3 and 4 of chromosome 6 aberrations which their intensity for the nucleus is 5, except for the group 2 that showed a slight increase for the intensity compared to other groups. The analysis using one-way ANOVA showed

the *p* value of 0.003, which is significant in respect to the outcome for FOXQ1 protein.

In addition, the survival analysis was done to compare the protein expression of FOXQ1 with UM patients' survival. Therefore, the expression of FOXQ1 been grouped into three groups based on the TS of the nucleus (Figure 4.6 B). This is because, as mentioned before, the expected expression of FOXQ1 is in the nucleus, which is similar to the outcome of this study. The TS score for the low expression group is between (0-2), the moderate expression group is between (3-5) and the high expression group us between (5-8). Therefore, the survival analysis showed no significant difference between the expression of FOXQ1 and the overall survival.

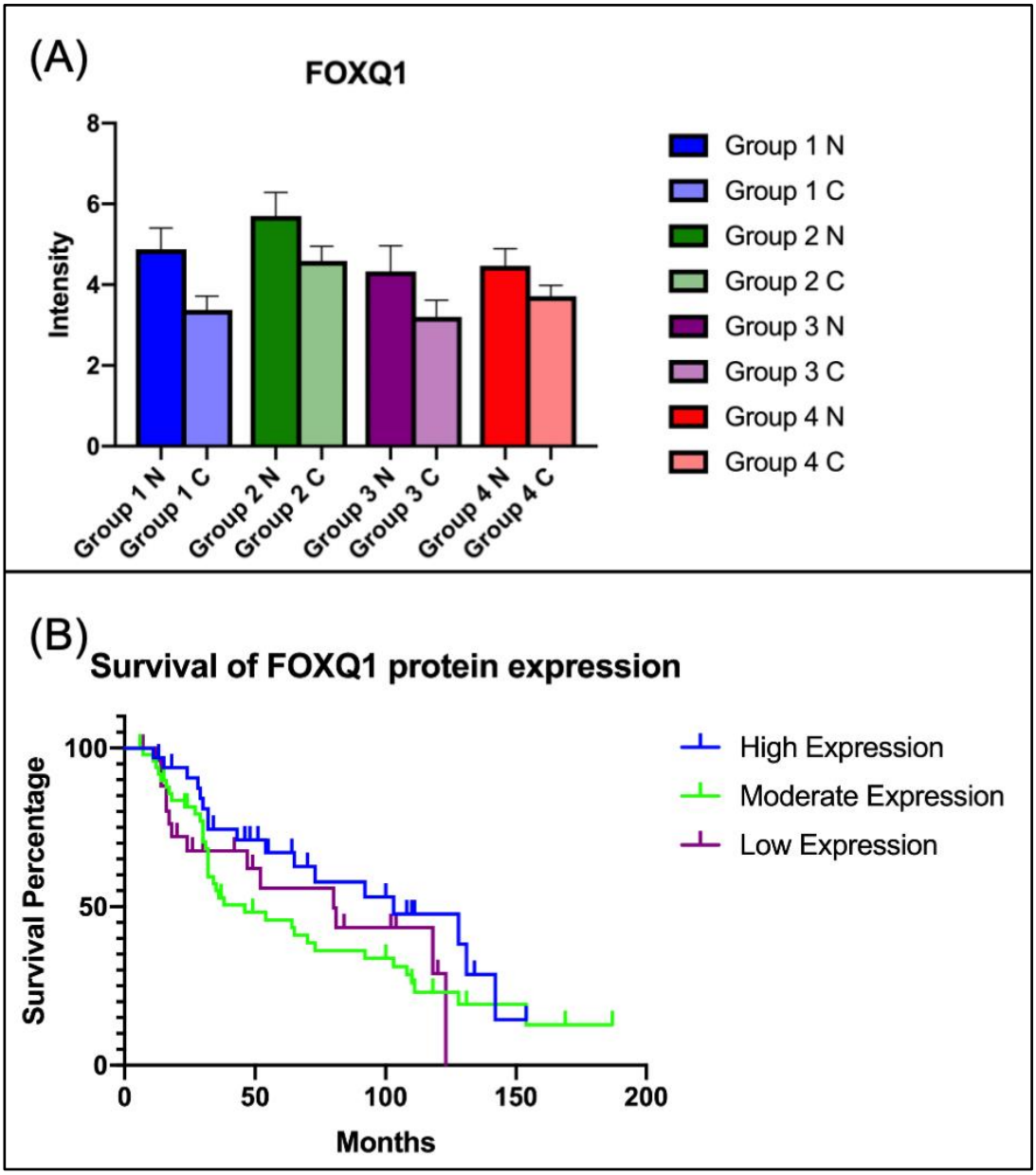

Figure 4.6: Allred scoring and Kaplan-Meier analysis of FOXQ1 protein expression.

(A) Based on the chromosome 6 groups, and the amount of TS for each nucleus (N) and cytoplasm (C) was calculated based on the Allred scoring system. It shows the staining is more in the nucleus than the cytoplasm. The results seemed broadly equal among in groups 1, 3 and 4 (5 for nucleus and 3 for cytoplasm) except a slight increase in group 2 (isochromosome 6p), around 6 for the nucleus and around 5 for cytoplasm. The *P* value is 0.003. **(B)** The Kaplan-Meier survival analysis for FOXQ1 shows that the X-axis represents the survival time in months and the Y-axis represents the percentage of survival among UM patients. The high, moderate and low nuclear protein expression for FOXQ1 shows no significant difference for survival.

All charts were designed and calculated using GraphPad Prism (v 8.0).

4.2.4.3 FARS2 protein expression

IHC was used to assess the expression of FARS2 protein in 80 UM tissue sections. The FARS2 protein is usually expressed in the cytoplasm. The control used to evaluate the protein expression of FARS2 was human colon carcinoma. This showed that the staining was mainly in the cytoplasm with a slight nuclear staining, in comparison to the negative human colon carcinoma tissue control (Figure 4.7 A and B).

The 80 UM FFPE tissue sections were stained with FARS2 antibody with the staining varying from tissue to another, regardless to their groups. For example, there was a low cytoplasmic and nucleus staining for FARS2 protein among some of the UM tissue samples (Figure 4.7 C). Additionally, some of the UM samples showed a strong FARS2 protein expression, as seen in Figure 4.7 D, while there was a mix cytoplasmic staining for some UM tissue sections for FARS2 that varies between low to moderate from cell to cell, as appeared in Figure 4.7 E. Thus, these UM samples showed more staining of the cytoplasm than the nucleus.

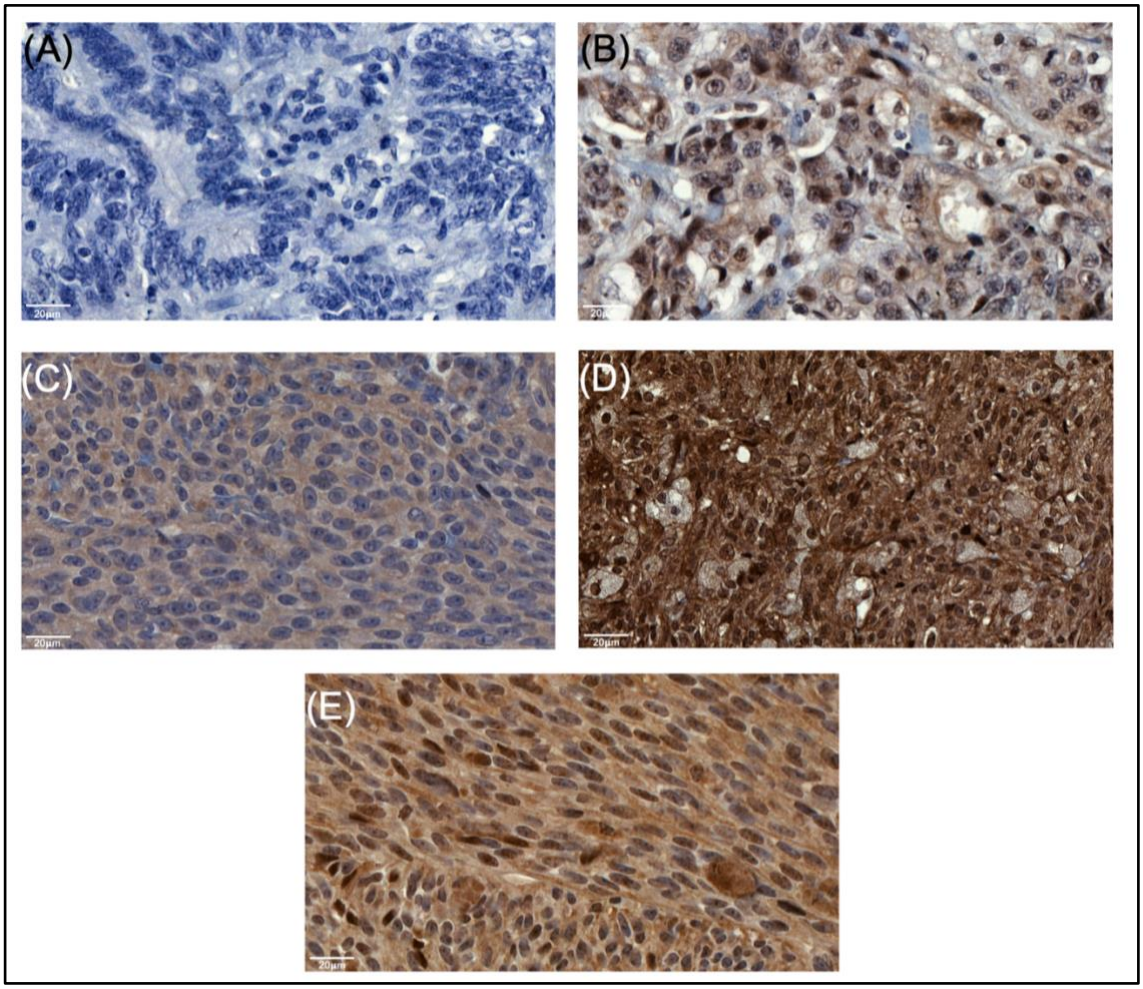

Figure 4.7: The expression of FARS2 protein in UM tissue sections using IHC.

(A) Negative control of human colon carcinoma FFPE tissue section without any FARS2 primary antibody and only haematoxylin counter staining. **(B)** Same human colon carcinoma FFPE tissue section with FARS2 primary antibody, showing some staining was in the cytoplasm (brown), while some of the immune staining in the nucleus varying between low and moderate. **(C)** The staining of FARS2 was low and neither the cytoplasm nor nucleus were strongly stained. In contrast, **(D)** the staining of FARS2 was high in the cytoplasm (brown) also encompassed the area of the nucleus. **(E)** Shows the mix staining for FRAS2 from one cell to another. All images were taken using Qupath software (v 0.1.0).

The analysis of FARS2 protein expression using the Allred scoring system revealed that the staining to be more in the cytoplasm than nucleus, as mentioned before, although there were broadly low among all chromosome 6 groups (Figure 4.8 A). The UM samples showed that there was no significant difference between chromosome 6 aberration groups and their intensity varies between the total of 2 to 4, expect for group 4 (no changes in chromosome 6) which had a slight increase. The analysis using one-way ANOVA showed a *p* value of <0.0001, indicating significance in the respect of the FARS2 protein.

Similar to FOXQ1, the survival analysis was done to compare the protein expression of FARS2 with patients' survival (Figure 4.8 B). Therefore, the expression of FARS was grouped into three groups based on the TS of the cytoplasm, because FARS2 was expected to be expressed in the cytoplasm more than nucleus, which similar to the outcome of this study. The TS of the low expression group is between (0-2), the moderate expression group is between (3-5) and the high expression group is between (5-8). Although the high FARS2 expression showed a lower survival at early months compared to the low FARS2 expression, the results showed that there is no significant difference between the expression of FARS2 and the overall survival.

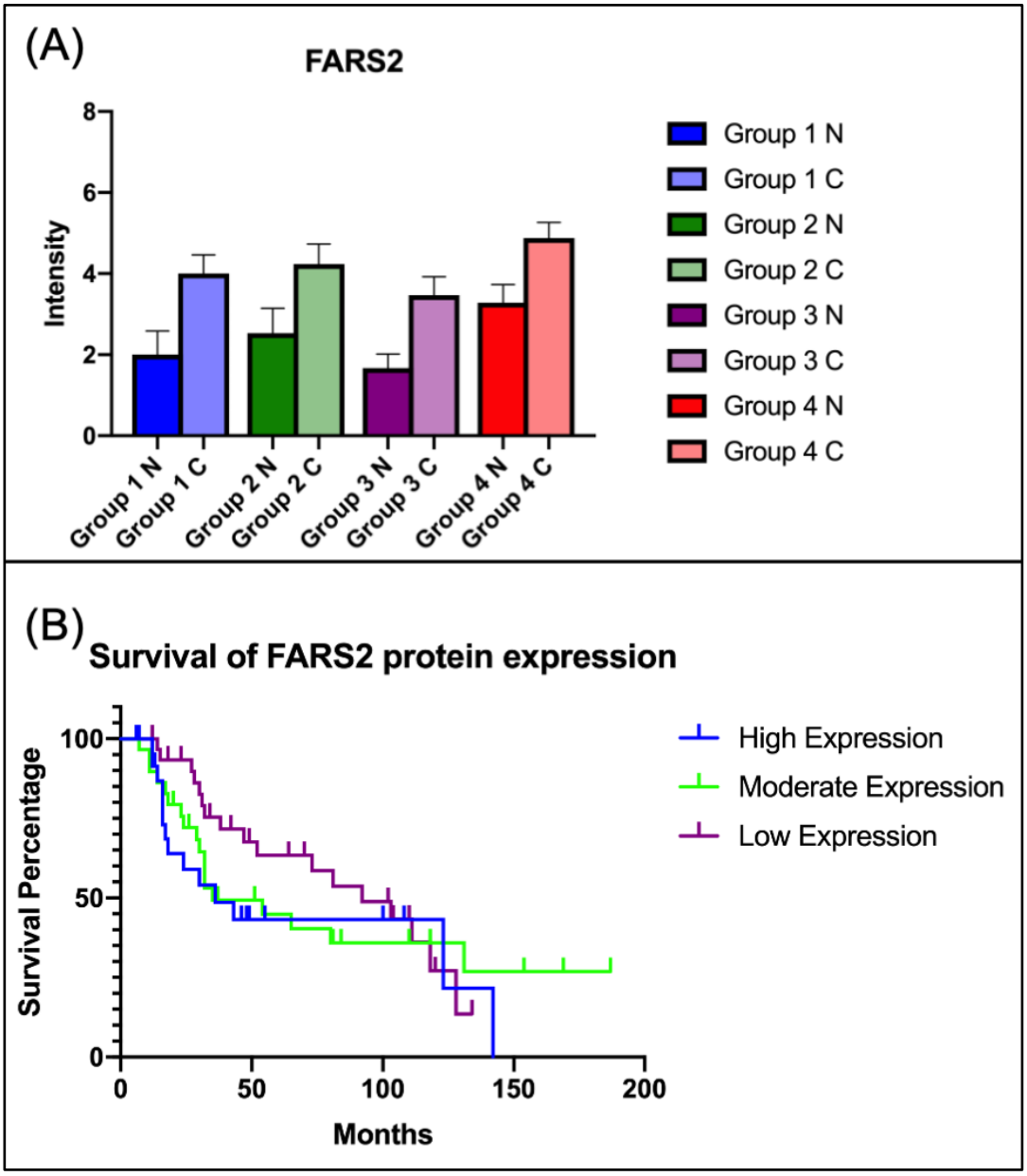

Figure 4.8: Allred scoring and Kaplan-Meier analysis of FARS2 protein expression.

(A) Based on the chromosome 6 groups, and the amount of TS for each nucleus (N) and cytoplasm (C) was calculated based on the Allred scoring system. The cytoplasm appeared to have more staining than the nucleus, as estimated before. The results between the three groups 1-3 seemed broadly the same (2 for nucleus and around 4 for cytoplasm) except for a slight increase in group 4 (no changes in chromosome 6), of around 5 for the cytoplasm and around 4 for nucleus. The *P* value is <0.0001. **(B)** The Kaplan-Meier survival analysis for FARS2 showed that the X-axis represents the survival time in months and the Y-axis represents the percentage of survival among UM patients. The high, moderate and low protein expression for FARS2 showed no significant difference for survival, although the high expression showed a slight lower survival at early months compared to the low FARS2 expression.

All charts were designed and calculated using GraphPad Prism (v 8.0).

4.2.4.4 AMD1 protein expression

Besides FOXQ1 and FARS2, IHC was used to assess the AMD1 protein expression in 80 UM tissue sections. The main site the AMD1 protein expression is cytoplasm. The control used to evaluate the protein expression of AMD1 was mammary cancer tissue section. Staining was evident in the cytoplasm more than the nucleus and it varies between moderate to high, in comparison with the negative mammary cancer tissue control (Figure 4.9 A and B).

The 80 UM FFPE tissue sections were stained with AMD1 antibody and it appeared there was a difference in the level of staining intensities among the UM tissue sections, regardless to their chromosome 6 groups. For example, there was low cytoplasm and nuclear staining for AMD1 protein among some of the UM tissue samples (Figure 4.9 C). Additionally, some of the UM sample had a high expression of AMD1 in the cytoplasm, as seen in Figure 4.9 D, while other UM had a mix of cytoplasm staining that varies between low to moderate from cell to cell, as appeared in Figure 4.9 E. Therefore, the expression of AMD1 in UM samples overall showed more cytoplasm staining than nucleus, which is consistent with the reported staining.

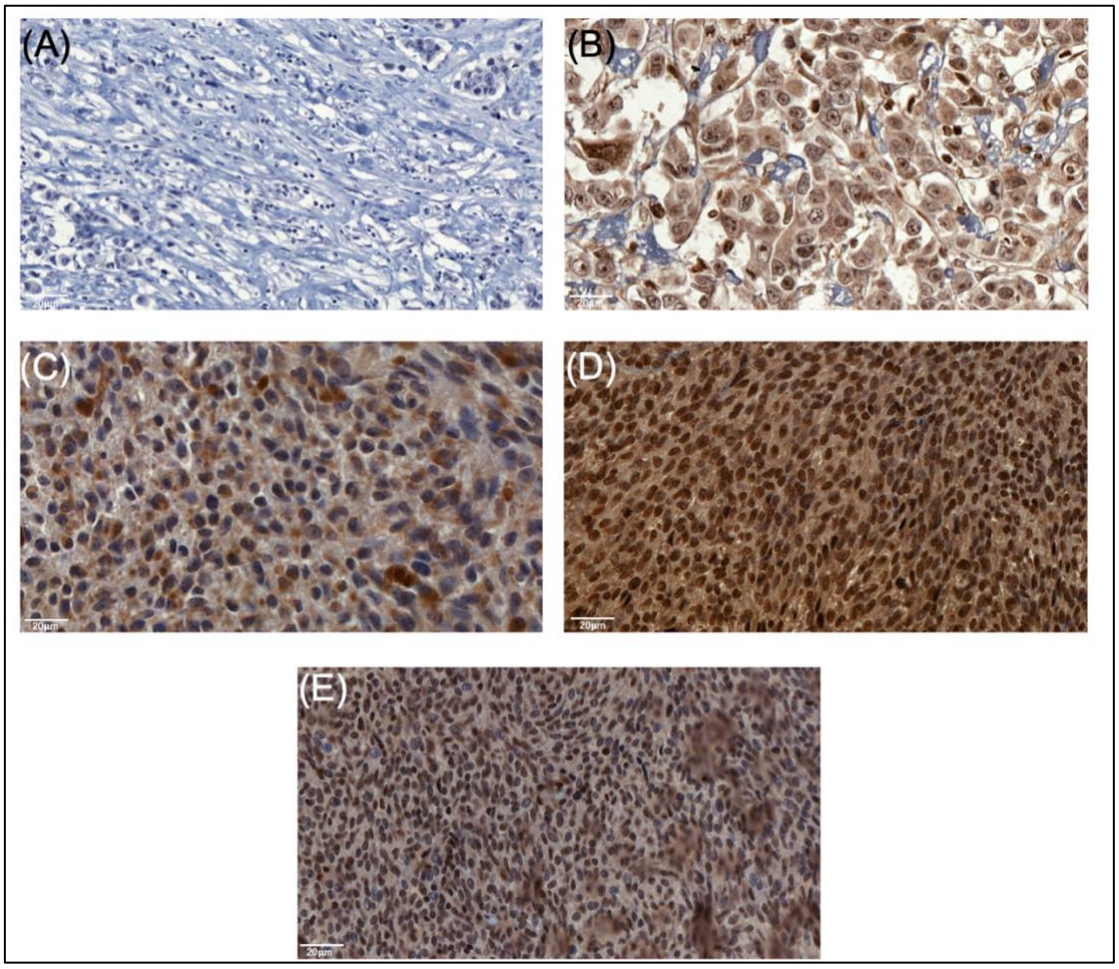

Figure 4.9: The expression of AMD1 protein in UM tissue sections using IHC.

(A) Negative control of mammary cancer FFPE tissue section without any AMD1 primary antibody and only haematoxylin counter staining. **(B)** Same mammary cancer FFPE tissue section with AMD1 primary antibody revealing some immune staining was mainly in the cytoplasm (brown) that appears to be between moderate to strong. **(C)** The staining of AMD1 was lower for both the cytoplasm and nucleus, and it showed a small amount of melanin pigmentation remaining even after the recommended treatment. In contrast, **(D)** the staining of AMD1 was high in the cytoplasm and nucleus also. **(E)** Show the mix of staining for AMD1 from one cell to another. All images were taken using Qupath software (v 0.1.0).

The analysis of AMD1 protein expression using the Allred scoring system revealed the cytoplasm is to be more stained than the nucleus amongst all the UM samples that were analysed (Figure 4.10 A). Remarkably, there was a significant difference between chromosome 6 aberration groups, based on the Allred scoring system. In group 1 (gain of chromosome 6p only), there was an increase in staining in both the nucleus and cytoplasm between 5 and 6, respectively, which is similar to group 4 (no chromosome 6 changes). Groups 2 (isochromosome 6p) and 3 (different aberrations in chromosome 6), however, showed a significant reduction in staining, at between 3 and 4 for both nucleus and cytoplasm. The analysis using one-way ANOVA showed *p* value of <0.0001 indicating a significance of the outcome in respect to AMD1 protein.

Moreover, the survival analysis was done to compare the protein expression of AMD1 with patients' survival and it was also grouped into three groups based on the TS of the cytoplasm (Figure 4.10 B). The TS of the low expression group is between (0-2), the moderate expression group is between (3-5) and the high expression group is between (5-8). Therefore, the survival analysis showed no significant difference between the expression of AMD1 and the overall survival. However, there was a slight difference between high expression and low or moderate expression of AMD1 for survival beyond 50 months. Conversely, this was the opposite to the survival for groups 2 and 3 where chromosome 6q was deleted (Figure 4.4 A)

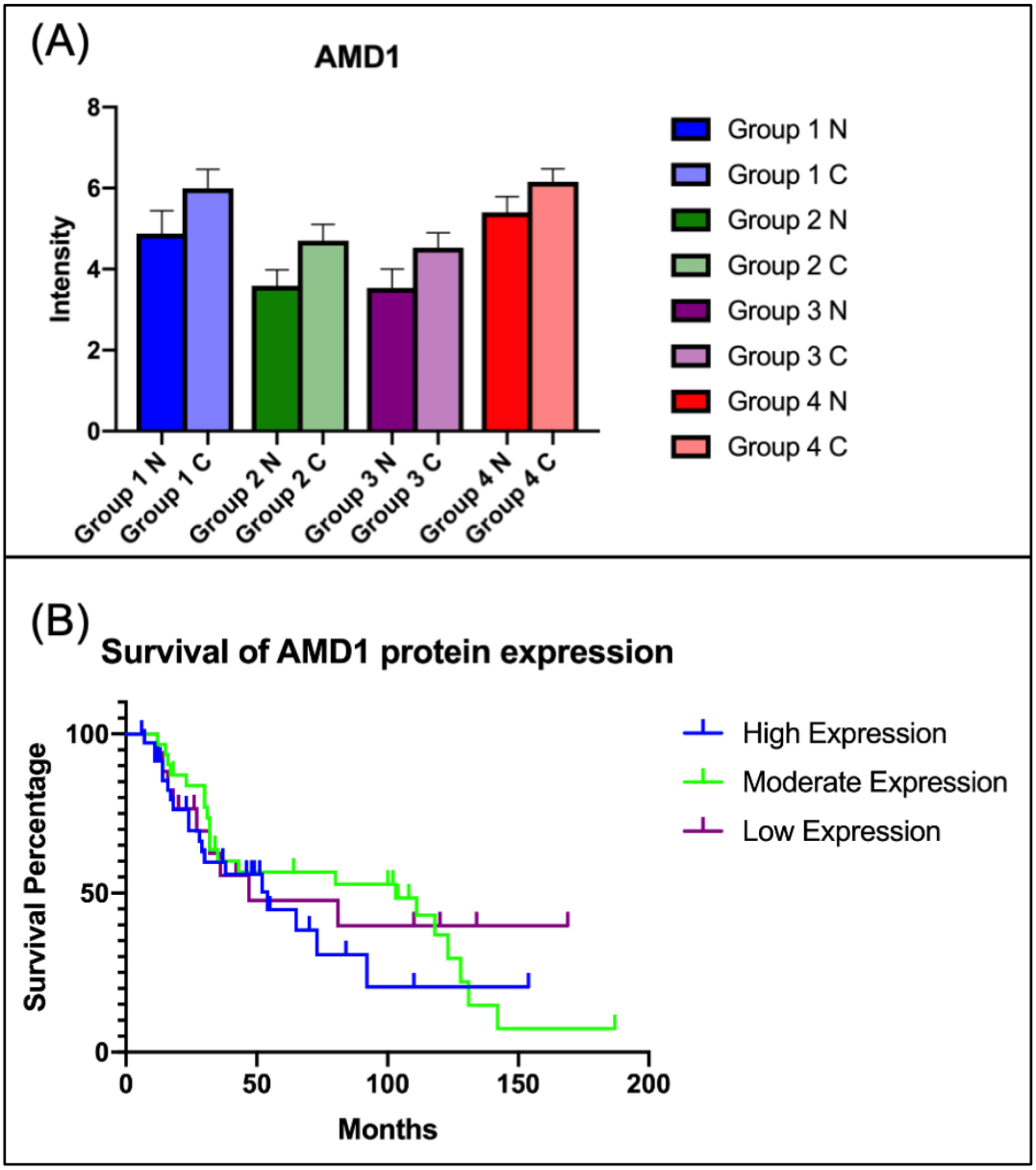

Figure 4.10: Allred scoring and Kaplan-Meier analysis of AMD1 protein expression.

(A) Based on the chromosome 6 groups, and the amount of TS for each nucleus (N) and cytoplasm (C) was calculated based on the Allred scoring system. The cytoplasm appeared to have more staining than the nucleus, as described earlier. Interestingly, the results for group 1 (gain in chromosome 6p) and group 4 (no changes in chromosome 6) appeared to be equal with a TS between 5 to 6. There was a decrease in groups 2 (isochromosome 6p) and group 3 (different changes in chromosome 6), in comparison with the other groups, however, with scores of between 3 and 4. The *P* value is <0.0001. **(B)** The Kaplan-Meier survival analysis for AMD1 showed that the X-axis represents the survival time in months and the Y-axis represents the percentage of survival among UM patients. The high, moderate and low protein expression for AMD1 showed no significant difference for survival, although from this figure the differences between these expressions of AMD1 appeared to occur after 50 months.

All charts were designed and calculated using GraphPad Prism (v 8.0).

4.3 Discussion

Here array-CGH on 22 UM samples confirmed groupings of chromosome 6 abnormalities and the previously identified genes (*FOXQ1*, *FARS2* and *AMD1*) were still implicated in different subsets of UM. Expression of target genes was investigated in a series of 80 UM samples that could be subdivided similarly on the basis of chromosome 6 changes. Based on the clinicopathological data of this study, the survival for UM patients were in agreement with a previous reports (McLean et al., 1982, Seregard and Kock, 1995, Kujala et al., 2003, Diener-West et al., 2005, Shields et al., 2009, Shields et al., 2012). The clinical data of this study were collected after the results been done and that indicated there were no selection bias toward any type of UM and there were treated anonymously to have a clear representation of the UM outcome.

4.3.1 Chromosome 6 changes and prognosis

The association of gain chromosome 6p with disomy 3 in UM appears to occur early in the progression of some UM (Parrella et al., 1999). The association of different chromosome 6 aberrations in UM with survival has recently been considered (Drabarek et al., 2019), which they found that gain of chromosome 6p and isochromosome 6p are considered as a good and intermediate prognostic markers in UM, respectively. Thus, the association in this study was also generated to confirm the effect of different chromosome 6 alterations on the patient's overall survival (Figure 4.4 A). Based on the chromosome 6 groups, it showed that group 1 (gain of chromosome 6p only) usually have the longest survival while group 2 (isochromosome 6p) have a shorter survival than group 1, however, group 3 (gain or deletion of whole chromosome 6) and group 4 (disomy 6) showed the worst prognosis and with a low survival rate. The findings of this current study confirm that chromosome 6q indicate a poorer outcome for UM patients and also confirmed the initial findings of the previous study undertaken by our group (Alshammari, 2017).

4.3.2 Confirmation of target genes

In the earlier study, Nexus software has been used as opposed to Agilent Workbench software used in the present study. The Nexus software uses an algorithm called FASST2 (Fast Adaptive States Segmentation Technique 2) for the aberration calls. This algorithm uses an approach of calling based on Hidden Markov Model (HMM), which estimates the copy number based on many states of the probe. Similar to the Nexus software, the algorithm of Agilent Genomic Workbench software that been used in this study is ADM-2, which makes the calls based on the states of the probes, yet it lacks the statistical tools that provided in the Nexus software to identify genes. The statistical tools that are available for Nexus software are significance testing for aberrant copy number (STAC) (Diskin et al., 2006), and genomic identification of significant targets in cancer (GISTIC) (Beroukhim et al., 2007). These statistical tools helped to precisely identify *FOXQ1*, *FARS2* and *AMD1* genes in the aberrant chromosome 6 (Alshammari, 2017). Therefore, despite lack of similar statistical tools and smaller sample, the results of this study were broadly supportive of the previous findings with FARS2 called for group 1 and AMD1 called for group 2; however, group 3 cases were not in this small series. This independent confirmation suggested that further exploration of these genes was warranted.

4.3.3 Are target genes potentially relevant to UM?

UMs are now well characterised by mutations of *BAP1* and preferential deletion of *BAP1* (Harbour et al., 2010), There has however been much debate as to whether the mutations of *BAP1* confer a poor outcome, as previous studies suggest that the expression of BAP1 in the nucleus is more reliable than the assessment of the mutations (Shah et al., 2013, Koopmans et al., 2014b, van de Nes et al., 2016, Field et al., 2018).

In this study, the expression of FOXQ1 did not appear to be predictive of outcome for UM patients (Figure 4.6). The *FOXQ1* gene on chromosome 6p25.3 consists of 2319bp which encode for FOXQ1 protein that has 403 amino acids (Bieller et al., 2001). It was first discovered in *Drosophila* melanogaster and there was little known about its function and effect in humans at that time (Weigel et al., 1989).

Subsequently, It has found that the forkhead box (FOX) family is a transcription factor and consists of more than 100 members that been classified into 19 subfamilies (Kaestner et al., 2000, Benayoun et al., 2011). These subfamilies are involved in various human cellular functions such as, cell proliferation, differentiation and apoptosis, as reviewed in Carlsson and Mahlapuu (2002). In addition to their cellular function, these genes have a role in different human health properties, as an example, embryonic development, metabolism of glucose and lipid, ageing and immune regulation.

Thus, *FOXQ1* is a key oncogenic transcription factor gene among the Fox family of genes and it has an essential role in tumorigenesis (Cao et al., 2004, Feuerborn et al., 2011). The overexpression and dysregulation of *FOXQ1* oncogene is also found in other types of cancers including ovarian and breast cancers (Gao et al., 2012, Sehrawat et al., 2013), cervical cancer (Fan et al., 2014), gastric cancer (Xiang et al., 2015), pancreatic cancer (Bao et al., 2014), bladder cancer (Zhu et al., 2013), glioma (Sun et al., 2013) and liver cancer (Xia et al., 2014).

The expression of FOXQ1 has a role within the Wnt pathway and the transforming growth factor (TGF) pathway, both of which are considered to be oncogenic signalling pathways that may transform normal cells into cancerous ones (Christensen et al., 2013, Fan et al., 2014). In addition, Peng et al, found that *FOXQ1* serves as a mediator between Wnt and TGF pathways during the tumorigenesis of colorectal cancer (Peng et al., 2015). However, lack of growth control in UM that is upregulated by TGF pathway has found to play a role in the progression of UM cells to the liver (Myatt et al., 2000, Woodward et al., 2002, Woodward et al., 2005). Although the *FOXQ1* oncogene implicated in the TGF pathway, the expression of FOXQ1 does not appear to be relevant to UM outcome.

Similar to FOXQ1, the expression of FARS2, on chromosome 6p25.1, was not significant and did not appear to be predictive of outcome for UM patients (Figure 4.8). *FARS2* gene is a nuclear gene encodes for mitochondrial aminoacyl-transfer RNA (tRNA) synthetases which use phenylalanine to catalyse and charge amino acids on their cognate tRNA. Mutations in this gene have been

linked to several infantile and adult diseases, as reviewed in Konovalova and Tyynismaa (2013). A few research studies have reported that mutation of *FARS2* mainly causes neurological autosomal recessive disorders such as combined oxidative phosphorylation deficiency 14 (COXPD14) (Elo et al., 2012, Shamseldin et al., 2012, Almalki et al., 2014) and spastic paraplegia 77 (SPG77) (Vernon et al., 2015, Yang et al., 2016). No studies however have examined whether the *FARS2* gene is linked to oncogenesis.

Based on the outcome of this study, *AMD1* is an interesting candidate for UM as it is supported by the findings of IHC analysis for AMD1 expression for groups that have a deletion in chromosome 6q, as seen in Figure 4.10 A. A common feature of tumour suppressor genes in different cancer types is somatic deletion that acts as a driver for tumorigenesis.

The *AMD1* gene is found on chromosome 6q21, which it consists of around 22kb and contains 9 exons (Maric et al., 1992). It encodes for S-adenosylmethionine decarboxylase 1 (AdoMetDC) which is the main enzyme in the biosynthesis of polyamines and its product serves as a major donor for the catalytic activity of various reactions involving DNA methylation, RNA, proteins and metabolites (Maric et al., 1995, Chiang et al., 1996, Roje, 2006, Pegg, 2009b, Lu and Mato, 2012). Additionally, AdoMetDC appear to have an imperative role for embryonic stem cell (ESC) self-renewal and the differentiation of neural precursor cells (Zhang et al., 2012). Scuoppo and colleagues identified a number of tumour suppressor genes that affect lymphoma, one of which was *AMD1* (Scuoppo et al., 2012). Beside lymphoma, the reduction in AMD1 expression in prostate cancer was associated with the inhibition of the polyamine pathway, leading to inhibition of cancer growth (Gerner et al., 2005, Kaul et al., 2010). In a recent study by Zabala-Letona et al., identified that when AMD1 is upregulated it activates the rapamycin complex 1 (mTORC1) pathway in prostate cancer, which regulates the dynamics of polyamine and is essential for tumorigenicity (Zabala-Letona et al., 2017). Furthermore, the inhibition of the mTOR pathway was also found to have a significant delay of the UM growth using cell lines and patient-derived xenograft (Amirouchene-Angelozzi et al., 2014). Although this current outcome of AMD1 represent a small study and the findings need to be validated

for those UM patients with chromosome 6q deletions, which seem to have the worse prognosis, the findings of IHC and survival seem to contradict the role of AMD1, as seen in Figure 4.10 B. Therefore, the increased expression of AMD1 correlates with the presence of chromosome 6q, which this study proposed that *AMD1* has a tumour suppressor role in UM.

In summary, this study independently confirmed potential genes of interest in the targeted regions of chromosome 6 that been previously identified using GISTIC and STAC by Alshammari (2017). This study validated these findings using IHC to determine the expression of those genes on UM tissue sections. The expression of AMD1 is the most interesting and significant, as shown in Figure 4.10 A. The effect therefore of *AMD1* on UM warrants further investigation to understand its implication to UM.

Chapter 5: The knockout effect of AMD1 on UM cell lines

5.1 Introduction

In the previous chapter, the assessment for AMD1 expression was significantly reduced among groups that have deletion in chromosome 6q (Figure 4.10 A). There was some indication that loss of chromosome 6q was associated with a poorer outcome (Figure 4.4 A), but the reduced expression of AMD1 did not associate with poorer prognosis, if anything the reverse was true.

As previously mentioned, *AMD1* is around 22kb, consists of 9 exons and encodes for S-adenosylmethionine decarboxylase (AdoMetDC), which is an essential enzyme for the polyamine pathway (Maric et al., 1992, Maric et al., 1995). There are three types of polyamines produced in mammals, putrescine, spermidine, and spermine, which are naturally found in all types of cells and have an essential role in proliferation and various cellular events, as reviewed by Pegg (2009a). These polyamines are positively charged and their charge allows them to bind with negatively charged molecules such as DNA, RNA and some proteins (Childs et al., 2003). Putrescine is formed by ornithine decarboxylase (ODC), which is therefore considered to be a rate-limiting factor in the polyamine pathway (Pegg, 2006). The overexpression of ODC activity has been reported to have a role in various types of cancers such as, squamous cell carcinoma, colorectal and prostate cancer (Zhang et al., 2006, Shukla-Dave et al., 2016, He et al., 2017).

The other rate-limiting enzyme in the biosynthesis of polyamine is AdoMetDC, which converts the putrescine into higher polyamines such as spermidine and spermine, respectively (Pegg et al., 1998). AMD1 has been shown to be essential for embryonic development in mice, and indeed the knockout of *AMD1* is lethal in mice (Nishimura et al., 2002). Besides ODC, *AMD1* acts as a tumour suppressor gene and has been correlated with a number of cancers, including lymphoma, colorectal and prostate cancers (Zhang et al., 2006, Scuoppo et al., 2012, Zabala-Letona et al., 2017). Targeting *AMD1* in polyamine biosynthesis pathway therefore offers the potential to understand in-depth its relation to the development and progression of UM.

In this current study, an initial exploration of AMD1 function in UM cell was undertaken. To achieve this, a relatively recent technology called Clustered Regularly Interspaced Short Palindromic Repeat (CRISPR) will be used, which was first found in *E.coli* as a natural defence system against viruses DNA (Ishino et al., 1987). The elements of CRISPR and its CRISPR-associated (Cas) proteins are linked as an adaptive immunity against viral DNA (Jansen et al., 2002). In 2013, DNA from mammalian cells was for the first time successfully transfected and cleaved using a combination of CRISPR and type II Cas protein from *Streptococcus pyogenes* (SpCas9) or the so-called CRISPR/Cas9 system (Cong et al., 2013, Mali et al., 2013).

The formation of CRISPR system to the target sequence allows the Cas9 to unwind the DNA and create a double-strand break (DSB). Consequently, the targeted cell will repair that break created using non-homologous end joining (NHEJ) that often creates different types of mutations that lead to loss-of-function for the targeted gene. Alternatively, the break will be repaired by homology directed repair (HDR) that needs a donor DNA strand to repair the break, which creates a precise mutation if the donor DNA was already altered, as reviewed in Pickar-Oliver and Gersbach (2019).

In summary, AMD1 is essential in polyamine biosynthesis and its effect on UM is still not fully known. This chapter therefore aims to knockout *AMD1* using CRISPR/Cas9 technology so as to determine its effect on the UM cells. To my knowledge, this is the first attempt to knockout *AMD1* on UM cell lines.

5.2 Results

5.2.1 UM cell lines and chromosomal aberrations

Four UM cell lines, MEL-577, MEL-585, MEL-627 and MEL-644, chosen to represent different aberrations of chromosome 6, were grown in RPMI-1640 media with supplements, as described in section 2.2.4, and incubated at 37 ºC with 5% CO_2. These cell lines were maintained and passaged every week depending on their confluency. In addition to these cell lines, a hepatocellular carcinoma cell line (HepG2) was used as an internal control for ICC and WB, as recommended by the antibody manufacturer; this was grown in similar conditions to the UM cell lines. These UM cell lines been chosen to represent different aberrations in chromosome 6. Chromosomal aberrations among those four UM cell lines were determined previously by members of our group using array-CGH.

The cellular characteristics of the MEL-577 cell line passage 59 showed a mixed cell morphology (Figure 5.1 A-B). The chromosomal aberrations of MEL-577 passage 53 represented typical UM chromosomal aberrations such as monosomy 3, gain of 8q and the aberration for chromosome 6 profile was partial gain of 6p and loss of 6q (pseudo-isochromosome 6p) (group 2) (Figure 5.1 C).

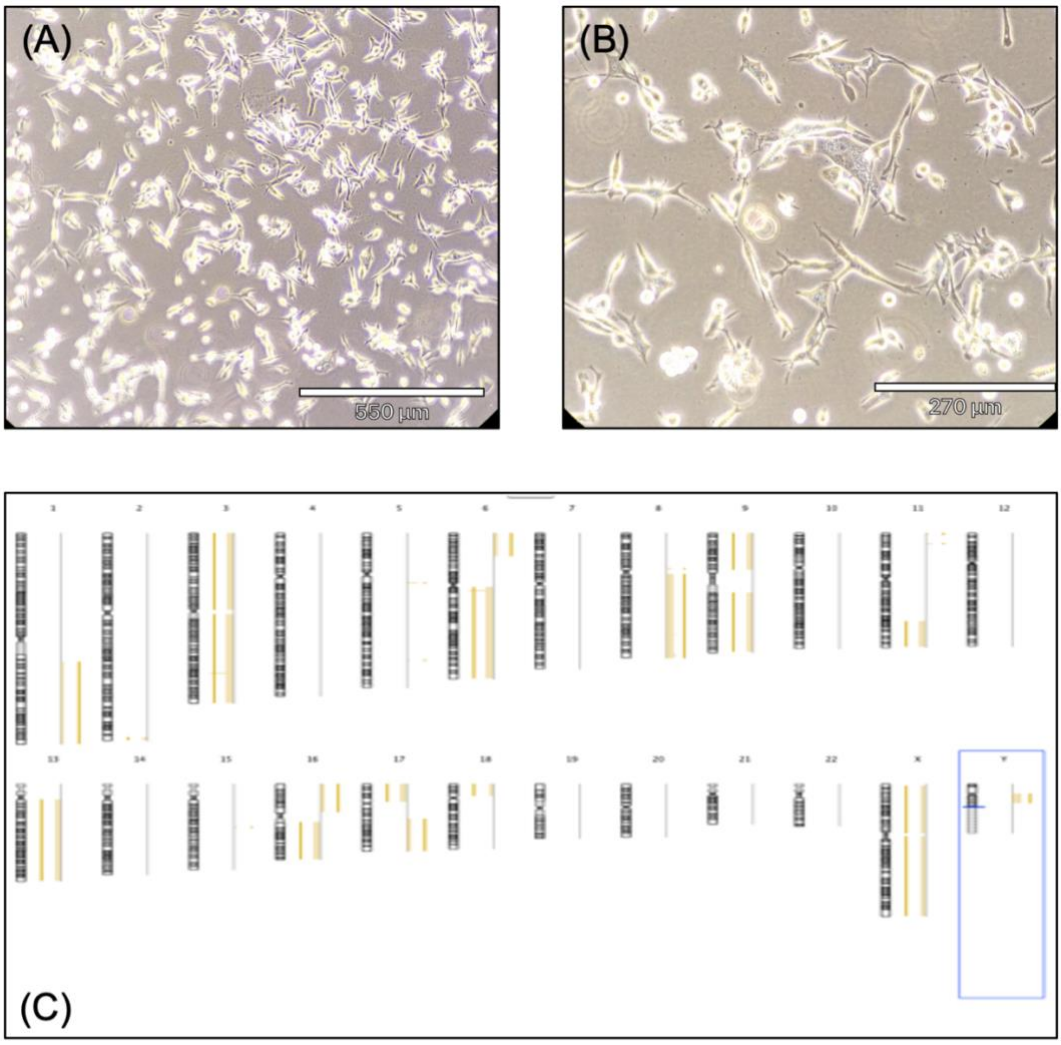

Figure 5.1: Phase contrast micrographs and array-CGH ideogram of MEL-577.

(A) The UM cell line MEL-577 passage 59 shows a mixed cell morphology on 10X magnification **(B)** the cells appear clearly under 20X magnification. **(C)** An ideogram of MEL-577 passage 53 showing a pseudo-isochromosome 6p, as well as aberrations such as gain of 1q, monosomy 3, gain of 8q, monosomy 9, partial loss of chromosome 11q, loss of chromosome 13, gain of 16p and loss of 16q, loss of 17p and gain of 17q and loss of 18p.

All microscope images were taken using REBEL ECHO (Avantor™). Images output for ideograms were taken from Agilent Genomic Workbench software v7.0.4.0. The ADM-2 algorithm was used to detect all the aberrations.

The cellular characteristics of MEL-585 passage 36 also showed a mixed cell morphology, as seen in Figure 5.2 A-B. In addition, the chromosomal profile for UM cell line MEL-585 passage 29 showed monosomy 3 and isochromosome 8q while the chromosome 6 aberration was pseudo-isochromosome 6p (group 2) (Figure 5.2).

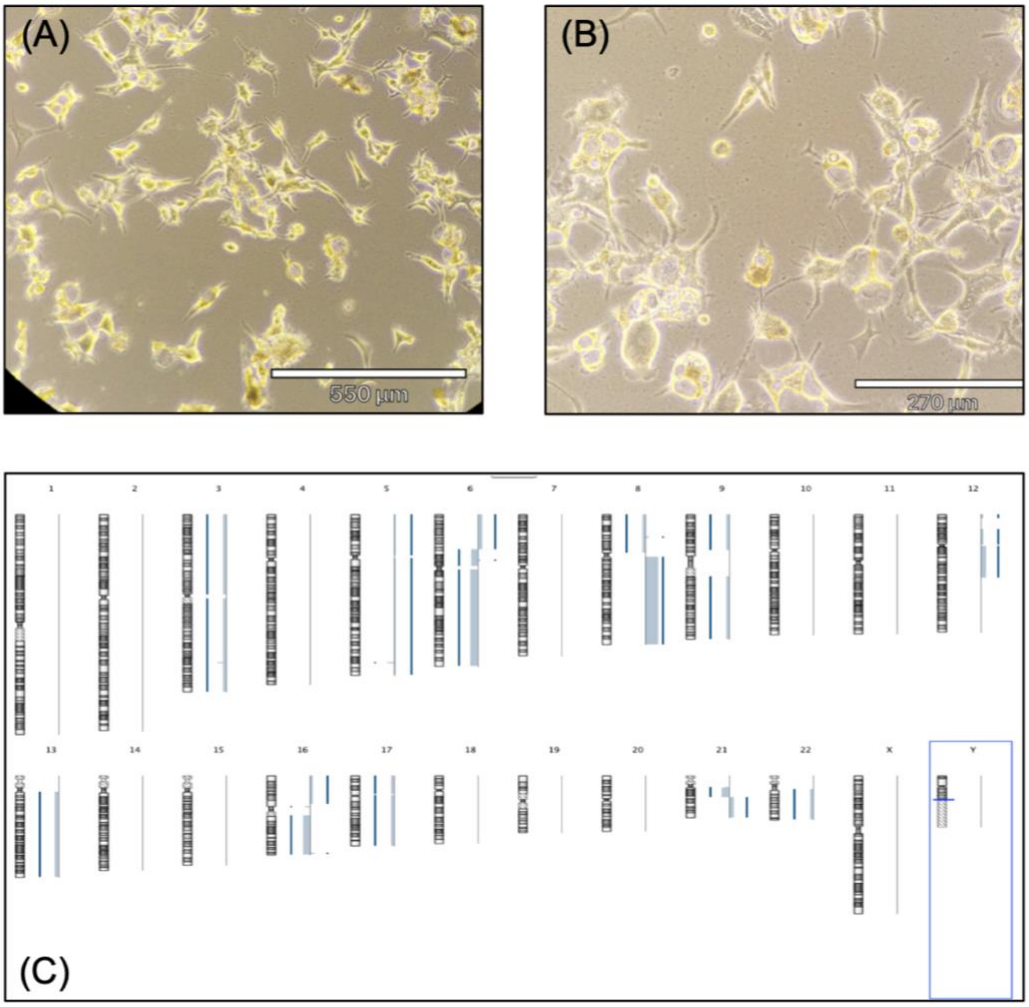

Figure 5.2: Phase contrast micrographs and array-CGH ideogram of MEL-585.

(A) The UM cell line MEL-585 passage 36 shows a mixed cell morphology on 10X magnification **(B)** the cells appear clearly under 20X magnification. **(C)** An ideogram of MEL-585 passage 29 showing a partial gain of chromosome 6p and loss of to the rest of chromosome 6 where the cells developed different aberrations such as monosomy 3, gain of chromosome 5, loss of 8p and gain of 8q, monosomy 9, partial gain of chromosome 12, loss of chromosome 13, gain of 16p and loss of 16q, loss of chromosome 17 and partial loss and gain of chromosome 21 and loss of chromosome 22.

All microscope images were taken using REBEL ECHO (Avantor™). Images output for ideograms were taken from Agilent Genomic Workbench software v7.0.4.0. The ADM-2 algorithm was used to detect all the aberrations.

The UM cell line of MEL-627 passage 27 showed an epithelioid cell morphology, as seen in Figure 5.3 A-B. The chromosomal aberrations for MEL-627 passage 25 were disomy 3, trisomy 8 and gain of chromosome 6p only, this representing group 1 (Figure 5.3 C).

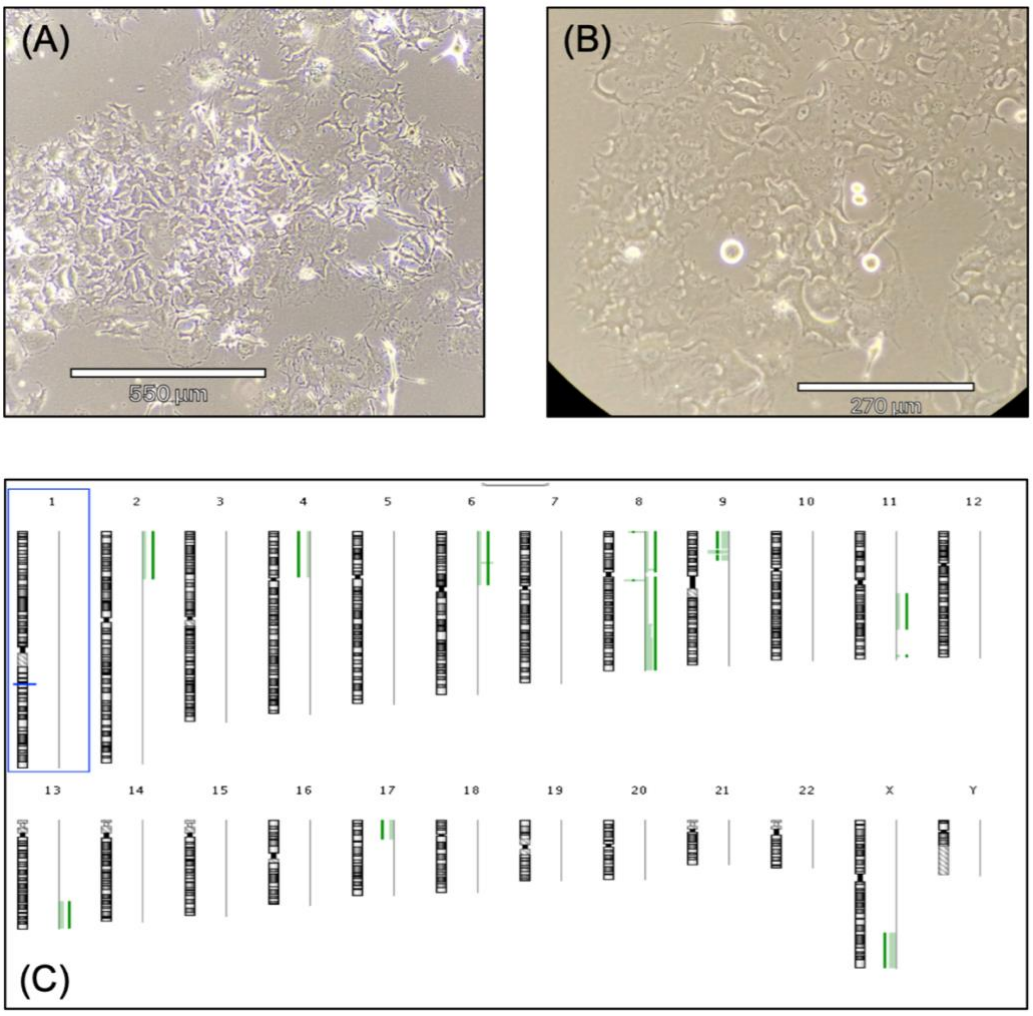

Figure 5.3: Phase contrast micrographs and array-CGH ideogram of MEL-627.

(A) The UM cell line MEL-627 passage 27 shows an epithelioid cell morphology on 10X magnification **(B)** the cells appear clearly under 20X magnification. **(C)** An ideogram of MEL-627 passage 25 showing gain of chromosome 6p where the cells developed different aberrations such as partial gain of chromosome 2p, loss of chromosome 4p, trisomy 8, loss of 9p, partial gain of chromosome 11q, partial gain of 13q and loss of 17p.

All microscope images were taken using REBEL ECHO (Avantor™). Images output for ideograms were taken from Agilent Genomic Workbench software v7.0.4.0. The ADM-2 algorithm was used to detect all the aberrations.

The cellular characteristics for MEL-644 passage 27 showed a spindle cell morphology, in contrast to the other three cell lines (Figure 5.4 A-B). The chromosomal aberrations for MEL-644 passage 22 exhibited classical UM aberrations such as loss of chromosome 1p, monosomy 3 and gain of 8q whereas there was no aberration for chromosome 6 (group 4) (Figure 5.4 C).

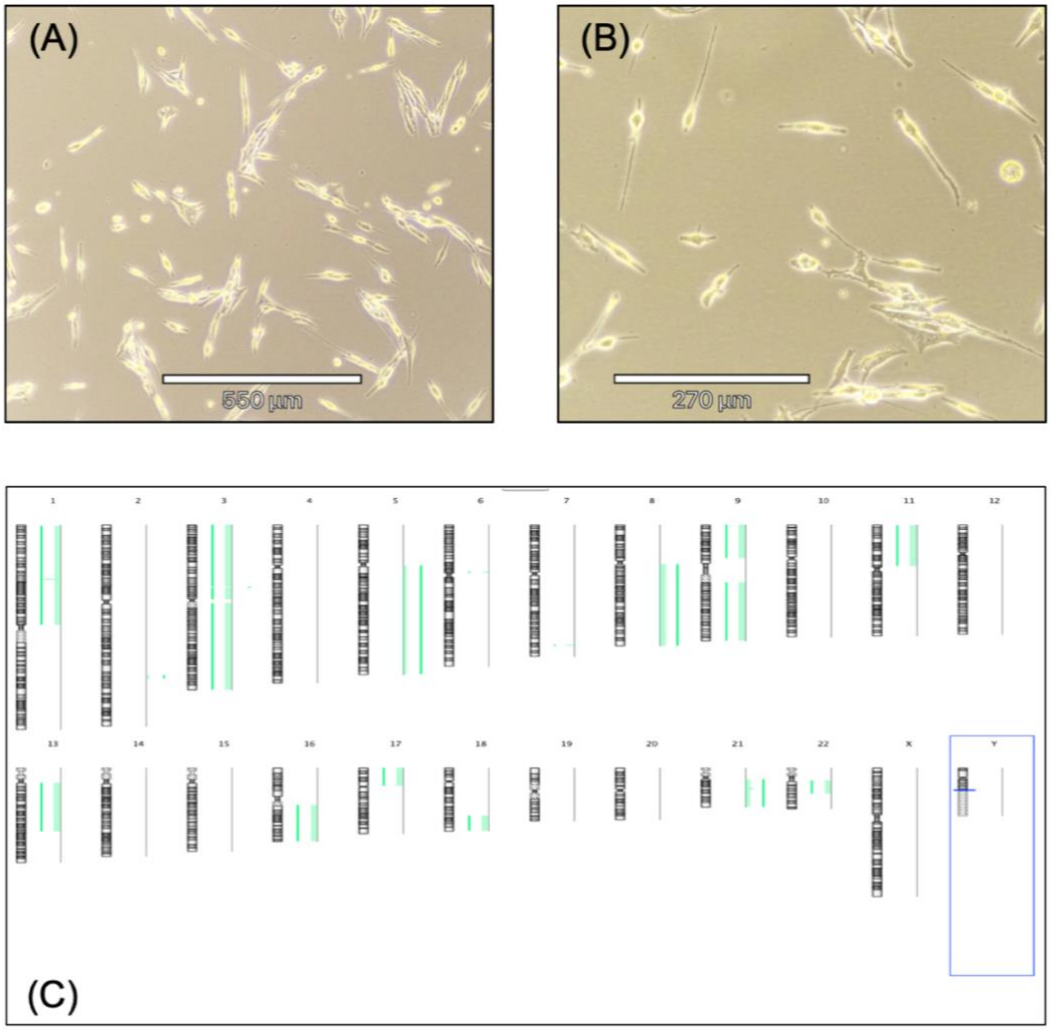

Figure 5.4: Phase contrast micrographs and array-CGH ideograms of MEL-644.

(A) The UM cell line MEL-644 passage 27 shows a spindle cell morphology on 10X magnification **(B)** the cells appeared clearly under 20X magnification. **(C)** An ideogram of MEL-627 passage 22 showing no aberration in chromosome 6 where the cells developed different aberrations such as loss of 1p, monosomy 3, gain of 5q, gain of 8q, monosomy 9, loss of 11p, partial loss of chromosome 13, loss of 16q, loss of 17p, partial loss of 18q, trisomy 21 and partial loss of chromosome 22.

All microscope images were taken using REBEL ECHO (Avantor™). Images output for ideograms were taken from Agilent Genomic Workbench software v7.0.4.0. The ADM-2 algorithm was used to detect all the aberrations.

5.2.2 Immunocytochemistry of UM cell lines

Immunocytochemistry (ICC) was conducted on the UM cell lines mentioned in order to determine the protein expression of AMD1. The UM cells were seeded on slides as mentioned in section 2.2.5, and fixed for used for the ICC. The AMD1 antibody that been used in this experiment was optimised based on the manufacturer's recommendation. This experiment was done to confirm the expression of AMD1 at a cellular level for those selected UM cell lines similar the IHC that was undertaken on UM tissue sections in the previous chapter.

The results showed that the HepG2 cells have a strong expression of AMD1 in the nucleus and cytoplasm compared to the negative control (Figure 5.5 A-B). Although it is known that the expression of AMD1 is mainly in the cytoplasm for IHC, the expression of AMD1 using ICC showed variation of expression in the cytoplasm while nuclear staining was stronger.

The four UM cell lines exhibited various AMD1 protein expression intensity (Figure 5.5 C-F). For instance, the mixed cell morphology of MEL-577 showed a moderate staining of AMD1 in the cytoplasm while there was a strong staining in the nucleus. Similarly, with MEL-585 the mixed cell morphology also showed a moderate staining in the nucleus and low staining in the cytoplasm. The epithelioid cell morphology of MEL-627, however, showed a low staining for AMD1 in the nucleus and no staining appeared in the cytoplasm. The staining for AMD1 on MEL-644, which has a spindle cell morphology, showed a strong staining in both nucleus and cytoplasm. Therefore, the increased of AMD1 expression among spindle cell morphology only may indicate a better prognosis for UM.

These UM cell lines have different chromosome 6 groups, and this explains the variation in the expression of AMD1 on these cells, as mentioned in the previous section. Although the cell lines (MEL-577 and MEL-585) represent (group 2), which is partial gain of chromosome 6p and loss of chromosome 6q, have same pattern as IHC analysis by exhibiting a lower expression of AMD1 in the cytoplasm, the other cell lines (MEL-627 and MEL-644) did not follow this same pattern as the IHC analysis.

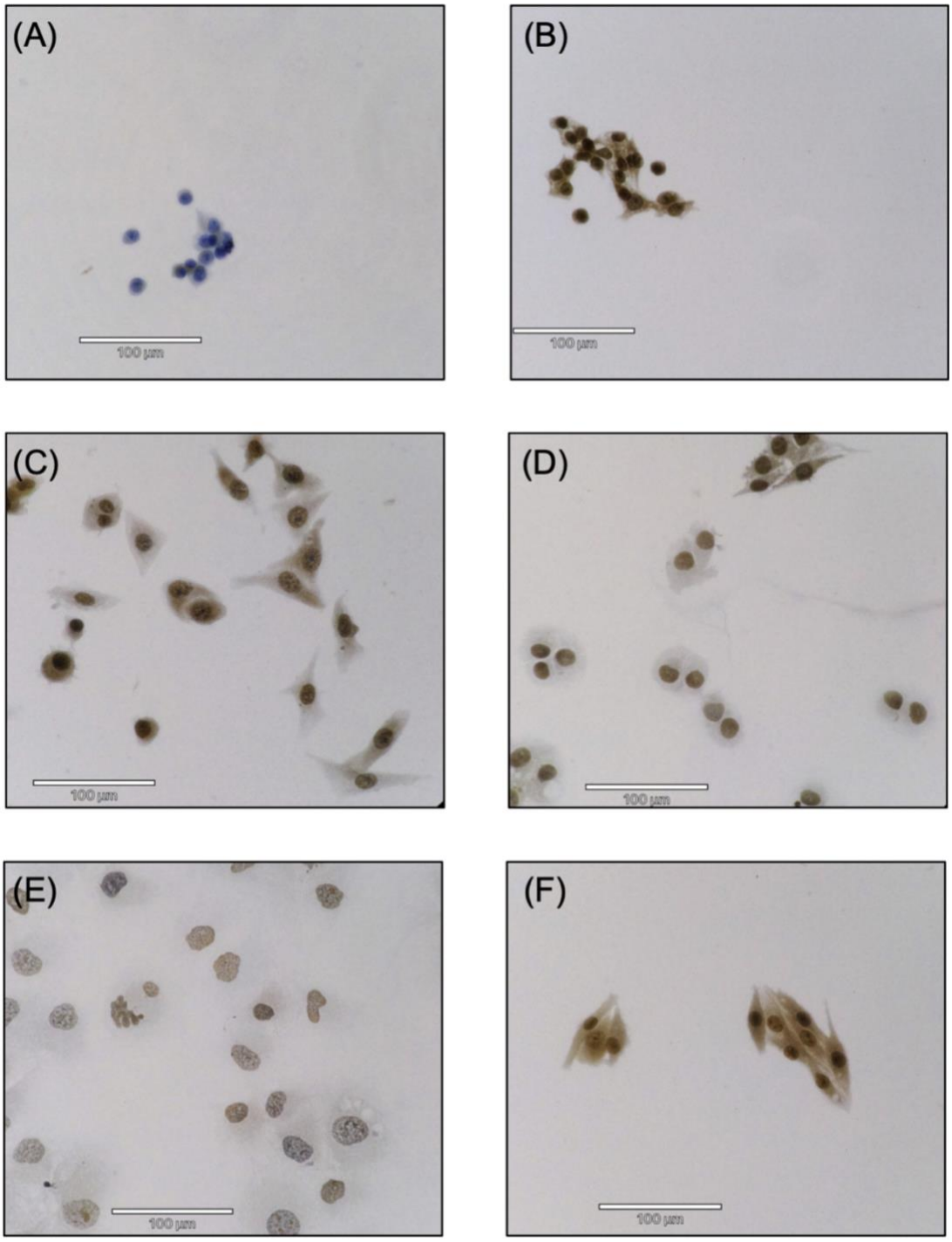

Figure 5.5: Immunocytochemistry for AMD1 antibody against UM cell lines.

(A) Negative control of HepG2 cells grown on slides without AMD1 staining and only haemoxylin. **(B)** Positive control for AMD1 using HepG2 cells. **(C)** Staining of AMD1 on MEL-577 cells showing the stronger staining in the nucleus than the cytoplasm. **(D)** Staining of AMD1 on MEL-585 showing a moderate staining in the nucleus than the cytoplasm. **(E)** Staining of AMD1 on MEL-627 showing a low staining in nucleus and no staining appeared in the cytoplasm. **(F)** Staining of AMD1 on MEL-644 showing a high staining in nucleus and moderate in the cytoplasm.

All microscope images were taken using REBEL ECHO (Avantor™).

5.2.3 AMD1 knockout using CRISPR/Cas9

The first step in knockout *AMD1* gene is to design an appropriate sgRNA to bind with the desired DNA target. The design of *AMD1* sgRNA was therefore done by using the Thermofisher website to generate a modified synthetic sgRNA. It appeared that the most efficient location for to knockout of *AMD1* was on exon 1, as explained in section 2.2.7. The UM cells were therefore transfected using lipofectamine (CRISPRMAX), a lipid transfection agent, that was mixed with the sgRNA and Cas9 protein to form ribonucleoprotein (RNP) complex and that complex was added to each UM cell line, which was then incubated at 37ºC and 5% CO_2 for 48 hours. The UM cell line MEL-585 was excluded from this experiment, however, due to its poor cellular growth which there was insufficient time to resolve. The downstream applications to assess the efficiency of the AMD1 knockout were done by extracting the DNA and protein from each UM cell line.

5.2.3.1 Assessment of AMD1 knockout efficiency using Genomic cleavage detection (GCD) assay

The DNA that was extracted from UM cell lines were used to calculate the efficiency of the *AMD1* knockout. The DNA was amplified using PCR around the target site, as explained in section 2.2.7. The amplified PCR products were then incubated with T7 Endonuclease I, which has the ability to recognize the heteroduplex mismatches and cleave them to produce a small two bands shorter than the original parental band. After amplifying the target and treating it with T7 Endonuclease I, the results showed that all transfected UM PCR products had a parental band and two shorter cut bands, which was as expected because of the cut between 202 bp and 398 bp in comparison with the untreated PCR product that only had one band, as seen in Figure 5.6 A. The calculation of the knockout efficiency from these bands was done using Image Lab (BioRad) to determine the percentage of each cleaved band in comparison with its parental band, based on the following equation:

$$Knockout\ efficiency = 1 - ((1 - fraction\ cleaved)^{\frac{1}{2}}).$$

This equation was applied to all samples so as to calculate the efficiency of AMD1 knockout (Figure 5.6 B). The positive control showed a 10.11% efficiency and the UM cell lines showed knockout efficiencies of 9.67% for MEL-644, 7.16% for MEL-577 and 6.94% for MEL-627.

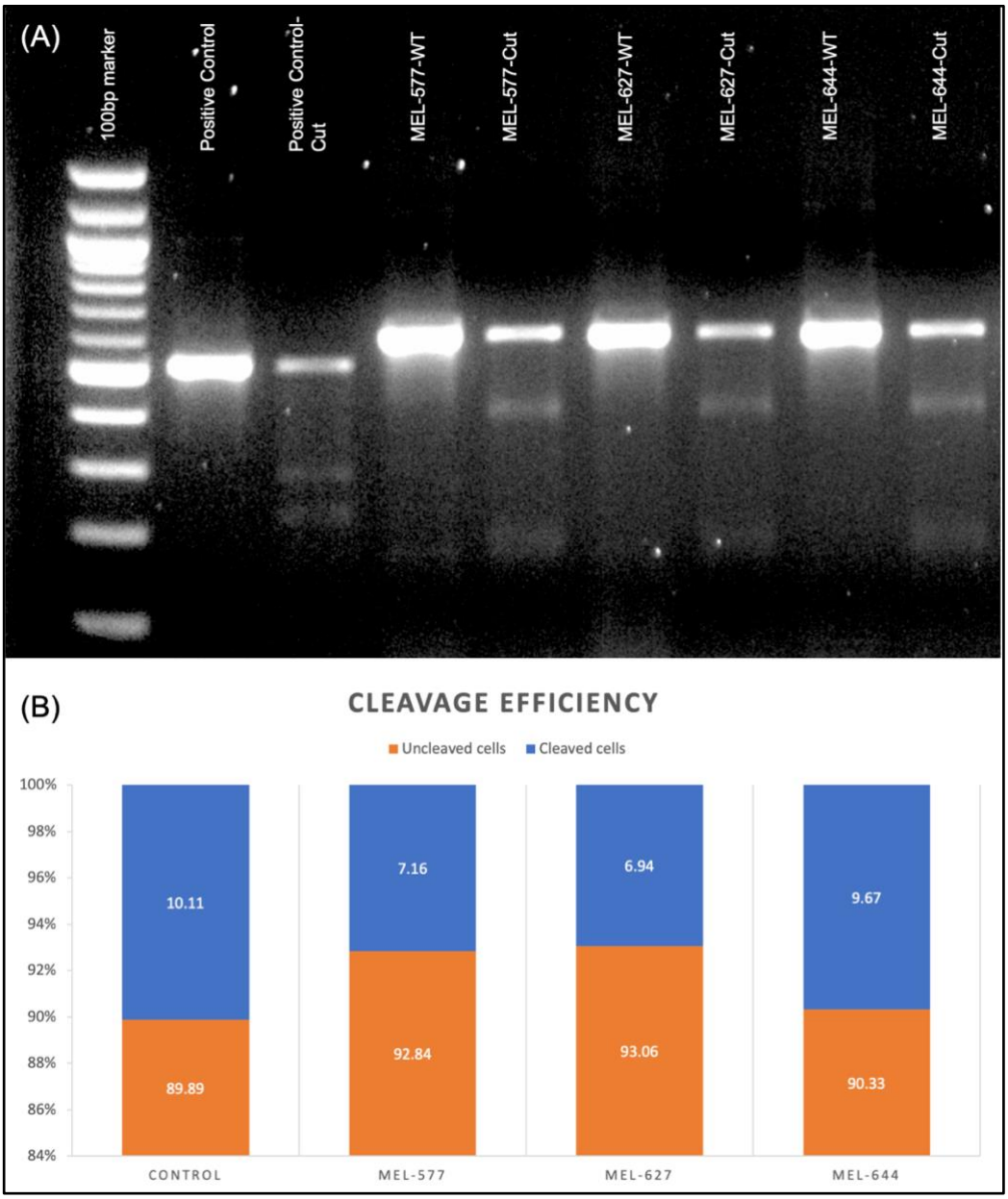

Figure 5.6: The cleavage efficiency for AMD1 knockout in UM cell lines.

(A) The gel electrophoresis of both undigested and digested UM cell lines showed that the amplified product was at 600 bp and the cuts were at 202 bp and 398 bp, as previously designed, while the internal positive control was amplified at 500 bp and the cut were at 225 bp and 291 bp, per the manufacturer's instructions. **(B)** The calculated total efficiency of the transfected cells showed that they were between 7 and 10% in comparison with the internal positive control, which was 10%.

5.2.3.2 Assessment of AMD1 knockout efficiency using Tracking indel by decomposition (TIDE)

The PCR products that were generated from the knockout and WT UM cell lines were sent to the sequencing core facility at the University of Sheffield. The results showed that all PCR products from WT UM cell lines and knockout *AMD1* achieved a good sequence trace (Figure 5.7). These sequences were then compared with the WT using an online quantifying method called Tracking of Indel by Decomposition (TIDE) http://tide.deskgen.com (Brinkman et al., 2014). This method is designed to determine the efficiency frequency from cell pools by adding the gRNA sequence before the software aligns this sequence with both the control and knockout sequence to calculate the percentage of the efficiency with the R^2 to confirm the findings. The sequence traces were uploaded so as to generate the total efficiency percentage by comparing the WT to the knockout. The data showed that MEL-644 had the highest total efficiency (7.5%) in comparison with the other UM cell lines, which had total efficiencies between 1 and 5.2%, as seen in Figure 5.6.

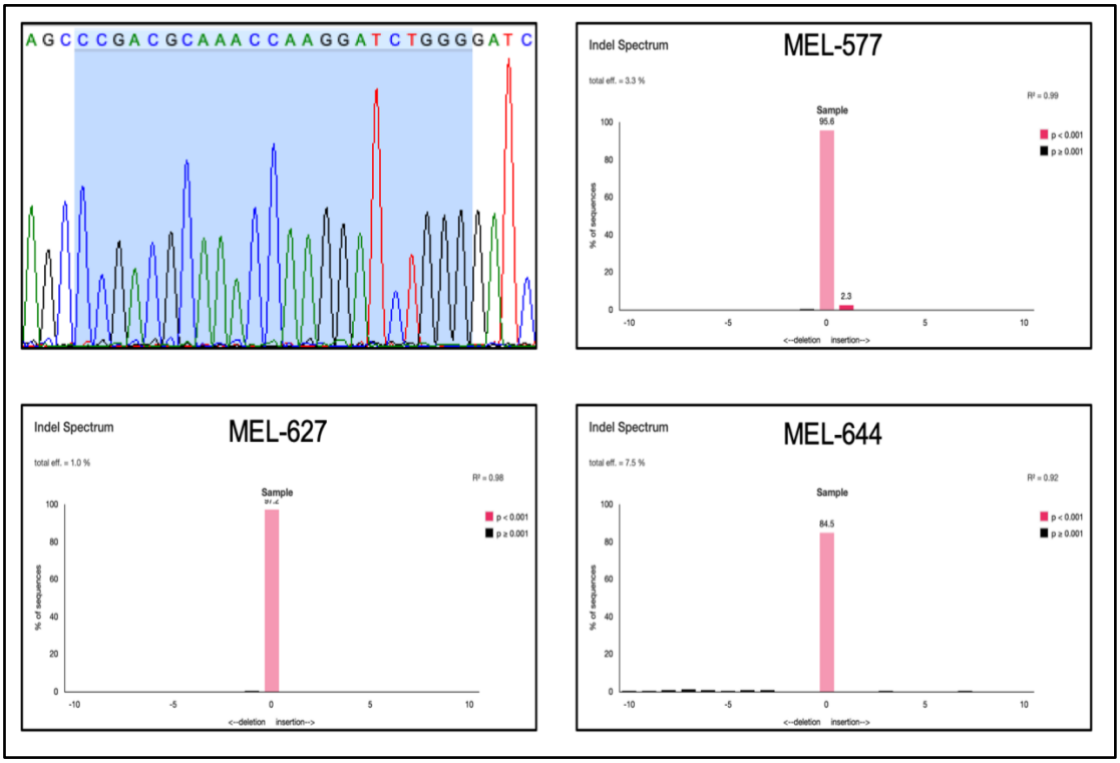

Figure 5.7: Chromatogram of AMD1 for UM cell lines and total efficiency calculation.

The chromatogram shows that UM cell lines sequenced for AMD1 having the area of sgRNA including PAM sequence. The total efficiency percentage calculation for UM cell lines using Tracking of Indel by Decomposition (TIDE) appeared to have a variation in the total efficiency percentage such as MEL-577 which has a total efficiency of 3.3%, MEL-585 of 1%, MEL-627 of 5.2% and MEL-644 of 7.5% with R^2 between 0.99 to 0.92.

5.2.3.3 Assessment of AMD1 knockout efficiency using Western blot

The protein in both WT and knockout UM cell lines were extracted in order to measure the protein expression of AMD1. The protein was extracted successfully from the HepG2 control and all the UM cell lines.

Numerous technical issues occurred when used the WB experiment to check the expression of AMD1 among UM lysates. For instance, when the SDS-PAGE was done and the gel was transferred to the PVDF membrane using the semi-dry method, no result was achieved. The wet transfer was therefore used, which was successful. Another issue was that while bands for beta-tubulin appeared, there were none for the AMD1 antibody. Because the first AMD1 antibody from Abcam™ did not work with the samples, the AMD1 antibody was changed to another company (ProteinTech™) which worked with the samples. In addition, the band for AMD1 was very faint and could not be detected. To overcome this issue, a long exposure time (two hours) was applied to give sufficient time for the membrane to develop the AMD1, and this worked with the lysate.

The results for AMD1 protein expression showed to have four bands for HepG2 (150 KDa, 80 KDa, 60 KDa and 30 KDa) (Figure 5.8 A). These bands are for the AMD1 at 30 KDa, proAMD1 at 60 KDa and an unspecific band at 80 KDa. In addition, the band at 150 KDa is also unspecific, which was only expressed with HepG2 cell line. Thus, the UM cell lines for both knockout and WT expressed only three bands (80 KDa, 60 KDa and 30 KDa) and these three bands did not change for the knockout in comparison with the WT UM cell lines. Remarkably, only the knockout MEL-644 showed a shift of the proAMD1 in comparison to the WT MEL-644 from 60KDa to 75KDa.

The experiment was repeated again to confirm the findings in the previous experiment and the proAMD1 for the knockout MEL-644 compared to the WT MEL-644 this time had only one band at 75 KDa without the unspecific band on 80 KDa (Figure 5.8 B). The beta-tubulin worked for all the samples, however, except for the knockout MEL-644.

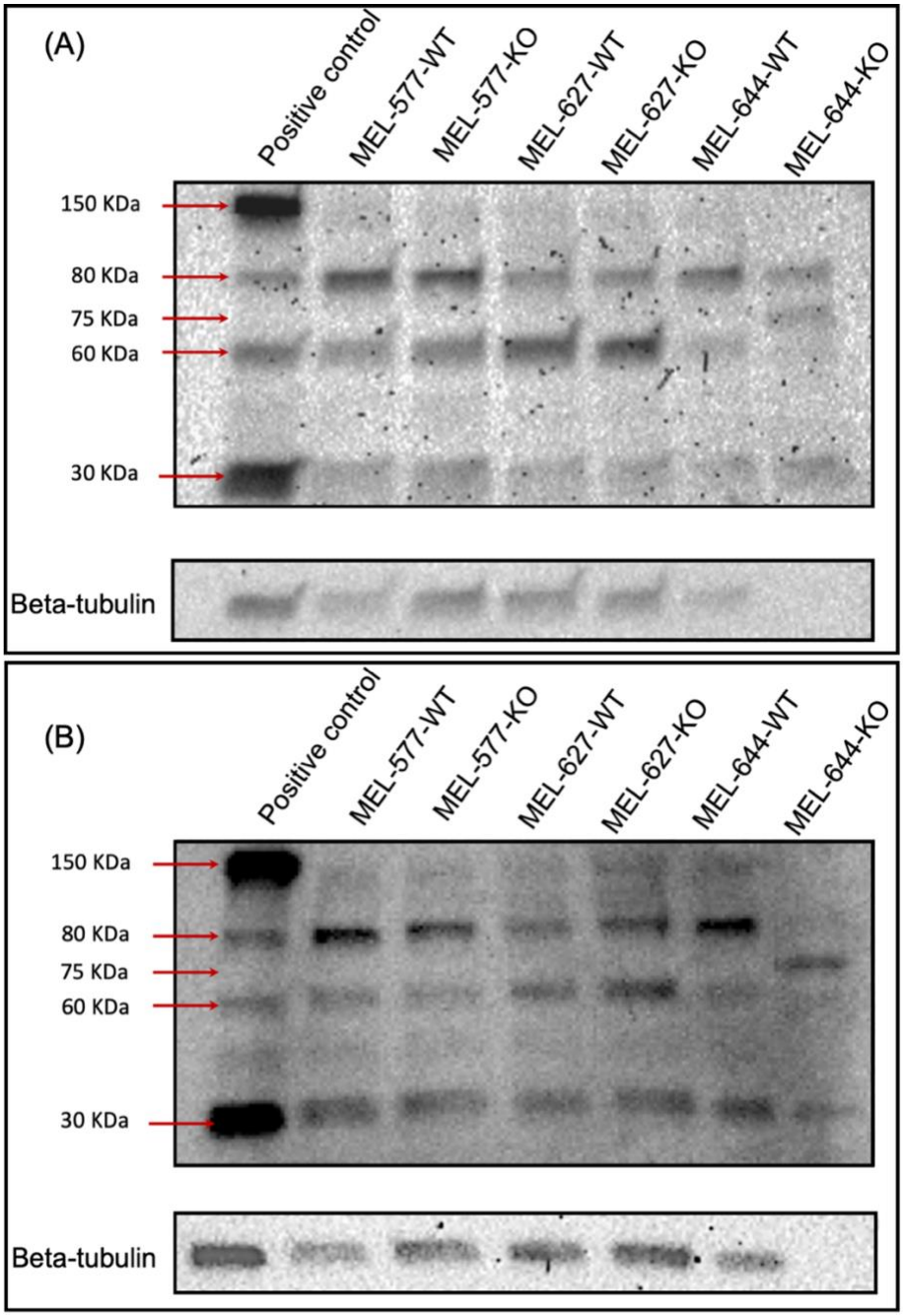

Figure 5.8: The effect of AMD1 protein expression knockout and WT UM cell lines.

(A) The positive control showed four bands for AMD1 in HepG2 while the UM cell lines showed only three bands. The first band at 30 KDa was for the AMD1, the band at 60 KDa was for the proAMD1 and the bands at 80 KDa and 150 KDa were unspecific band. MEL-644-KO, however, showed a shift in the proAMD1 to 75 KDa in comparison with its WT. The beta-tubulin appeared at 50 KDa for all samples except MEL-644-KO. **(B)** The experiment was repeated to confirm the findings and MEL-644-KO showed the AMD1 at 30KDa and only shifted band at 75KDa without the unspecific band at 80KDa. Similar to the previous experiment, beta-tubulin appeared in all the test samples except for MEL-644-KO.

5.2.3.4 Proliferation assay for WT and knockout UM cell lines

The UM cell lines that were transfected with *AMD1* sgRNA and the WT were tested to check for any differences in biological growth, as explained in section 2.2.8. For this, Mr. Ahmad Alshammari kindly performed the MTT for this study due to the limit time for this project and his prior experience with this technique. The objective of this experiment was to determine the biological effect of *AMD1* knockout UM cell lines in comparison with the WT UM cell lines.

The results for MTT showed that there was no significant difference between WT UM cell lines MEL- 577 and MEL-627 and the AMD1 knockout, as seen in Figure 5.9 A-B. Interestingly, the WT UM cell line MEL-644 showed a doubling time of around 58 hours while the knockout UM cell line appeared to has a lower doubling time of around 50 hours (Figure 5.9 C). This experiment was repeated at least three times to confirm the finding and the mean was calculated with SEM.

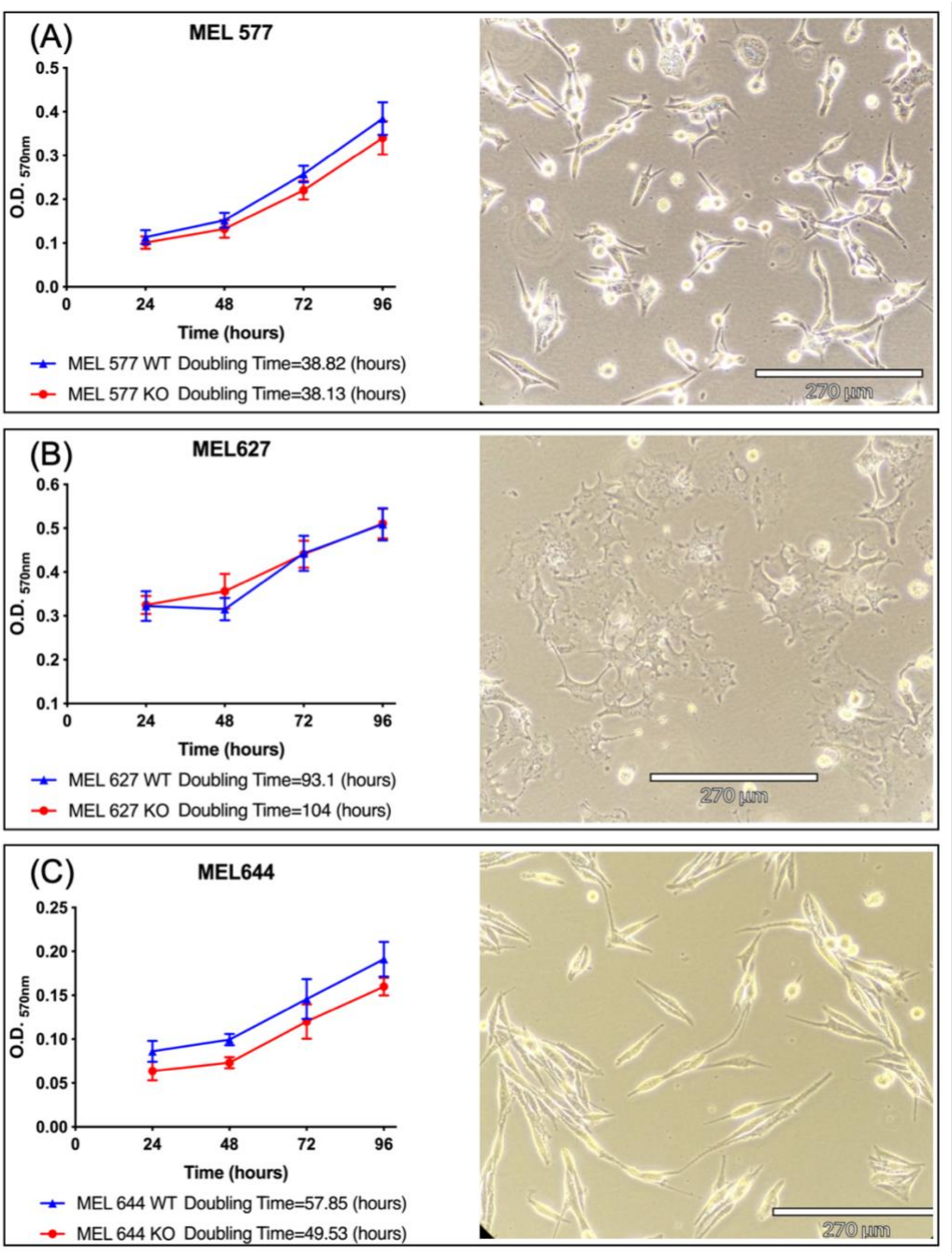

Figure 5.9: Analysis of UM cell viability using MTT assay after AMD1 knockout.

These results show the calculation of MTT on O.D. 570nm with images of each knockout cell line. **(A)** The cell viability for both MEL-577 WT and KO showed no difference and the doubling time was almost the same. **(B)** There was a slight difference of MEL-627 between the WT and the KO of MEL-627 with the doubling time being 93.1 and 104 hours, respectively; this may due to the erroneous reading difference after 48 hours because at 24, 72 and 96 hours the cell growth rates were the same. **(C)** However, the doubling time for MEL-644 the WT and KO were different (57.85 and 49.53 hours, respectively). All microscope images were taken using REBEL ECHO (Avantor™). These charts were designed and calculated using GraphPad Prism (v 8.0).

5.3 Discussion

This current study, for the first time, knocked out *AMD1* in UM cell lines with various chromosome 6 abnormalities so as determine its effect using genetic and protein analysis. Four UM cell lines were chosen, therefore, representing groups 1, 2 and 4 of different chromosome 6 aberrations to evaluate the knockout of *AMD1* in UM cell lines. The determination of the AMD1 protein expression among UM cell lines using ICC showed that MEL-644, which is spindle cell morphology, had the highest AMD1 expression compared to the other UM cell lines. These UM cell lines were then transfected by CRISPR/Cas9 to knockout *AMD1* exon 1 using sgRNA to determine the effect of AMD1 expression on UM cell lines.

This chapter used the CRISPR/Cas9 knockout instead knock-in of *AMD1* gene because the knock-in is harder to achieve and has a low efficiency rate. This depends on the design of the inserted dsDNA and the number of base pairs that should be inserted to the target DNA, as reviewed in Carroll (2016). In addition, homology-direct repair (HDR) is necessary to insert the desired dsDNA to the targeted DNA, however, the occurrences of error-free HDR in the cells are less than the error-prone NHEJ. This is because HDR occurs only in S- or G2-phase of the cycle where NHEJ occurs in throughout the cell cycle (Soutoglou et al., 2007, Zierhut and Diffley, 2008). Furthermore, HDR needs a donor DNA template to insert the desired dsDNA to the targeted DNA which NHEJ does not need to make the DSB. Subsequently, these issues make knock-in for any piece of dsDNA harder to achieve than knockout using CRISPR/Cas9.

Interestingly, AMD1 showed different sites of expression using WB and that may be due to unspecific expression sites of AMD1 appearing in the blot, as recently argued by Zabala-Letona et al. (2017). They found that after using WB for AMD1 expression on their prostate cancer cell lines other expression sites were shown as being expressed in the WB, rather than just proAMD1 or AMD1. They also exposed their membrane for a longer time to determine the presence of the proAMD1, which is similar to the presented WB for both proAMD1 and AMD1. This shift of proAMD1 may due the effect of the knockout of *AMD1* in UM cell lines which may lead to an upregulation of mTOR pathway. This is because the

AMD1 is produced as a proAMD1 which is self-cleaved and resulting in an active form of AMD1 (Pegg, 2006). However, the knockout of *AMD1* in UM cells may disturb the normal cleavage process of the proAMD1 and result in an upregulation of the mTOR pathway.

5.3.1 What is the correlation between AMD1 and mTOR pathway?

As mentioned earlier, it appears that there is a relationship between chromosomal aberrations and genetic mutations. For example, prostate cancer has a similar loss of chromosome 6q to that of UM cells (Nupponen et al., 1998). In that case, Nupponen et al., used CGH technology to determine the chromosomal aberrations among their prostate cancer cell lines and found that the deletion of chromosome 6q was significant in most of their prostate cancer cell lines. The correlation in this study between AMD1 and chromosome 6q in UM is therefore similar to the prostate cancer.

In addition, AMD1 expression is upregulated in prostate cancer cells by activating the mTOR pathway (Zabala-Letona et al., 2017). The mTOR pathway is part of the PTEN-PI3K pathway and together they sustain the growth and proliferation of cancer cells (Zoncu et al., 2011, Efeyan et al., 2015). The inhibition of the mTOR pathway in UM cells showed a reduction in the growth for the UM cells (Ho et al., 2012, Amirouchene-Angelozzi et al., 2014). It is plausible, therefore, that *AMD1* act as a tumour suppressor gene because when this gene is mutated, it may affect UM cells by upregulating the mTOR pathway.

5.3.2 The knockout efficiency differences in CRISPR

The knockout efficiency percentages were determined using both GCD assay and TIDE to estimate the effect of AMD1 knockout on UM cell lines. The GCD assay used T7 endonuclease I to detect and cleave any structural abnormalities in the amplified heteroduplex DNA (Mashal et al., 1995). This assay is considered to be a simple and cost-effective technique which is also easy to interpret for CRISPR edits. A comparison between GCD assay using both T7 endonuclease I and Surveyor nuclease revealed T7 endonuclease I to be the more sensitive

technique for measuring the editing efficiency of sgRNA (Vouillot et al., 2015). Other work has argued that the GCD assay using T7 endonuclease I, however, may not be highly sensitive because it is may influenced by various factors such as the length of the mismatch, secondary structure, flanking sequence and the abundance of mutated sequences (Mashal et al., 1995, Vouillot et al., 2015).

Sentmanat et al. (2018) evaluated the strategies of different techniques used to determine the editing efficiency of CRISPR in comparison to next generation sequencing (NGS). They found that the T7 endonuclease I did not accurately measure the cells edited by CRISPR in comparison with NGS. On the other hand, they also found TIDE has a similar accuracy to that of the. TIDE is an algorithm created by Brinkman et al. (2014) which calculates the Sanger sequence traces after amplifying the PCR product to detect edited cells created by CRISPR compared to the WT cells. Although NGS is more sensitive and reliable more than other techniques, it is a high cost and labour intensive approach, and thus TIDE was chosen here as a reliable technique for a low number of samples (Sentmanat et al., 2018). The results of this study revealed that MEL-644 had the highest editing efficiency of the various tested UM cell lines.

5.3.3 The effect of polyamines on beta-tubulin

The absence of beta-tubulin expression in the membrane for the knockout UM cell line MEL-644, may be due to a relationship between microtubules (alpha- and beta-tubulin) and the polyamines (Figure 5.8). Thus, Pohjanpelto et al. (1981) found that the starvation of polyamines may cause a disappearance of microtubule and actin filaments in the mammalian cells, as reviewed in Bouchereau et al. (1999). In addition, Mechulam and colleagues found that there was a relation between microtubules and the polyamines such as spermidine and spermine both *in vitro* and *in vivo* (Mechulam et al., 2009). Therefore, this relation between the polyamines and tubulin may have an effect on the edited MEL-644 which showed a shift in proAMD1 from 60 KDa to 75 KDa compared to the WT, while there was no expression for beta-tubulin in that edited sample (Figure 5.8). In addition, this relation may also affect the proliferation of the knockout of AMD1 in MEL-644 which showed an increase in the growth rate compared to the WT UM cell line, as seen in Figure 5.9 C. Consequently, there may a relationship

between one of the polyamines regulators (AMD1) and beta-tubulin that leads to a diffusion of beta-tubulin in the knockout UM cell line in comparison to its WT. Although there are a correlation AMD1 and beta-tubulin, the diffusion in beta-tubulin may have resulted from unexpected off-target effect from CRISPR technology.

In summary, this chapter used CRISPR as a new technology to knockout *AMD1* so as to determine its effect on UM cell lines. The knockout of *AMD1* was achieved in the UM cell line (MEL-644) with normal chromosome 6 and the efficiency was determined to be effective. Although it is known in this study that spindle cell morphology is correlated with good prognosis, this UM cell line exhibits chromosomal aberrations such as monosomy 3 and gain of chromosome 8q, which indicates a poor prognosis. In addition, this study also showed that the results effectively produce less of the AMD1 and therefore it has a tumour suppressor gene role in UM. Although the result of this study found a shift of proAMD1 to a higher molecular weight, this outcome needs to be repeated to confirm this effect of *AMD1* on knockout UM cells. However, due to the limited time of this PhD, the repeat of knocking out *AMD1* in UM cell line was not achievable and that will be done in the future to confirm this outcome. Accordingly, further exploration of AMD1 in UM may help in understanding how changes of chromosome 6 affect UM development and influence prognosis.

Chapter 6: General discussion

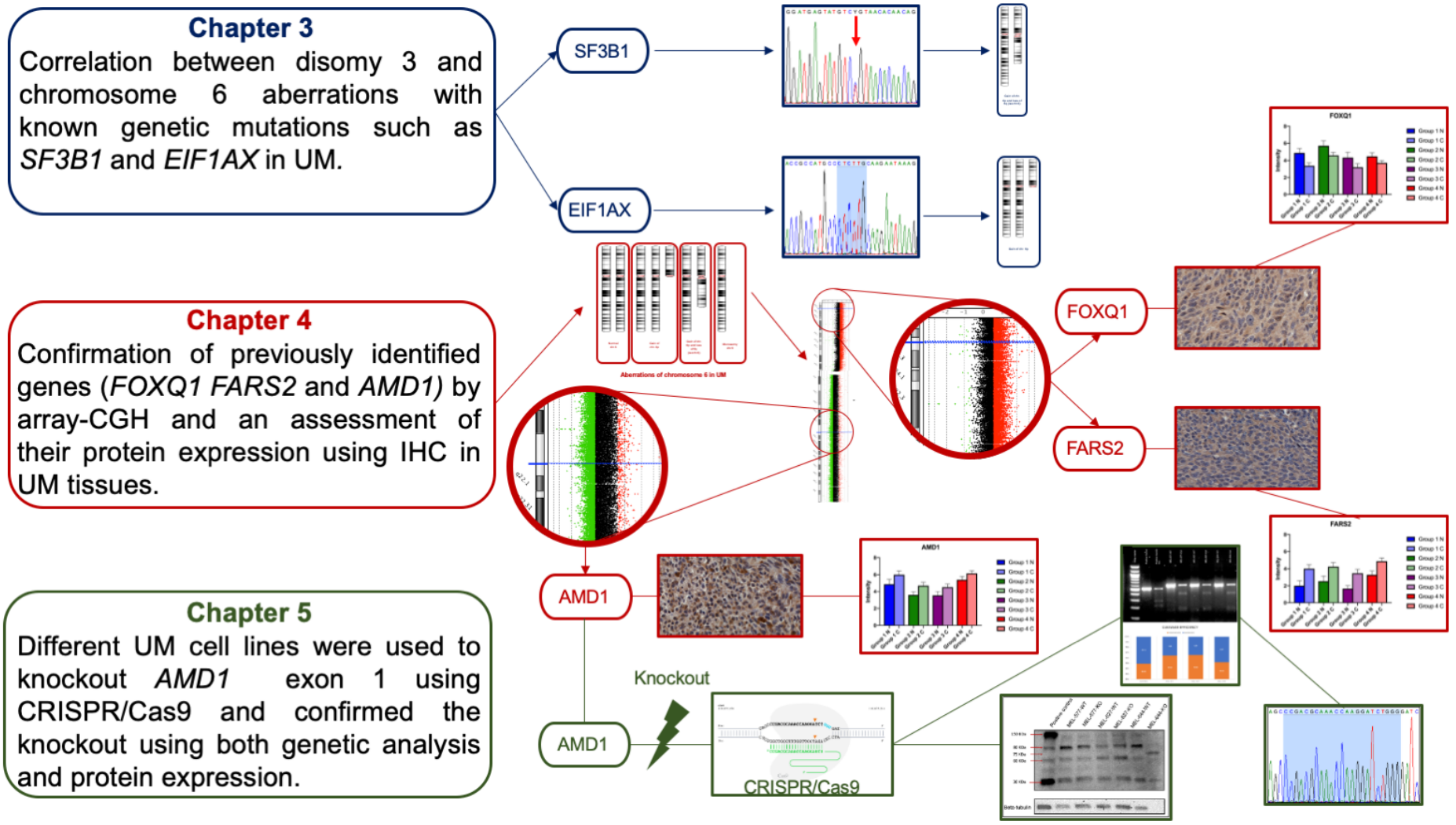

Figure 6.1: Summary of this study and the findings for each chapter.

6.1 Overview of this study

The clinical, histopathological and genetic prognostic factors for UM have been well characterised in numerous previous research studies (Mooy and De Jong, 1996, Sisley et al., 1997, Singh et al., 2001, Coupland et al., 2013). Although the chromosomal aberrations in UM have previously been correlated with prognosis (Sisley et al., 1990, Prescher et al., 1996, Sisley et al., 1997), these chromosomal aberrations have not been explored in detail to identify the relevant drivers of UM and its metastasis. Furthermore, although genes may be implicated, such as *BAP1*, the relationship between its mutation, expression and prognosis is unclear (Harbour et al., 2010, Koopmans et al., 2014b, Van Beek et al., 2015). The role of chromosome 6 has not been fully as extensively studied as other common chromosomes changes found in UM, such as chromosomes 3 and 8 (Sisley et al., 1997, Cross et al., 2006, van de Nes et al., 2016, Dogrusoz et al., 2017). Therefore, the aim of this current thesis was to evaluate in-depth chromosome 6 aberrations and identify driver genes that may help understand the progression of UM, as summarised in Figure 6.1.

This study started with a comparison between the common chromosome 6 aberrations in UM along with their relationship to other known genetic biomarkers such as *SF3B1*, *EIF1AX* and *TERTp* (Furney et al., 2013, Harbour et al., 2013, Martin et al., 2013, Dono et al., 2014, Yavuzyigitoglu et al., 2016b). The outcome of chapter 3 proposed an alternative sequence of events in UM considering disomy 3 with isochromosome 6p followed by mutations in *SF3B1* and then gain of chromosome 8q as one of the events that affect the prognosis of UM (Figures 3.9).

Moreover, this study broadly confirmed the target genes of interest on chromosome 6 (*FOXQ1*, *FARS2* and *AMD1*) using a small number of cases, which been identified previously by Alshammari (2017). This study also evaluated the protein expression of those targeted genes using IHC and found that there was a significant reduction of AMD1 expression among groups with chromosome 6q deletion (Figure 4.10).

Furthermore, in chapter 5, the *AMD1* gene was knocked out in UM cell lines using CRISPR/Cas9 technology, for the first time, in order to evaluate the efficiency and determine its effect on UM cell lines. In addition, the findings from the specific targeting of *AMD1* raised a number of questions specifically a depletion beta-tubulin (Figure 5.8). It was also found that specific targeting of *AMD1* raised a number of questions, specifically a depletion of beta-tubulin, as seen in Figure 5.8.

6.1.1 Can the importance of AMD1 to UM be independently validated?

The Cancer Genome Atlas (TCGA), which is a project supported by the National Institute of Health (NIH), aims to provide an extensive genetic analysis for different types of cancers, correlated with their clinical outcomes. Robertson and colleagues analysed 80 primary UM samples together with their clinico-pathological profiles, genomic alterations and mutational status and NGS, and published their data on TCGA (Robertson et al., 2017). They classified the genetic mutations of *EIF1AX* and *SF3B1* similarly to the classification used in Chapter 3 of this thesis. In addition, the SCNA of UM were categorised into four categories based on monosomy 3, gain of chromosome 8q and gain of chromosome 6p. Therefore, TCGA is a good approach to correlate our outcome on AMD1 and confirm this gene in a published database.

The University of California Santa Cruz (UCSC) developed an online analysis tool called Xena to explore the TCGA data and analyse them directly from their website (www.xenabrowser.net). This online tool allows the users to explore genomic data and correlate them with genomic or phenotypic data. This study used Xena to explore *AMD1* with the outcome of UM TCGA of 80 UM samples and generate a correlation between the gene and the published data on UM. It was found that *AMD1* is lost in 22 out of 80 samples (27.5%) and gained in 6 samples only (7.5%). Loss of *AMD1* was correlated with the isochromosome 6p while the gain of *AMD1* appeared to be correlated with a gain of whole chromosome 6, as appears in Figure 6.2 column C and D. Similarly, loss of *AMD1* showed a low gene expression with an isochromosome 6p while there was

different high and low gene expressions for the gain of chromosome 6, as shown in Figure 6.2 column E.

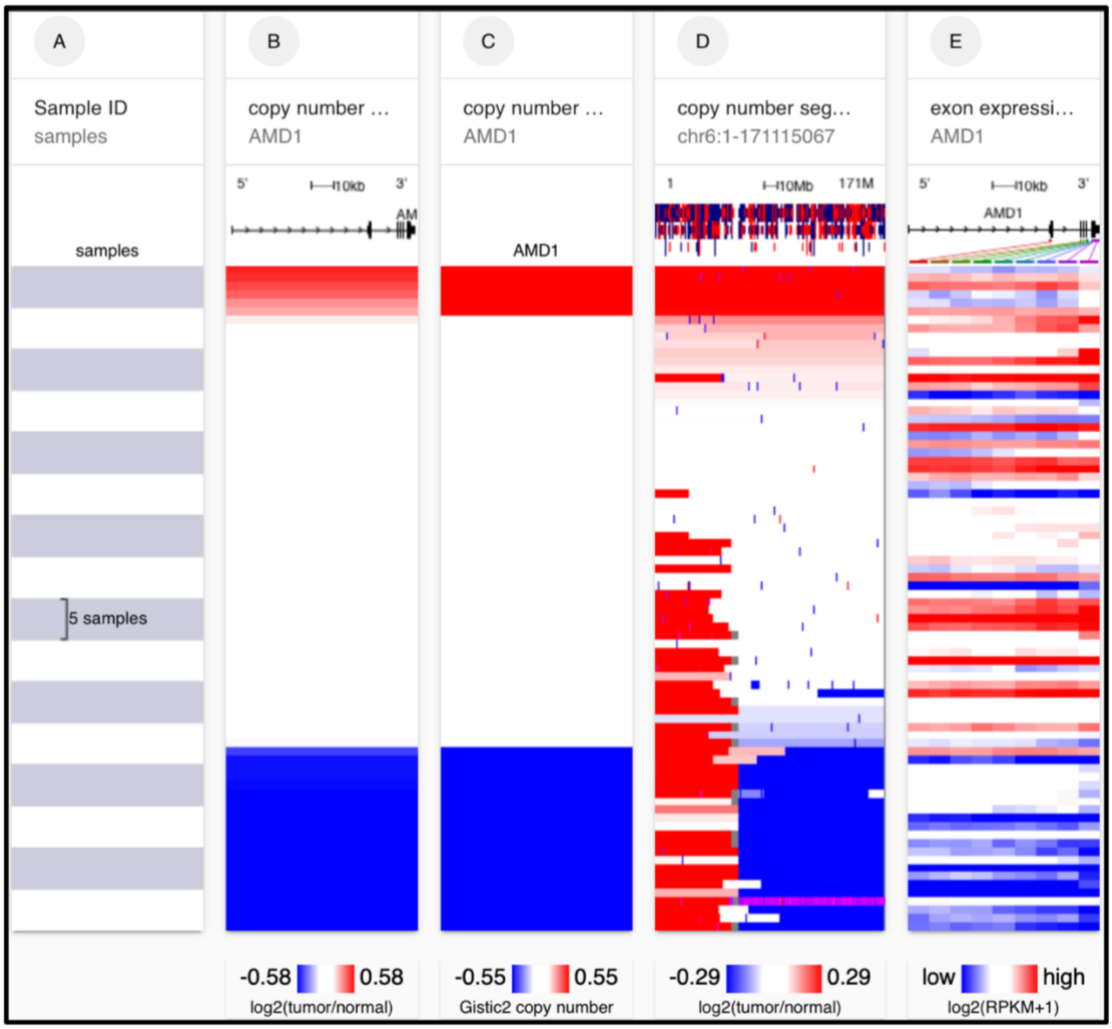

Figure 6.2: Analysis using UCSC Xena for AMD1.

The figure shows that in column **(A)** the sample ID and **(B)** the copy number of gene level of AMD1; **(C)** similar to column B but without the germline mutations. **(D)** The copy number segregation of chromosome 6; (E) showed the gene expression profile of AMD1.

The Kaplan-Meier analysis for chromosome 6 alterations with *AMD1* showed that patients have a poor overall survival with loss of *AMD1* than with its gain (Figure 6.3). Indeed, the loss of *AMD1* in UM patients have a lower overall survival, although the overall survival in *AMD1* gain cases showed to have a late effect on

overall survival. This is because the overall survival for both *AMD1* gain and loss have decreased at about three and half years. This suggests that the loss of *AMD1* has particularly striking early effect on overall survival in comparison with the *AMD1* gain. Therefore, the outcome from TCGA is interesting and indicates that *AMD1* may have a role in the development of UM and subsequent prognosis, which is supporting the findings of this study.

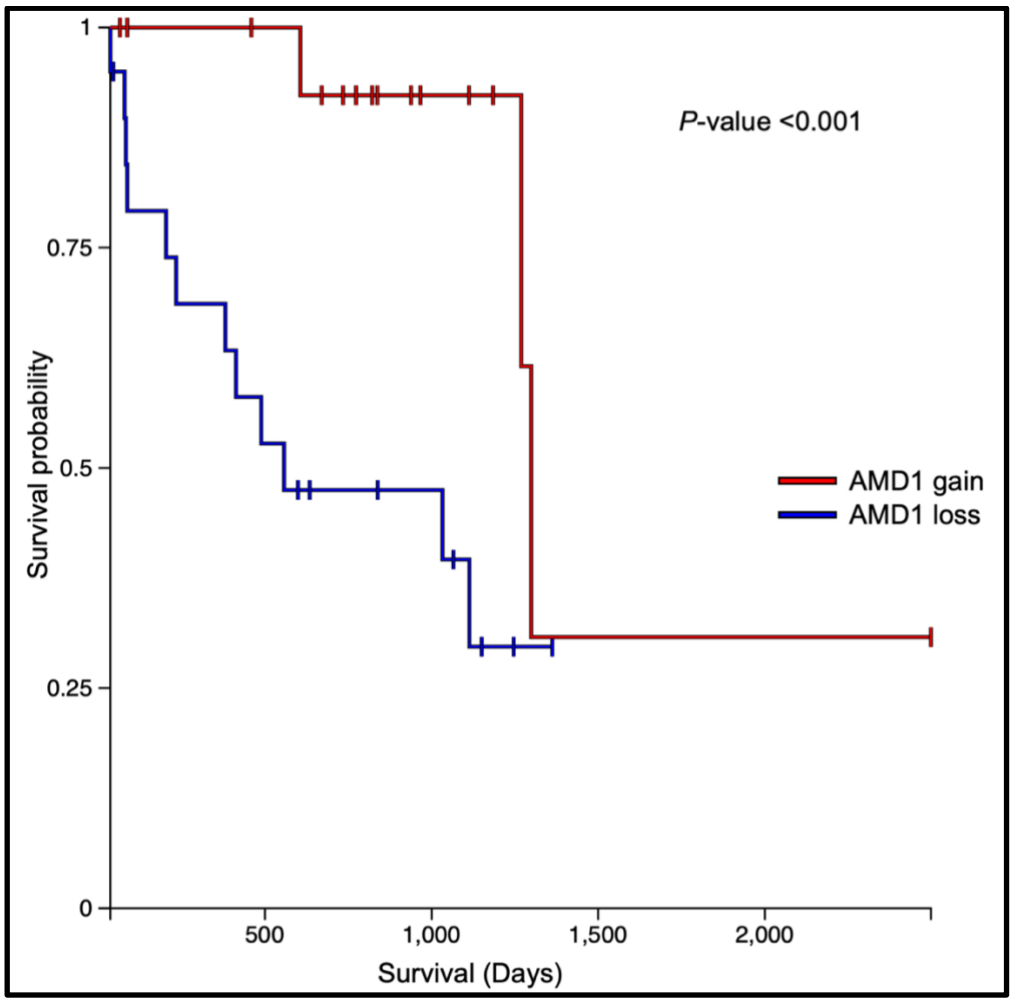

Figure 6.3: The Kaplan-Meier analysis of AMD1 gain and loss.

The analysis of AMD1 in TCGA using Xena showed that the loss of *AMD1* in UM cells appeared to decrease the survival rate in comparison with the gain of *AMD1*.

6.2 Study limitations

Although this study found an interesting gene (*AMD1*) that may have a relationship to the development and metastasis of UM that has not been reported, there were limitations. Technical challenges towards the end of the project did not allow in-depth analysis of the functional impact of *AMD1* on UM development and were limited by the remaining time of the study. In addition, another important constrain is that Nexus software licence was not available for analysis in chapter 4 and some of the clinical follow-up information was limited. In chapter 5, the transfection of *AMD1* using CRISPR/Cas9 needs to be repeated to confirm the findings in UM cell lines and the protein expression of UM among those cell lines. Moreover, the gene expression should be measured after the transfection to determine any differences in the expression of AMD1 when it was knocked out in comparison with its normal status.

6.3 Future direction

This thesis used a novel approached to identify *AMD1* as a plausible target for the future research. Based on this finding, CRISPR/Cas9 knockout for *AMD1* should be done again and including a control cell line such as human embryonic kidney (HEK293) to compare the efficiency between the UM cell line and the control cell line. It would be advisable to increase the number of UM cell lines in order to compare the effect of transfection and thus potentially of generate a higher knockout efficiency. Furthermore, although the relationship between AMD1 and beta-tubulin showed that there may be an off-target effect resulted from CRISPR, it is still an acceptable approach for further exploration which needs to be considered for future research.

In addition, a single cell colony should be achieved after the transfection using fluorescence activated cell sorting (FACS) because the cells were in mixed cell pools post CRISPR transfection, i.e. some of them were transfected and others not, and the single cell colony technique will generate a unified knockout AMD1 in the UM cell line. This knockout cell line will allow the application of other

approaches to validate the *AMD1* gene expression in *vitro* such as gene expression, genetic analysis and protein expression. In addition, the use of NGS for the UM knockout cells may give a detailed information about other genes that may be mutated. After validating the knockout cell line, it would be interesting to check the effect of knockout *AMD1* on an UM cell line in *vivo* by transfecting those cells into an animal model to check the effect of knockout of *AMD1* on the animal.

References

Aalto, Y., Eriksson, L., Seregard, S., Larsson, O. and Knuutila, S. (2001) 'Concomitant loss of chromosome 3 and whole arm losses and gains of chromosome 1, 6, or 8 in metastasizing primary uveal melanoma', *Invest Ophthalmol Vis Sci,* 42(2), pp. 313-7.

Abdel-Rahman, M. H., Christopher, B. N., Faramawi, M. F., Said-Ahmed, K., Cole, C., McFaddin, A., Ray-Chaudhury, A., Heerema, N. and Davidorf, F. H. (2011) 'Frequency, molecular pathology and potential clinical significance of partial chromosome 3 aberrations in uveal melanoma', *Mod Pathol,* 24(7), pp. 954-62.

Albertson, D. G. and Pinkel, D. (2003) 'Genomic microarrays in human genetic disease and cancer', *Human Molecular Genetics,* 12, pp. R145-R152.

Allred, D. C., Harvey, J. M., Berardo, M. and Clark, G. M. (1998) 'Prognostic and predictive factors in breast cancer by immunohistochemical analysis', *Mod Pathol,* 11(2), pp. 155-68.

Almalki, A., Alston, C. L., Parker, A., Simonic, I., Mehta, S. G., He, L., Reza, M., Oliveira, J. M., Lightowlers, R. N., McFarland, R., Taylor, R. W. and Chrzanowska-Lightowlers, Z. M. (2014) 'Mutation of the human mitochondrial phenylalanine-tRNA synthetase causes infantile-onset epilepsy and cytochrome c oxidase deficiency', *Biochim Biophys Acta,* 1842(1), pp. 56-64.

Alsafadi, S., Houy, A., Battistella, A., Popova, T., Wassef, M., Henry, E., Tirode, F., Constantinou, A., Piperno-Neumann, S., Roman-Roman, S., Dutertre, M. and Stern, M. H. (2016) 'Cancer-associated SF3B1 mutations affect alternative splicing by promoting alternative branchpoint usage', *European Journal of Cancer,* 61, pp. S94-S95.

Alshammari, N. (2017) *Genetic biomarkers in uveal melanoma: an exploration using high-resolution array comparative genomic hybridization.* PhD Thesis, University of Sheffield.

Amirouchene-Angelozzi, N., Nemati, F., Gentien, D., Nicolas, A., Dumont, A., Carita, G., Camonis, J., Desjardins, L., Cassoux, N., Piperno-Neumann, S., Mariani, P., Sastre, X., Decaudin, D. and Roman-Roman, S. (2014) 'Establishment of novel cell lines recapitulating the genetic landscape of uveal melanoma and preclinical validation of mTOR as a therapeutic target', *Molecular Oncology,* 8(8), pp. 1508-1520.

Anbunathan, H., Verstraten, R., Singh, A. D., Harbour, J. W. and Bowcock, A. M. (2019) 'Integrative Copy Number Analysis of Uveal Melanoma Reveals Novel Candidate Genes Involved in Tumorigenesis Including a Tumor Suppressor Role for PHF10/BAF45a', *Clinical Cancer Research,* 25(16), pp. 5156-5166.

Aoude, L. G., Vajdic, C. M., Kricker, A., Armstrong, B. and Hayward, N. K. (2013) 'Prevalence of germline BAP1 mutation in a population-based sample of uveal melanoma cases', *Pigment Cell Melanoma Res,* 26(2), pp. 278-9.

Aronow, M., Sun, Y., Saunthararajah, Y., Biscotti, C., Tubbs, R., Triozzi, P. and Singh, A. D. (2012) 'Monosomy 3 by FISH in Uveal Melanoma: Variability

in Techniques and Results', *Survey of Ophthalmology,* 57(5), pp. 463-473.
Augsburger, J. J., Correa, Z. M. and Shaikh, A. H. (2009) 'Effectiveness of treatments for metastatic uveal melanoma', *Am J Ophthalmol,* 148(1), pp. 119-27.
Bao, B., Azmi, A. S., Aboukameel, A., Ahmad, A., Bolling-Fischer, A., Sethi, S., Ali, S., Li, Y., Kong, D., Banerjee, S., Back, J. and Sarkar, F. H. (2014) 'Pancreatic cancer stem-like cells display aggressive behavior mediated via activation of FoxQ1', *J Biol Chem,* 289(21), pp. 14520-33.
Bartosch, B. (2010) 'Hepatitis B and C Viruses and Hepatocellular Carcinoma', *Viruses-Basel,* 2(8), pp. 1504-1509.
Basen-Engquist, K. and Chang, M. (2011) 'Obesity and cancer risk: recent review and evidence', *Curr Oncol Rep,* 13(1), pp. 71-6.
Bastian, B. C., LeBoit, P. E., Hamm, H., Brocker, E. B. and Pinkel, D. (1998) 'Chromosomal gains and losses in primary cutaneous melanomas detected by comparative genomic hybridization', *Cancer Res,* 58(10), pp. 2170-5.
Bastian, B. C., Olshen, A. B., LeBoit, P. E. and Pinkel, D. (2003) 'Classifying melanocytic tumors based on DNA copy number changes', *Am J Pathol,* 163(5), pp. 1765-70.
Bauer, J., Kilic, E., Vaarwater, J., Bastian, B. C., Garbe, C. and de Klein, A. (2009) 'Oncogenic GNAQ mutations are not correlated with disease-free survival in uveal melanoma', *Br J Cancer,* 101(5), pp. 813-5.
Bedi, D. G., Gombos, D. S., Ng, C. S. and Singh, S. (2006) 'Sonography of the eye', *AJR Am J Roentgenol,* 187(4), pp. 1061-72.
Bedikian, A. Y. (2006) 'Metastatic uveal melanoma therapy: current options', *Int Ophthalmol Clin,* 46(1), pp. 151-66.
Benayoun, B. A., Caburet, S. and Veitia, R. A. (2011) 'Forkhead transcription factors: key players in health and disease', *Trends Genet,* 27(6), pp. 224-32.
Berenblum, I. and Shubik, P. (1947) 'The role of croton oil applications, associated with a single painting of a carcinogen, in tumour induction of the mouse's skin', *Br J Cancer,* 1(4), pp. 379-82.
Beroukhim, R., Getz, G., Nghiemphu, L., Barretina, J., Hsueh, T., Linhart, D., Vivanco, I., Lee, J. C., Huang, J. H., Alexander, S., Du, J., Kau, T., Thomas, R. K., Shah, K., Soto, H., Perner, S., Prensner, J., Debiasi, R. M., Demichelis, F., Hatton, C., Rubin, M. A., Garraway, L. A., Nelson, S. F., Liau, L., Mischel, P. S., Cloughesy, T. F., Meyerson, M., Golub, T. A., Lander, E. S., Mellinghoff, I. K. and Sellers, W. R. (2007) 'Assessing the significance of chromosomal aberrations in cancer: methodology and application to glioma', *Proc Natl Acad Sci U S A,* 104(50), pp. 20007-12.
Beroukhim, R., Mermel, C. H., Porter, D., Wei, G., Raychaudhuri, S., Donovan, J., Barretina, J., Boehm, J. S., Dobson, J., Urashima, M., Mc Henry, K. T., Pinchback, R. M., Ligon, A. H., Cho, Y. J., Haery, L., Greulich, H., Reich, M., Winckler, W., Lawrence, M. S., Weir, B. A., Tanaka, K. E., Chiang, D. Y., Bass, A. J., Loo, A., Hoffman, C., Prensner, J., Liefeld, T., Gao, Q., Yecies, D., Signoretti, S., Maher, E., Kaye, F. J., Sasaki, H., Tepper, J. E., Fletcher, J. A., Tabernero, J., Baselga, J., Tsao, M. S., Demichelis, F., Rubin, M. A., Janne, P. A., Daly, M. J., Nucera, C., Levine, R. L., Ebert, B. L., Gabriel, S., Rustgi, A. K., Antonescu, C. R.,

Ladanyi, M., Letai, A., Garraway, L. A., Loda, M., Beer, D. G., True, L. D., Okamoto, A., Pomeroy, S. L., Singer, S., Golub, T. R., Lander, E. S., Getz, G., Sellers, W. R. and Meyerson, M. (2010) 'The landscape of somatic copy-number alteration across human cancers', *Nature,* 463(7283), pp. 899-905.

Biankin, A. V. and Waddell, N. and Kassahn, K. S. and Gingras, M. C. and Muthuswamy, L. B. and Johns, A. L. and Miller, D. K. and Wilson, P. J. and Patch, A. M. and Wu, J. and Chang, D. K. and Cowley, M. J. and Gardiner, B. B. and Song, S. and Harliwong, I. and Idrisoglu, S. and Nourse, C. and Nourbakhsh, E. and Manning, S. and Wani, S. and Gongora, M. and Pajic, M. and Scarlett, C. J. and Gill, A. J. and Pinho, A. V. and Rooman, I. and Anderson, M. and Holmes, O. and Leonard, C. and Taylor, D. and Wood, S. and Xu, Q. and Nones, K. and Fink, J. L. and Christ, A. and Bruxner, T. and Cloonan, N. and Kolle, G. and Newell, F. and Pinese, M. and Mead, R. S. and Humphris, J. L. and Kaplan, W. and Jones, M. D. and Colvin, E. K. and Nagrial, A. M. and Humphrey, E. S. and Chou, A. and Chin, V. T. and Chantrill, L. A. and Mawson, A. and Samra, J. S. and Kench, J. G. and Lovell, J. A. and Daly, R. J. and Merrett, N. D. and Toon, C. and Epari, K. and Nguyen, N. Q. and Barbour, A. and Zeps, N. and Australian Pancreatic Cancer Genome, I. and Kakkar, N. and Zhao, F. and Wu, Y. Q. and Wang, M. and Muzny, D. M. and Fisher, W. E. and Brunicardi, F. C. and Hodges, S. E. and Reid, J. G. and Drummond, J. and Chang, K. and Han, Y. and Lewis, L. R. and Dinh, H. and Buhay, C. J. and Beck, T. and Timms, L. and Sam, M. and Begley, K. and Brown, A. and Pai, D. and Panchal, A. and Buchner, N. and De Borja, R. and Denroche, R. E. and Yung, C. K. and Serra, S. and Onetto, N. and Mukhopadhyay, D. and Tsao, M. S. and Shaw, P. A. and Petersen, G. M. and Gallinger, S. and Hruban, R. H. and Maitra, A. and Iacobuzio-Donahue, C. A. and Schulick, R. D. and Wolfgang, C. L. and Morgan, R. A. and Lawlor, R. T. and Capelli, P. and Corbo, V. and Scardoni, M. and Tortora, G. and Tempero, M. A. and Mann, K. M. and Jenkins, N. A. and Perez-Mancera, P. A. and Adams, D. J. and Largaespada, D. A. and Wessels, L. F. and Rust, A. G. and Stein, L. D. and Tuveson, D. A. and Copeland, N. G. and Musgrove, E. A. and Scarpa, A. and Eshleman, J. R. and Hudson, T. J. and Sutherland, R. L. and Wheeler, D. A. and Pearson, J. V. and McPherson, J. D. and Gibbs, R. A. and Grimmond, S. M. (2012) 'Pancreatic cancer genomes reveal aberrations in axon guidance pathway genes', *Nature,* 491(7424), pp. 399-405.

Bieller, A., Pasche, B., Frank, S., Glaser, B., Kunz, J., Witt, K. and Zoll, B. (2001) 'Isolation and characterization of the human forkhead gene FOXQ1', *DNA Cell Biol,* 20(9), pp. 555-61.

Boshart, M., Gissmann, L., Ikenberg, H., Kleinheinz, A., Scheurlen, W. and zur Hausen, H. (1984) 'A new type of papillomavirus DNA, its presence in genital cancer biopsies and in cell lines derived from cervical cancer', *EMBO J,* 3(5), pp. 1151-7.

Bouchereau, A., Aziz, A., Larher, F. and Martin-Tanguy, J. (1999) 'Polyamines and environmental challenges: recent development', *Plant Science,* 140(2), pp. 103-125.

Boveri, T. (1902) 'Über mehrpolige mitosen als mittel zur analyse des zellkerns'.

Brady, G., MacArthur, G. J. and Farrell, P. J. (2007) 'Epstein-Barr virus and Burkitt lymphoma', *J Clin Pathol,* 60(12), pp. 1397-402.
Bray, F., Ferlay, J., Soerjomataram, I., Siegel, R. L., Torre, L. A. and Jemal, A. (2018) 'Global cancer statistics 2018: GLOBOCAN estimates of incidence and mortality worldwide for 36 cancers in 185 countries', *CA Cancer J Clin,* 68(6), pp. 394-424.
Brinkman, E. K., Chen, T., Amendola, M. and van Steensel, B. (2014) 'Easy quantitative assessment of genome editing by sequence trace decomposition', *Nucleic Acids Res,* 42(22), pp. e168.
Brookes, P. and Lawley, P. D. (1964) 'Evidence for the Binding of Polynuclear Aromatic Hydrocarbons to the Nucleic Acids of Mouse Skin : Relation between Carcinogenic Power of Hydrocarbons and their Binding to Deoxyribonucleic Acid', *Nature,* 202(4934), pp. 781-784.
Calle, E. E., Rodriguez, C., Walker-Thurmond, K. and Thun, M. J. (2003) 'Overweight, obesity, and mortality from cancer in a prospectively studied cohort of US adults', *New England Journal of Medicine,* 348(17), pp. 1625-1638.
Callender, G. R. (1931) 'Malignant melanotic tumors of the eye: a study of histologic types in 111 cases', *Trans Am Acad Ophthalmol Otolaryngol,* 36(131), pp. e42.
Cancer Genome Atlas, N. (2012) 'Comprehensive molecular portraits of human breast tumours', *Nature,* 490(7418), pp. 61-70.
Cancer Research UK (2016). Available at: https://www.cancerresearchuk.org/health-professional/cancer-statistics/incidence/all-cancers-combined#heading-Zero (Accessed: 30/01/2020.
Cao, D., Hustinx, S. R., Sui, G., Bala, P., Sato, N., Martin, S., Maitra, A., Murphy, K. M., Cameron, J. L., Yeo, C. J., Kern, S. E., Goggins, M., Pandey, A. and Hruban, R. H. (2004) 'Identification of novel highly expressed genes in pancreatic ductal adenocarcinomas through a bioinformatics analysis of expressed sequence tags', *Cancer Biol Ther,* 3(11), pp. 1081-9; discussion 1090-1.
Carless, M. A. and Griffiths, L. R. (2008) 'Cytogenetics of melanoma and nonmelanoma skin cancer', *Adv Exp Med Biol,* 624, pp. 227-40.
Carlsson, P. and Mahlapuu, M. (2002) 'Forkhead transcription factors: key players in development and metabolism', *Dev Biol,* 250(1), pp. 1-23.
Carroll, D. (2016) 'Genome editing: progress and challenges for medical applications', *Genome Medicine,* 8.
Carvajal, R. D., Antonescu, C. R., Wolchok, J. D., Chapman, P. B., Roman, R. A., Teitcher, J., Panageas, K. S., Busam, K. J., Chmielowski, B., Lutzky, J., Pavlick, A. C., Fusco, A., Cane, L., Takebe, N., Vemula, S., Bouvier, N., Bastian, B. C. and Schwartz, G. K. (2011) 'KIT as a therapeutic target in metastatic melanoma', *JAMA,* 305(22), pp. 2327-34.
Cassoux, N., Rodrigues, M. J., Plancher, C., Asselain, B., Levy-Gabriel, C., Lumbroso-Le Rouic, L., Piperno-Neumann, S., Dendale, R., Sastre, X., Desjardins, L. and Couturier, J. (2014) 'Genome-wide profiling is a clinically relevant and affordable prognostic test in posterior uveal melanoma', *British Journal of Ophthalmology,* 98(6), pp. 769-774.
Cebulla, C. M., Binkley, E. M., Pilarski, R., Massengill, J. B., Rai, K., Liebner, D. A., Marino, M. J., Singh, A. D. and Abdel-Rahman, M. H. (2015)

'Analysis of BAP1 Germline Gene Mutation in Young Uveal Melanoma Patients', *Ophthalmic Genet,* 36(2), pp. 126-31.
Cesare, A. J. and Reddel, R. R. (2010) 'Alternative lengthening of telomeres: models, mechanisms and implications', *Nat Rev Genet,* 11(5), pp. 319-30.
Char, D. H. and Miller, T. (1995) 'Accuracy of Presumed Uveal Melanoma Diagnosis before Alternative Therapy', *British Journal of Ophthalmology,* 79(7), pp. 692-696.
Chattopadhyay, C., Kim, D. W., Gombos, D. S., Oba, J., Qin, Y., Williams, M. D., Esmaeli, B., Grimm, E. A., Wargo, J. A., Woodman, S. E. and Patel, S. P. (2016) 'Uveal melanoma: From diagnosis to treatment and the science in between', *Cancer*.
Chaudhuri, J., Si, K. and Maitra, U. (1997) 'Function of eukaryotic translation initiation factor 1A (eIF1A) (formerly called eIF-4C) in initiation of protein synthesis', *J Biol Chem,* 272(12), pp. 7883-91.
Cheng, K. W., Lahad, J. P., Kuo, W. L., Lapuk, A., Yamada, K., Auersperg, N., Liu, J., Smith-McCune, K., Lu, K. H., Fishman, D., Gray, J. W. and Mills, G. B. (2004) 'The RAB25 small GTPase determines aggressiveness of ovarian and breast cancers', *Nat Med,* 10(11), pp. 1251-6.
Chiang, P. K., Gordon, R. K., Tal, J., Zeng, G. C., Doctor, B. P., Pardhasaradhi, K. and McCann, P. P. (1996) 'S-Adenosylmethionine and methylation', *FASEB J,* 10(4), pp. 471-80.
Childs, A. C., Mehta, D. J. and Gerner, E. W. (2003) 'Polyamine-dependent gene expression', *Cell Mol Life Sci,* 60(7), pp. 1394-406.
Chokhachi Baradaran, P., Kozovska, Z., Furdova, A. and Smolkova, B. (2020) 'Targeting Epigenetic Modifications in Uveal Melanoma', *Int J Mol Sci,* 21(15).
Choo, Q. L., Kuo, G., Weiner, A. J., Overby, L. R., Bradley, D. W. and Houghton, M. (1989) 'Isolation of a cDNA clone derived from a blood-borne non-A, non-B viral hepatitis genome', *Science,* 244(4902), pp. 359-62.
Christensen, J., Bentz, S., Sengstag, T., Shastri, V. P. and Anderle, P. (2013) 'FOXQ1, a novel target of the Wnt pathway and a new marker for activation of Wnt signaling in solid tumors', *PLoS One,* 8(3), pp. e60051.
Cohen, Y., Goldenberg-Cohen, N., Parrella, P., Chowers, I., Merbs, S. L., Pe'er, J. and Sidransky, D. (2003) 'Lack of BRAF mutation in primary uveal melanoma', *Invest Ophthalmol Vis Sci,* 44(7), pp. 2876-8.
COMS (1990) 'Accuracy of Diagnosis of Choroidal Melanomas in the Collaborative Ocular Melanoma Study', *Archives of Ophthalmology,* 108(9), pp. 1268.
Cong, L., Ran, F. A., Cox, D., Lin, S. L., Barretto, R., Habib, N., Hsu, P. D., Wu, X. B., Jiang, W. Y., Marraffini, L. A. and Zhang, F. (2013) 'Multiplex Genome Engineering Using CRISPR/Cas Systems', *Science,* 339(6121), pp. 819-823.
Coupland, S. E., Lake, S. L., Zeschnigk, M. and Damato, B. E. (2013) 'Molecular pathology of uveal melanoma', *Eye (Lond),* 27(2), pp. 230-42.
Cross, N. A., Ganesh, A., Parpia, M., Murray, A. K., Rennie, I. G. and Sisley, K. (2006) 'Multiple locations on chromosome 3 are the targets of specific deletions in uveal melanoma', *Eye (Lond),* 20(4), pp. 476-81.

Cross, N. A., Murray, A. K., Rennie, I. G., Ganesh, A. and Sisley, K. (2003) 'Instability of microsatellites is an infrequent event in uveal melanoma', *Melanoma Research,* 13(5), pp. 435-440.
Daley, G. Q. and Baltimore, D. (1988) 'Transformation of an Interleukin-3-Dependent Hematopoietic-Cell Line by the Chronic Myelogenous Leukemia-Specific P210ber/Abl Protein', *Proceedings of the National Academy of Sciences of the United States of America,* 85(23), pp. 9312-9316.
Damato, B. (2006) 'Treatment of primary intraocular melanoma', *Expert Rev Anticancer Ther,* 6(4), pp. 493-506.
Damato, B. (2010) 'Does ocular treatment of uveal melanoma influence survival?', *Br J Cancer,* 103(3), pp. 285-90.
Damato, B., Dopierala, J., Klaasen, A., van Dijk, M., Sibbring, J. and Coupland, S. E. (2009) 'Multiplex ligation-dependent probe amplification of uveal melanoma: correlation with metastatic death', *Invest Ophthalmol Vis Sci,* 50(7), pp. 3048-55.
Damato, B., Dopierala, J. A. and Coupland, S. E. (2010) 'Genotypic profiling of 452 choroidal melanomas with multiplex ligation-dependent probe amplification', *Clin Cancer Res,* 16(24), pp. 6083-92.
Damato, B., Duke, C., Coupland, S. E., Hiscott, P., Smith, P. A., Campbell, I., Douglas, A. and Howard, P. (2007) 'Cytogenetics of uveal melanoma: a 7-year clinical experience', *Ophthalmology,* 114(10), pp. 1925-31.
Damato, B., Kacperek, A., Errington, D. and Heimann, H. (2013) 'Proton beam radiotherapy of uveal melanoma', *Saudi J Ophthalmol,* 27(3), pp. 151-7.
Dane, D. S., Cameron, C. H. and Briggs, M. (1970) 'Virus-like particles in serum of patients with Australia-antigen-associated hepatitis', *Lancet,* 1(7649), pp. 695-8.
Davies, H., Bignell, G. R., Cox, C., Stephens, P., Edkins, S., Clegg, S., Teague, J., Woffendin, H., Garnett, M. J., Bottomley, W., Davis, N., Dicks, E., Ewing, R., Floyd, Y., Gray, K., Hall, S., Hawes, R., Hughes, J., Kosmidou, V., Menzies, A., Mould, C., Parker, A., Stevens, C., Watt, S., Hooper, S., Wilson, R., Jayatilake, H., Gusterson, B. A., Cooper, C., Shipley, J., Hargrave, D., Pritchard-Jones, K., Maitland, N., Chenevix-Trench, G., Riggins, G. J., Bigner, D. D., Palmieri, G., Cossu, A., Flanagan, A., Nicholson, A., Ho, J. W., Leung, S. Y., Yuen, S. T., Weber, B. L., Seigler, H. F., Darrow, T. L., Paterson, H., Marais, R., Marshall, C. J., Wooster, R., Stratton, M. R. and Futreal, P. A. (2002) 'Mutations of the BRAF gene in human cancer', *Nature,* 417(6892), pp. 949-54.
Davis, M. D., Fine, S. L. and Kupfer, C. (1994) 'The collaborative Ocular Melanoma Study', *Arch Ophthalmol,* 112(6), pp. 730-1.
DeBoever, C., Ghia, E. M., Shepard, P. J., Rassenti, L., Barrett, C. L., Jepsen, K., Jamieson, C. H., Carson, D., Kipps, T. J. and Frazer, K. A. (2015) 'Transcriptome sequencing reveals potential mechanism of cryptic 3' splice site selection in SF3B1-mutated cancers', *PLoS Comput Biol,* 11(3), pp. e1004105.
Decatur, C. L., Ong, E., Garg, N., Anbunathan, H., Bowcock, A. M., Field, M. G. and Harbour, J. W. (2016) 'Driver Mutations in Uveal Melanoma: Associations With Gene Expression Profile and Patient Outcomes', *JAMA Ophthalmol,* 134(7), pp. 728-33.
DePinho, R. A. (2000) 'The age of cancer', *Nature,* 408(6809), pp. 248-54.

Desjardins, L., Dorval, T., Lévy, C., Cojean, I., Schlienger, P., Salmon, R., Validire, P. and Asselain, B. (1998) 'Randomised study on adjuvant therapy by DTIC in choroidal melanoma', *Ophtalmologie,* 12(3), pp. 168-173.

Dhillon, A. S., Hagan, S., Rath, O. and Kolch, W. (2007) 'MAP kinase signalling pathways in cancer', *Oncogene,* 26(22), pp. 3279-3290.

Diener-West, M., Reynolds, S. M., Agugliaro, D. J., Caldwell, R., Cumming, K., Earle, J. D., Hawkins, B. S., Hayman, J. A., Jaiyesimi, I., Jampol, L. M., Kirkwood, J. M., Koh, W. J., Robertson, D. M., Shaw, J. M., Straatsma, B. R., Thoma, J. and Collaborative Ocular Melanoma Study, G. (2005) 'Development of metastatic disease after enrollment in the COMS trials for treatment of choroidal melanoma: Collaborative Ocular Melanoma Study Group Report No. 26', *Arch Ophthalmol,* 123(12), pp. 1639-43.

Dienerwest, M., Hawkins, B. S., Markowitz, J. A. and Schachat, A. P. (1992) 'A Review of Mortality from Choroidal Melanoma .2. A Metaanalysis of 5-Year Mortality-Rates Following Enucleation, 1966 through 1988', *Archives of Ophthalmology,* 110(2), pp. 245-250.

Diskin, S. J., Eck, T., Greshock, J., Mosse, Y. P., Naylor, T., Stoeckert, C. J., Jr., Weber, B. L., Maris, J. M. and Grant, G. R. (2006) 'STAC: A method for testing the significance of DNA copy number aberrations across multiple array-CGH experiments', *Genome Res,* 16(9), pp. 1149-58.

Dogrusoz, M., Bagger, M., van Duinen, S. G., Kroes, W. G., Ruivenkamp, C. A., Bohringer, S., Andersen, K. K., Luyten, G. P., Kiilgaard, J. F. and Jager, M. J. (2017) 'The Prognostic Value of AJCC Staging in Uveal Melanoma Is Enhanced by Adding Chromosome 3 and 8q Status', *Invest Ophthalmol Vis Sci,* 58(2), pp. 833-842.

Doherty, R. E., Alfawaz, M., Francis, J., Lijka-Jones, B. and Sisley, K. (2018) 'Genetics of Uveal Melanoma', in Scott, J.F. & Gerstenblith, M.R. (eds.) *Noncutaneous Melanoma*. Brisbane (AU).

Dono, M., Angelini, G., Cecconi, M., Amaro, A., Esposito, A. I., Mirisola, V., Maric, I., Lanza, F., Nasciuti, F., Viaggi, S., Gualco, M., Bandelloni, R., Truini, M., Coviello, D. A., Zupo, S., Mosci, C. and Pfeffer, U. (2014) 'Mutation frequencies of GNAQ, GNA11, BAP1, SF3B1, EIF1AX and TERT in uveal melanoma: detection of an activating mutation in the TERT gene promoter in a single case of uveal melanoma', *Br J Cancer,* 110(4), pp. 1058-65.

Drabarek, W., Yavuzyigitoglu, S., Obulkasim, A., van Riet, J., Smit, K. N., van Poppelen, N. M., Vaarwater, J., Brands, T., Eussen, B., Verdijk, R. M., Naus, N. C., Mensink, H. W., Paridaens, D., Boersma, E., van de Werken, H. J. G., Kilic, E., de Klein, A. and Rotterdam Ocular Melanoma Study, G. (2019) 'Multi-Modality Analysis Improves Survival Prediction in Enucleated Uveal Melanoma Patients', *Invest Ophthalmol Vis Sci,* 60(10), pp. 3595-3605.

Durst, M., Gissmann, L., Ikenberg, H. and zur Hausen, H. (1983) 'A papillomavirus DNA from a cervical carcinoma and its prevalence in cancer biopsy samples from different geographic regions', *Proc Natl Acad Sci U S A,* 80(12), pp. 3812-5.

Efeyan, A., Comb, W. C. and Sabatini, D. M. (2015) 'Nutrient-sensing mechanisms and pathways', *Nature,* 517(7534), pp. 302-310.

Ehlers, J. P. and Harbour, J. W. (2005) 'NBS1 expression as a prognostic marker in uveal melanoma', *Clinical Cancer Research,* 11(5), pp. 1849-1853.
Ehlers, J. P., Worley, L., Onken, M. D. and Harbour, J. W. (2005) 'DDEF1 is located in an amplified region of chromosome 8q and is overexpressed in uveal melanoma', *Clinical Cancer Research,* 11(10), pp. 3609-3613.
Ehlers, J. P., Worley, L., Onken, M. D. and Harbour, J. W. (2008) 'Integrative genomic analysis of aneuploidy in uveal melanoma', *Clin Cancer Res,* 14(1), pp. 115-22.
Elo, J. M., Yadavalli, S. S., Euro, L., Isohanni, P., Gotz, A., Carroll, C. J., Valanne, L., Alkuraya, F. S., Uusimaa, J., Paetau, A., Caruso, E. M., Pihko, H., Ibba, M., Tyynismaa, H. and Suomalainen, A. (2012) 'Mitochondrial phenylalanyl-tRNA synthetase mutations underlie fatal infantile Alpers encephalopathy', *Hum Mol Genet,* 21(20), pp. 4521-9.
Epstein, M. A., Achong, B. G. and Barr, Y. M. (1964) 'Virus Particles in Cultured Lymphoblasts from Burkitt's Lymphoma', *Lancet,* 1(7335), pp. 702-3.
Eskelin, S. and Kivela, T. (2002) 'Mode of presentation and time to treatment of uveal melanoma in Finland', *Br J Ophthalmol,* 86(3), pp. 333-8.
Eslick, G. D., Lim, L. L., Byles, J. E., Xia, H. H. and Talley, N. J. (1999) 'Association of Helicobacter pylori infection with gastric carcinoma: a meta-analysis', *Am J Gastroenterol,* 94(9), pp. 2373-9.
Evangelidou, P., Sismani, C., Ioannides, M., Christodoulou, C., Koumbaris, G., Kallikas, I., Georgiou, I., Velissariou, V. and Patsalis, P. C. (2010) 'Clinical application of whole-genome array CGH during prenatal diagnosis: Study of 25 selected pregnancies with abnormal ultrasound findings or apparently balanced structural aberrations', *Mol Cytogenet,* 3, pp. 24.
Fabian, I. D., Stacey, A. W., Papastefanou, V., Al Harby, L., Arora, A. K., Sagoo, M. S., Cohen, V. M. and Medscape (2017) 'Primary photodynamic therapy with verteporfin for small pigmented posterior pole choroidal melanoma', *Eye (Lond),* 31(4), pp. 519-528.
Fakiris, A. J., Lo, S. S., Henderson, M. A., Witt, T. C., Worth, R. M., Danis, R. P., Des Rosiers, P. M. and Timmerman, R. D. (2007) 'Gamma-knife-based stereotactic radiosurgery for uveal melanoma', *Stereotact Funct Neurosurg,* 85(2-3), pp. 106-12.
Fan, D. M., Feng, X. S., Qi, P. W. and Chen, Y. W. (2014) 'Forkhead factor FOXQ1 promotes TGF-beta1 expression and induces epithelial-mesenchymal transition', *Mol Cell Biochem,* 397(1-2), pp. 179-86.
Feng, X., Degese, M. S., Iglesias-Bartolome, R., Vaque, J. P., Molinolo, A. A., Rodrigues, M., Zaidi, M. R., Ksander, B. R., Merlino, G., Sodhi, A., Chen, Q. and Gutkind, J. S. (2014) 'Hippo-independent activation of YAP by the GNAQ uveal melanoma oncogene through a trio-regulated rho GTPase signaling circuitry', *Cancer Cell,* 25(6), pp. 831-45.
Feuerborn, A., Srivastava, P. K., Kuffer, S., Grandy, W. A., Sijmonsma, T. P., Gretz, N., Brors, B. and Grone, H. J. (2011) 'The Forkhead factor FoxQ1 influences epithelial differentiation', *J Cell Physiol,* 226(3), pp. 710-9.
Field, M. G., Decatur, C. L., Kurtenbach, S., Gezgin, G., van der Velden, P. A., Jager, M. J., Kozak, K. N. and Harbour, J. W. (2016) 'PRAME as an Independent Biomarker for Metastasis in Uveal Melanoma', *Clin Cancer Res,* 22(5), pp. 1234-42.

Field, M. G., Durante, M. A., Anbunathan, H., Cai, L. Z., Decatur, C. L., Bowcock, A. M., Kurtenbach, S. and Harbour, J. W. (2018) 'Punctuated evolution of canonical genomic aberrations in uveal melanoma', *Nature Communications,* 9.

Furney, S. J., Pedersen, M., Gentien, D., Dumont, A. G., Rapinat, A., Desjardins, L., Turajlic, S., Piperno-Neumann, S., de la Grange, P., Roman-Roman, S., Stern, M. H. and Marais, R. (2013) 'SF3B1 mutations are associated with alternative splicing in uveal melanoma', *Cancer Discov,* 3(10), pp. 1122-9.

Gao, M., Shih Ie, M. and Wang, T. L. (2012) 'The role of forkhead box Q1 transcription factor in ovarian epithelial carcinomas', *Int J Mol Sci,* 13(11), pp. 13881-93.

Garbe, C. and Leiter, U. (2009) 'Melanoma epidemiology and trends', *Clin Dermatol,* 27(1), pp. 3-9.

Gautrey, H., Jackson, C., Dittrich, A. L., Browell, D., Lennard, T. and Tyson-Capper, A. (2015) 'SRSF3 and hnRNP H1 regulate a splicing hotspot of HER2 in breast cancer cells', *RNA Biol,* 12(10), pp. 1139-51.

Gerami, P., Mafee, M., Lurtsbarapa, T., Guitart, J., Haghighat, Z. and Newman, M. (2010) 'Sensitivity of fluorescence in situ hybridization for melanoma diagnosis using RREB1, MYB, Cep6, and 11q13 probes in melanoma subtypes', *Arch Dermatol,* 146(3), pp. 273-8.

Gerner, E. W., Ignatenko, N. A., Lance, P. and Hurley, L. H. (2005) 'A comprehensive strategy to combat colon cancer targeting the adenomatous polyposis coli tumor suppressor gene', *Ann N Y Acad Sci,* 1059, pp. 97-105.

Glaser, S. L., Lin, R. J., Stewart, S. L., Ambinder, R. F., Jarrett, R. F., Brousset, P., Pallesen, G., Gulley, M. L., Khan, G., O'Grady, J., Hummel, M., Preciado, M. V., Knecht, H., Chan, J. K. and Claviez, A. (1997) 'Epstein-Barr virus-associated Hodgkin's disease: epidemiologic characteristics in international data', *Int J Cancer,* 70(4), pp. 375-82.

Gordon, K., Char, D., Obrien, J., Ghazvini, S., Choi, E., Elbakri, H. and Kroll, S. (1993) 'Use of Comparative Genomic Hybridization for Cytogenetic Analysis of Uveal Melanomas', *Investigative Ophthalmology & Visual Science,* 34(4), pp. 890-890.

Gordon, K. B., Thompson, C. T., Char, D. H., Obrien, J. M., Kroll, S., Ghazvini, S. and Gray, J. W. (1994) 'Comparative Genomic Hybridization in the Detection of DNA Copy Number Abnormalities in Uveal Melanoma', *Cancer Research,* 54(17), pp. 4764-4768.

Gragoudas, E. S., Egan, K. M., Seddon, J. M., Glynn, R. J., Walsh, S. M., Finn, S. M., Munzenrider, J. E. and Spar, M. D. (1991) 'Survival of patients with metastases from uveal melanoma', *Ophthalmology,* 98(3), pp. 383-9; discussion 390.

Griewank, K. G., Murali, R., Schilling, B., Scholz, S., Sucker, A., Song, M., Susskind, D., Grabellus, F., Zimmer, L., Hillen, U., Steuhl, K. P., Schadendorf, D., Westekemper, H. and Zeschnigk, M. (2013) 'TERT promoter mutations in ocular melanoma distinguish between conjunctival and uveal tumours', *Br J Cancer,* 109(2), pp. 497-501.

Hammer, H., Olah, J. and Toth-Molnar, E. (1996) 'Dysplastic nevi are a risk factor for uveal melanoma', *Eur J Ophthalmol,* 6(4), pp. 472-4.

Hammond, D. W., Al-Shammari, N. S., Danson, S., Jacques, R., Rennie, I. G. and Sisley, K. (2015) 'High-Resolution Array CGH Analysis Identifies Regional Deletions and Amplifications of Chromosome 8 in Uveal Melanoma', *Invest Ophthalmol Vis Sci,* 56(6), pp. 3460-6.
Hanahan, D. and Weinberg, R. A. (2000) 'The hallmarks of cancer', *Cell,* 100(1), pp. 57-70.
Hanahan, D. and Weinberg, R. A. (2011) 'Hallmarks of cancer: the next generation', *Cell,* 144(5), pp. 646-74.
Harbour, J. W., Onken, M. D., Roberson, E. D., Duan, S., Cao, L., Worley, L. A., Council, M. L., Matatall, K. A., Helms, C. and Bowcock, A. M. (2010) 'Frequent mutation of BAP1 in metastasizing uveal melanomas', *Science,* 330(6009), pp. 1410-3.
Harbour, J. W., Roberson, E. D., Anbunathan, H., Onken, M. D., Worley, L. A. and Bowcock, A. M. (2013) 'Recurrent mutations at codon 625 of the splicing factor SF3B1 in uveal melanoma', *Nat Genet,* 45(2), pp. 133-5.
Harvey, J. M., Clark, G. M., Osborne, C. K. and Allred, D. C. (1999) 'Estrogen receptor status by immunohistochemistry is superior to the ligand-binding assay for predicting response to adjuvant endocrine therapy in breast cancer', *J Clin Oncol,* 17(5), pp. 1474-81.
Hausler, T., Stang, A., Anastassiou, G., Jockel, K. H., Mrzyk, S., Horsthemke, B., Lohmann, D. R. and Zeschnigk, M. (2005) 'Loss of heterozygosity of 1p in uveal melanomas with monosomy 3', *International Journal of Cancer,* 116(6), pp. 909-913.
He, W., Roh, E., Yao, K., Liu, K., Meng, X., Liu, F., Wang, P., Bode, A. M. and Dong, Z. (2017) 'Targeting ornithine decarboxylase (ODC) inhibits esophageal squamous cell carcinoma progression', *NPJ Precis Oncol,* 1(1), pp. 13.
Healy, E., Belgaid, C., Takata, M., Harrison, D., Zhu, N. W., Burd, D. A. R., Rigby, H. S., Matthews, J. N. S. and Rees, J. L. (1998) 'Prognostic significance of allelic losses in primary melanoma', *Oncogene,* 16(17), pp. 2213-2218.
Hecht, S. S. (2002) 'Cigarette smoking and lung cancer: chemical mechanisms and approaches to prevention', *Lancet Oncol,* 3(8), pp. 461-9.
Heng, B., Glenn, W. K., Ye, Y., Tran, B., Delprado, W., Lutze-Mann, L., Whitaker, N. J. and Lawson, J. S. (2009) 'Human papilloma virus is associated with breast cancer', *Br J Cancer,* 101(8), pp. 1345-50.
Henriquez, F., Janssen, C., Kemp, E. G. and Roberts, F. (2007) 'The T1799A BRAF mutation is present in iris melanoma', *Invest Ophthalmol Vis Sci,* 48(11), pp. 4897-900.
Hijiya, N., Zhang, J., Ratajczak, M. Z., Kant, J. A., DeRiel, K., Herlyn, M., Zon, G. and Gewirtz, A. M. (1994) 'Biologic and therapeutic significance of MYB expression in human melanoma', *Proc Natl Acad Sci U S A,* 91(10), pp. 4499-503.
Hillman, S. C., Pretlove, S., Coomarasamy, A., McMullan, D. J., Davison, E. V., Maher, E. R. and Kilby, M. D. (2011) 'Additional information from array comparative genomic hybridization technology over conventional karyotyping in prenatal diagnosis: a systematic review and meta-analysis', *Ultrasound in Obstetrics & Gynecology,* 37(1), pp. 6-14.
Hirsch, D., Kemmerling, R., Davis, S., Camps, J., Meltzer, P. S., Ried, T. and Gaiser, T. (2013) 'Chromothripsis and focal copy number alterations

determine poor outcome in malignant melanoma', *Cancer research,* 73(5), pp. 1454-1460.
Ho, A. L., Musi, E., Ambrosini, G., Nair, J. S., Vasudeva, S. D., de Stanchina, E. and Schwartz, G. K. (2012) 'Impact of Combined mTOR and MEK Inhibition in Uveal Melanoma Is Driven by Tumor Genotype', *Plos One,* 7(7).
Hoglund, M., Gisselsson, D., Hansen, G. B., White, V. A., Sall, T., Mitelman, F. and Horsman, D. (2004) 'Dissecting karyotypic patterns in malignant melanomas: temporal clustering of losses and gains in melanoma karyotypic evolution', *Int J Cancer,* 108(1), pp. 57-65.
Holly, E. A., Aston, D. A., Char, D. H., Kristiansen, J. J. and Ahn, D. K. (1990) 'Uveal melanoma in relation to ultraviolet light exposure and host factors', *Cancer Res,* 50(18), pp. 5773-7.
Horn, S., Figl, A., Rachakonda, P. S., Fischer, C., Sucker, A., Gast, A., Kadel, S., Moll, I., Nagore, E., Hemminki, K., Schadendorf, D. and Kumar, R. (2013) 'TERT promoter mutations in familial and sporadic melanoma', *Science,* 339(6122), pp. 959-61.
Horsman, D. E. and White, V. A. (1993) 'Cytogenetic Analysis of Uveal Melanoma - Consistent Occurrence of Monosomy 3 and Trisomy 8q', *Cancer,* 71(3), pp. 811-819.
Huang, F. W., Hodis, E., Xu, M. J., Kryukov, G. V., Chin, L. and Garraway, L. A. (2013) 'Highly recurrent TERT promoter mutations in human melanoma', *Science,* 339(6122), pp. 957-9.
IARC, W. G. o. t. E. o. C. R. t. H. (2012) 'Radiation', *IARC Monogr Eval Carcinog Risks Hum,* 100(Pt D), pp. 7-303.
International Human Genome Sequencing, C. (2004) 'Finishing the euchromatic sequence of the human genome', *Nature,* 431(7011), pp. 931-45.
Ishaq, S. and Nunn, L. (2015) 'Helicobacter pylori and gastric cancer: a state of the art review', *Gastroenterol Hepatol Bed Bench,* 8(Suppl 1), pp. S6-S14.
Ishino, Y., Shinagawa, H., Makino, K., Amemura, M. and Nakata, A. (1987) 'Nucleotide-Sequence of the Iap Gene, Responsible for Alkaline-Phosphatase Isozyme Conversion in Escherichia-Coli, and Identification of the Gene-Product', *Journal of Bacteriology,* 169(12), pp. 5429-5433.
Jager, M. J., Brouwer, N. J. and Esmaeli, B. (2018) 'The Cancer Genome Atlas Project: An Integrated Molecular View of Uveal Melanoma', *Ophthalmology,* 125(8), pp. 1139-1142.
Jansen, R., van Embden, J. D. A., Gaastra, W. and Schouls, L. M. (2002) 'Identification of genes that are associated with DNA repeats in prokaryotes', *Molecular Microbiology,* 43(6), pp. 1565-1575.
Jeggo, P. A., Pearl, L. H. and Carr, A. M. (2016) 'DNA repair, genome stability and cancer: a historical perspective', *Nat Rev Cancer,* 16(1), pp. 35-42.
Jemal, A., Siegel, R., Xu, J. and Ward, E. (2010) 'Cancer statistics, 2010', *CA Cancer J Clin,* 60(5), pp. 277-300.
Jensen, D. E., Proctor, M., Marquis, S. T., Gardner, H. P., Ha, S. I., Chodosh, L. A., Ishov, A. M., Tommerup, N., Vissing, H., Sekido, Y., Minna, J., Borodovsky, A., Schultz, D. C., Wilkinson, K. D., Maul, G. G., Barlev, N., Berger, S. L., Prendergast, G. C. and Rauscher, F. J. (1998) 'BAP1: a novel ubiquitin hydrolase which binds to the BRCA1 RING finger and

enhances BRCA1-mediated cell growth suppression', *Oncogene,* 16(9), pp. 1097-1112.
Jinek, M., Chylinski, K., Fonfara, I., Hauer, M., Doudna, J. A. and Charpentier, E. (2012) 'A programmable dual-RNA-guided DNA endonuclease in adaptive bacterial immunity', *Science,* 337(6096), pp. 816-21.
Johansson, P., Aoude, L. G., Wadt, K., Glasson, W. J., Warrier, S. K., Hewitt, A. W., Kiilgaard, J. F., Heegaard, S., Isaacs, T., Franchina, M., Ingvar, C., Vermeulen, T., Whitehead, K. J., Schmidt, C. W., Palmer, J. M., Symmons, J., Gerdes, A. M., Jonsson, G. and Hayward, N. K. (2016) 'Deep sequencing of uveal melanoma identifies a recurrent mutation in PLCB4', *Oncotarget,* 7(4), pp. 4624-4631.
Kaestner, K. H., Knochel, W. and Martinez, D. E. (2000) 'Unified nomenclature for the winged helix/forkhead transcription factors', *Genes Dev,* 14(2), pp. 142-6.
Kaliki, S., Shields, C. L. and Shields, J. A. (2015) 'Uveal melanoma: estimating prognosis', *Indian J Ophthalmol,* 63(2), pp. 93-102.
Kalirai, H., Dodson, A., Faqir, S., Damato, B. E. and Coupland, S. E. (2014) 'Lack of BAP1 protein expression in uveal melanoma is associated with increased metastatic risk and has utility in routine prognostic testing', *Br J Cancer,* 111(7), pp. 1373-80.
Kang, Y. H., Lee, H. S. and Kim, W. H. (2002) 'Promoter methylation and silencing of PTEN in gastric carcinoma', *Lab Invest,* 82(3), pp. 285-91.
Kath, R., Hayungs, J., Bornfeld, N., Sauerwein, W., Hoffken, K. and Seeber, S. (1993) 'Prognosis and treatment of disseminated uveal melanoma', *Cancer,* 72(7), pp. 2219-23.
Kaul, D., Wu, C. L., Adkins, C. B., Jordan, K. W., Defeo, E. M., Habbel, P., Peterson, R. T., McDougal, W. S., Pohl, U. and Cheng, L. L. (2010) 'Assessing prostate cancer growth with mRNA of spermine metabolic enzymes', *Cancer Biol Ther,* 9(9), pp. 736-42.
Kilic, E., Naus, N. C., van Gils, W., Klaver, C. C., van Til, M. E., Verbiest, M. M., Stijnen, T., Mooy, C. M., Paridaens, D., Beverloo, H. B., Luyten, G. P. and de Klein, A. (2005) 'Concurrent loss of chromosome arm 1p and chromosome 3 predicts a decreased disease-free survival in uveal melanoma patients', *Invest Ophthalmol Vis Sci,* 46(7), pp. 2253-7.
Kilic, E., van Gils, W., Lodder, E., Beverloo, H. B., van Til, M. E., Mooy, C. M., Paridaens, D., de Klein, A. and Luyten, G. P. (2006) 'Clinical and cytogenetic analyses in uveal melanoma', *Invest Ophthalmol Vis Sci,* 47(9), pp. 3703-7.
Kim, E. K. and Choi, E. J. (2010) 'Pathological roles of MAPK signaling pathways in human diseases', *Biochimica Et Biophysica Acta-Molecular Basis of Disease,* 1802(4), pp. 396-405.
Knudson, A. G. (1971) 'Mutation and Cancer - Statistical Study of Retinoblastoma', *Proceedings of the National Academy of Sciences of the United States of America,* 68(4), pp. 820-&.
Knudson, A. G. (1988) 'The Genetics of Childhood-Cancer', *Bulletin Du Cancer,* 75(1), pp. 135-138.
Knudson, A. G. (1993) 'Antioncogenes and Human Cancer', *Proceedings of the National Academy of Sciences of the United States of America,* 90(23), pp. 10914-10921.

Knudson, A. G. (2001) 'Two genetic hits (more or less) to cancer', *Nat Rev Cancer,* 1(2), pp. 157-62.
Kong, Y., Krauthammer, M. and Halaban, R. (2014) 'Rare SF3B1 R625 mutations in cutaneous melanoma', *Melanoma Res,* 24(4), pp. 332-4.
Konovalova, S. and Tyynismaa, H. (2013) 'Mitochondrial aminoacyl-tRNA synthetases in human disease', *Mol Genet Metab,* 108(4), pp. 206-11.
Koopmans, A. E., Ober, K., Dubbink, H. J., Paridaens, D., Naus, N. C., Belunek, S., Krist, B., Post, E., Zwarthoff, E. C., de Klein, A., Verdijk, R. M. and Rotterdam Ocular Melanoma Study, G. (2014a) 'Prevalence and implications of TERT promoter mutation in uveal and conjunctival melanoma and in benign and premalignant conjunctival melanocytic lesions', *Invest Ophthalmol Vis Sci,* 55(9), pp. 6024-30.
Koopmans, A. E., Vaarwater, J., Paridaens, D., Naus, N. C., Kilic, E., de Klein, A. and Rotterdam Ocular Melanoma Study, g. (2013) 'Patient survival in uveal melanoma is not affected by oncogenic mutations in GNAQ and GNA11', *Br J Cancer,* 109(2), pp. 493-6.
Koopmans, A. E., Verdijk, R. M., Brouwer, R. W., van den Bosch, T. P., van den Berg, M. M., Vaarwater, J., Kockx, C. E., Paridaens, D., Naus, N. C., Nellist, M., van, I. W. F., Kilic, E. and de Klein, A. (2014b) 'Clinical significance of immunohistochemistry for detection of BAP1 mutations in uveal melanoma', *Mod Pathol,* 27(10), pp. 1321-30.
Kottschade, L. A., McWilliams, R. R., Markovic, S., Block, M. S., Bisneto, J. V., Pham, A. Q. and Dronca, R. S. (2015) 'The use of pembrolizumab for the treatment of metastatic uveal melanoma.', *Journal of Clinical Oncology,* 33(15).
Kroll, S., Char, D. H., Quivey, J. and Castro, J. (1998) 'A comparison of cause-specific melanoma mortality and all-cause mortality in survival analyses after radiation treatment for uveal melanoma', *Ophthalmology,* 105(11), pp. 2035-45.
Kujala, E., Makitie, T. and Kivela, T. (2003) 'Very long-term prognosis of patients with malignant uveal melanoma', *Invest Ophthalmol Vis Sci,* 44(11), pp. 4651-9.
Landreville, S., Agapova, O. A. and Harbour, J. W. (2008) 'Emerging insights into the molecular pathogenesis of uveal melanoma', *Future Oncol,* 4(5), pp. 629-36.
Lane, A. M., Egan, K. M., Harmon, D., Holbrook, A., Munzenrider, J. E. and Gragoudas, E. S. (2009) 'Adjuvant Interferon Therapy for Patients with Uveal Melanoma at High Risk of Metastasis', *Ophthalmology,* 116(11), pp. 2206-2212.
Lepez-Otin, C., Blasco, M. A., Partridge, L., Serrano, M. and Kroemer, G. (2013) 'The Hallmarks of Aging', *Cell,* 153(6), pp. 1194-1217.
Lin, W. M., Baker, A. C., Beroukhim, R., Winckler, W., Feng, W., Marmion, J. M., Laine, E., Greulich, H., Tseng, H., Gates, C., Hodi, F. S., Dranoff, G., Sellers, W. R., Thomas, R. K., Meyerson, M., Golub, T. R., Dummer, R., Herlyn, M., Getz, G. and Garraway, L. A. (2008) 'Modeling genomic diversity and tumor dependency in malignant melanoma', *Cancer Res,* 68(3), pp. 664-73.
Lu, S. C. and Mato, J. M. (2012) 'S-adenosylmethionine in liver health, injury, and cancer', *Physiol Rev,* 92(4), pp. 1515-42.

Luch, A. (2005) 'Nature and nurture - lessons from chemical carcinogenesis', *Nat Rev Cancer,* 5(2), pp. 113-25.
Luscan, A., Just, P. A., Briand, A., Burin des Roziers, C., Goussard, P., Nitschke, P., Vidaud, M., Avril, M. F., Terris, B. and Pasmant, E. (2015) 'Uveal melanoma hepatic metastases mutation spectrum analysis using targeted next-generation sequencing of 400 cancer genes', *Br J Ophthalmol,* 99(4), pp. 437-9.
Lutz, J. M., Cree, I., Sabroe, S., Kvist, T. K., Clausen, L. B., Afonso, N., Ahrens, W., Ballard, T. J., Bell, J., Cyr, D., Eriksson, M., Fevotte, J., Guenel, P., Hardell, L., Jockel, K. H., Miranda, A., Merletti, F., Morales-Suarez-Varela, M. M., Stengrevics, A. and Lynge, E. (2005) 'Occupational risks for uveal melanoma results from a case-control study in nine European countries', *Cancer Causes Control,* 16(4), pp. 437-47.
Ma, Y. L. and Li, M. D. (2017) 'Establishment of a Strong Link Between Smoking and Cancer Pathogenesis through DNA Methylation Analysis', *Scientific Reports,* 7.
Malaponte, G., Libra, M., Gangemi, P., Bevelacqua, V., Mangano, K., D'Amico, F., Mazzarino, M. C., Stivala, F., McCubrey, J. A. and Travali, S. (2006) 'Detection of BRAF gene mutation in primary choroidal melanoma tissue', *Cancer Biol Ther,* 5(2), pp. 225-7.
Malcovati, L., Papaemmanuil, E., Bowen, D. T., Boultwood, J., Della Porta, M. G., Pascutto, C., Travaglino, E., Groves, M. J., Godfrey, A. L., Ambaglio, I., Galli, A., Da Via, M. C., Conte, S., Tauro, S., Keenan, N., Hyslop, A., Hinton, J., Mudie, L. J., Wainscoat, J. S., Futreal, P. A., Stratton, M. R., Campbell, P. J., Hellstrom-Lindberg, E., Cazzola, M., Chronic Myeloid Disorders Working Group of the International Cancer Genome, C. and of the Associazione Italiana per la Ricerca sul Cancro Gruppo Italiano Malattie, M. (2011) 'Clinical significance of SF3B1 mutations in myelodysplastic syndromes and myelodysplastic/myeloproliferative neoplasms', *Blood,* 118(24), pp. 6239-46.
Mali, P., Yang, L. H., Esvelt, K. M., Aach, J., Guell, M., DiCarlo, J. E., Norville, J. E. and Church, G. M. (2013) 'RNA-Guided Human Genome Engineering via Cas9', *Science,* 339(6121), pp. 823-826.
Mancini, M., Vegna, M. L., Castoldi, G. L., Mecucci, C., Spirito, F., Elia, L., Tafuri, A., Annino, L., Pane, F., Rege-Cambrin, G., Gottardi, M., Leoni, P., Gallo, E., Camera, A., Luciano, L., Specchia, G., Torelli, G., Sborgia, M., Gabbas, A., Tedeschi, A., Della Starza, I., Cascavilla, N., Di Raimondo, F., Mandelli, F. and Foa, R. (2002) 'Partial deletions of long arm of chromosome 6: biologic and clinical implications in adult acute lymphoblastic leukemia', *Leukemia,* 16(10), pp. 2055-2061.
Maric, S. C., Crozat, A. and Janne, O. A. (1992) 'Structure and organization of the human S-adenosylmethionine decarboxylase gene', *J Biol Chem,* 267(26), pp. 18915-23.
Maric, S. C., Crozat, A., Louhimo, J., Knuutila, S. and Janne, O. A. (1995) 'The human S-adenosylmethionine decarboxylase gene: nucleotide sequence of a pseudogene and chromosomal localization of the active gene (AMD1) and the pseudogene (AMD2)', *Cytogenet Cell Genet,* 70(3-4), pp. 195-9.
Martin, J. W., Squire, J. A. and Zielenska, M. (2012) 'The genetics of osteosarcoma', *Sarcoma,* 2012, pp. 627254.

Martin, M., Masshofer, L., Temming, P., Rahmann, S., Metz, C., Bornfeld, N., van de Nes, J., Klein-Hitpass, L., Hinnebusch, A. G., Horsthemke, B., Lohmann, D. R. and Zeschnigk, M. (2013) 'Exome sequencing identifies recurrent somatic mutations in EIF1AX and SF3B1 in uveal melanoma with disomy 3', *Nat Genet,* 45(8), pp. 933-6.
Mashal, R. D., Koontz, J. and Sklar, J. (1995) 'Detection of mutations by cleavage of DNA heteroduplexes with bacteriophage resolvases', *Nat Genet,* 9(2), pp. 177-83.
Mashayekhi, A., Shields, C. L., Rishi, P., Atalay, H. T., Pellegrini, M., McLaughlin, J. P., Patrick, K. A., Morton, S. J., Remmer, M. H., Parendo, A., Schlitt, M. A. and Shields, J. A. (2015) 'Primary transpupillary thermotherapy for choroidal melanoma in 391 cases: importance of risk factors in tumor control', *Ophthalmology,* 122(3), pp. 600-9.
McCannel, T. A. (2013) 'Fine-needle aspiration biopsy in the management of choroidal melanoma', *Curr Opin Ophthalmol,* 24(3), pp. 262-6.
McLean, I. W., Foster, W. D. and Zimmerman, L. E. (1982) 'Uveal melanoma: location, size, cell type, and enucleation as risk factors in metastasis', *Hum Pathol,* 13(2), pp. 123-32.
McLean, I. W., Foster, W. D., Zimmerman, L. E. and Gamel, J. W. (1983) 'Modifications of Callender's classification of uveal melanoma at the Armed Forces Institute of Pathology', *Am J Ophthalmol,* 96(4), pp. 502-9.
McLean, M. J., Foster, W. D. and Zimmerman, L. E. (1977) 'Prognostic factors in small malignant melanomas of choroid and ciliary body', *Arch Ophthalmol,* 95(1), pp. 48-58.
Mechulam, A., Chernov, K. G., Mucher, E., Hamon, L., Curmi, P. A. and Pastre, D. (2009) 'Polyamine Sharing between Tubulin Dimers Favours Microtubule Nucleation and Elongation via Facilitated Diffusion', *Plos Computational Biology,* 5(1).
Melia, B. M., DienerWest, M., Bennett, S. R., Folk, J. C., Montague, P. R. and Weingeist, T. A. (1997) 'Factors predictive of growth and treatment of small choroidal melanoma - COMS report no. 5', *Archives of Ophthalmology,* 115(12), pp. 1537-1544.
Merlo, A., Herman, J. G., Mao, L., Lee, D. J., Gabrielson, E., Burger, P. C., Baylin, S. B. and Sidransky, D. (1995) '5' Cpg Island Methylation Is Associated with Transcriptional Silencing of the Tumor-Suppressor P16/Cdkn2/Mts1 in Human Cancers', *Nature Medicine,* 1(7), pp. 686-692.
Millikin, D., Meese, E., Vogelstein, B., Witkowski, C. and Trent, J. (1991) 'Loss of heterozygosity for loci on the long arm of chromosome 6 in human malignant melanoma', *Cancer Res,* 51(20), pp. 5449-53.
Minca, E. C., Tubbs, R. R., Portier, B. P., Wang, Z., Lanigan, C., Aronow, M. E., Triozzi, P. L., Singh, A., Cook, J. R., Sauntharajah, Y., Plesec, T. P., Schoenfield, L., Cawich, V., Sulpizio, S. and Schultz, R. A. (2014) 'Genomic microarray analysis on formalin-fixed paraffin-embedded material for uveal melanoma prognostication', *Cancer Genet,* 207(7-8), pp. 306-15.
Mitelman, F., Johansson, B. and Mertens, F. (1994) *Catalog of chromosome aberrations in cancer.* 5th edn. (2 vols). New York: Wiley-Liss.
Moon, S., Lee, Y. K., Lee, S. W. and Um, S. J. (2017) 'Suppressive role of OGT-mediated O-GlcNAcylation of BAP1 in retinoic acid signaling',

Biochemical and Biophysical Research Communications, 492(1), pp. 89-95.
Moore, A. R., Ceraudo, E., Sher, J. J., Guan, Y., Shoushtari, A. N., Chang, M. T., Zhang, J. Q., Walczak, E. G., Kazmi, M. A., Taylor, B. S., Huber, T., Chi, P., Sakmar, T. P. and Chen, Y. (2016) 'Recurrent activating mutations of G-protein-coupled receptor CYSLTR2 in uveal melanoma', *Nat Genet,* 48(6), pp. 675-80.
Mooy, C. M. and De Jong, P. T. (1996) 'Prognostic parameters in uveal melanoma: a review', *Surv Ophthalmol,* 41(3), pp. 215-28.
Muller, M., Rink, K., Krause, H. and Miller, K. (2000) 'PTEN/MMAC1 mutations in prostate cancer', *Prostate Cancer Prostatic Dis,* 3(S1), pp. S32.
Mullis, K., Faloona, F., Scharf, S., Saiki, R., Horn, G. and Erlich, H. (1986) 'Specific enzymatic amplification of DNA in vitro: the polymerase chain reaction', *Cold Spring Harb Symp Quant Biol,* 51 Pt 1, pp. 263-73.
Murphree, A. L. and Benedict, W. F. (1984) 'Retinoblastoma - Clues to Human Oncogenesis', *Science,* 223(4640), pp. 1028-1033.
Myatt, N., Aristodemou, P., Neale, M. H., Foss, A. J., Hungerford, J. L., Bhattacharya, S. and Cree, I. A. (2000) 'Abnormalities of the transforming growth factor-beta pathway in ocular melanoma', *J Pathol,* 192(4), pp. 511-8.
Nakaya, K., Yamagata, H. D., Arita, N., Nakashiro, K. I., Nose, M., Miki, T. and Hamakawa, H. (2007) 'Identification of homozygous deletions of tumor suppressor gene FAT in oral cancer using CGH-array', *Oncogene,* 26(36), pp. 5300-8.
Namiki, T., Yanagawa, S., Izumo, T., Ishikawa, M., Tachibana, M., Kawakami, Y., Yokozeki, H., Nishioka, K. and Kaneko, Y. (2005) 'Genomic alterations in primary metaphase comparative genomic cutaneous melanomas detected by hybridization with laser capture or manual microdisSsection: 6p gains may predict poor outcome', *Cancer Genetics and Cytogenetics,* 157(1), pp. 1-11.
Naus, N. C., van Drunen, E., de Klein, A., Luyten, G. P., Paridaens, D. A., Alers, J. C., Ksander, B. R., Beverloo, H. B. and Slater, R. M. (2001) 'Characterization of complex chromosomal abnormalities in uveal melanoma by fluorescence in situ hybridization, spectral karyotyping, and comparative genomic hybridization', *Genes Chromosomes Cancer,* 30(3), pp. 267-73.
Nishimura, K., Nakatsu, F., Kashiwagi, K., Ohno, H., Saito, T. and Igarashi, K. (2002) 'Essential role of S-adenosylmethionine decarboxylase in mouse embryonic development', *Genes Cells,* 7(1), pp. 41-7.
Nowell, P. C. and Hungerford, D. A. (1960) 'Chromosome studies on normal and leukemic human leukocytes', *J Natl Cancer Inst,* 25(1), pp. 85-109.
Nupponen, N. N., Hyytinen, E. R., Kallioniemi, A. H. and Visakorpi, T. (1998) 'Genetic alterations in prostate cancer cell lines detected by comparative genomic hybridization', *Cancer Genetics and Cytogenetics,* 101(1), pp. 53-57.
O'Keeffe, L. M., Taylor, G., Huxley, R. R., Mitchell, P., Woodward, M. and Peters, S. A. E. (2018) 'Smoking as a risk factor for lung cancer in women and men: a systematic review and meta-analysis', *Bmj Open,* 8(10).

Ogino, S., Kawasaki, T., Kirkner, G. J., Ogawa, A., Dorfman, I., Loda, M. and Fuchs, C. S. (2006) 'Down-regulation of p21 (CDKN1A/CIP1) is inversely associated with microsatellite instability and CpG island methylator phenotype (CIMP) in colorectal cancer', *J Pathol,* 210(2), pp. 147-54.

Onken, M. D., Worley, L. A., Char, D. H., Augsburger, J. J., Correa, Z. M., Nudleman, E., Aaberg, T. M., Jr., Altaweel, M. M., Bardenstein, D. S., Finger, P. T., Gallie, B. L., Harocopos, G. J., Hovland, P. G., McGowan, H. D., Milman, T., Mruthyunjaya, P., Simpson, E. R., Smith, M. E., Wilson, D. J., Wirostko, W. J. and Harbour, J. W. (2012) 'Collaborative Ocular Oncology Group report number 1: prospective validation of a multi-gene prognostic assay in uveal melanoma', *Ophthalmology,* 119(8), pp. 1596-603.

Onken, M. D., Worley, L. A., Ehlers, J. P. and Harbour, J. W. (2004) 'Gene expression profiling in uveal melanoma reveals two molecular classes and predicts metastatic death', *Cancer Res,* 64(20), pp. 7205-9.

Onken, M. D., Worley, L. A., Long, M. D., Duan, S., Council, M. L., Bowcock, A. M. and Harbour, J. W. (2008) 'Oncogenic mutations in GNAQ occur early in uveal melanoma', *Invest Ophthalmol Vis Sci,* 49(12), pp. 5230-4.

Onken, M. D., Worley, L. A., Tuscan, M. D. and Harbour, J. W. (2010) 'An accurate, clinically feasible multi-gene expression assay for predicting metastasis in uveal melanoma', *J Mol Diagn,* 12(4), pp. 461-8.

Ozaki, T., Schaefer, K. L., Wai, D., Buerger, H., Flege, S., Lindner, N., Kevric, M., Diallo, R., Bankfalvi, A., Brinkschmidt, C., Juergens, H., Winkelmann, W., Dockhorn-Dworniczak, B., Bielack, S. S. and Poremba, C. (2002) 'Genetic imbalances revealed by comparative genomic hybridization in osteosarcomas', *International Journal of Cancer,* 102(4), pp. 355-365.

Packer, S. and Rotman, M. (1980) 'Radiotherapy of choroidal melanoma with iodine 125', *Int Ophthalmol Clin,* 20(2), pp. 135-42.

Pan, H., Jia, R., Zhang, L., Xu, S., Wu, Q., Song, X., Zhang, H., Ge, S., Xu, X. L. and Fan, X. (2015) 'BAP1 regulates cell cycle progression through E2F1 target genes and mediates transcriptional silencing via H2A monoubiquitination in uveal melanoma cells', *Int J Biochem Cell Biol,* 60, pp. 176-84.

Pane, A. R. and Hirst, L. W. (2000) 'Ultraviolet light exposure as a risk factor for ocular melanoma in Queensland, Australia', *Ophthalmic Epidemiol,* 7(3), pp. 159-67.

Park, J. J., Diefenbach, R. J., Byrne, N., Kefford, R., Long, G. V., Scolyer, R. A., Gray, E., Carlino, M. S. and Rizos, H. (2020) 'Circulating tumor DNA (ctDNA) in patients (pts) with metastatic uveal melanoma (UM) treated with protein kinase C inhibitor (PKCi)', *Journal of Clinical Oncology,* 38(15_suppl), pp. e22054-e22054.

Parrella, P., Caballero, O. L., Sidransky, D. and Merbs, S. L. (2001) 'Detection of c-myc amplification in uveal melanoma by fluorescent in situ hybridization', *Investigative Ophthalmology & Visual Science,* 42(8), pp. 1679-1684.

Parrella, P., Fazio, V. M., Gallo, A. P., Sidransky, D. and Merbs, S. L. (2003) 'Fine mapping of chromosome 3 in uveal melanoma: Identification of a minimal region of deletion on chromosomal arm 3p25.1-p25.2', *Cancer Research,* 63(23), pp. 8507-8510.

Parrella, P., Sidransky, D. and Merbs, S. L. (1999) 'Allelotype of posterior uveal melanoma: implications for a bifurcated tumor progression pathway', *Cancer Res,* 59(13), pp. 3032-7.
Parsonnet, J., Friedman, G. D., Vandersteen, D. P., Chang, Y., Vogelman, J. H., Orentreich, N. and Sibley, R. K. (1991) 'Helicobacter pylori infection and the risk of gastric carcinoma', *N Engl J Med,* 325(16), pp. 1127-31.
Patel, K. A., Edmondson, N. D., Talbot, F., Parsons, M. A., Rennie, I. G. and Sisley, K. (2001) 'Prediction of prognosis in patients with uveal melanoma using fluorescence in situ hybridisation', *British Journal of Ophthalmology,* 85(12), pp. 1440-1444.
Pegg, A. E. (2006) 'Regulation of ornithine decarboxylase', *J Biol Chem,* 281(21), pp. 14529-32.
Pegg, A. E. (2009a) 'Mammalian polyamine metabolism and function', *IUBMB Life,* 61(9), pp. 880-94.
Pegg, A. E. (2009b) 'S-Adenosylmethionine decarboxylase', *Essays Biochem,* 46, pp. 25-45.
Pegg, A. E., Xiong, H., Feith, D. J. and Shantz, L. M. (1998) 'S-adenosylmethionine decarboxylase: structure, function and regulation by polyamines', *Biochem Soc Trans,* 26(4), pp. 580-6.
Peng, X., Luo, Z., Kang, Q., Deng, D., Wang, Q., Peng, H., Wang, S. and Wei, Z. (2015) 'FOXQ1 mediates the crosstalk between TGF-beta and Wnt signaling pathways in the progression of colorectal cancer', *Cancer Biol Ther,* 16(7), pp. 1099-109.
Pickar-Oliver, A. and Gersbach, C. A. (2019) 'The next generation of CRISPR-Cas technologies and applications', *Nat Rev Mol Cell Biol,* 20(8), pp. 490-507.
Pohjanpelto, P., Virtanen, I. and Holtta, E. (1981) 'Polyamine Starvation Causes Disappearance of Actin-Filaments and Microtubules in Polyamine-Auxotrophic Cho Cells', *Nature,* 293(5832), pp. 475-477.
Prescher, G., Bornfeld, N. and Becher, R. (1990) 'Nonrandom chromosomal abnormalities in primary uveal melanoma', *J Natl Cancer Inst,* 82(22), pp. 1765-9.
Prescher, G., Bornfeld, N., Friedrichs, W., Seeber, S. and Becher, R. (1995) 'Cytogenetics of twelve cases of uveal melanoma and patterns of nonrandom anomalies and isochromosome formation', *Cancer Genet Cytogenet,* 80(1), pp. 40-6.
Prescher, G., Bornfeld, N., Hirche, H., Horsthemke, B., Jockel, K. H. and Becher, R. (1996) 'Prognostic implications of monosomy 3 in uveal melanoma', *Lancet,* 347(9010), pp. 1222-5.
Renehan, A. G., Tyson, M., Egger, M., Heller, R. F. and Zwahlen, M. (2008) 'Body-mass index and incidence of cancer: a systematic review and meta-analysis of prospective observational studies', *Lancet,* 371(9612), pp. 569-78.
Rennie, I. G. (1997) 'The Ashton Lecture - Uveal melanoma: The past, the present and the future', *Eye,* 11, pp. 255-264.
Rey, J. A., Bello, M. J., de Campos, J. M., Ramos, M. C. and Benitez, J. (1985) 'Cytogenetic findings in a human malignant melanoma metastatic to the brain', *Cancer Genet Cytogenet,* 16(2), pp. 179-83.

Rietschel, P., Panageas, K. S., Hanlon, C., Patel, A., Abramson, D. H. and Chapman, P. B. (2005) 'Variates of survival in metastatic uveal melanoma', *J Clin Oncol,* 23(31), pp. 8076-80.
Rizvi, M. M., Alam, M. S., Ali, A., Mehdi, S. J., Batra, S. and Mandal, A. K. (2011) 'Aberrant promoter methylation and inactivation of PTEN gene in cervical carcinoma from Indian population', *J Cancer Res Clin Oncol,* 137(8), pp. 1255-62.
Robertson, A. G., Shih, J., Yau, C., Gibb, E. A., Oba, J., Mungall, K. L., Hess, J. M., Uzunangelov, V., Walter, V., Danilova, L., Lichtenberg, T. M., Kucherlapati, M., Kimes, P. K., Tang, M., Penson, A., Babur, O., Akbani, R., Bristow, C. A., Hoadley, K. A., Iype, L., Chang, M. T., Network, T. R., Cherniack, A. D., Benz, C., Mills, G. B., Verhaak, R. G. W., Griewank, K. G., Felau, I., Zenklusen, J. C., Gershenwald, J. E., Schoenfield, L., Lazar, A. J., Abdel-Rahman, M. H., Roman-Roman, S., Stern, M. H., Cebulla, C. M., Williams, M. D., Jager, M. J., Coupland, S. E., Esmaeli, B., Kandoth, C. and Woodman, S. E. (2017) 'Integrative Analysis Identifies Four Molecular and Clinical Subsets in Uveal Melanoma', *Cancer Cell,* 32(2), pp. 204-220 e15.
Rodriguez, J. M. P., de Olza, M. O., Codes, M., Lopez-Martin, J. A., Berrocal, A., Garcia, M., Gurpide, A., Homet, B. and Martin-Algarra, S. (2014) 'Phase II study evaluating ipilimumab as a single agent in the first-line treatment of adult patients (Pts) with metastatic uveal melanoma (MUM): The GEM-1 trial.', *Journal of Clinical Oncology,* 32(15).
Rodriguez-Rodero, S., Fernandez-Morera, J. L., Menendez-Torre, E., Calvanese, V., Fernandez, A. F. and Fraga, M. F. (2011) 'Aging Genetics and Aging', *Aging and Disease,* 2(3), pp. 186-195.
Roje, S. (2006) 'S-Adenosyl-L-methionine: beyond the universal methyl group donor', *Phytochemistry,* 67(15), pp. 1686-98.
Rowley, J. D. (1973a) 'Chromosomal patterns in myelocytic leukemia', *N Engl J Med,* 289(4), pp. 220-1.
Rowley, J. D. (1973b) 'Letter: A new consistent chromosomal abnormality in chronic myelogenous leukaemia identified by quinacrine fluorescence and Giemsa staining', *Nature,* 243(5405), pp. 290-3.
Royds, J. A., Sharrard, R. M., Parsons, M. A., Lawry, J., Rees, R., Cottam, D., Wagner, B. and Rennie, I. G. (1992) 'C-myc oncogene expression in ocular melanomas', *Graefes Arch Clin Exp Ophthalmol,* 230(4), pp. 366-71.
Sanger, F., Nicklen, S. and Coulson, A. R. (1977) 'DNA sequencing with chain-terminating inhibitors', *Proc Natl Acad Sci U S A,* 74(12), pp. 5463-7.
Sarwari, N. M., Khoury, J. D. and Hernandez, C. M. (2016) 'Chronic Epstein Barr virus infection leading to classical Hodgkin lymphoma', *BMC Hematol,* 16, pp. 19.
Schadendorf, D., Fisher, D. E., Garbe, C., Gershenwald, J. E., Grob, J. J., Halpern, A., Herlyn, M., Marchetti, M. A., McArthur, G., Ribas, A., Roesch, A. and Hauschild, A. (2015) 'Melanoma', *Nat Rev Dis Primers,* 1, pp. 15003.
Schmidt-Pokrzywniak, A., Jockel, K. H., Bornfeld, N., Sauerwein, W. and Stang, A. (2009) 'Positive interaction between light iris color and ultraviolet radiation in relation to the risk of uveal melanoma: a case-control study', *Ophthalmology,* 116(2), pp. 340-8.

Schmittel, A., Schmidt-Hieber, M., Martus, P., Bechrakis, N. E., Schuster, R., Siehl, J. M., Foerster, M. H., Thiel, E. and Keilholz, U. (2006) 'A randomized phase II trial of gemcitabine plus treosulfan versus treosulfan alone in patients with metastatic uveal melanoma', *Ann Oncol,* 17(12), pp. 1826-9.

Scholes, A. G. M., Damato, B. E., Nunn, J., Hiscott, P., Grierson, I. and Field, J. K. (2003) 'Monosomy 3 in uveal melanoma: Correlation with clinical and histologic predictors of survival', *Investigative Ophthalmology & Visual Science,* 44(3), pp. 1008-1011.

Scholz, S. L., Moller, I., Reis, H., Susskind, D., van de Nes, J. A. P., Leonardelli, S., Schilling, B., Livingstone, E., Schimming, T., Paschen, A., Sucker, A., Murali, R., Steuhl, K. P., Schadendorf, D., Westekemper, H. and Griewank, K. G. (2017) 'Frequent GNAQ, GNA11, and EIF1AX Mutations in Iris Melanoma', *Invest Ophthalmol Vis Sci,* 58(9), pp. 3464-3470.

Scuoppo, C., Miething, C., Lindqvist, L., Reyes, J., Ruse, C., Appelmann, I., Yoon, S., Krasnitz, A., Teruya-Feldstein, J., Pappin, D., Pelletier, J. and Lowe, S. W. (2012) 'A tumour suppressor network relying on the polyamine-hypusine axis', *Nature,* 487(7406), pp. 244-8.

Seddon, J., Egan, K., Gragoudas, E., Glynn, R. and Ryan, S. (1989) 'Epidemiology of uveal melanoma', *Retina,* 1, pp. 717-24.

Seddon, J. M., Gragoudas, E. S., Glynn, R. J., Egan, K. M., Albert, D. M. and Blitzer, P. H. (1990) 'Host factors, UV radiation, and risk of uveal melanoma. A case-control study', *Arch Ophthalmol,* 108(9), pp. 1274-80.

Sehrawat, A., Kim, S. H., Vogt, A. and Singh, S. V. (2013) 'Suppression of FOXQ1 in benzyl isothiocyanate-mediated inhibition of epithelial-mesenchymal transition in human breast cancer cells', *Carcinogenesis,* 34(4), pp. 864-73.

Sentmanat, M. F., Peters, S. T., Florian, C. P., Connelly, J. P. and Pruett-Miller, S. M. (2018) 'A Survey of Validation Strategies for CRISPR-Cas9 Editing', *Sci Rep,* 8(1), pp. 888.

Seregard, S. and Kock, E. (1995) 'Prognostic indicators following enucleation for posterior uveal melanoma. A multivariate analysis of long-term survival with minimized loss to follow-up', *Acta Ophthalmol Scand,* 73(4), pp. 340-4.

Shah, A. A., Bourne, T. D. and Murali, R. (2013) 'BAP1 protein loss by immunohistochemistry: a potentially useful tool for prognostic prediction in patients with uveal melanoma', *Pathology,* 45(7), pp. 651-6.

Shain, A. H., Bagger, M. M., Yu, R., Chang, D., Liu, S., Vemula, S., Weier, J. F., Wadt, K., Heegaard, S., Bastian, B. C. and Kiilgaard, J. F. (2019) 'The genetic evolution of metastatic uveal melanoma', *Nat Genet,* 51(7), pp. 1123-1130.

Shamseldin, H. E., Alshammari, M., Al-Sheddi, T., Salih, M. A., Alkhalidi, H., Kentab, A., Repetto, G. M., Hashem, M. and Alkuraya, F. S. (2012) 'Genomic analysis of mitochondrial diseases in a consanguineous population reveals novel candidate disease genes', *J Med Genet,* 49(4), pp. 234-41.

Shay, J. W. and Bacchetti, S. (1997) 'A survey of telomerase activity in human cancer', *Eur J Cancer,* 33(5), pp. 787-91.

Shields, C. L., Dalvin, L. A., Vichitvejpaisal, P., Mazloumi, M., Ganguly, A. and Shields, J. A. (2019) 'Prognostication of uveal melanoma is simple and highly predictive using The Cancer Genome Atlas (TCGA) classification: A review', *Indian Journal of Ophthalmology,* 67(12), pp. 1959-1963.
Shields, C. L., Furuta, M., Thangappan, A., Nagori, S., Mashayekhi, A., Lally, D. R., Kelly, C. C., Rudich, D. S., Nagori, A. V., Wakade, O. A., Mehta, S., Forte, L., Long, A., Dellacava, E. F., Kaplan, B. and Shields, J. A. (2009) 'Metastasis of uveal melanoma millimeter-by-millimeter in 8033 consecutive eyes', *Arch Ophthalmol,* 127(8), pp. 989-98.
Shields, C. L., Ganguly, A., Bianciotto, C. G., Turaka, K., Tavallali, A. and Shields, J. A. (2011) 'Prognosis of uveal melanoma in 500 cases using genetic testing of fine-needle aspiration biopsy specimens', *Ophthalmology,* 118(2), pp. 396-401.
Shields, C. L., Ganguly, A., Materin, M. A., Teixeira, L., Mashayekhi, A., Swanson, L. A., Marr, B. P. and Shields, J. A. (2007) 'Chromosome 3 analysis of uveal melanoma using fine-needle aspiration biopsy at the time of plaque radiotherapy in 140 consecutive cases', *Trans Am Ophthalmol Soc,* 105, pp. 43-52; discussion 52-3.
Shields, C. L., Kaliki, S., Furuta, M., Mashayekhi, A. and Shields, J. A. (2012) 'Clinical spectrum and prognosis of uveal melanoma based on age at presentation in 8,033 cases', *Retina,* 32(7), pp. 1363-72.
Shields, C. L., Manalac, J., Das, C., Ferguson, K. and Shields, J. A. (2014) 'Choroidal melanoma: clinical features, classification, and top 10 pseudomelanomas', *Curr Opin Ophthalmol,* 25(3), pp. 177-85.
Shields, C. L., Shields, J. A., De Potter, P., Cater, J., Tardio, D. and Barrett, J. (1996) 'Diffuse choroidal melanoma. Clinical features predictive of metastasis', *Arch Ophthalmol,* 114(8), pp. 956-63.
Shields, C. L., Shields, J. A., Materin, M., Gershenbaum, E., Singh, A. D. and Smith, A. (2001) 'Iris melanoma: risk factors for metastasis in 169 consecutive patients', *Ophthalmology,* 108(1), pp. 172-8.
Shields, J. and Shields, C. (1992) 'Posterior uveal melanoma: clinical and pathologic features', *Intraocular tumors. A Text and Atlas, WB Saunders Company, Philadelphia*, pp. 117-136.
Shields, J. A. and Shields, C. L. (2015) 'Management of posterior uveal melanoma: past, present, and future: the 2014 Charles L. Schepens lecture', *Ophthalmology,* 122(2), pp. 414-28.
Shukla, S. A., Rooney, M. S., Rajasagi, M., Tiao, G., Dixon, P. M., Lawrence, M. S., Stevens, J., Lane, W. J., Dellagatta, J. L., Steelman, S., Sougnez, C., Cibulskis, K., Kiezun, A., Hacohen, N., Brusic, V., Wu, C. J. and Getz, G. (2015) 'Comprehensive analysis of cancer-associated somatic mutations in class I HLA genes', *Nat Biotechnol,* 33(11), pp. 1152-8.
Shukla-Dave, A., Castillo-Martin, M., Chen, M., Lobo, J., Gladoun, N., Collazo-Lorduy, A., Khan, F. M., Ponomarev, V., Yi, Z., Zhang, W., Pandolfi, P. P., Hricak, H. and Cordon-Cardo, C. (2016) 'Ornithine Decarboxylase Is Sufficient for Prostate Tumorigenesis via Androgen Receptor Signaling', *Am J Pathol,* 186(12), pp. 3131-3145.
Siegel, R. L., Miller, K. D. and Jemal, A. (2019) 'Cancer statistics, 2019', *CA Cancer J Clin,* 69(1), pp. 7-34.
Sikuade, M. J., Salvi, S., Rundle, P. A., Errington, D. G., Kacperek, A. and Rennie, I. G. (2015) 'Outcomes of treatment with stereotactic

radiosurgery or proton beam therapy for choroidal melanoma', *Eye (Lond),* 29(9), pp. 1194-8.
Singh, A. D., Eagle, R. C., Jr., Shields, C. L. and Shields, J. A. (2003) 'Clinicopathologic reports, case reports, and small case series: enucleation following transpupillary thermotherapy of choroidal melanoma: clinicopathologic correlations', *Arch Ophthalmol,* 121(3), pp. 397-400.
Singh, A. D., Rennie, I. G., Seregard, S., Giblin, M. and McKenzie, J. (2004) 'Sunlight exposure and pathogenesis of uveal melanoma', *Surv Ophthalmol,* 49(4), pp. 419-28.
Singh, A. D., Shields, C. L., DePotter, P., Shields, J. A., Troch, B., Cater, J. and Pastore, D. (1996a) 'Familial uveal melanoma - Clinical observations on 56 patients', *Archives of Ophthalmology,* 114(4), pp. 392-399.
Singh, A. D., Shields, C. L. and Shields, J. A. (2001) 'Prognostic factors in uveal melanoma', *Melanoma Res,* 11(3), pp. 255-63.
Singh, A. D. and Topham, A. (2003) 'Incidence of uveal melanoma in the United States: 1973-1997', *Ophthalmology,* 110(5), pp. 956-61.
Singh, A. D., Tubbs, R., Biscotti, C., Schoenfield, L. and Trizzoi, P. (2009) 'Chromosomal 3 and 8 Status Within Hepatic Metastasis of Uveal Melanoma', *Archives of Pathology & Laboratory Medicine,* 133(8), pp. 1223-1227.
Singh, A. D., Turell, M. E. and Topham, A. K. (2011) 'Uveal melanoma: trends in incidence, treatment, and survival', *Ophthalmology,* 118(9), pp. 1881-5.
Singh, A. D., Wang, M. X., Donoso, L. A., Shields, C. L., DePotter, P., Shields, J. A., Elston, R. C. and Fijal, B. (1996b) 'Familial uveal melanoma .3. Is the occurrence of familial uveal melanoma coincidental?', *Archives of Ophthalmology,* 114(9), pp. 1101-1104.
Sisley, K. (2015) 'Tumors of the eye', *Cancer Cytogenetics*: John Wiley & Sons, Ltd, pp. 538-554.
Sisley, K., Doherty, R. and Cross, N. A. (2011) 'What hope for the future? GNAQ and uveal melanoma', *Br J Ophthalmol,* 95(5), pp. 620-3.
Sisley, K., Parsons, M. A., Garnham, J., Potter, A. M., Curtis, D., Rees, R. C. and Rennie, I. G. (2000) 'Association of specific chromosome alterations with tumour phenotype in posterior uveal melanoma', *British Journal of Cancer,* 82(2), pp. 330-338.
Sisley, K., Rennie, I. G., Cottam, D. W., Potter, A. M., Potter, C. W. and Rees, R. C. (1990) 'Cytogenetic findings in six posterior uveal melanomas: involvement of chromosomes 3, 6, and 8', *Genes Chromosomes Cancer,* 2(3), pp. 205-9.
Sisley, K., Rennie, I. G., Parsons, M. A., Jacques, R., Hammond, D. W., Bell, S. M., Potter, A. M. and Rees, R. C. (1997) 'Abnormalities of chromosomes 3 and 8 in posterior uveal melanoma correlate with prognosis', *Genes Chromosomes Cancer,* 19(1), pp. 22-8.
Sisley, K., Tattersall, N., Dyson, M., Smith, K., Mudhar, H. S. and Rennie, I. G. (2006) 'Multiplex fluorescence in situ hybridization identifies novel rearrangements of chromosomes 6, 15, and 18 in primary uveal melanoma', *Exp Eye Res,* 83(3), pp. 554-9.

Smittenaar, C. R., Petersen, K. A., Stewart, K. and Moitt, N. (2016) 'Cancer incidence and mortality projections in the UK until 2035', *British Journal of Cancer,* 115(9), pp. 1147-1155.
Soria, J. C., Lee, H. Y., Lee, J. I., Wang, L., Issa, J. P., Kemp, B. L., Liu, D. D., Kurie, J. M., Mao, L. and Khuri, F. R. (2002) 'Lack of PTEN expression in non-small cell lung cancer could be related to promoter methylation', *Clin Cancer Res,* 8(5), pp. 1178-84.
Soutoglou, E., Dorn, J. F., Sengupta, K., Jasin, M., Nussenzweig, A., Ried, T., Danuser, G. and Misteli, T. (2007) 'Positional stability of single double-strand breaks in mammalian cells', *Nat Cell Biol,* 9(6), pp. 675-82.
Spagnolo, F., Caltabiano, G. and Queirolo, P. (2012) 'Uveal melanoma', *Cancer Treat Rev,* 38(5), pp. 549-53.
Spagnolo, F., Grosso, M., Picasso, V., Tornari, E., Pesce, M. and Queirolo, P. (2013) 'Treatment of metastatic uveal melanoma with intravenous fotemustine', *Melanoma Res,* 23(3), pp. 196-8.
Speicher, M. R., Prescher, G., Dumanoir, S., Jauch, A., Horsthemke, B., Bornfeld, N., Becher, R. and Cremer, T. (1994) 'Chromosomal Gains and Losses in Uveal Melanomas Detected by Comparative Genomic Hybridization', *Cancer Research,* 54(14), pp. 3817-3823.
Spendlove, H. E., Damato, B. E., Humphreys, J., Barker, K. T., Hiscott, P. S. and Houlston, R. S. (2004) 'BRAF mutations are detectable in conjunctival but not uveal melanomas', *Melanoma Res,* 14(6), pp. 449-52.
Stephens, P. J., Greenman, C. D., Fu, B., Yang, F., Bignell, G. R., Mudie, L. J., Pleasance, E. D., Lau, K. W., Beare, D., Stebbings, L. A., McLaren, S., Lin, M. L., McBride, D. J., Varela, I., Nik-Zainal, S., Leroy, C., Jia, M., Menzies, A., Butler, A. P., Teague, J. W., Quail, M. A., Burton, J., Swerdlow, H., Carter, N. P., Morsberger, L. A., Iacobuzio-Donahue, C., Follows, G. A., Green, A. R., Flanagan, A. M., Stratton, M. R., Futreal, P. A. and Campbell, P. J. (2011) 'Massive genomic rearrangement acquired in a single catastrophic event during cancer development', *Cell,* 144(1), pp. 27-40.
Sternberg, S. H., Redding, S., Jinek, M., Greene, E. C. and Doudna, J. A. (2014) 'DNA interrogation by the CRISPR RNA-guided endonuclease Cas9', *Nature,* 507(7490), pp. 62-7.
Stratton, M. R., Campbell, P. J. and Futreal, P. A. (2009) 'The cancer genome', *Nature,* 458(7239), pp. 719-724.
Sun, H. T., Cheng, S. X., Tu, Y., Li, X. H. and Zhang, S. (2013) 'FoxQ1 promotes glioma cells proliferation and migration by regulating NRXN3 expression', *PLoS One,* 8(1), pp. e55693.
Tagawa, H., Karnan, S., Suzuki, R., Matsuo, K., Zhang, X., Ota, A., Morishima, Y., Nakamura, S. and Seto, M. (2005) 'Genome-wide array-based CGH for mantle cell lymphoma: identification of homozygous deletions of the proapoptotic gene BIM', *Oncogene,* 24(8), pp. 1348-58.
Te Raa, G. D., Derks, I. A., Navrkalova, V., Skowronska, A., Moerland, P. D., van Laar, J., Oldreive, C., Monsuur, H., Trbusek, M., Malcikova, J., Loden, M., Geisler, C. H., Hullein, J., Jethwa, A., Zenz, T., Pospisilova, S., Stankovic, T., van Oers, M. H., Kater, A. P. and Eldering, E. (2015) 'The impact of SF3B1 mutations in CLL on the DNA-damage response', *Leukemia,* 29(5), pp. 1133-42.

The Collaborative Ocular Melanoma Study (1998) 'The Collaborative Ocular Melanoma Study (COMS) randomized trial of pre-enucleation radiation of large choroidal melanoma III: local complications and observations following enucleation COMS report no. 11', *Am J Ophthalmol,* 126(3), pp. 362-72.

The Collaborative Ocular Melanoma Study (2001) 'Assessment of metastatic disease status at death in 435 patients with large choroidal melanoma in the Collaborative Ocular Melanoma Study (COMS): COMS report no. 15', (0003-9950 (Print)).

Theriault, B. L., Dimaras, H., Gallie, B. L. and Corson, T. W. (2014) 'The genomic landscape of retinoblastoma: a review', *Clin Exp Ophthalmol,* 42(1), pp. 33-52.

Thijsen, S., Schuurhuis, G., van Oostveen, J. and Ossenkoppele, G. (1999) 'Chronic myeloid leukemia from basics to bedside', *Leukemia,* 13(11), pp. 1646-74.

Thomas, N. E., Berwick, M. and Cordeiro-Stone, M. (2006) 'Could BRAF mutations in melanocytic lesions arise from DNA damage induced by ultraviolet radiation?', *J Invest Dermatol,* 126(8), pp. 1693-6.

Trolet, J., Hupe, P., Huon, I., Lebigot, I., Decraene, C., Delattre, O., Sastre-Garau, X., Saule, S., Thiery, J. P., Plancher, C., Asselain, B., Desjardins, L., Mariani, P., Piperno-Neumann, S., Barillot, E. and Couturier, J. (2009) 'Genomic profiling and identification of high-risk uveal melanoma by array CGH analysis of primary tumors and liver metastases', *Invest Ophthalmol Vis Sci,* 50(6), pp. 2572-80.

Tschentscher, F., Prescher, G., Horsman, D. E., White, V. A., Rieder, H., Anastassiou, G., Schilling, H., Bornfeld, N., Bartz-Schmidt, K. U., Horsthemke, B., Lohmann, D. R. and Zeschnigk, M. (2001) 'Partial deletions of the long and short arm of chromosome 3 point to two tumor suppressor genes in uveal melanoma', *Cancer Research,* 61(8), pp. 3439-3442.

Tsihlias, J., Kapusta, L. and Slingerland, J. (1999) 'The prognostic significance of altered cyclin-dependent kinase inhibitors in human cancer', *Annual Review of Medicine,* 50, pp. 401-+.

Vajdic, C. M., Kricker, A., Giblin, M., McKenzie, J., Aitken, J., Giles, G. G. and Armstrong, B. K. (2003) 'Incidence of ocular melanoma in Australia from 1990 to 1998', *Int J Cancer,* 105(1), pp. 117-22.

Van Beek, J. G., Koopmans, A. E., Vaarwater, J., Verdijk, R. M., de Klein, A., Naus, N. C. and Kilic, E. (2015) 'Metastatic disease in uveal melanoma: importance of a genetic profile?', *Melanoma Res,* 25(5), pp. 447-9.

van de Nes, J. A., Nelles, J., Kreis, S., Metz, C. H., Hager, T., Lohmann, D. R. and Zeschnigk, M. (2016) 'Comparing the Prognostic Value of BAP1 Mutation Pattern, Chromosome 3 Status, and BAP1 Immunohistochemistry in Uveal Melanoma', *Am J Surg Pathol,* 40(6), pp. 796-805.

van den Bosch, T., Kilic, E., Paridaens, D. and de Klein, A. (2010) 'Genetics of uveal melanoma and cutaneous melanoma: two of a kind?', *Dermatol Res Pract,* 2010, pp. 360136.

van der Kooij, M. K., Speetjens, F. M., van der Burg, S. H. and Kapiteijn, E. (2019) 'Uveal Versus Cutaneous Melanoma; Same Origin, Very Distinct Tumor Types', *Cancers (Basel),* 11(6).

van Gils, W., Lodder, E. M., Mensink, H. W., Kilic, E., Naus, N. C., Bruggenwirth, H. T., van Ijcken, W., Paridaens, D., Luyten, G. P. and de Klein, A. (2008) 'Gene expression profiling in uveal melanoma: two regions on 3p related to prognosis', *Invest Ophthalmol Vis Sci,* 49(10), pp. 4254-62.

Van Raamsdonk, C. D., Bezrookove, V., Green, G., Bauer, J., Gaugler, L., O'Brien, J. M., Simpson, E. M., Barsh, G. S. and Bastian, B. C. (2009) 'Frequent somatic mutations of GNAQ in uveal melanoma and blue naevi', *Nature,* 457(7229), pp. 599-602.

Van Raamsdonk, C. D., Griewank, K. G., Crosby, M. B., Garrido, M. C., Vemula, S., Wiesner, T., Obenauf, A. C., Wackernagel, W., Green, G., Bouvier, N., Sozen, M. M., Baimukanova, G., Roy, R., Heguy, A., Dolgalev, I., Khanin, R., Busam, K., Speicher, M. R., O'Brien, J. and Bastian, B. C. (2010) 'Mutations in GNA11 in uveal melanoma', *N Engl J Med,* 363(23), pp. 2191-9.

Vernon, H. J., McClellan, R., Batista, D. A. and Naidu, S. (2015) 'Mutations in FARS2 and non-fatal mitochondrial dysfunction in two siblings', *Am J Med Genet A,* 167A(5), pp. 1147-51.

Vijg, J. and Suh, Y. (2013) 'Genome instability and aging', *Annu Rev Physiol,* 75, pp. 645-68.

Violanti, S. S., Bononi, I., Gallenga, C. E., Martini, F., Tognon, M. and Perri, P. (2019) 'New Insights into Molecular Oncogenesis and Therapy of Uveal Melanoma', *Cancers,* 11(5).

Virgili, G., Gatta, G., Ciccolallo, L., Capocaccia, R., Biggeri, A., Crocetti, E., Lutz, J. M., Paci, E. and Group, E. W. (2007) 'Incidence of uveal melanoma in Europe', *Ophthalmology,* 114(12), pp. 2309-15.

Vouillot, L., Thelie, A. and Pollet, N. (2015) 'Comparison of T7E1 and surveyor mismatch cleavage assays to detect mutations triggered by engineered nucleases', *G3 (Bethesda),* 5(3), pp. 407-15.

Wang, L., Lawrence, M. S., Wan, Y., Stojanov, P., Sougnez, C., Stevenson, K., Werner, L., Sivachenko, A., DeLuca, D. S., Zhang, L., Zhang, W., Vartanov, A. R., Fernandes, S. M., Goldstein, N. R., Folco, E. G., Cibulskis, K., Tesar, B., Sievers, Q. L., Shefler, E., Gabriel, S., Hacohen, N., Reed, R., Meyerson, M., Golub, T. R., Lander, E. S., Neuberg, D., Brown, J. R., Getz, G. and Wu, C. J. (2011) 'SF3B1 and other novel cancer genes in chronic lymphocytic leukemia', *N Engl J Med,* 365(26), pp. 2497-506.

Weigel, D., Jurgens, G., Kuttner, F., Seifert, E. and Jackle, H. (1989) 'The homeotic gene fork head encodes a nuclear protein and is expressed in the terminal regions of the Drosophila embryo', *Cell,* 57(4), pp. 645-58.

White, J. S., McLean, I. W., Becker, R. L., Director-Myska, A. E. and Nath, J. (2006) 'Correlation of comparative genomic hybridization results of 100 archival uveal melanomas with patient survival', *Cancer Genet Cytogenet,* 170(1), pp. 29-39.

White, V. A., Chambers, J. D., Courtright, P. D., Chang, W. Y. and Horsman, D. E. (1998) 'Correlation of cytogenetic abnormalities with the outcome of patients with uveal melanoma', *Cancer,* 83(2), pp. 354-9.

Wilson, M. A. and Nathanson, K. L. (2012) 'Molecular testing in melanoma', *Cancer J,* 18(2), pp. 117-23.

Woodward, J. K. L., Elshaw, S. R., Murray, A. K., Nichols, C. E., Cross, N., Laws, D., Rennie, I. G. and Sisley, K. (2002) 'Stimulation and inhibition of uveal melanoma invasion by HGF, GRO, IL-alpha and TGF-beta', *Investigative Ophthalmology & Visual Science,* 43(10), pp. 3144-3152.

Woodward, J. K. L., Rennie, I. G., Burn, J. L. and Sisley, K. (2005) 'A potential role for TGF beta in the regulation of uveal melanoma adhesive interactions with the hepatic endothelium', *Investigative Ophthalmology & Visual Science,* 46(10), pp. 3473-3477.

Wu, X. Q., Huang, C., He, X., Tian, Y. Y., Zhou, D. X., He, Y., Liu, X. H. and Li, J. (2013) 'Feedback regulation of telomerase reverse transcriptase: new insight into the evolving field of telomerase in cancer', *Cell Signal,* 25(12), pp. 2462-8.

Xia, L., Huang, W., Tian, D., Zhang, L., Qi, X., Chen, Z., Shang, X., Nie, Y. and Wu, K. (2014) 'Forkhead box Q1 promotes hepatocellular carcinoma metastasis by transactivating ZEB2 and VersicanV1 expression', *Hepatology,* 59(3), pp. 958-73.

Xiang, X. J., Deng, J., Liu, Y. W., Wan, L. Y., Feng, M., Chen, J. and Xiong, J. P. (2015) 'MiR-1271 Inhibits Cell Proliferation, Invasion and EMT in Gastric Cancer by Targeting FOXQ1', *Cell Physiol Biochem,* 36(4), pp. 1382-94.

Yang, Y., Liu, W., Fang, Z., Shi, J., Che, F., He, C., Yao, L., Wang, E. and Wu, Y. (2016) 'A Newly Identified Missense Mutation in FARS2 Causes Autosomal-Recessive Spastic Paraplegia', *Hum Mutat,* 37(2), pp. 165-9.

Yavuzyigitoglu, S., Drabarek, W., Smit, K. N., van Poppelen, N., Koopmans, A. E., Vaarwater, J., Brands, T., Eussen, B., Dubbink, H. J., van Riet, J., van de Werken, H. J., Beverloo, B., Verdijk, R. M., Naus, N., Paridaens, D., Kilic, E., de Klein, A. and Rotterdam Ocular Melanoma Study, G. (2016a) 'Correlation of Gene Mutation Status with Copy Number Profile in Uveal Melanoma', *Ophthalmology*.

Yavuzyigitoglu, S., Koopmans, A. E., Verdijk, R. M., Vaarwater, J., Eussen, B., van Bodegom, A., Paridaens, D., Kilic, E., de Klein, A. and Rotterdam Ocular Melanoma Study, G. (2016b) 'Uveal Melanomas with SF3B1 Mutations: A Distinct Subclass Associated with Late-Onset Metastases', *Ophthalmology,* 123(5), pp. 1118-28.

Yu, F. X., Luo, J., Mo, J. S., Liu, G., Kim, Y. C., Meng, Z., Zhao, L., Peyman, G., Ouyang, H., Jiang, W., Zhao, J., Chen, X., Zhang, L., Wang, C. Y., Bastian, B. C., Zhang, K. and Guan, K. L. (2014) 'Mutant Gq/11 promote uveal melanoma tumorigenesis by activating YAP', *Cancer Cell,* 25(6), pp. 822-30.

Yuan, P., Cao, J. L., Abuduwufuer, A., Wang, L. M., Yuan, X. S., Lv, W. and Hu, J. (2016) 'Clinical Characteristics and Prognostic Significance of TERT Promoter Mutations in Cancer: A Cohort Study and a Meta-Analysis', *PLoS One,* 11(1), pp. e0146803.

Zabala-Letona, A., Arruabarrena-Aristorena, A., Martin-Martin, N., Fernandez-Ruiz, S., Sutherland, J. D., Clasquin, M., Tomas-Cortazar, J., Jimenez, J., Torres, I., Quang, P., Ximenez-Embun, P., Bago, R., Ugalde-Olano, A., Loizaga-Iriarte, A., Lacasa-Viscasillas, I., Unda, M., Torrano, V., Cabrera, D., van Liempd, S. M., Cendon, Y., Castro, E., Murray, S., Revandkar, A., Alimonti, A., Zhang, Y., Barnett, A., Lein, G., Pirman, D., Cortazar, A. R., Arreal, L., Prudkin, L., Astobiza, I., Valcarcel-Jimenez,

L., Zuniga-Garcia, P., Fernandez-Dominguez, I., Piva, M., Caro-Maldonado, A., Sanchez-Mosquera, P., Castillo-Martin, M., Serra, V., Beraza, N., Gentilella, A., Thomas, G., Azkargorta, M., Elortza, F., Farras, R., Olmos, D., Efeyan, A., Anguita, J., Munoz, J., Falcon-Perez, J. M., Barrio, R., Macarulla, T., Mato, J. M., Martinez-Chantar, M. L., Cordon-Cardo, C., Aransay, A. M., Marks, K., Baselga, J., Tabernero, J., Nuciforo, P., Manning, B. D., Marjon, K. and Carracedo, A. (2017) 'mTORC1-dependent AMD1 regulation sustains polyamine metabolism in prostate cancer', *Nature,* 547(7661), pp. 109-113.

Zhang, B., Liu, X. X., Zhang, Y., Jiang, C. Y., Hu, H. Y., Gong, L., Liu, M. and Teng, Q. S. (2006) 'Polyamine depletion by ODC-AdoMetDC antisense adenovirus impairs human colorectal cancer growth and invasion in vitro and in vivo', *J Gene Med,* 8(8), pp. 980-9.

Zhang, D., Zhao, T., Ang, H. S., Chong, P., Saiki, R., Igarashi, K., Yang, H. and Vardy, L. A. (2012) 'AMD1 is essential for ESC self-renewal and is translationally down-regulated on differentiation to neural precursor cells', *Genes Dev,* 26(5), pp. 461-73.

Zhu, Z., Zhu, Z., Pang, Z., Xing, Y., Wan, F., Lan, D. and Wang, H. (2013) 'Short hairpin RNA targeting FOXQ1 inhibits invasion and metastasis via the reversal of epithelial-mesenchymal transition in bladder cancer', *Int J Oncol,* 42(4), pp. 1271-8.

Zielinski, B., Gratias, S., Toedt, G., Mendrzyk, F., Stange, D. E., Radlwimmer, B., Lohmann, D. R. and Lichter, P. (2005) 'Detection of chromosomal imbalances in retinoblastoma by matrix-based comparative genomic hybridization', *Genes Chromosomes & Cancer,* 43(3), pp. 294-301.

Zierhut, C. and Diffley, J. F. (2008) 'Break dosage, cell cycle stage and DNA replication influence DNA double strand break response', *EMBO J,* 27(13), pp. 1875-85.

Zimmer, L., Vaubel, J., Mohr, P., Hauschild, A., Utikal, J., Simon, J., Garbe, C., Herbst, R., Enk, A., Kampgen, E., Livingstone, E., Bluhm, L., Rompel, R., Griewank, K. G., Fluck, M., Schilling, B. and Schadendorf, D. (2015) 'Phase II DeCOG-Study of Ipilimumab in Pretreated and Treatment-Naive Patients with Metastatic Uveal Melanoma', *Plos One,* 10(3).

Zimmerman, L. E., McLean, I. W. and Foster, W. D. (1978) 'Does enucleation of the eye containing a malignant melanoma prevent or accelerate the dissemination of tumour cells', *Br J Ophthalmol,* 62(6), pp. 420-5.

Zoncu, R., Efeyan, A. and Sabatini, D. M. (2011) 'mTOR: from growth signal integration to cancer, diabetes and ageing', *Nature Reviews Molecular Cell Biology,* 12(1), pp. 21-35.

Appendices

Appendix 1: Mapping for genes used in this study and mutations hotspots

GNAQ exon 4 codon R183

Forward primer: TCTTTTTCTCCCACCCCTTGC

Reverse primer: TTGTTTTGAAGCCTACACATGATTCC

Product size = 509bp

TCTTTTTCTCCCACCCCTTGCCTCTGGGGAGTATGAGTTCTAATTGATAATAAGAGAA
GAAATGAGAACTATGGTGTGTATGTAATCCATAGATGGATAACCTTCCAGTAATGGAA
GGTTGACTTTATCTTTCTTTTCCACAGACTCCTCTACCACTTTCTGATATTTTTCTTT
CTCTTCTTTACTTCTCTGTTAGGACTCATTTTTGTCCTTCCCTTTCCGTAGACAGCTT
TGGTGTGATGGTGTCACTGACATTCTCATTGTGTCTTCCCTCCTCTAGCTATCTTAAT
GACTTGGACCGCGTAGCTGACCCTGCCTACCTGCCTACGCAACAAGATGTGCTTAGAG
TTCGAGTCCCCACCACAGGGATCATCGAATACCCCTTTGACTTACAAAGTGTCATTTT
CAGGTAGTAACTGAGTCCATGAAACCTATTTCCCAGCTTTTATGCCTTGAGTACATTT
GGTAAACTCTATAAATACTGGAATCATGTGTAGGCTTCAAAACAA

Mutation hotspot, primers and sequencing area

GNAQ exon 5 codon Q209

Forward primer: AGAAGTAAGTTCACTCCATTCCC

Reverse primer: TTCCCTAAGTTTGTAAGTAGTGC

Product size = 317bp

AGAAGTAAGTTCACTCCATTCCCCACACCCTACTTTCTATCATTTACTTGTATCAGAT
AATAAAATGATAATCCATTGCCTGTCTAAAGAACACTTACCTCATTGTCTGACTCCAC
GAGAACTTGATCATATTCACTAAGCGCTACTAGAAACATGATAGAGGTGACATTTTCA
AAGCAGTGTATCCATTTTCTTCTCTCTGACCTTTGGCCCCCTACATCGACCATTCTGC
AAGGTTAACAATACTCATATTAATAACATATAAAGTAAAACTAAAAAGTCAACATAAA
TATAGCACTACTTACAAACTTAGGGAA

Mutation hotspot, primers and sequencing area

GNA11 exon 4 codon R183

Forward primer: GTGCTGTGTCCCTGTCCTG

Reverse primer: GGCAAATGAGCCTCTCAGTG

Product size = 249bp

GTGCTGTGTCCCTGTCCTGCCCCCCCACCCCCGGCAGCCGGCCTGAGCACCCACCGCT
GTGTTGCAGCTACCTGACCGACGTTGACCGCATCGCCACCTTGGGCTACCTGCCCACC
CAGCAGGACGTGCTGCGGGTCCGCGTGCCCACCACCGGCATCATCGAGTACCCTTTCG
ACCTGGAGAACATCATCTTCCGGTACCGCCCGGGCCACAGCAGGCGGGGAGGGGGCAC
TGAGAGGCTCATTTGCC

Mutation hotspot, primers and sequencing area

GNA11 exon 5 codon Q209

Forward primer: CGCTGTGTCCTTTCAGGATG

Reverse primer: CCTCGTTGTCCGACT

Product size =147bp

GAGCGTCCTTGCCCGTTCTAAGAGTGGGGGCTCTTCCTGCTCCAGCCGATGTCAGTCT
GGTGTGGCAGGAGGGGCTTGGGTGGGAGCCGTCCTGGGATTGCAGATTGGGCCTTGGG
GCGCCAGGTGGCTGAGTCCTGGCGCTGTGTCCTTTCAGGATGGTGGATGTGGGGGGCC
AGCGGTCGGAGCGGAGGAAGTGGATCCACTGCTTTGAGAACGTGACATCCATCATGTT
TCTCGTCGCCCTCAGCGAATACGACCAAGTCCTGGTGGAGTCGGACAACGAGGTGGGC
CCTGCCCTGAGCAGGGGCAGCGTTGGGGGCCGGGCCTTCCCCACCTGCCAAGCCTGGG
TCCCCTCACCTGGGTCCCCCCAGCTGCCCCTTGGGCTGTGTGCAGTGGGGAGGGCCCC
TCTGATTCCCTCTG

Mutation hotspot, primers and sequencing area

EIF1AX exon 1

Forward primer: GAAAAGCGACGCAAAGAGTC

Reverse primer: CTGGGTGACCTGCAATCTAC

Product size =320bp

GAGTCAGTCGGCCACGCCTGCGTCATAAAGCCTGGGGGCGGGCCCAGCCGGCGACGGG
AGGCGGGGAAAAGCGACGCAAAGAGTCGCGGCGCCATTTGCTGCCGCCGAGCGTGGAC
GCAGGCGGATCTCTGAAGAGCTGGGTCGCCAGCCTCTCCCGCGCACGTTGCCTGGCCT
CCAGCACCTACTTGGTCCCGCGCGCTCCCTCGTGTCGCCCCTCGGAGCAGCAGCCGCC
GCGGTCGCCGCTACCCGGAAAGAAGTCAGAGACGCCGCGAGGTCGCCGCCACCGCCAT
GCCCCAAGAATAAAGGTAATGCCGCCCGGACCCCCGGACCACGGCTCTGCTCGGCCGGG
TCTCCCAGGTCCTGCCCGTAGATTGCAGGTCACCCAGGCCGCAGTGACCCTT

Mutation hotspot, primers and sequencing area

EIF1AX exon 2 codon K3

Forward primer: GGGTAGGGAGGTGATAATGTG

Reverse primer: CTGTAATCGTGCCACCACAC

Product size =406bp

TTTAACATAATATCTGCTATTTATGTGTATTTTATGTCAGAAAAATCCCCAAAGGAAA
TTCCAAGAAGGGTAGGGAGGTGATAATGTGTTAATGTTGGGATTGGAGATTGTAAATT
TAATATGATTGTGTAGCTAAAATAGATGAATTTTTTAATTTAAGTGATCTTTTAAAAA
ATGGTTTTATAAGCCTTAATTTCATTTTATTTCATACTGTTTTACAGATAATTAATGT
CATTTACCTCCTTTTCTTTTTTTTAAACCATCAGGTAAAGGAGGTAAAAACAGACGCA
GGGGTAAGAATGAGAATGAATCTGAAAAAAGAGAACTGGTATTCAAAGAGGATGGTCA
GGGTAAGTGTTTTCATAAATTACGCTTTTTAAAATAACATCCTTTCTTTTTTAGCTGG
GGACTTTATTTTTTTGAGACAGCGTCTTGCCCATCGCCCAGGGTGAAGTGTGGTGGCA
CGATTACAGCCCACTG

Mutation hotspot, primers and sequencing area

SF3B1 exon 14

Forward primer: TGATTATGGAAAGAAATGGTTGAAG

Reverse primer: CATGTTCAATGATTTCAACTAAACTTC

Product size =343bp

TGATTATGGAAAGAAATGGTTGAAGATTAATATTACCAACTCATGACTGTCCTTTCTT
TGTTTACATTTTAGGCTGCTGGTCTGGCTACTATGATCTCTACCATGAGACCTGATAT
AGATAACATGGATGAGTATGTCCGTAACACAACAGCTAGAGCTTTTGCTGTTGTAGCC
TCTGCCCTGGGCATTCCTTCTTTATTGCCCTTCTTAAAAGCTGTGTGCAAAAGCAAGA
AGTCCTGGCAAGCGAGACACACTGGTATTAAGATTGTACAACAGATAGCTATTCTTAT
GGGCTGTGCCATCTTGCCACATCTTAGAAGTTTAGTTGAAATCATTGAACATG

Mutation hotspot, primers and sequencing area

TERT promoter

Forward primer: GTCCTGCCCCTTCACCTT

Reverse primer: GCTTCCCACGTGCGCA

Product size =187bp

GACCGCGCTTCCCACGTGGCGGAGGGACTGGGGACCCGGGCACCCGTCCTGCCCCTTC
ACCTTCCAGCTCCGCCTCCTCCGCGCGGACCCCGCCCCGTCCCGACCCCTCCCGGGTC
CCCGGCCCAGCCCCCTCCGGGCCCTCCCAGCCCCTCCCCTTCCTTTCCGCGGCCCCGC
CCTCTCCTCGCGGCGCGAGTTTCAGGCAGCGCTGCGTCCTGCTGCGCACGTGGGAAGC
CCTGGCCCCGGCCACCCCCGCGATGCC

Mutation hotspot, primers and sequencing area

Appendix 2: Samples clinical data

Sample No.	Sex	Age	Location*	Cell Type	Mean Diameter (mm)	Survival
157	Male	71	C	Epithelioid	22.15	Died from liver metastasis 14 months
158	Male	54	C	Spindle	17	Alive 187 months
161	Female	68	CB/C	Mixed	14	Died 81 months from unrelated death
166	Female	74	C	Spindle	15	Died from liver metastasis 17 months
167	Female	88	CB	Mixed	15	Died from liver metastasis 16 months
169	Female	76	C	Spindle	12	Died from unrelated 142 months
170	Male	56	CB	Mixed	17	Died from liver metastasis 30 months
171	Female	75	CB	Spindle	NA	Died from liver metastasis 23 months
209	Female	64	C	Mixed	14.5	Died from liver metastasis 12 months
218	Male	42	C	Mixed	12	Died from liver metastasis 38 months
235	Female	71	CB/C	Mixed	14	Died from metastasis 32 months
244	Female	54	CB	Spindle	7.58	Alive 102 months
255	Female	63	C/CB	Spindle	16	Died from liver metastasis 35 months
284	Male	61	C	Spindle	13.5	Died from liver metastasis 30 months
300	Male	52	C	Spindle	14	Alive 154 months
301	Male	27	C	Mixed	NA	Alive 49 months but lost follow up
304	Female	45	C	Spindle	16.72	Died from metastasis 65 months
305	Male	67	CB	Spindle	15.01	Died from liver metastasis 32 months
306	Male	78	C	Mixed	11.55	Died from unrelated 27 months
308	Male	71	C	Spindle	NA	Alive 64 months but lost follow up
316	Male	75	C	NA	NA	Died from liver metastasis 36 months
317	Male	70	CB	Mixed	15.8	Died from liver metastasis 30 months

Sample No.	Sex	Age	Location*	Cell Type	Mean Diameter (mm)	Survival
312	NA	NA	NA	NA	NA	Died from metastasis 15 months
323	Female	56	C	Spindle	12.1	Alive 169 months
324	Female	41	CB	Spindle	9.6	Alive 18 months but follow up
325	Male	71	C	Spindle	11.05	Alive 118 months
327	Male	68	C	Epithelioid	20.2	Died from liver metastasis 24 months
328	Male	81	C	Spindle	15.2	Died from unrelated 54 months
330	Male	27	C	Spindle	14.4	Died from metastasis 118 months
335	Female	60	C	NA	12.6	Died from metastasis 11 months
341	Female	63	C	Mixed	15	Died from liver metastasis 7 months
342	Male	53	C	Spindle	13.15	Alive 110 months
343	Female	77	C	Spindle	9.7	Alive 111 months
344	Female	54	C	Spindle	12.5	Died 111 months cause not confirmed
345	Female	55	C	NA	21.2	Alive 108 months
346	Male	62	C	Mixed	13.45	Alive 110 months
352	NA	NA	NA	NA	NA	Died from metastasis 18 months
353	Female	65	CB/C	Epithelioid	16.7	Died 92 months cause unknown
355	Male	59	C	Spindle	14.05	Alive 104 months
375	Female	30	CB/C	NA	13.7	Alive 84 months
392	Male	58	CB	Spindle	20	Died from liver metastasis 131 months
401	Male	52	CB	Mixed	12.59	Died from liver metastasis 32 months
408	Male	57	C	Spindle	12.5	Died from liver metastasis 18 months
409	Male	50	C	Epithelioid	14.7	Died from liver metastasis 32 months
410	Female	57	CB	Spindle	19.55	Died 73 months cause not confirmed
411	Male	69	CB/C	Mixed	18.29	Died 16 months cause unknown

Sample No.	Sex	Age	Location*	Cell Type	Mean Diameter (mm)	Survival
412	Female	13	C	Spindle	14.65	Died from liver metastasis 103 months
429	Male	46	CB	Epithelioid	10.1	Died from liver metastasis 12 months
432	Female	77	C	Spindle	11.74	Alive 81 months
442	Female	47	C	Spindle	NA	Died from metastases 123 months
450	Male	73	CB	Mixed	19.75	Died from metastases 15 months
454	Male	60	C	Spindle	12.7	Alive 100 months
456	Male	69	C	Spindle	13.6	Alive 134 months
457	Female	79	C	Mixed	14.95	Died from metastasis 18 months
463	Male	76	C	Mixed	NA	Died from liver metastasis 14 months
467	Female	56	C	Spindle	9.8	Died 128 months cause unknown
472	Male	54	C	Mixed	20.75	Died from metastasis 11 months
485	NA	NA	NA	NA	NA	Alive 55 months
486	NA	NA	NA	NA	NA	Alive 61 months
489	NA	NA	NA	NA	NA	Alive 63 months
491	NA	NA	NA	NA	NA	Alive 50 months
492	NA	NA	NA	NA	NA	Alive 50 months
497	Male	63	C	Mixed	15.3	Died 31 months cause unknown
498	Male	80	CB	Spindle	13.2	Died from liver metastasis 28 months
520	Female	21	CB	Spindle	10.16	Alive 120 months
521	NA	NA	NA	NA	NA	Died from metastasis 10 months
522	NA	NA	NA	NA	NA	Died from metastasis 2 months
523	NA	NA	NA	NA	NA	Died from metastasis 38 months
524	NA	NA	NA	NA	NA	Died from metastasis 11 months
528	NA	NA	NA	NA	NA	Died from metastasis 4 months

Sample No.	Sex	Age	Location*	Cell Type	Mean Diameter (mm)	Survival
529	NA	NA	NA	NA	NA	Alive 36 months
530	NA	NA	NA	NA	NA	Alive 38 months
532	Male	45	C	Mixed	13	Alive 70 months
547	Male	48	C	Mixed	15.3	Died from liver metastasis 80 months
551	Female	31	C	Spindle	NA	Alive 6 months
578	Male	83	CB/C	Mixed	16.35	Died 17 months cause unknown
579	Male	72	CB	Mixed	11.6	Died from liver metastasis 43 months
580	Male	23	CB	Mixed	NA	Alive 55 months
581	Female	40	C	Spindle	13.4	Alive 13 months
582	Male	58	CB/C	Mixed	NA	Alive 12 months
583	Female	87	CB/C	Mixed	12	Died 14 months cause unknown
584	Male	76	I/CB/C	Mixed	9.26	Alive 34 months
585	Male	59	C	Mixed	16.36	Alive 26 months
586	Female	89	CB/C	Epithelioid	11.1	Died from liver metastasis 16 months
587	Female	64	CB/C	Mixed	NA	Alive 30 months
588	Male	54	C	Mixed	13.53	Alive 18 months
589	NA	62	CB/C	Mixed	NA	Alive 20 months
590	Male	74	C	Spindle	13.66	Alive 7 months
591	Female	69	C	NA	NA	Died 52 months cause not confirmed
592	Male	70	C	Spindle	12.605	Alive 51 months
593	Female	61	C	Spindle	13.37	Alive 6 months
594	Male	54	C	Mixed	13.835	Died from liver metastasis 29 months
595	Female	84	C	NA	15.44	Died 47 months cause unknown
596	Female	64	C	Mixed	13.045	Alive 49 months

Sample No.	Sex	Age	Location*	Cell Type	Mean Diameter (mm)	Survival
598	Female	61	CB/C	Mixed	15.785	Died from liver metastasis 24 months
599	Female	69	CB/C	Epithelioid	13.54	Alive 48 months
601	Female	54	CB/C	NA	14.125	Alive 46 months
604	Male	50	C	Mixed	16.17	Alive 42 months
605	Male	81	C	Mixed	15.48	Alive 23 months
611	Male	68	C	Epithelioid	14.655	Alive 37 months
652	NA	NA	NA	NA	NA	NA
654	NA	NA	NA	NA	NA	NA
655	NA	NA	NA	NA	NA	NA
656	NA	NA	NA	NA	NA	NA
657	NA	NA	NA	NA	NA	NA
658	NA	NA	NA	NA	NA	NA
659	NA	NA	NA	NA	NA	NA
660	NA	NA	NA	NA	NA	NA
661	NA	NA	NA	NA	NA	NA
663	NA	NA	NA	NA	NA	NA
664	NA	NA	NA	NA	NA	NA
665	NA	NA	NA	NA	NA	NA
667	NA	NA	NA	NA	NA	NA
670	NA	NA	NA	NA	NA	NA
671	NA	NA	NA	NA	NA	NA
672	NA	NA	NA	NA	NA	NA
*** Location: C=Choroid, I=Iris, CB=Ciliary body, NA=Not Applicable**						

Appendix 3: Western blot images

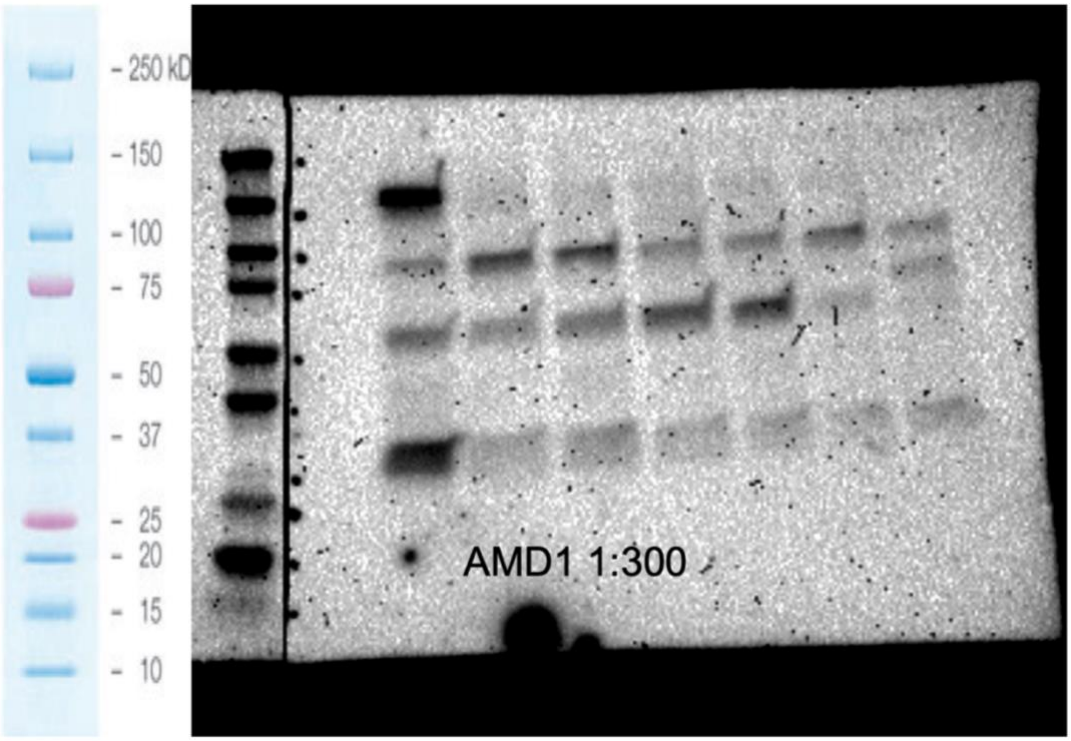

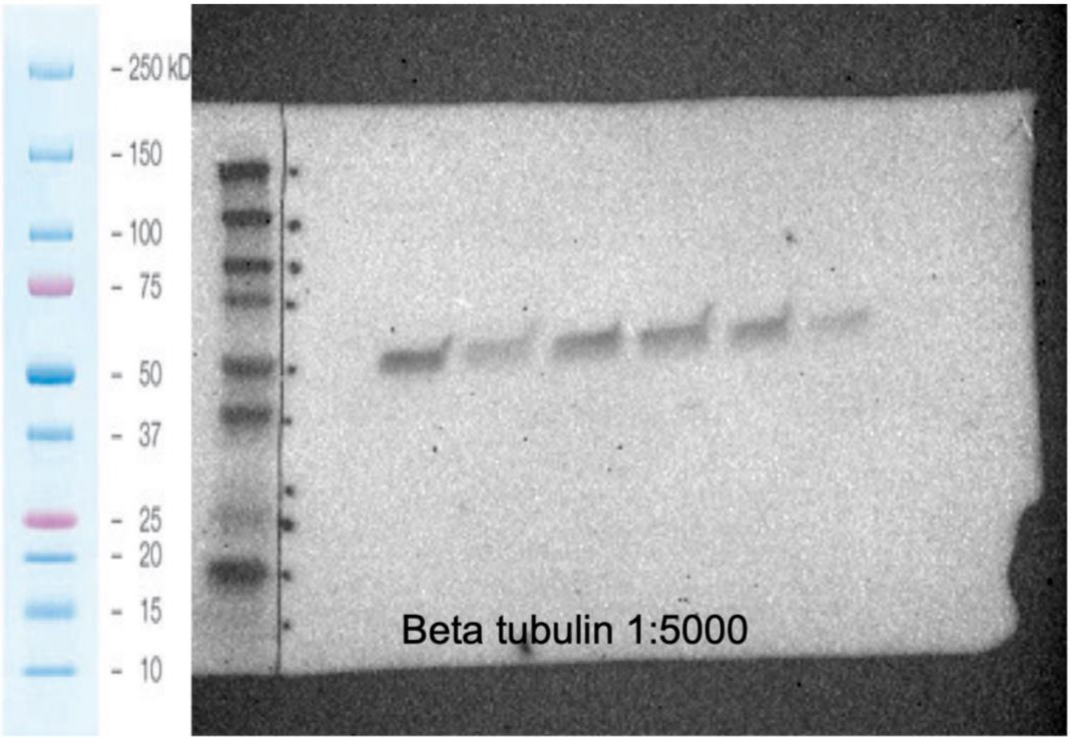

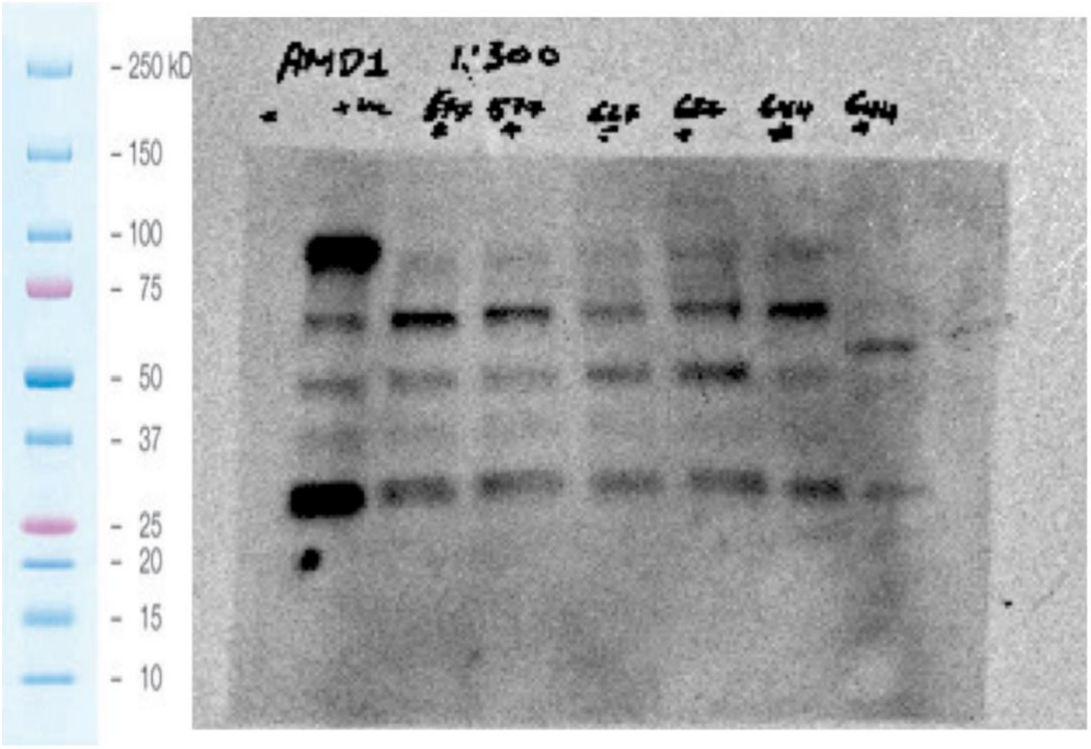
AMD1 1:300
- 250 kD
- 150
- 100
- 75
- 50
- 37
- 25
- 20
- 15
- 10

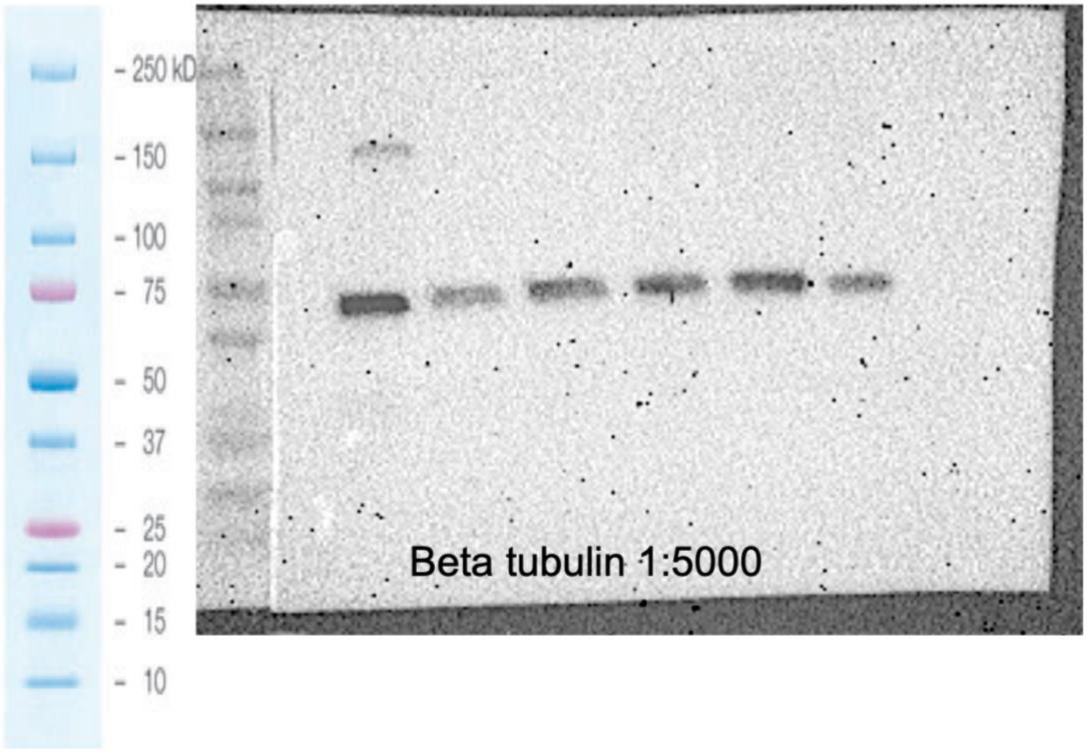
- 250 kD
- 150
- 100
- 75
- 50
- 37
- 25
- 20
- 15
- 10
Beta tubulin 1:5000